UNIVERSITAT DE BARCELONA

ZeGRIN: Using zebrafish GRIN-related disorders models for disease understanding and therapeutic discovery

Sílvia Locubiche Serra

UNIVERSITAT DE BARCELONA

Ze*GRIN*: Using zebrafish *GRIN*-related disorders models for disease understanding and therapeutic discovery

Doctoral Thesis dissertation presented by

Sílvia Locubiche Serra

to apply for the degree of Doctor by the Universitat de Barcelona

Directed by
Dr. Javier Terriente Félix
(ZeClinics S.L.)
Dr. Xavier Altafaj Tardío
(Universitat de Barcelona)

Doctoral Program in Biomedicine - Neurosciences
School of Medicine and Health Sciences. Universitat de Barcelona
ZeClinics S.L.
September 2024

ZeClinics®
Powering discovery with Zebrafish

To all GRIN
families

Acknowledgements

En primer lugar, me gustaría agradecer a mis directores de tesis, Javier Terriente y Xavier Altafaj, que me dieran la oportunidad de poder realizar este proyecto y por darme total libertad en su transcurso. Gracias por confiar en mí y decidir hacer este ambicioso proyecto juntos. Y sobre todo gracias por todo el apoyo que me habéis dado, por motivarme a seguir y por estar siempre allí.

Special thanks to Dr. Laetitia Mony, Dr. Sandra Acosta, Dr. Josep Dalmau, Dr. Daniel Tornero and Dr. Cristina Pujadas for being part of my thesis defence committee and substitutes. Thanks in advance for the stimulating discussion we will have, which I know is going to be extremely refreshing.

Xavi, moltíssimes gràcies per escollir aquella noia que encara no havia acabat la carrera i buscava un laboratori on començar les pràctiques, a la que ara ajudes a acabar la tesi doctoral. Gràcies per ensenyar-me què són els NMDARs, dels quals em vaig enamorar i no he deixat anar després de tants anys. Gràcies per les llargues converses parlant de ciència i de no-ciència, per ser com ets i per donar-me sempre suport. I gràcies a tot el iGluRs lab, aquell petit grup que em va ensenyar totes les bases del que sé del laboratori. Aquelles tardes a la Flama són inoblidables.

Maca, mi mentora, mil gracias por enseñarme a dar mis primeros pasos en el lab. Por esas "cerves", esos subfraccionamientos eternos (pero preciosos), y esas inmunos fantásticas seguidas de largas sesiones de microscopio. Gracias por confiar en mí desde el principio, y apostar por mí. Esa primera FENS en Berlín es algo que llevaré siempre conmigo. Y, por supuesto, gracias por seguir allí, por seguir siendo mi mentora y mi motivación siempre que lo necesite. ¡Qué suerte tuve de tenerte!

Cris, mi otra pieza esencial, clave en el iGluRs lab, muchísimas gracias por todo. Me enseñaste a ser ordenada con mis experimentos y con la vida, a ser extremadamente cuidadosa y, sobre todo, a hacer una fantasía de cultivos primarios de hipocampo y córtex. Y, aunque nadie los hace como tú, no se puede tener mejor profesora. Tu apoyo fue esencial, y aunque han pasado ya unos años, sigues siendo un referente para mí. "Yo de mayor quiero ser como tú".

Ana, ¡mi compañera de aventuras en el lab! Gracias por tantas horas, mano a mano, sacando adelante juntas nuestros proyectos. Eres la otra pieza clave del iGluRs lab, y sin ti nada hubiese sido igual. A los demás miembros del laboratorio de Neurofarmacología del Dr. Ciruela, gracias por las risas, las casas rurales, y el apoyo fantástico que

supusisteis en mis primeros años. Siempre me sacáis una sonrisa y me hace una tremenda ilusión encontrarnos, casualmente, en todos los congresos científicos.

Gràcies a tot el laboratori de Neurofisiologia, Xavi (un altre cop), Xavi, David, Núria, Gerard, Mar, Fede, Anna, Anna, Javi, Aïda, Paula i els que potser em deixo, per estar sempre allà, encara que sigui a la distància. Sou el meu laboratori una mica virtual, i sé que sempre que ho necessito tinc un suport en vosaltres.

Gracias a la gente de Sant Joan de Déu, con los que he compartido congresos, formaciones, jornadas y muy buenos momentos. Àngels, Natàlia, Alfonso y Uliana, muchas gracias por vuestro apoyo y por la energía y positividad que me transmitís.

Moviéndome a la que ha sido mi segunda casa durante este proyecto, ZeClinics, gracias a absolutamente todos por formar parte de esta aventura. De nuevo, gracias Javi por haber confiado en mí desde el inicio. Gracias por tu rigor científico, por nuestras charlas formales-informales y por darme apoyo en mis momentillos. Gràcies Ignasi per ser-hi sempre, per la confiança i per compartir amor per la ciència. Espero que ens quedin moltes més converses *frikis* per endavant. Y gracias a todos los directores por haber apostado por mi desde el inicio. Al final parece que contratar a "la chica del pelo azul" nos ha dado buenos momentos, ¿no?

Especial mención a mi "Jefe", Davide Rubbini, mi mentor en el inicio de mi "Pe Hache Dé". Gracias por el apoyo, por enseñarme las bases del Zebrafish, las *in situs* y lo importante que es ser cuidadosa y rigurosa en el laboratorio. Gracias por seguir allí pese a no estarlo físicamente. Y gracias por nuestras charletas de videojuegos aleatorias. Grim Fandango fue una recomendación maravillosa. ¡Lo que Zelda ha unido, que no lo separe nadie!

Gracias a todos los miembros del ZeLab (o Pezqueñines) con los que he tenido el placer de trabajar y han dejado una huella importante en mí. Sara, Marc, Cris, Roger, Samu, Nadia, Carles, Rafa, Sergio, Davide, Víctor, Jone, Santi, Júlia, David, Laura, Bea, Jessica, Helena, Katka, Tanita, Anna, Gentzane, Michele, Flavia, Lucía, Sofía, Irina, Joselyne, Claudia, Vin, Laia, Carole, Ángeles, Xris, Sylvia, Ferran, Edu, Sergi, Elena, Javi y los que posiblemente me esté dejando. Gracias también al resto del equipo, Loreto, Miriam, Dani, Anna, Tizi, Isabella, Vacys, Dimitra, Valentina, Eli, Simo, Davide e Ignasi. ¡Todos y cada uno de vosotros tenéis un huequecito en mi corazón! Sin vosotros esta aventura no hubiese sido la misma.

A todos aquellos que os habéis hecho un huequito especial, mil gracias. Bea, gracias por las risas, por el apoyo y por ser como eres. Sin ti, mis días en el lab serían mucho más tristes. A todo el equipo técnico, Lucía, Sofía, Irina y Joselyne, muchas gracias por la energía y el buen rollo que desprendéis. Trabajar junto a vosotras es pura fantasía. Michele, mil gracias por tu apoyo, tus consejos, tu ayuda y tu energía. El *Michelese* es ahora una lengua co-oficial en el lab, con todos los buenos momentos que ello conlleva. Flavia, muchísimas gracias por todo el apoyo que me has ofrecido, por las charlas, y por todo. Trabajar junto a ti ha sido realmente maravilloso.

Al petit grup que ha sorgit d'entre els tancs de l'animalari de Zebrafish, gràcies. Marc, Roger, Cris i Samu, moltíssimes gràcies per acceptar-me com infiltrada sense pijama verd. Moltes gràcies pels riures i somriures, pels bons moments, per les festes, pels concerts i per les hamburgueses compartides. El vostre recolzament i suport ha estat imprescindible durant aquesta etapa. Gràcies Sara per ser la meva companya del Vallès. Gràcies pels consells, pels cafès i tés compartits, pels viatges en cotxe, els esmorzars i per tot el que has fet per mi.

Un gracias especial a los doctorandos que me han acompañado en esta aventura, compartiendo oficina, laboratorio y algún que otro café. Helena, la teva entrada a ZeClinics va ser una glopada d'aire fresc per mi. Moltes gràcies per la teva energia i per compartir llargues tardes i caps de setmana amb mi. Gràcies per ser sempre un suport. I gràcies per ser-hi per la ciència i també per lo personal. Ferran, el meu baixista de Paradíso preferit, moltes gràcies per les bones estones, el *frikisme* i els concerts (i els que estan per venir). Katka, my old-blue-haired dearest friend, thank you so much for all the adventures we've lived in and outside the lab. Thank you for your amazing energy, your enthusiasm and for sharing with me your passion for science. Thank you for our coffees, our talks, our exchange of memes, cat pictures and beers. Tanita, my dearest μάλακα (with love), thank you for being there, always. Thank you for sharing, for caring, and for everything. Thank you for all the Friends references that kept our mental health on the toughest days. Thank you for being there for me (□).

Gracias a mis "*minions*" favoritos, Héctor, Alejandro y Míriam, con los que he tenido el placer de compartir tantas PCRs, preparaciones de buffers y, sobre todo, risas y buenos momentos.

A todos aquellos que he conocido trabajando y que sabéis que no sois sólo compañeros, que sois mis *colegos*, mis amigos, muchísimas gracias por todo, de corazón. Gracias a vosotros, soy Blue.

Gracias a toda la gente con la que he tenido el placer de cruzarme dentro del mundo de la neurociencia. A todos aquellos que he conocido en congresos, cursos (¡mi Carmona querida!), talleres de divulgación, etc. gracias por hacer que nunca vaya sola a ningún congreso, ya que siempre estáis allí para acogerme, sea donde sea.

Gracias a todas las familias GRIN, a las que he tenido el placer de conocer durante las distintas jornadas y conferencias, y a las que no conozco, pero sé que están allí. Gracias a todos por el esfuerzo, por ser como sois y por todo lo que hacéis, de corazón. El apoyo de la Asociación Española de GRINpatías ha sido indispensable durante el transcurso de este proyecto, y hacéis que todo tenga un sentido. Sobre todo, gracias a Sandra, que des de antes de empezar en este proyecto ha sido siempre un gran apoyo para mí. I am equally indebted to the GRIN families I've had the pleasure to meet from GRIN Europe. Every time we have seen each other you have given me the strength I needed to continue. Thank you all for all your effort, your enthusiasm and for everything you do.

Una mención especial al equipo de GTM ediciones, que aunque "sólo hacen su trabajo" (já), han sido un apoyo indispensable durante el transcurso de esta tesis. A Juan, Juanpe, Ramis, José y todos los que estáis detrás, mil gracias por ser como sois. La revista GTM, Kaibun, los podcasts (y el grumito), los libros, todo el contenido que generáis y vuestra brutal energía han sido una de mis grandes válvulas de escape. Muchas gracias por darme mi queridísimo nuevo apodo de "la cabesita loca". Realmente me representa, no nos vamos a engañar. Gracias por saber sacarme una sonrisa siempre que lo he necesitado.

I passant a un punt de vista més personal, vull començar agraint al meu grup d'amigues simplement per ser-hi. Què faria jo sense el meu estimadíssim Procrastination Club. Alba, Aïda, Ariadna i Marta, les gràcies es queden curtes. Gràcies per haver estat el meu suport incondicional des d'inicis de carrera. Gràcies per haver compartit classes, exàmens, Biofestes, matins (i ChocoBombs) a la biblioteca, dinars a la gespeta, sleepovers, cap d'anys i tot el que se'ns posi per davant. Gràcies per ser el meu confort, la meva casa, el meu lloc segur on podem parlar d'absolutament de tot i de res alhora (baixeu un dit, si). Gràcies per, per molta distancia que hi hagi i per molt que passin els anys, seguir sent-hi sempre. Jope, us estimo molt, de debò.

A tots els amics amb els que puc compartir milers d'estones, opinions, jocs de taula, campanyes de Dungeons & Dragons i, sobretot, cerveses. David, Sergi, Xexis, Ferran, Moi, Marc, Richi, Andy, Luís, Paula, Edu, Gabriel, Sergio, Ignacio y, de nuevo, a los que me pueda estar dejando, muchísimas gracias a todos.

David, moltíssimes gràcies per tot i més. Gràcies per ser un dels meus pilars, una peça fonamental que em dona sempre recolzament, per ser-hi i per ajudar-me en tot, sempre. Gràcies per compartir alegries, penes, atacs de riure i *comilonas* meravelloses. I gràcies per la realització de la fantasia de portada que té aquesta tesi. No podria haver escollit res millor que una il·lustració feta per tu. Sense tu, tot hagués estat molt més difícil. Gràcies per tot. També gràcies a la teva família, Bea, Laia i tota la resta, que sou sempre un gran suport per mi.

Gràcies a la meva família, i en especial als meus pares Eva i Pedro i el meu germà Sergi (el primer Dr. Locubiche). Sense el vostre recolzament no podria haver arribat on soc. Gràcies per ser-hi sempre, a les bones i a les dolentes, per donar-me sempre el vostre punt de vista i per aconsellar-me quan m'he sentit perduda. Gràcies per tants anys escoltant-me parlar de *phosphorylations,* de pòsters i presentacions que sempre semblen iguals, i per acompanyar-me durant aquesta aventura. Moltes gràcies sobretot per aguantar-me, sé que no és senzill.

No m'oblido de les nostres estimades gates, Bimba i Lola, que han estat sempre allà donant-me suport i demanant-me mimis i menjar. Les llargues temporades d'anàlisi i les llargues nits de feina no haguessin estat el mateix sense vosaltres, gatiques.

Finalment, gràcies a aquells dels qui potser m'he oblidat però, tot i així, saben perfectament que els agraeixo l'impacte que han tingut en mi. Gràcies a tots els que heu fet que aquest projecte sigui inoblidable.

Abstract

The glutamatergic neurotransmission system is crucial for brain function, and its dysregulation is involved in several neurological diseases, including developmental, psychiatric and neurodegenerative disorders. Recently, high-throughput genetic studies in patients with idiopathic developmental encephalopathies allowed the identification of GRIN-Related Disorders (GRDs). GRD is a group of genetic rare neurodevelopmental diseases, caused by the presence of *de novo* mutations of *GRIN* genes that encode for the *N*-methyl-D-aspartate receptor (NMDAR) GluN subunits. Since NMDARs play a critical role in glutamatergic neurotransmission, their dysregulation results in a range of moderate to severe neurological disorders with a clinical spectrum including intellectual disability, locomotor alterations, epilepsy, gastrointestinal dysfunction and visual problems among others.

This study focuses on generating zebrafish models of *GRIN* gene loss-of-function, specifically targeting *GRIN1*, *GRIN2A*, and *GRIN2B* homologous genes in zebrafish, to better understand the mechanisms underlying GRD pathophysiology and to evaluate potential therapeutic strategies. Along this Thesis we successfully developed and characterised an *in vivo* library of loss-of-function *grin1a*, *grin1b*, *grin2Aa*, *grin2Ab*, *grin2Ba* and *grin2Bb* zebrafish models, with the identification of GRD-like phenotypic abnormalities in a genotype-dependent manner. In addition to the deep-characterisation of these genetic models, we developed novel tools to assess GRD-related secondary alterations, such as gastrointestinal function distress and visual disturbances.

Finally, using these models will allow us to conduct drug screening aimed at identifying compounds that can rescue NMDAR function. The identified compounds hold therapeutic potential not only for GRD patients but also for other conditions involving NMDAR dysfunction that are displaying comorbidities. In that sense, in parallel with the creation of zebrafish *grin* genetic models, an innovative and cost-effective platform to study genetic-based diseases with strong phenotypes (using epilepsy as proof-of-principle) and to perform large-scale drug screening was developed. Overall, the results from this Thesis are contributing to the development of novel, targeted therapies for NMDAR-related diseases.

Resum

El sistema de neurotransmissió glutamatèrgica és crucial per la funció cerebral, i la seva desregulació està relacionada amb diferents malalties neurològiques, incloent malalties del neurodesenvolupament, psiquiàtriques i neurodegeneratives. Recentment, estudis genètics d'alt rendiment en pacients amb encefalopaties idiopàtiques del desenvolupament han permès identificar els trastorns relacionats amb els gens GRIN (GRDs, de l'anglès, GRIN-related disorders). Les GRDs són un grup de malalties genètiques rares del neurodesenvolupament, causades per la presència de mutacions *de novo* en els gens *GRIN*, que codifiquen per a les subunitats GluN del receptor N-metil-D-aspartat (NMDAR). Atès que els NMDAR tenen un paper crític en la transmissió glutamatèrgica, la desregulació de la seva funció resulta en una sèrie de trastorns neurològics de moderats a greus, amb un espectre clínic que inclou discapacitat intel·lectual, alteracions locomotores, epilèpsia, disfunció gastrointestinal i problemes visuals, entre altres.

Aquest projecte es centra en la generació de models de peix zebra amb pèrdua de funció dels gens *GRIN*, focalitzant-nos específicament als gens homòlegs *grin1*, *grin2A* i *grin2B* en peix zebra. Això ens permetrà entendre millor els mecanismes subjacents a la fisiopatologia de les GRDs, així com avaluar possibles estratègies terapèutiques. Al llarg d'aquesta tesi, hem desenvolupat i caracteritzat amb èxit una biblioteca *in vivo* de models de peix zebra amb pèrdua de funció dels gens *grin1a*, *grin1b*, *grin2Aa*, *grin2Ab*, *grin2Ba* i *grin2Bb*, identificant anomalies fenotípiques similars a les GRDs de manera dependent del genotip. A més de la caracterització d'aquests models genètics, hem desenvolupat noves eines per avaluar alteracions secundàries relacionades amb les GRDs, com ara trastorns de la funció gastrointestinal i alteracions visuals.

Finalment, l'ús d'aquests models ens permetrà dur a terme un cribratge de fàrmacs orientat a identificar compostos capaços de restaurar la funció dels NMDARs Els compostos identificats tindran potencial terapèutic no només per als pacients amb GRD, sinó també per a altres malalties relacionades amb disfuncions dels NMDARs. En aquest sentit, paral·lelament a la creació dels models genètics *GRIN* en peix zebra, s'ha desenvolupat una plataforma innovadora i rendible per estudiar malalties genètiques amb fenotips robustos (utilitzant l'epilèpsia com a prova de concepte) i realitzar cribratges de fàrmacs a gran escala. En conjunt, els resultats d'aquesta tesi contribueixen al desenvolupament de noves teràpies dirigides per a malalties relacionades amb els NMDARs.

Index

Abbreviations and acronyms

A

AD: Alzheimer's Disease

ADHD: Attention-deficit and hyperactivity disorder

AED: Antiepileptic drugs

AMPA: α-amino-3-hydroxy-5-methyl-4-isoxazolepropioninc acid

AMPAR: AMPA Receptor

ANOVA: Analysis of Variance

ASD: Autism Spectrum Disorders

B

BCIP: 5-bromo-4-chloro-3-indolyl-phosphate

BMD: Benchmark Dose (LD10)

Bpi: Blue Preference Index

BSA: Bovine Serum Albumine

C

cDNA: Complementary DNA

cLTP: Chemical long-term potentiation

CNS: Central Nervous System

CRISPR: Clustered Regularly Interspaced Short Palindromic Repeats

crRNA: CRISPR RNA

CTD: Carboxyl-Terminal Domain

D

DIG: Digoxigenin

DMSO: Dimethylsulfoxide

DNA: Deoxyribonucleic acid

dpf: Days post-fertilisation

E

E3: Embryo Media

F

FET: Fish Embryo Toxicity Test

G

GABA: γ-aminobutyric acid

GI: Gastrointestinal

GIT: Gastrointestinal tract

GLYT1: Glycine Transporter Type 1

GoF: Gain-of-function

GRD: GRIN-related disorders

H

HD: Hungtinton's Disease

HEK: Human embryonic kidney

hpf: Hours post-fertilisation

HYB: Hybridisation

I

IDT: Integrated DNA Technologies

iGluR: Ionotropic Glutamate Receptor

iNGS: Inactivated Normal Goat Serum

ISH: *In situ* Hybridisation

K

KA: Kainate acid

KAR: Kainate acid Receptor

KI: Knock-in

KO: Knockout

L

LBD: Ligand Binding Domain

LC10: Lethal Concentration for 10% of the population

LoF: Loss-of-function

LTD: Long-term depression

LTP: Long-term potentiation

M

mGluR: Metabotropic Glutamate Receptor

MK-801: (+) MK-801 or dizocilpine

mRNA: Messenger RNA

N

NAM: Negative Allosteric Modulator

NBT: Nitro Blue Tetrazolium Chloride

NHEJ: Non-Homologous End Joining

NMDA: N-Methyl-D-Aspartate

NMDAR: NMDA Receptor

NTD: Amino-Terminal Domain

NTMT: Alkaline Phosphate Buffer

O

OECD: Organisation for Economic Co-operation and Development

P

PAM: Positive Allosteric Modulator

PBS: Phosphate-buffered saline

PBST: Phosphate-buffered saline with Tween-20

PCA: Principal Component Analysis

PCR: Polymerase Chain Reaction

PD: Parkinson's Disease

PFA: Paraformaldehyde

PNS: Peripheral Nervous System

PsAM: Protospacer Adjacent Motif

PSD: Post-synaptic density

PTU: Phenylthiourea

PTZ: Pentylenetetrazole

R

RNA: Ribonucleic acid

S

sgRNA: Single guide RNA

SR: Serine Racemase

SSC: Saline Sodium Citrate

T

TARPs: Transmembrane AMPA receptor regulatory proteins

Tg: Transgenic

TMD: Transmembrane Domain

tracrRNA: Trans-activating CRISPR RNA

TSGD: Teleost-specific genome duplication

V

VAST: Vertebrate Automated Screening Technology

VGLUT: Vesicular Glutamate Transporters

v-SNARE: Vesicle Soluble NSF Attachment Protein

W

WISH: Whole mount *in situ* hybridization

WT: Wild-type

Introduction

1. Zebrafish as a research model

Zebrafish (*Danio rerio*) is a vertebrate animal model usually used in biomedical research as a complement organism of mammalian models. As a vertebrate, the zebrafish provides a high genetic conservation, extensive to anatomy and several biological processes. Furthermore, it has been described to offer several experimental advantages when compared both to higher and lower complexity models (Vorhees et al., 2021).

Zebrafish and humans evolved from a common ancestor. Therefore, both species are sharing genes that may conserve similar functions along evolution. Specifically, ~70% of the zebrafish genes are homologous to human genes. Interestingly, in terms of disease-associated genes, 82% of the human genes linked to genetic disorders are homologous in zebrafish (Howe et al., 2013; Vorhees et al., 2021).

This high genetic homology is only one of the several reasons why the zebrafish has an emerging interest in the study of several human disorders. One of the most interesting reasons is the low maintenance costs, given by the small size, compared with other models like rodents, which allow keeping them in tanks in large numbers, reducing the space required for their maintenance (Zon, 1999).

Another interesting characteristic of zebrafish is related to the reproductive and developmental cycle. Indeed, the fertilisation occurs *ex utero*, along with the embryo development within a transparent protective membrane (chorion). In early stages of zebrafish development, not only the chorion is transparent, but also the whole animal is almost see-through. This feature facilitates the visual monitoring of zebrafish larvae development, by means of real-time *in vivo* imaging.

Furthermore, the progeny of a zebrafish breeding is tremendously large, increasing the sample size of the experimental groups. Besides the fact that a breeding of adult fertile zebrafish can lay more than 200 eggs every week, the development of the zebrafish larvae also happens in a short period of time. Development occurs rapidly from the zygote to a small larva, with major organs such as the heart, brain, liver, intestine, and eye differentiated within a day and fully functional by 120 hours post-fertilization (hpf) (Ingham, 1997). Moreover, larvae can continue to obtain nutrients from the yolk until 10 dpf. However, they are usually kept without feeding up to 5 dpf, when they are transferred to a nursery system to continue their development, if required.

At only 5 dpf, still in larval period, the larvae have begun to actively swim, developing the essential swimming bladder, showing a characteristic swimming behaviour. At these stages, also the larvae start moving the jaw, opercular flaps, pectoral fins and eyes. The development of these structures allows the swift scape responses and herald respiration, the seeking of prey and feeding. As early as 7 dpf, the majority of morphogenesis and primary neurogenesis processes have been completed (Boueid et al., 2023; Chapouton & Godinho, 2010; Peng et al., 2016; Rieger et al., 2011; Schmidt et al., 2013). In accordance with their rapid development at the initial developmental stages, zebrafish also reach sexual maturity relatively early, around 2 months of age, allowing the rapid generation of stable lines to study the function and dysfunction of several important genes (Zon, 1999).

1.1. Zebrafish conservation and drug discovery

Given the genetic conservation, zebrafish display a conserved metabolism and response to drugs, making them highly suitable in vivo models for drug discovery assays.

First, the screening of different compounds in zebrafish are performed in living embryos or larvae. These present a complexity of biological processes and possess fully integrated organ systems. Thus, compared to cell culture assays, a broad range of phenotypes can be assayed and are currently widely used for drug-screening.

The highly homologous zebrafish genome also has an impact in metabolism and drug discovery. While the primary sequence of the zebrafish proteome is only relatively conserved with the human proteome, key proteins such as ion channels, membrane receptors or enzymatic regulatory and catalytic domains (common pharmacological targets) are highly conserved. These sites have retained the ability to bind to the same molecules and ions, conserving their function. Therefore, compounds or therapies with an impact in zebrafish are highly likely to have an effect in mammalian models (P. Goldsmith, 2004; MacRae & Peterson, 2015).

Furthermore, in terms of an integrated multisystemic evaluation of pharmacological effects, the study of drug effects on an intact animal provides a comprehensive understanding of pharmacokinetics, bioavailability, responses. These advantages are particularly relevant in the context of neuroscience drug-discovery, in which cell interactions, neural modulation and endocrine signalling are key for the assessment of drug tolerability and efficacy.

Overall, zebrafish embryos are widely used in large-scale high-throughput drug screening of small molecules, in a cost- and time-effective manner (MacRae & Peterson, 2015; Parng et al., 2002).

1.2. Zebrafish as a suitable model for brain diseases modelling

Along evolutionary processes, vertebrates have highly conserved the nervous system structures, functions, and sensitivity to chemical challenges. This phylogenetic conservation, together with the cost- and time-saving intrinsic properties show the zebrafish as a suitable model for high-throughput neuroscience-related studies, over more commonly used vertebrate models, such as mice and rats.

Not only the nervous system is conserved as vertebrates, but zebrafish also share several genetic, developmental, pharmacological and behavioural characteristics analogous to other mammals, including humans. However, also important limitations and differences exist, sometimes affecting the translation of the obtained data with the zebrafish to other mammals, and overall humans. For these reasons, zebrafish is still considered an alternative and complementary animal model along with other mammal models.

However, one important difference when addressing the zebrafish neuronal system is the brain architecture. The predominant external layer in zebrafish brain is the optic tectum, while in other mammals like rats and mice is the neocortex. The zebrafish have a little telencephalon, with the midbrain or mesencephalon as the main structure (Kozol et al., 2016) (Figure 1).

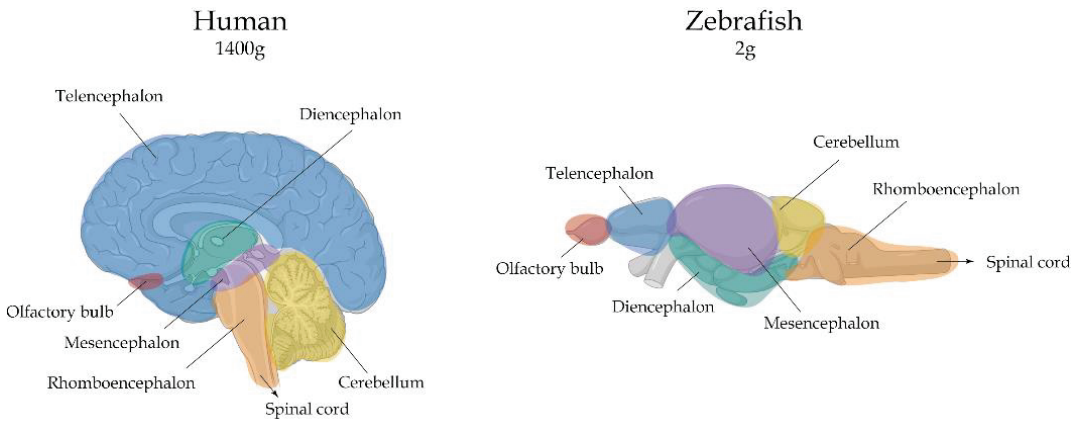

Figure 1. Conserved brain structures between zebrafish and humans. Telencephalon is represented in blue, Diencephalon in green, Mesencephalon in purple, Olfactory bulb in red, Rhomboencephalon in orange, Cerebellum in yellow and Spinal cord is indicated with an arrow. Created with BioRender. Adapted from ZeClinics website, https://www.zeclinics.com/.

However, there is a degree of conservation of the neuron-targeted compound effects in zebrafish and other mammal models. This is explained because the similarities in the cellular and synaptic structure, which is highly conserved among these vertebrate species. The specification of a conserved neurobiological mechanism, like the protein structure, the neurotransmitter implied, the post-synaptic density composition, etc. is critical for the translation of zebrafish discoveries to mammals (Bayés et al., 2017; Guo, 2009).

An example of the use of zebrafish in neuroscience research is the study of rug neurotoxicity. Neurotoxicity assays take advantage of the high similarity between zebrafish and human CNS structure and function to predict with accuracy the possible neurotoxic consequences of new compounds exposure (Cornet et al., 2017). Importantly, neurotoxicity and neurotoxic response in mammals have shown that sex differences have to be taken into account. Zebrafish, and teleost fish in general, have also sex characteristics, but these are determined differently than in mammals, and occur later in development, so larvae are not affected by sex determinants. The sex characteristics in the zebrafish are defined mainly by environmental conditions in juvenile and adult phases of their development. Nevertheless, in larvae the sex characteristics are not yet defined, and no differences can be measured, and this must be considered when translating the information to mammals. On the other hand, this can also be considered an advantage since we directly do not have an interaction of either of the sexes in our results.

The behavioural test batteries developed and currently used in zebrafish models provide analogous assessments to rodent sensorimotor and cognitive functions. Also, zebrafish models can provide valuable mechanistic information regarding the neurodevelopmental processes that may be affected by specific genetic conditions or the exposure to different potential toxic reagents.

In general, zebrafish provides a wide array of translatable mechanistic pathways, mechanisms of action within neurodevelopment and toxicity. At the same time, it also provides non-homologous genes that may influence gene expression and whose influence is not directly relevant to humans. This is complicated further by the genome duplication of teleost fish.

As a general vision, zebrafish is a valuable model that can be considered complementary to mammalian models. As such, zebrafish are extremely useful for genetic disease modelling, target discovery and high throughput drug/chemical screening, but always followed by study in rodent models.

Specifically, the zebrafish is a very suitable model for the study of developmental conditions (J. R. Goldsmith & Jobin, 2012), including neurodevelopmental diseases such as ASD, epilepsy, or the recently described rare disease, GRIN-related disorders.

2. Glutamate and the glutamatergic system

Glutamate is the principal excitatory amino acid neurotransmitter in the brain. Glutamate excitatory properties in the mammalian nervous system have been known since the 1950's (D. Curtis et al., 1959; Hayashi, 2021), but it was not until the 1970's where it was recognized as the principal excitatory neurotransmitter (D. R. Curtis & Johnston, 1974; Fonnum, 1984; Fonnum et al., 1981; Fonnum, Gottesfeld, et al., 1978; Fonnum, Grofová, et al., 1978; Roberts, 1981). Within the synapse, presynaptic neuron accumulates L-glutamate-filled synaptic vesicles from glutamate turn-over provided by *i)* the synthesis from α-ketoglutarate (Krebs cycle) or from *ii)* astrocyte-released glutamine metabolised into glutamate. Upon action potential in the presynaptic neuron, calcium influx promotes neurotransmitter vesicles fusion with presynaptic membrane and L-glutamate is released into the synaptic cleft (Bak et al., 2006), binding to glutamate receptors and activation of ionotropic and/or metabotropic pathways. Glutamate-mediated neurotransmission is present both in the central nervous system (CNS) and peripheral nervous system (PNS), and both in neuronal and non-neuronal cells.

2.1. Glutamatergic synthesis

Glutamate is ubiquitously distributed in the brain, with a powerful excitatory function. Initially, given the high concentration of glutamate in the brain, this amino-acid was considered a metabolite (Krebs, 1935). Its role as excitatory neurotransmitter was initially doubted, given the widespread action and the lack of knowledge of a system that stopped glutamate function. The identification of GABA effects on neurons (D. Curtis et al., 1959) and the relationship between the metabolism of GABA and glutamate suggested that glutamate could have an important role in the neuronal function.

The identification of GABA effects on neurons (D. Curtis et al., 1959) and the relationship between the metabolism of GABA and glutamate suggested that glutamate could have an important role in the neuronal function. This hypothesis was further confirmed by biochemical and neurobiological findings. These approaches demonstrated that glutamate fulfils the main criteria of a neurotransmitter: *i)* presynaptic localization in specific types of neurons (glutamatergic neurons), release to the synaptic cleft in response to a physiological stimulus, and ability to elicit a postsynaptic response; *ii)* identity of action, with response to agonists and antagonists; *iii)* the existence of mechanisms to rapidly terminate the transmitter action or response (D. Curtis et al., 1959; Fonnum, 1984).

In neurons, *de novo* glutamate synthesis occurs from tricarboxylic acid cycle (TCS, Krebs cycle), the common pathway for oxidation of carbohydrates, lipids, and proteins (Akram, 2014). In this pathway, GABA (γ-Aminobutyric acid), the main inhibitory neurotransmitter in the mammalian cortex (Petroff, 2002), is synthesised directly from glutamate. Furthermore, the amino- group of the GABA molecule is transaminated into glutamate during the GABA degradation pathway. Therefore, beyond their functional interaction, glutamate excitatory GABA inhibitory neurotransmission systems are intrinsically biochemically related.

2.2. Glutamate neurotransmission function

Glutamatergic neurotransmission uses glutamate as the primary signalling molecule and is involved in major brain functions. Due to the wide heterogeneity of cell types releasing glutamate, in combination with their relative target cells or receptors, glutamate-mediated neuronal communication is highly diverse and can mediate

multiple functions in the neuronal effectors (Anaparti et al., 2015; Chenu et al., 1998; Du et al., 2016; Genever et al., 1999; S. Gill et al., 2007; S. S. Gill & Pulido, 2001; Mattson, 2008; McKenna, 2007; Takahashi et al., 2019; Tomé, 2018; Yano et al., 1998). While considering their diversity, glutamate-mediated functions can be grouped in the following categories: sensation, movement control, learning and memory mechanisms.

2.3. The tripartite glutamatergic synapse

In the last century, synapses were traditionally described as morphological structures formed by and allowing the communication of two neurons, namely the presynaptic and the postsynaptic neurons. Nonetheless, seminal works from Araque and others showed that, in the vertebrate CNS, glutamatergic signalling requires the presence and activity of glial cells (Araque et al., 1999; Lalo et al., 2021; Perea et al., 2009). The prevailing majority view acknowledges the participation of astrocytic cells, a third actor, in addition to the presynaptic and postsynaptic neurons. Therefore, there are three main cellular players involved in the synapse: the presynaptic neuron releasing glutamate to the synaptic cleft, the postsynaptic neuron responding to glutamate-binding to specific glutamate receptors, and glial cells (mainly astrocytes) that regulate the homeostasis of the synaptic button (i.e. uptake of glutamate / release of gliotransmitters).

Importantly, glial cells express different types of glutamate receptors and transporters, to sense synaptic activity and modulate their physiology to regulate the proper activity (in the short and long term), respectively. Moreover, after postsynaptic neuron activation, several signalling cascades lead to transcriptional and translational modifications of proteins critically involved in glutamate metabolism, glial activity and, overall, the glutamatergic neurotransmission process (Liu et al., 2018; Nishida & Okabe, 2007; Noriega-Prieto & Araque, 2021; Rossi, 2015).

2.3.1. Presynaptic neuron

Glutamatergic neurons synthesise and release L-Glutamate into the synaptic cleft. Upon glutamate synthesis, glutamate is transported via vesicular glutamate transporters (VGLUT) and stored in neurotransmitter vesicles in the presynaptic button. Glutamate exocytosis or release is finely regulated and requires the propagation of the action potential to the presynaptic terminal, activating voltage-dependent calcium channels that, in turn, will allow a transient calcium influx. This Ca2+ will directly interact with

primed synaptic vesicle proteins and induce their fusion with the presynaptic plasma membrane and the release of glutamate in the synaptic cleft (Lodish et al., 2000) and further binding to the different types of glutamate receptors mostly located in the postsynaptic neuron, although presynaptic glutamate receptors (autoreceptors) are also present and regulate release process, with an impact on neuronal processes (*e.g.* neuronal plasticity).

The three families of Ionotropic Glutamate Receptors (iGluRs): AMPARs (α-amino-3-hydroxy-5-methyl-4-isoxazonle Propionic Acid Receptors), KARs (Kainate Receptors) and NMDARs (*N*-methyl-D-aspartate Receptors) participate in the regulation of the synaptic transmission, mostly facilitating the neurotransmission. Presynaptic Metabotropic Glutamate Receptors (mGluRs) might be facilitating or inhibiting the synaptic transmission depending on the signalling and the specific coupled G-protein (Pinheiro & Mulle, 2008) (Figure 2).

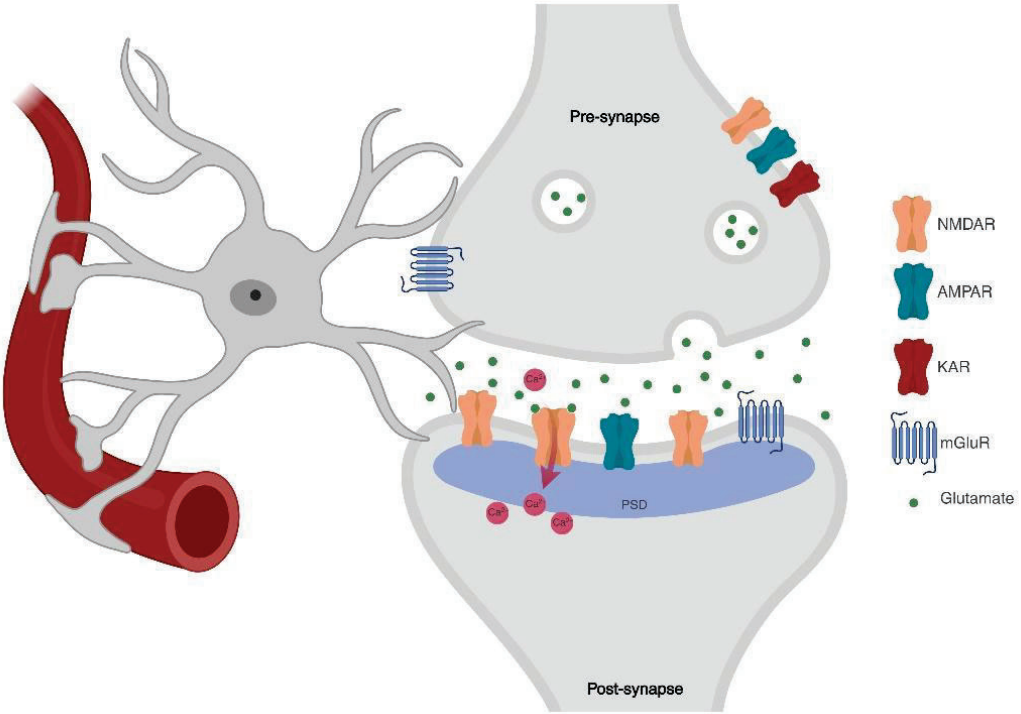

Figure 2. Schematic representation of the tripartite glutamatergic synapse. The different receptors (AMPAR, KAR, NMDAR and mGluR) are represented in a schematic version of the synapse. In the presynaptic neuron autoreceptors can be find, and glutamate accumulates in the vesicles. This is released into the synaptic cleft, interacting with the receptors in the postsynaptic terminal, where the post-synaptic density (PSD) allows the receptor clustering. Activation of glutamate receptors generates a calcium influx, activating different signalling pathways. The astrocyte is also present in the tripartite glutamatergic synapse. Created with BioRender.

Along with glutamate, additional molecules directly involved in glutamatergic neurotransmission are also released in the synaptic cleft. This is the case for glycine, a co-agonist of the *N*-methyl D-aspartate type (NMDAR) of ionotropic glutamate receptors. Glycine concentration is regulated in the synaptic cleft by GLYT1 (glycine transporter type 1), which couples the glycine transport with two Na^+ cations and a Cl^- anion (Erdem et al., 2019). Similarly to glycine, D-Serine is also acting as an NMDAR co-agonist. In the brain, D-Serine can be synthetized *de novo* from L-Serine, by the action of Serine Racemase (SR). This enzyme is widely expressed in astrocytes, and these glial cells are releasing D-Serine gliotransmitter in the synaptic cleft, contributing to the regulation of glutamatergic neurotransmission (Kartvelishvily et al., 2006; Kim et al., 2005; Schell et al., 1995).

2.3.2. Postsynaptic neuron

The postsynaptic side of the tripartite synapse is specialised in the reception and transduction of the neurotransmitter signal (*e.g.* glutamate) released from the presynaptic terminal. Different glutamate receptors types are concentrated in the postsynaptic membrane, and ready to receive the presynaptic signaling. The receptors are embedded in a protein network, formed by scaffolding and anchoring molecules, enzymes and cytoskeletal components. This high-density protein network, visualized as a dark electrodense structure in electron microscopy studies, corresponds to the so-called Post-Synaptic Density (PSD), and contains molecular components essential for several neuronal functions, such as memory and learning processes (Sheng & Kim, 2011).

Glutamate receptors are functionally classified in two main categories, namely **metabotropic receptors** (mGluRs) and **ionotropic receptors** (iGluRs). Metabotropic-type mGluRs are ligand-dependent receptors coupled to G-proteins. They consist of proteins with seven transmembrane domains that form dimers, and they are classified in three different groups: Group I (mGluR1 and mGluR5), coupled to G_q/G_{11} proteins, Group II (mGluR2 and mGluR3), and Group III (mGluR4, mGluR6, mGluR7 and mGluR8), both coupled to G_i/G_o proteins (Nicoletti et al., 2011). Functionally, mGluRs are associated with slow responses (minutes-hours) (Pin & Duvoisin, 1995).

Inotropic-type iGluRs are ion channels forming a membrane pore allowing cations influx in response to agonist binding, mediating fast excitatory neurotransmission (Hollmann & Heinemann, 1994). iGluRs are permeable to different cations (Na^+, K^+ and Ca^{2+}) in a receptor type-dependent (Paoletti et al., 2013; Sanz-Clemente et al., 2013; Traynelis et al., 2010). iGluRs-mediated cation influx can directly modulate intracellular proteins and/or alter the postsynaptic potential, generating excitatory postsynaptic potentials (EPSP) that can contribute to generate action potentials in the postsynaptic neuron (Traynelis et al., 2010).

The ionotropic glutamate receptors are tetrameric membrane proteins. Each tetramer is composed of four large subunits forming a central ionic channel pore permeable to cations. Each subunit presents different characteristic domains: a large extracellular amino-terminal domain (ATD), an extracellular ligand-binding domain (LBD), a transmembrane domain (TMD) with three transmembrane helix (M1, M3 and M4) and a re-entrant loop (M2), and finally an intracellular carboxyl-terminal domain (CTD). The architecture of the receptors is shared by all the ionotropic glutamate receptors (Figure 3).

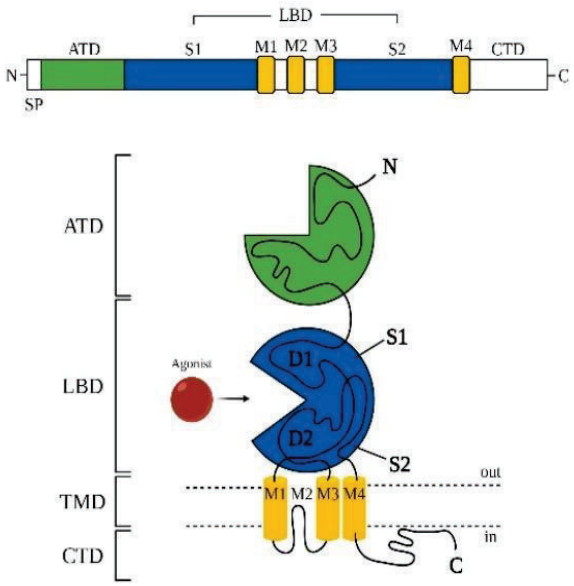

Figure 3. Structure and domain organisation of glutamate receptors. Linear representation and schematic illustration of the structure of the different subunits. The different domains are represented: Amino-terminal domain (ATD) in green, ligand-binding domain (LBD) in blue, transmembrane domain (TMD) in orange and carboxyl-terminal domain (CTD), in black at the end of the structure. SP: Signal Peptide. Adapted from Traynellis et al 2010. Created with BioRender

While keeping in mind that iGluRs are responding to L-Glutamate, the endogenous agonist, this family of glutamate receptors can be pharmacologically classified in their differential response to glutamate analogues, resulting on the following classification:

- **α-Amino-3-hydroxy-5-Methyl-4-isoxazonle Propionic Acid Receptors (AMPARs)**: They are composed by GluA1-GluA4 subunits, and form quaternary complexes with AMPAR-associated proteins (e.g. TARPs).

- **Kainate Acid Receptors (KARs)**: Composed by GluK1-GluK5 subunits. Lead to small currents, and have low activation and deactivation kinetics.

- ***N*-methyl-D-aspartate Receptors (NMDARs)**: Composed by two obligatory GluN1 subunits and a combination of GluN2A-D and/or GluN3A-B subunits. The subunit composition and physiology of the NMDAR will be described in the next section.

In addition to these well-studied iGluRs, a fourth group of glutamate ionotropic receptors namely Glutamate Delta Receptors (GluDs: GluRδ1 and GluRδ2) have been reported. GluDs have been described as playing a role in synapse formation and maturation, and their alteration has been associated with psychiatric and neurodevelopmental disorders. These receptors present a weak sequence identity (20-25%) to the other three iGluRs families. Although it is assumed that the Delta Receptors form ligand-gated ion channels, there are no known agonists for GluD channels themselves. Recently, it has been reported that GluRδ2 could function as an ion channel responding to the co-agonists D-Serine and glycine, but only in specific complex formations (Carrillo et al., 2021; Itoh et al., 2024). However, many fundamental questions regarding their mechanism of action and function remain unknown (Carrillo et al., 2021; Hansen et al., 2009; Itoh et al., 2024; Lomeli et al., 1993; Schmid & Hollmann, 2008).

The different iGluR subunits are encoded by different genes. These are named according to the functional type of receptor they form (Collingridge et al., 2009; Traynelis et al., 2010) (Table 1).

Receptor	Protein subunits (Alternative names)	Codifying genes
AMPAR	GluA1 (GluR1, GluRA)	*GRIA1*
	GluA2 (GluR2, GluRB)	*GRIA2*
	GluA3 (GluR3, GluRC)	*GRIA3*
	GluA4 (GluR4, GluRD)	*GRIA4*
KAR	GluK1 (GluR5)	*GRIK1*
	GluK2 (GluR6)	*GRIK2*
	GluK3 (GluR7)	*GRIK3*
	GluK4 (KA1)	*GRIK4*
	GluK5 (KA2)	*GRIK5*
NMDAR	GluN1 (NMDAR1, NR1, GluRε1)	*GRIN1*
	GluN2A (NMDAR2A, NR2A, GluRϵ1)	*GRIN2A*
	GluN2B (NMDAR2B, NR2B, GluRϵ2)	*GRIN2B*
	GluN2C (NMDAR2C, NR2C, GluRϵ3)	*GRIN2C*
	GluN2D (NMDAR2D, NR2D, GluRϵ4)	*GRIN2D*
	GluN3A (NR3A)	*GRIN3A*
	GluN3B (NR3B)	*GRIN3B*
DeltaR	GluD1 (δ1, GluR delta-1)	*GRID1*
	GluD2 (δ2, GluR delta-2)	*GRID2*

345 1. Summary of the different iGluRs, their nomenclature and the name of their genes. The protein subunits name is the current IUPHAR nomenclature, and in brackets are the other common names. The genes are listed with their HUGO symbol. Adapted from Traynelis et al., 2010.

2.3.3. Astrocytes

Traditionally, glial cells and particularly astrocytes, have been considered as cellular elements of the brain providing a supportive structure to neurons. This classical vision has evolved, and nowadays glial cells are considered as functional and active players in brain communication, homeostasis and physiology. In particular, astrocytes are cellular processors of processing, transfer and storage of information in the nervous system, having a crucial role in synaptic communication and plasticity (Perea et al., 2009; Santello et al., 2012).

Among other important roles, the astrocytes participating in the glutamatergic synapse are part of the blood brain barrier structure, and regulate extracellular levels of K^+ and different gliotransmitters, modulating the synapse function. Regarding their role in the glutamatergic transmission, astrocytes are involved in glutamate clearance that is required to terminate glutamatergic signalling (after glutamate release and glutamatergic receptor activation), not only for the signalling within the direct synapse, but also to avoid diffusion to neighbour synapses and excitotoxicity (Zhou & Danbolt, 2014).

3. The NMDA Receptor

3.1. Composition of the NMDA Receptor

The NMDAR (*N*-methyl-D-aspartate Receptors) ionotropic glutamate receptors are heterotetrameric structures composed of four large GluN subunits. NMDARs are formed by the combination of two obligatory GluN1 subunits and two variable GluN subunits (GluN2A-D and/or GluN3A-B) (Cull-Candy et al., 2001; Paoletti, 2011; Paoletti et al., 2013; Traynelis et al., 2010).

Furthermore, several isoforms have been described for GluN1, GluN2A and GluN3A subunits, resulting from alternative splicing (Paoletti et al., 2013; Warming et al., 2019). The assembling of the different GluN subunits results in the formation of di-heteromeric (variable subunits are identical) or triheteromeric NMDARs (different variable subunits within the same NMDAR) (Figure 4). Functionally, the molecular heterogeneity of NMDAR is crucial, since their composition determines the biophysical and pharmacological properties of the channel. In addition, the NMDAR composition also

determines the subcellular distribution and interactions with other proteins (Paoletti, 2011; Paoletti et al., 2013).

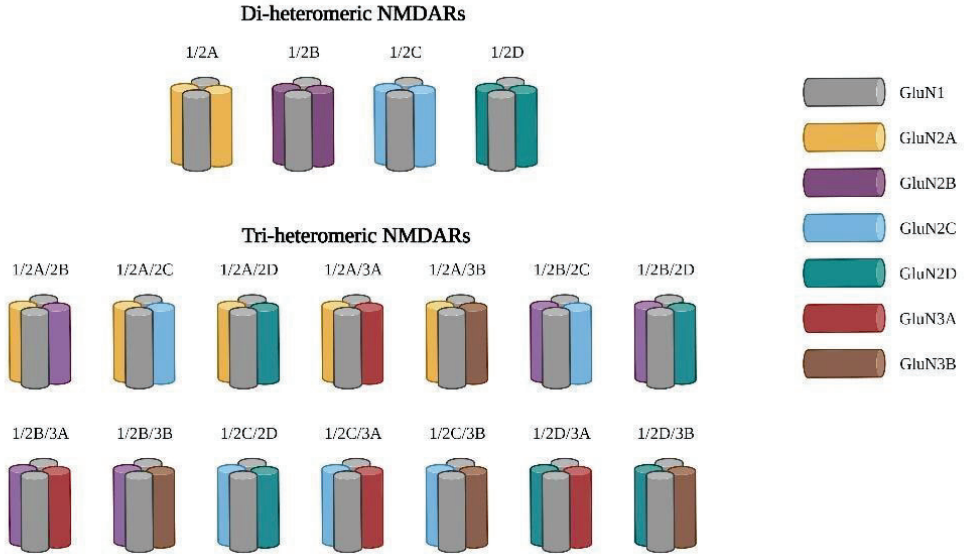

Figure 4. Summary and representation of the different populations of heteromeric NMDARs. The distinct possibilities of combination of the different subunits are displayed. Adapted from Paoletti et al., 2013. Created with BioRender.

Notably, GluN2A- and GluN2B-subunit containing NMDARs -the major expressed variable GluN subunits- have different developmental, subcellular, biophysical and functional features. GluN2A subunit-containing NMDARs are more expressed in the synaptic sites and play a role in long-term potentiation (LTP). In contrast, GluN2B subunit-containing NMDARs are more present in extrasynaptic sites of mature neurons and are more involved in the production of long-term depression (LTD) (Massey et al., 2004). NMDARs show different spatio-temporal expression profiles, together with specific biophysical properties. This differential expression has been reported in humans (Laurie & Seeburg, 1994), rat (Paoletti, 2011), mice (Paoletti et al., 2013) and zebrafish (Cox et al., 2005; Zoodsma et al., 2020).

3.2. Structural characteristics of the NMDA Receptor

NMDAR are composed by different large domains: an extracellular amino-terminal domain (ATD), a ligand-binding domain (LBD), a transmembrane domain (TMD) where the pore of the channel is formed, and an intracellular carboxyl-terminal domain (CTD).

The ATD differs the most among the different GluN subunits and functionally binds to allosteric modulators on a subunit-dfependent manner (Karakas et al., 2009). In addition, ATD also mediates the dimer formation through disulfide bonds, and regulates receptor trafficking.

The LBD contains a structure, formed by two lobes (S1 and S2) and a pocket specific for agonists binding. Therefore, this domain is critical for gating and activation responses to agonist binding (Traynelis et al., 2010).

The TMD is formed by three transmembrane helices, M1, M3 and M4, and a re-entrant loop, M2. The TMD of the four different ensembled GluN subunits constitute the pore of the ion channel that dictates the ion selectivity, permeability and blockade of the channel. This specific structure is determinant for the permeability of NMDAR to cations Na^+, K^+ and Ca^{2+}. In addition, it is blocked by Mg^{2+} depending on membrane potential. This domain is also involved in receptor trafficking (Kaniakova et al., 2012; Traynelis et al., 2010).

Lastly, the CTD is characterised by containing several motifs for binding intracellular proteins. These interactions play a crucial role in NMDAR post-translational modifications, trafficking, docking, conductance and gating. The CTD complex interactome and domain flexibility make it unable to resolve the crystallographic structure (Hayashi, 2021; Horak & Wenthold, 2009; Kennedy, 2018; Maki et al., 2012; Yong et al., 2021).

3.3. NMDAR activation

NMDAR activation requires the temporal coincidence of different factors. The NMDAR is a ligand-gated ion channel that requires specific membrane potential (voltage-dependency) conditions to be activated. Accordingly, NMDA receptors are known to

act as coincidence detectors of presynaptic activity (release of glutamate) and postsynaptic sustained activation (membrane depolarisation) (Figure 5).

Firstly, the co-agonists need to be released and bound to NMDAR subunits (glycine or D-Serine binding to GluN1, glutamate binding to GluN2 subunit) (Paoletti et al., 2013). However, the presence of co-agonists binding does not allow ion influx, since NMDAR pore is blocked by extracellular magnesium (Mg^{2+}) under resting membrane potential. The Mg^{2+} blockade is voltage-dependent and, to be unlocked, NMDAR requires postsynaptic depolarisation, which is mainly triggered by glutamate-induced AMPAR activation. Therefore, the NMDAR activation obligatorily needs the depolarisation of the postsynaptic terminal and the binding of the co-agonists to the receptor. NMDAR gating results in a conformational change of the LBD, in which the lobes S1 and S2 close around the ligand and prevents its dissociation (Dolino et al., 2016).

It is hypothesised that the co-agonists binding may trigger the movement of the TMD and LBD linkers. This movement would cause M3 segment rearrangement, resulting in the opening of the ion channel. Subsequently, Na^{+} and especially Ca^{2+} ions permeate through the channel pore, increasing their intracellular concentration and triggering several signalling cascades that modify the synaptic response and strength (Furukawa et al., 2005).

Calcium influx into the postsynaptic neuron plays a key role in several critical neuronal processes, such as changes in membrane excitability, synaptic transmission, and exocytosis, among others. Thus, NMDAR activity and the consequent calcium influx must be tightly regulated in order to properly maintain physiological functions, both in excitatory and inhibitory synapses (Bouvier et al., 2015; Sun et al., 2016). NMDAR are considered key actors in several physiological but also pathological conditions (Rebola et al., 2010).

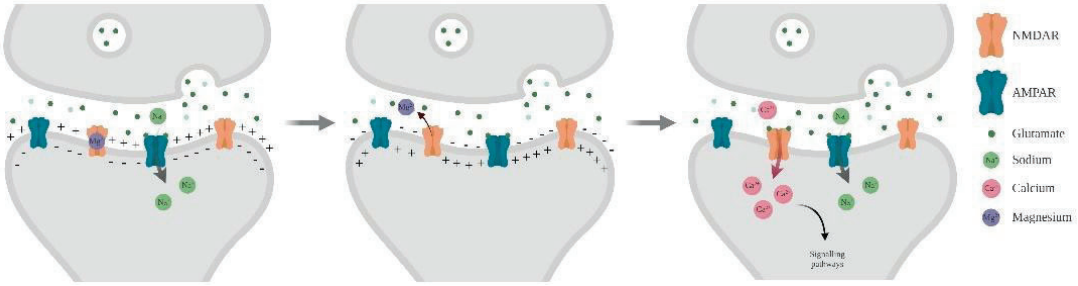

Figure 5. **Schematic simplification of NMDAR activation pathway.** After glutamate release from the presynaptic neuron to the synaptic cleft, AMPAR are activated, and a Na^+ influx depolarises the postsynaptic membrane. This depolarisation releases the Mg^{2+} blockade of the NMDAR, allowing their activation. A Ca^{2+} influx through NMDAR will activate different signalling pathways.

3.4. Pathophysiological role of NMDAR in neurological conditions

NMDAR function is tightly regulated, which is indicative of their relevance in neuronal function. Concomitantly, dysregulation of the NMDAR function has been related with several neurological disorders. Many neuropsychiatric disorders are linked to synaptic defects, also named synaptopathies, and NMDAR dysfunction. NMDAR hyperactivity is deleterious, given that excessive Ca^{2+} influx in the neuron leads to excitotoxicity and neuronal death (Bliss & Collingridge, 1993; Hardingham & Bading, 2010). Furthermore, NMDAR hypofunction is also linked to several CNS disorders. Therefore, both agonists and antagonists of NMDARs are considered potential CNS therapies.

3.4.1. Neuropathic pain

NMDA Receptors play a crucial role in the peripheral and central sensitisation mechanisms of neuropathic pain (Bliss et al., 2016; Liang et al., 2021). GluN2B-containing receptors have been reported to play an important role in the development of neuropathic pain in nerve injury models (Yi-Wen et al., 2021). Despite GluN2A subunit may also be involved in pain, their role is still controversial. However, Zinc (Zn^{2+}) binding to these subunits could be a fundamental molecular event in pain transmission and development (Nozaki et al., 2015).

Furthermore, preclinical and clinical studies have shown that NMDAR antagonists are effective in the reduction of pain besides their neuroprotective effect when administered

shortly after a traumatic brain injury or insults in animal models (Mony et al., 2009; Paoletti et al., 2013). Nevertheless, several and important side effects may appear after the administration of broad-spectrum antagonists, such as memory impairment or motor incoordination (Wu & Zhuo, 2009).

3.4.2. Neurodegenerative disorders

Chronically increased extracellular glutamate levels and overactivation of glutamate-mediating signalisation contribute to synapse loss and, consequently, neuronal dysfunction / death in several degenerative conditions, such as Alzheimer's Disease (AD), Parkinson's Disease (PD) and Huntington's Disease (HD).

In AD, amyloid-beta peptide accumulation is proposed to promote NMDAR-derived excitotoxicity. Accordingly, the low-affinity NMDAR uncompetitive antagonist memantine is clinically used for the treatment of moderate to severe AD patients, and also is used as a pro-cognitive treatment.

PD is a neurodegenerative disease with a histological hallmark of degenerating dopaminergic neurons in the substantia nigra, which results on dopamine depletion from the nigro-stratial pathway that overactivate the glutamatergic projections to striatum and basal ganglia. Accordingly, some NMDAR antagonists have been tested as possible treatments for PD. Despite these compounds showed beneficial antidyskinetic activity in some animal models, they are not devoid of important side-effects, including cognitive deficits, amnesia and dissociative effects (Mony et al., 2009; Nutt et al., 2008).

HD is characterised by specific GABAergic neuronal degeneration caused by the expression of mutant forms of the *huntingtin* gene. Some studies relate mutant forms of the huntingtin protein and NMDAR dysregulation, leading to excitotoxic damage and neuronal loss. Specifically, striatal GABAergic loss shows a selective enhancement of GluN2B-containing NMDAR currents (Zeron et al., 2002). Thus, early treatment with NMDAR antagonists, or more specifically GluN2B-selective antagonists, may become a therapeutic strategy for early stages of the disorder.

3.4.3. Depression

Different findings suggest a relationship between depression and NMDAR dysfunction. Depression is associated with various stressors, such as magnesium deficiency, inflammation or bioenergetic dysfunction. In addition, various NMDAR antagonists present antidepressant activity in humans and animal models, like ketamine, memantine or zinc (Adell, 2020; Jelen & Stone, 2021; Marsden, 2011). Recently, GluN2A-containing NMDAR have been identified as a promising target for development of novel depression therapies, limiting the side-effects observed when using broad-spectrum NDMAR antagonists (Wang et al., 2024).

3.4.4. Anxiety

Anxiety is a key component of the acute stress response to potential threatening situations. However, the persistence (chronicity) of anxiety, that may occur even in the absence of noxious situations, can result on neurological disorders. Dysregulation of NMDAR has been proposed as an underlying cause of this disorder, since the glutamatergic system is tightly related with fear-mediated learning and emotional processing of stressful events. Therefore, NMDAR dysregulation might cause misprocessing of the events, triggering an unnecessary defence response and contributing to anxiety (Bermudo-Soriano et al., 2012).

3.4.5. Autism Spectrum Disorders

Autism Spectrum Disorders (ASD) are clinically described as persistent in each of three areas of social communication and interaction. Genetic variants of several genes have been associated with ASD, and multiple ASD candidate genes converge on biological pathways related with glutamatergic synapse function and plasticity (https://gene.sfari.org/). Either a reduction or enhancement of NMDAR function has been linked with ASD, although the mechanisms remain unclear. The pathophysiological heterogeneity might result from the fact that NMDAR dysfunction may occur both at excitatory synapses on interneurons, decreasing the inhibitory input; but also in modulatory neurons related with other neurotransmitters signalling, having an influence in both excitatory and inhibitory neurons (E.-J. Lee et al., 2015; K. Lee et al., 2022, p. 202; Paoletti et al., 2013). In that sense, *GRIN* genes are considered high-susceptibility ASD genes (O'Roak et al., 2012; Tarabeux et al., 2011).

Patients harbouring *GRIN* mutations, including gain- and loss-of-function variants, frequently exhibit ASD traits (García-Recio et al., 2021). In line with the role of NMDAR in ASD, a recent study of anti-NMDAR autoimmune encephalitis supported the relation between NMDAR hypofunction and ASD (Gibson et al., 2019).

3.4.6. Cognitive impairment and ageing

Ageing and an impairment in the memory and cognitive functions are generally linked to a synaptic plasticity impairment. NMDAR function is key in synaptic plasticity mechanisms, underlying learning and memory processes. Functional alterations of NMDAR have been observed in aged animals, specifically with a particular reduction of specific NMDAR subunits expression. For instance, a decrease in GluN2B-containing NMDAR correlates with an impairment in learning and LTP formation in rats (Clayton et al., 2002). In a consistent manner, the overexpression of GluN2B in mice show an enhancement of LTP and superior learning and memory functions, including individuals at senile stages (Paoletti et al., 2013). Hence, a potentiation treatment could be helpful to save the cognitive impairment related to ageing and other conditions coursing with a decrease in NMDAR function.

3.4.7. Epilepsy

Epileptic seizures can be triggered by glutamate-mediated neuronal hyperexcitation and the resulting overactivation of NMDARs and AMPARs, which represent major clinical targets in epilepsy research. Irregular activity of both receptors may be a cause of seizure disorders. Specifically for NMDAR, seizures occur both in hypo- and hyper-functionality of the receptor. Hyperfunctionality correlates with continuous and generalized epilepsies, while hypofunctional NMDAR are related with focal seizures (Ghasemi & Schachter, 2011; Hanada, 2020). In line with this, recent genetic studies reported the association between *GRIN* genetic variants and epilepsy (García-Recio et al., 2021; Gjerulfsen et al., 2024; Reutlinger et al., 2010). Additionally, anti-NMDAR autoimmune encephalitis has also been related with epilepsy (Husari & Dubey, 2019). Therefore, molecules regulating NMDAR function (both increasing or decreasing NMDAR activity), may be potential therapies for antiepileptic drugs (AED) refractory patients.

3.4.8. Schizophrenia

Schizophrenia is a multifactorial psychiatric disorder, characterised by positive symptoms (hallucinations, delusions or aberrant motor behaviour), negative symptoms (social and emotional alterations), and cognitive impairment. Negative and cognitive symptoms have been adscribed to NMDAR hypofunction. In fact, NMDAR blockers administration (i.e. phencyclidine (PCP), ketamine) in neurotypical individuals can trigger psychotic and negative symptoms, along with cognitive impairment, mimicking schizophrenia symptoms. Moreover, when used in schizophrenic patients, the symptoms were exacerbated (Adell, 2020). Additionally, MK-801 administration (non reversible uncompetitive NMDAR antagonist) is widely used as a pharmacological model of schizophrenia, mimicking both positive and negative symptoms of schizophrenia (sociability alterations, motor disturbance, anxiety behaviours) (Rung et al., 2005). Besides pharmacological interventions, *GRIN* variants have been associated with schizophrenia onset (Tarabeux et al., 2011) and anti-NMDAR autoimmune encephalitis is widely reported as an immune trigger of acute schizophrenia (Kayser & Dalmau, 2016).

Therefore, NMDAR agonists or activity potentiators could be suitable treatments for schizophrenia. Specifically, the activity of GluN2A-containing NMDAR seems to be essential for the excitatory-inhibitory circuits in schizophrenia patients. Consequently, GluN2A-selective potentiators could be potential therapies (Paoletti et al., 2013).

3.4.9. Autoimmune anti-NMDAR encephalitis

Autoimmune anti-NMDAR encephalitis is associated with severe neurological and psychiatric symptoms (Dalmau et al., 2008, 2019; Kayser & Dalmau, 2016). Mechanistically, the presence of anti-NMDAR antibodies (specifically anti-GluN1 auto-antibodies) cause the internalisation of surface NMDAR, resulting in a decrease of the receptor surface density and, therefore, a decrease in NMDAR activity (Hughes et al., 2010; Planagumà et al., 2016). Recent works support the use of NMDAR potentiators (e.g. SGE-301) as a second line for the treatment of the long-lasting alterations in the post-acute phase of the disease (Mannara et al., 2020; Maudes et al., 2024; Radosevic et al., 2022).

3.4.10. GRIN-Related Disorders

Recently, an association between *GRIN* variants and neurodevelopmental disorders has been identified (Benke et al., 2021; Camp et al., 2023; Chen et al., 2017; Endele et al., 2010; Hu et al., 2016; Reutlinger et al., 2010). Pathogenic mutations in *GRIN* genes directly disrupt the NMDAR function, contributing to the onset of several neuronal conditions. Below we will describe thoroughly some of the findings related to this group of diseases.

4. GRIN-related disorders

GRIN-related disorders (GRD, also called "GRINpathies") refer to a novel group of rare inherited neurodevelopmental disorders caused by the presence of disease-causing *GRIN* genes variants. These mutations occur *de novo* and have an autosomal dominant inheritance pattern. Accordingly, the majority of GRD patients only present one affected *GRIN* allele with a dominant negative effect on NMDAR function, ultimately resulting on disease-associated clinical spectrum.

Nowadays, the number of diagnosed and referred GRD cases is ~650 patients worldwide, although this would represent a strong underestimation. Indeed, considering the incidence of *GRIN1*, *GRIN2A* and *GRIN2B* variants in ASD (https://gene.sfari.org/database/ gene-scoring/) and in idiopathic paediatric epilepsy (~5,000 European patients harbouring a *GRIN* variant), the estimated prevalence of GRD is ~2:10,000 births, resulting on a predicted >1 million GRD patients worldwide (Lemke, 2020).

The first association between *GRIN* mutations and neurodevelopmental phenotypes was described in 2010 by Endele et al., 2010.

4.1. GRIN variants and disease association

Genetic variants of *GRIN* genes are scattered along the exons ensemble. However, the genetic vulnerability or tolerance (disease association or polymorphism) to missense variants differs on a gene-, domain- and residue-dependent manner, as revealed by a recent work conducted by our team on the analysis of more than 4000 missense *GRIN* variants (García-Recio et al., 2021). Pathogenic mutations in *GRIN* genes are mostly affecting *GRIN1, GRIN2A* and *GRIN2B* genes (around 18% of the variants are disease-associated) (Figure 6). In addition, the variants are mainly concentrated in the LBD and

TMD. In contrast, about 95% of reported missense variants in *GRIN2C, GRIN2D, GRIN3A* and *GRIN3B* are neutral, and homogeneously distributed across all domains (García-Recio et al., 2021)

The mapping of *GRIN* variants pathogenicity is extensive, but the functional annotation of the pathogenic *GRIN* variants is still incomplete. The annotation of the variants allows their classification into loss-of-function and gain-of-function. In the context of GRD patients, this annotation is essential towards their stratification and to allow personalised medicine, enhancing or attenuating the receptors' function or focusing on subunit specificity.

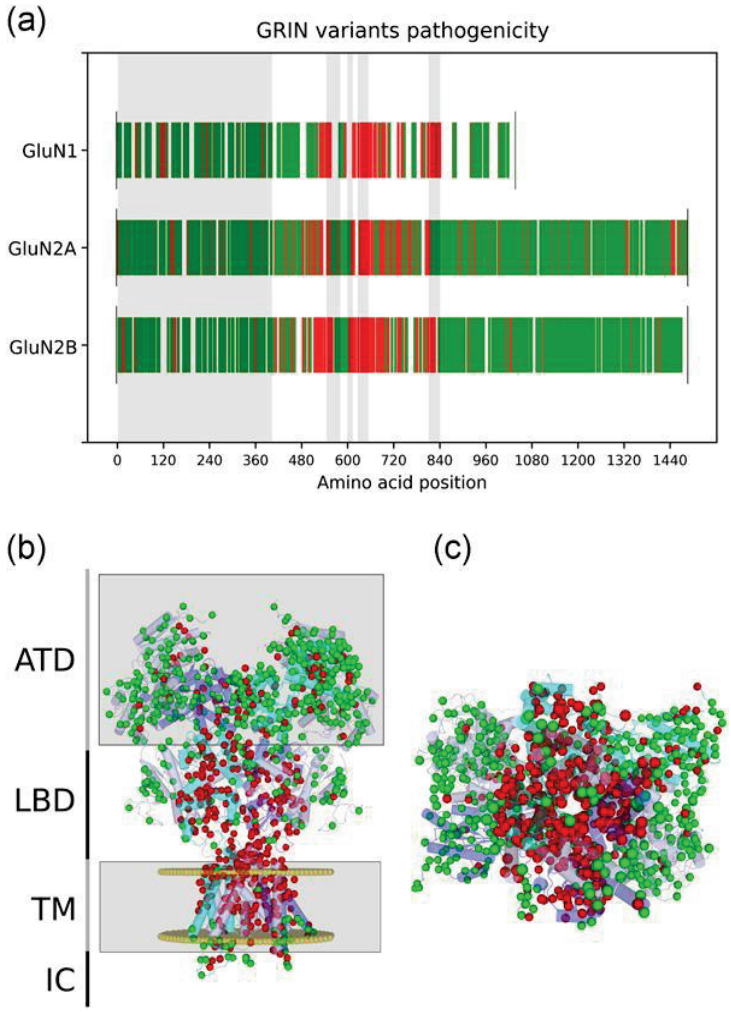

Figure 6. GRIN variants pathogenicity. A. Scatter plot representing *GRIN1*, *GRIN2A*, and *GRIN2B* variants' disease association and distribution along the *GluN1*, *GluN2A*, and *GluN2B* protein sequence. Spikes undefined colour code: disease-associated *GRIN* variants in red; not associated with disease in green; no reported variant in white. Juxtaposed topological domains are represented in alternate colours (amino-terminal domain [ATD], M1,M2, M3, and M4 highlighted in grey) and the protein termination with a black spike. B. *GRIN1*, *GRIN2A*, and

GRIN2B variants pathogenicity mapped on the structural model of the trihetromeric (GluN1)2-GluN2A/GluN2B NMDA receptor. Lateral view of the structural model of the NMDAR, composed of two GluN1 (pale blue), one GluN2A (cyan), and one GluN2B (purple) subunits. Note the high density of disease-associated *GRIN* variants in the ligand-binding domain (LBD) and transmembrane domain (TMD). (c) Molecularmodel of the N-methyl-D-aspartate receptor (cytosolic side view). The pore channel and the GluN subunit interfaces are highly pathogenic. A position is considered as associated with disease (in red) if at least one disease-associated mutation is found. Neutral variants (in green) are those not reported as disease-associated; TM, transmembrane. From García-Recio et al. 2020.

4.2. GRD Clinical spectrum

The available clinical information, along with the GRIN database (GRINdb, García-Recio et al., 2021) and the growing number of research articles describing genotype-phenotype association in GRD individuals (Benke et al., 2021; Burnashev & Szepetowski, 2015; De Ligt et al., 2012; Endele et al., 2010; Epi4K Consortium & Epilepsy Phenome/Genome Project, 2013; Freunscht et al., 2013; Gjerulfsen et al., 2024; Hamdan et al., 2011; Hu et al., 2016; Kellner et al., 2021; Kenny et al., 2014; Lemke et al., 2014; Mielnik et al., 2021; R. A. Myers et al., 2011; S. J. Myers et al., 2019; O'Roak et al., 2012; Pierson et al., 2014; Platzer et al., 2017; Platzer & Lemke, 2018; Reutlinger et al., 2010; Santos-Gómez, Miguez-Cabello, García-Recio, et al., 2021; Santos-Gómez, Miguez-Cabello, Juliá-Palacios, et al., 2021; Soto et al., 2019; Strehlow et al., 2016; Tarabeux et al., 2011), allowed the identification of GRD clinical spectrum, with the variable presence and severity of the following symptoms: intellectual disability, developmental delay, schizophrenia, autism spectrum disorder (ASD) traits, epilepsy, attention-deficit and hyperactivity disorder (ADHD), hypotonia, movement disorders, hypotonia, cortical visual impairment and microcephaly. As aforementioned, the severity is variable and this is particularly relevant regarding intellectual severity (from moderate to severe), verbal communication (absent, poor, moderate), motor function and epilepsy manifestations. Regarding the latter, GRD individuals can exhibit (or not) different epileptic syndromes, such as epilepsy with continuous spike and wave during sleep, benign childhood epilepsy with centro-temporal spikes, Landau-Kleffner syndrome of childhood, focal epilepsy and discrete epileptic seizures (Carvill et al., 2013; Conroy et al., 2014; DeVries & Patel, 2013; Dimassi et al., 2014; Lemke et al., 2013; Lesca et al., 2012, 2013).

The clinical spectrum is indicative that, despite being autosomal dominant, the different *GRIN* variants are provoking a spectrum of NMDAR functional effects dictated by the affected gene identity, the structural domain alterations, the mutated residue, that can affect NMDAR biogenesis and/or biophysical properties. GRD result from the disturbed functionality of the mutant NMDARs which, as for other channelopathies, are roughly classified into those variants that provoke either a gain-of-function (GoF) or a loss-of-function (LoF). In that sense, several efforts have been focused to delineate the relationship between *GRIN* genetic variants and their functional outcomes (NMDAR-mediated currents in receptors containing *GRIN* variants). To merge all the available information, our group created the "GRIN database" GRINdb (https://alf06.uab.es/grindb/home), which is a unified, non-redundant curated database that offers all the available information of the described *GRIN* variants. Besides automatically collecting *GRIN* variants, GRIN database provides a manual curation of GRIN variants-associated data and stratification (e.g. gain/loss-of-function) upon functional annotation availability (García-Recio et al., 2021).

This database has provided valuable information in terms of vulnerable/resilient NMDAR structural domains, as well as regarding the functional outcomes. In general, there is a higher number of LoF annotated variants compared with GoF variants. The compilation of *GRIN* variants-associated clinical phenotypes aimed at defining the clinical range of GRDs and investigating potential genotype- and domain-specific clinical symptoms. The analysis revealed that *GRIN1* pathogenic variants are clinically manifested by Intellectual Disability (ID) (82%), Developmental Delay (DD) (71%) and epilepsy (57%). *GRIN2A* variants are highly associated with epilepsy (89%), ID and DD (variable depending on functional annotation). *GRIN2B* disease-associated mutations are almost invariably associated with ID (93%) and DD (68%), with variable occurrence of epilepsy (47%). The phenotypic data was summarised in García-Recio et al., 2021 and is displayed in Table 2.

	GRIN1			*GRIN2A*			*GRIN2B*		
	GoF	LoF	Total	GoF	LoF	Total	GoF	LoF	Total
Reported phenotypes	7	16	56	18	26	99	12	40	91
Autism spectrum disorder	0	6% (1)	18% (10)	0	4% (1)	6% (6)	0	40% (16)	29% (26)
Cortical visual impairment	57% (4)	19% (3)	25% (14)	0	0	0	42% (5)	3% (1)	7% (6)
Developmental delay	86% (6)	81% (13)	71% (40)	83% (15)	46% (12)	38% (38)	100% (12)	75% (30)	68% (62)
Epilepsy (ECSWS, FE, BECTS, LKS)	57% (4)	56% (9)	57% (32)	83% (15)	100% (26)	89% (88)	83% (10)	40% (16)	47% (43)
Hypotonia	43% (3)	38% (6)	30% (17)	11% (2)	4% (1)	3% (3)	8% (1)	38% (15)	21% (19)
Intellectual disability	71% (5)	100% (16)	82% (46)	89% (16)	46% (12)	49% (49)	100% (12)	100% (40)	93% (85)
Microcephaly	0	6% (1)	4% (2)	0	0	1% (1)	50% (6)	8% (3)	14% (13)
Movement disorder	0	31% (5)	13% (7)	6% (1)	0	1% (1)	0	13% (5)	9% (8)
Schizophrenia	0	0	5% (3)	0	0	4% (4)	0	5% (2)	5% (5)
Speech disorder	0	19% (3)	7% (4)	50% (9)	73% (19)	57% (56)	0	0	0

Table 2. Clinical phenotypes of disease-associated *GRIN1*, *GRIN2A* and *GRIN2B* variants. From Garcia-Recio et al 2020.

Beyond the presence of primary CNS-related symptoms, GRD individuals also exhibit systemic alterations, with ongoing natural history delineation. Recently, and prompted by the feedback from GRD patients' families, our group was exploring in collaboration with an international consortium the gastrointestinal (GI) function and related symptoms (sleep alterations, visceral pain) in GRD children. To this end, a GI distress evaluation survey was filled by the parents of GRD children, revealing the presence of gastrointestinal distress and sleep alterations associated with *GRIN* pathogenic mutations (unpublished data, Figure 7).

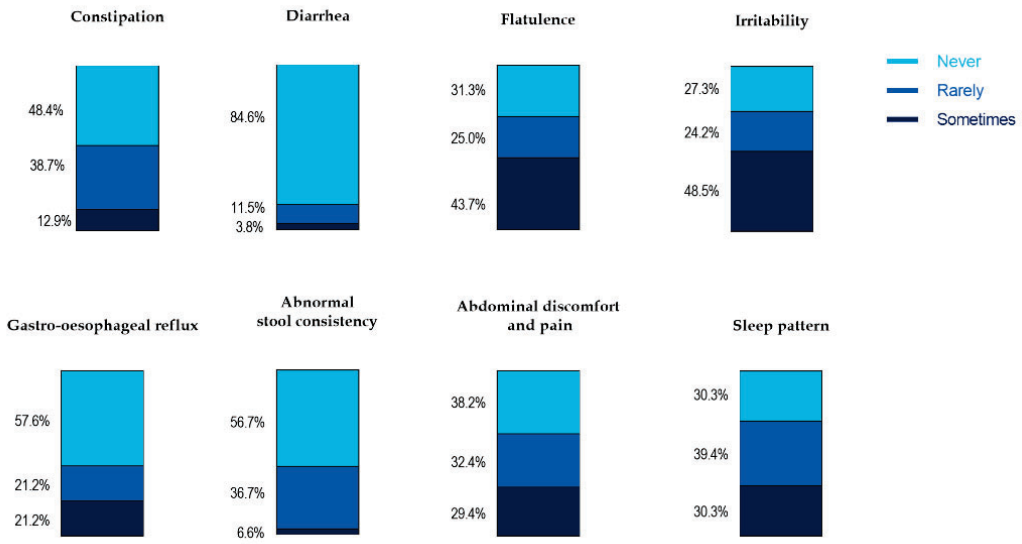

Figure 7. Representation of relevant results from patients' survey of a variety of symptoms. Some of the most relevant phenotypes related with systemic alterations. "Never" events are represented in light blue, "Rarely" events in blue and "Sometimes" in dark blue. Unpublished data.

4.3. GRD treatment and research

GRD is a novel group of developmental encephalopathies and, despite the NMDAR has been the target of extensive pharmacological research, currently the therapeutic weapons are very scarce. Indeed, treatment of GRD is facing several hurdles: *i)* GRD has been recently identified, and the pathophysiological mechanisms (related with GoF, LoF GRIN variants) are still currently under investigation; *ii)* GRD is a rare condition and, despite the NMDAR dysfunction has a severe health burden and can be a converging factor in CNS disorders, the low prevalence of GRD is limiting the interest of the pharmacological industry; *iii)* GRIN variants result on several functional effects on NMDARs (GoF, LoF) and different strategies (personalised medicine) are required for their treatment; *iv)* the preclinical models and assays are under development; *v)* the usage of broad-range NMDAR modulators is not devoid of side-effects.

Despite all these difficulties, the translational initiatives are investigating novel personalised therapies for GRD, with some important advances. In relation with GRIN-

LoF patients' treatment, the strategy is focusing on the treatment with NMDAR activity enhancers. Currently, there is only one treatment consisting of L-Serine administration for LoF GRD patients (Den Hollander et al., 2023; Juliá-Palacios et al., 2024; Krey et al., 2022; Soto et al., 2019). L-serine treatment results in an improvement of the communication, sociability and motor performance of GRD-LoF patients, while being well tolerated. Despite these benefits in GRD-LoF patients, the amelioration is limited and additional therapeutic options are required, and are currently investigated. Regarding the treatment of GRD-GoF patients, the strategy is focused on the reduction of NMDAR activity. In that line, initial studies were performed with the non-competitive NMDAR antagonist memantine, but the benefits were very limited (Platzer et al., 2017). More recently, Radiprodil -a selective GluN2B negative allosteric modulator (NAM)- has shown promising effects (Bertocchi et al., 2024). Indeed, GRIN Therapeutics Inc., is currently enrolling in Europe for a clinical trial and performing one in the United States to verify the therapeutic advantages of Radiprodil in GoF GRD patients (https://grintherapeutics.com/). Recent results of the Radiprodil phase 1B clinical trial showed a reduction in seizures present in GRD-GoF patients. Of the 15 patients enrolled, eight experienced regular seizures before the trial. After Radiprodil treatment, the seizures were reported to be reduced by a median of 86%. In addition, the potential treatment also led to clinical improvements in other symptoms. It was well tolerated by the patients from a safety perspective (GRIN Therapeutics, 2024).

However, there is a current need for further annotations of GRD pathogenic variants for better stratification, but also a need for GRD models to identify and characterise novel GRD potential therapies. Currently, there are some cellular models, mice models and zebrafish models available.

4.3.1. Cellular studies for GRD research

The most extended method used to study *GRIN* variants pathogenicity, pathophysiological mechanisms and to investigate potential treatments, is based on the use of the heterologous expression in cellular systems. Briefly, recombinant DNA encoding GluN subunits are genetically-edited and transfected in mammalian cell lines, in neuronal primary cultures or in *Xenopus laevis* oocytes to study the impact of mutant GRIN genes on NMDAR functions. This methodology is employed to study NMDAR protein stability, assembling, trafficking as well as to analyze the electrophysiological properties of the mutant NMDAR (co-agonists affinities, channel conductance, kinetics,

modulatory effects of Mg^{2+}, Zn^{2+}, protons, etc.), allowing the functional stratification of GRIN variants, which is necessary to define a personalized treatment (J. Li et al., 2019; S. J. Myers et al., 2023; Santos-Gómez, Miguez-Cabello, García-Recio, et al., 2021, 2021; Soto et al., 2019; XiangWei et al., 2018; Xu et al., 2024). The obtained information is extremely important to determine the nature of the mutation and, potentially, to preclinically evaluate and/or to treat the GRD patient with an adapted NMDAR modulator to rescue NMDAR function.

4.3.2. Animal models for disease understanding

Animal models are valuable tools for unveiling disease pathophysiological mechanisms studies and, importantly, for the evaluation of novel therapeutic strategies. Since NMDAR dysregulation is a key factor in several CNS diseases, several efforts have been focused on the generation of NMDAR dysfunction models and the exploration of therapeutic strategies.

4.3.2.1. GRD murine models

The generation of a full *Grin1*$^{-/-}$ knockout mouse model was initially attempted. Nevertheless, *Grin1*$^{-/-}$ mice pups presented neonatal lethality. This mortality suggested that early development depends on the GluN1 subunit (Forrest et al., 1994). Concurrent with this groundbreaking investigation, a *Grin1* knockdown (KD) was generated. In this model, GluN1 subunit levels were around 5-10% of wildtype GluN1 expression levels (Mohn et al., 1999). The latest has been widely used to study *Grin1* LoF.

Grin1 KD mice have some phenotypical characteristic traits, such as small size during early developmental stages, hyperlocomotion, self-injury behaviour, stereotypies, decreased anxiety behaviour, impaired social interactions or cognitive impairment. In some studies, fertility problems have also been reported. Moreover, synaptic alterations and brain metabolism disruption have been also observed (Duncan et al., 2002, 2004; Dzirasa et al., 2009; Halene et al., 2009; Lipina et al., 2022; Mohn et al., 1999; Moy et al., 2006; Ramsey et al., 2011). In the context of GRD, some knock-in mouse models have been recently generated and/or are currently under development (Sullivan et al., 2024; Umemori et al., 2013).

Regarding *Grin2a* models, a constitutive *Grin2a*$^{-/-}$ knockout mouse model was successfully generated in the 90's (Ito et al., 1997). The main phenotypes identified in

this Grin2a-LoF model were related with hyperlocomotion, memory alterations, impaired learning functions, attention deficits, anxiety-like behaviours, reduced depressive-like behaviours, communication impairment and sleep disturbances. At the cellular level, impaired hippocampal long-term potentiation and dendritic changes were also reported (Bannerman et al., 2008; Boyce-Rustay & Holmes, 2006; Brigman et al., 2008; Ito et al., 1997; Kannangara et al., 2014, 2015; Kiyama et al., 1998; Miyamoto et al., 2001; Salmi et al., 2019). Similarly to *Grin1*, different *Grin2a* knock-in models of some disease-associated genetic variants have been recently generated, showing phenotypes that recapitulate particular symptoms of GRD patients (Amador et al., 2020; Zhao et al., 2023).

Finally, a constitutive full *Grin2b*$^{-/-}$ knockout has been successfully generated. However, this full knockout has been reported to be perinatally lethal due to lack of suckling reflex (Kutsuwada et al., 1996). Nevertheless, heterozygous *Grin2b*$^{+/-}$ mice are viable and exhibit reduced NMDAR-mediated EPSCs and LTP alterations. From a behavioural point of view, *Grin2b*$^{+/-}$ mice models present sensorimotor gating alterations (Ito et al., 1997). Additionally, conditional KO-*Grin2b* mouse models towards deletion of protein expression in specific brain regions have been generated. Deletion of GluN2B expression in the forebrain results in hyperactivity, memory impairment, visual alterations and reduced anxiety-like phenotype (Von Engelhardt et al., 2008). Knock-in models with *Grin2b* mutations have been generated, showing similar results to the knockout model and mimicking GRD-associated behavioural alterations (Farsi et al., 2023; Shin et al., 2020).

4.3.2.2. Zebrafish as a model to study NMDAR

All the aforementioned characteristics make the zebrafish a very suitable model for the study of developmental conditions (J. R. Goldsmith & Jobin, 2012), including neurodevelopmental conditions such as GRIN-related disorders.

Zebrafish (*Danio rerio*) is an excellent model organism for studying the growth of neurons and the function of neurotransmitter receptors in the formation of neuronal circuitry. Among several advantages (discussed in previous sections), the *ex-utero* development and transparency of the embryos are key. Thus, *Danio rerio* has been, and currently still is, a useful model for performing vertebrate nervous system studies (Chandrasekhar et al., 1997; Chitnis & Kuwada, 1990; Collier et al., 2023; Doszyn et al.,

2024; Hashimoto & Hibi, 2012; Hibi & Shimizu, 2012; Kimmel et al., 1995; Lewis & Eisen, 2003; Lu et al., 2021; McLean & Fetcho, 2008; Saint-Amant, 2010; Schweitzer & Driever, 2009; Zada et al., 2024). Subsequently, the glutamate circuit has been considerably studied in this model (Borghuis et al., 2014; Higashijima et al., 2004; Martin et al., 1998; Marvin et al., 2013; Swain et al., 2004). However, the knowledge around NMDAR is still limited.

An ancestor of teleost fishes experienced a whole-genome duplication, which has been implicated in the evolution of teleost fishes, and Zebrafish are not an exception (Glasauer & Neuhauss, 2014). By PCR cloning techniques, it was described that the genes codifying for all the NMDAR subunits are duplicated in the zebrafish genome (Cox et al., 2005).

The different GluN subunit sequences are highly conserved across zebrafish and humans (Cox et al., 2005, Figure 8A). The two zebrafish GluN1 subunits share approximately a 90% of the human protein. The region containing the four transmembrane domains, and therefore forming the ionic pore of the channel, as well as the Mg^{++} biding domain, are the most conserved (Figure 8B). These regions are also highly conserved in the subunits GluN2A-D. This high conservation argues that there is a low tolerance even for conserved amino acid changes in these regions. This supports the idea that, mutations in these regions tend to be pathogenic. The N-terminal region is more divergent, but still shares more than 60% of the amino acid sequence. The C-terminal tail diverges in the different subunits, with substantial changes in their length.

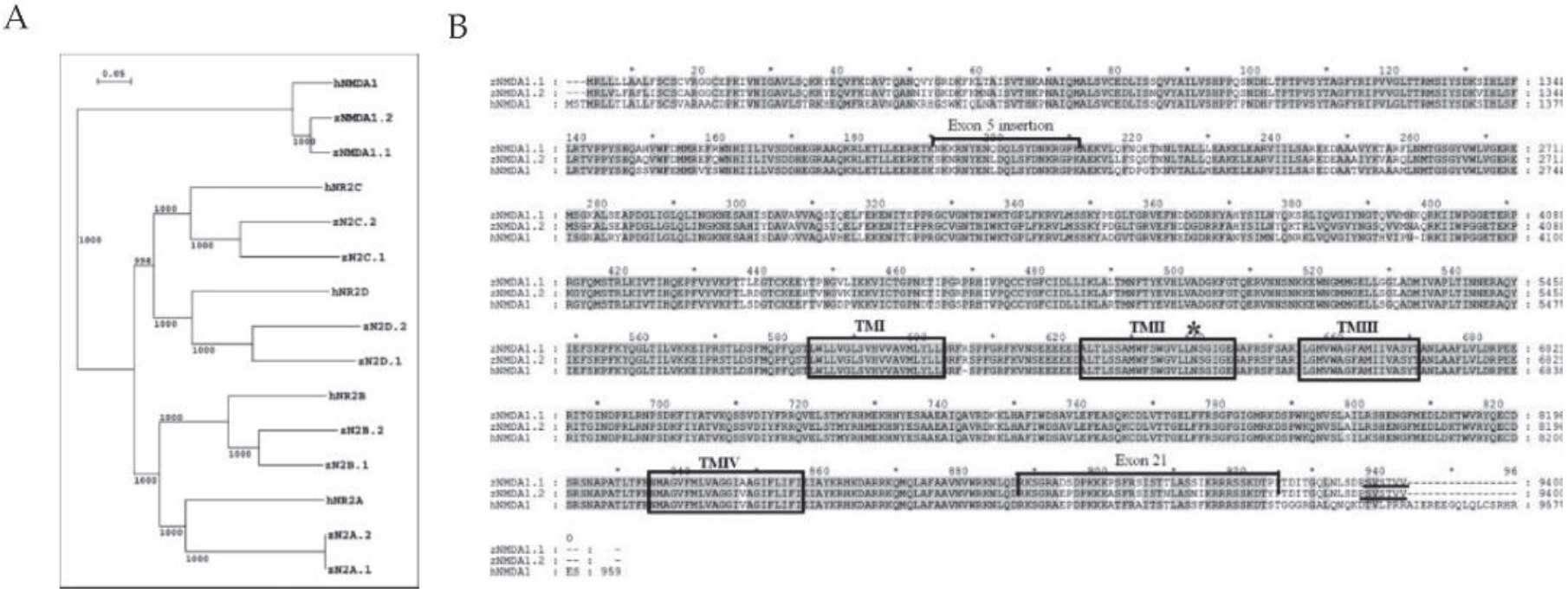

Figure 8. Genetic conservation of zebrafish NMDA subunits compared to human NMDA (hNMDA) subunits. A. Phylogenetic tree of zebrafish and human NMDAR. This tree was generated using Clustal X and was based on the multiple alignment output of all 10 full-length zebrafish proteins and five hu-man subunits, with the tree calculated and bootstrapped using the neighbor-joining method. The numbers at the branch points are the bootstrap values from 1,000 iterations. B. Protein alignment for the most common NMDAR1 splice variant from zebrafish (zNMDA-1.1 and zNMDA-1.2) and human (hNMDA-1). Adapted from Cox. J., et al. 2005.

In addition, it has been reported that all the NMDAR subunits are expressed in the zebrafish during the development (Cox et al., 2005; Zoodsma et al., 2020, 2022).

Regarding the behavioural studies in zebrafish, Zoodsma et al. generated *grin1* zebrafish models, knocking out both paralogs of the zebrafish *grin1a* and *grin1b*. Surprisingly, complete knockout larvae were able to survive through early development, with a mortality observed around 10dpf. Furthermore, these larvae lacking NMDAR were able to initiate a variety of behaviours, like burst swimming, responses to visual and acoustic stimuli or prey-capture. However, these larvae presented deficits in these stimuli when compared to wild-type animals.

Nevertheless, the NMDAR studies in zebrafish are still scarce. Regarding the zebrafish advantages in genetic modelling but also in pharmacological screening, further exploration is needed to use *Danio rerio* as a suitable animal model for pharmacological discovery.

Hypothesis and Objectives

GRIN-related disorders is a group of rare developmental encephalopathies reported less than ten years ago. Given the recent identification of this genetic condition, the understanding of GRD pathophysiological mechanisms is still scarce and there are few therapeutic options under evaluation. Therefore, there is an urgent need to generate GRD animal models to both unravel the pathophysiological mechanisms, but also to generate research tools that allow identifying personalised therapeutic strategies.

This Thesis is based on the hypothesis that the generation and deep phenotypic characterization of zebrafish genetic GRD models will provide valuable insights on the pathophysiology of GRD and will allow the *in vivo* high-throughput pharmacological screening of potential candidates for GRD precision treatment.

The overarching goal of this PhD project is to generate GRD zebrafish models and to identify the associated endophenotypes for their correction using pharmacological approaches. These biological models and the readouts will represent an innovative and efficient tool to study GRD which, in turn, will enable high throughput pharmacological screening of potential personalised therapeutic strategies. Overall, this project will contribute to defining GRD pathophysiology, to identify novel therapeutic targets and to evaluate personalised pharmacotherapies for GRD.

In order to tackle this objective, and in line with the current translational research on GRIN-related disorders performed by our team, the following objectives have been defined for the **principal project**:

- **Zebra-GRIN**: generation of an *in vivo* library of GRD models. Genome editing tools will be used to modify *Grin* genes in Zebrafish and to develop *Grin* models, duplicating the situation observed in GRD individuals. Based on *GRIN* gene variants prevalently associated with GRD, GRIN1, GRIN2A and GRIN2B paralogous genes have been selected.

- **Pheno-GRIN**: Comprehensive phenotyping of Zebra-GRIN models will allow defining GRD-like alterations that will be further used in pharmacological assays. Together with the identification of CNS-related endophenotypes, novel methods will be developed towards the study of potential GRD-associated non-neurologic phenotypes.

- **Pharma-GRIN**: evaluation of the therapeutic efficacy of NMDAR allosteric modulators to correct the identified endophenotypes of Zebra-GRIN models.

This evaluation will be performed together with toxicity assays of the evaluated drugs.

GRD is a clinical spectrum frequently associated with epilepsy and, interestingly, along this Thesis we identified the presence of convulsant phenotypes in the generated Zebra-GRIN models. Indeed, similar epilepsy phenotypes have been described both in patients and in genetic models of genes playing a crucial role in the glutamatergic synapse. Therefore, a **secondary project** has been performed in parallel to the main objective of this thesis project to advance the modelling of epilepsy in zebrafish larvae. Additionally, this project is closely aligned to address a growing demand from customers and associates of the hosting company ZeClinics.

This complementary project consisted on the generation and refinement of a new gene editing tool that will allow the evaluation of the epileptic phenotype of different genes related with paediatric epilepsies in CRISPANTS, highly penetrant F0 knockouts generated using the CRISPR technology. In addition, a fast screening of potential anti-epileptic drugs will be performed in those CRISPANTS presenting an evident epileptic phenotype. Based on the functional convergence of those genes in the regulation of the glutamatergic synapse, we hypothesised that those compounds able to rescue particular gene-associated epilepsies could potentially mitigate the epileptic phenotypes observed in ZebraGRIN models.

In order to tackle this secondary project, the following objectives were defined the following objectives:

- **Design and characterization of CRISPANTS**: design of the strategy and the new genetic tools to generate an *in vivo* CRISPANT zebrafish models library. This library will consist of a selection of genes strongly associated with paediatric epilepsy, and their further phenotypic assessment.
- **Pharmacological screening of anti-epileptic drugs**: evaluation of the anti-epileptic effect of different pharmacological candidates using epilepsy-manifesting CRISPANTS.

Materials and Methods

Chapter 1: Generation of *GRIN*-related disorders models and deep endophenotypic evaluation

1. Zebrafish husbandry and breeding

Zebrafish are grown in an animal facility specially designed and ensuring the optimal conditions for animal health and the correct development and growth of the animals. The main system where the different used fish lines are maintained is a water system with a constant temperature of 27.5 ± 1ºC, an optimal pH of 7.5 ± 0.5 and a conductivity between 600-900µS. The entire facility follows a 14:10 hours light:dark cycle, with progressive light ramps of 1h at both the beginning and end of the daylight hours (Westerfield, 2000).

During daylight hours, fish receive three feedings. The given food is selected depending on the developmental stage of each fish tank, following the guideline:

- Zebrafish larvae, from their entrance in the facility at 5 dpf to 15 dpf, are fed with commercial fine powdered breeding food with zooplankton (18% krill) and phytoplankton (51% spirulina) (sera Micron Nature, #00720, SAP-Mat.-Nº: 45474)
- Zebrafish juveniles, from 16 dpf to 30 dpf, are fed with a 1:1 mixture of the abovementioned breeding food and Zebrafeed <100µm (Sparos I&D), that consists of premium quality granulated food with a balanced composition, specific for zebrafish breeding.
- Zebrafish adults, from 30 dpf onwards, are fed with different size Zebrafeed mixtures according to the manufacturer's recommendation. In addition, adult zebrafish are also fed with artemia, promoting their motivation and promoting their prey-capture mechanisms. From 30 dpf to 45 dpf, zebrafish were fed with Zebrafeed <100µm; from 45 dpf to 60 dpf, with Zebrafeed 100-200µm; from 60 dpf to 90 dpf, with Zebrafeed 200-400µm; and from 90 dpf onwards, with Zebrafeed 400-600µm.

For breeding, adult zebrafish are placed in mating tanks, either spawning or in pairs depending on the experimental needs. A thin net in the lower part of the tanks allows

the laid eggs to safely pass through, protecting them from their progenitors until collected. The mating crosses are set up after the last feeding, and the resulting eggs are collected the following day, two to four hours from the artificial dawn.

The eggs are collected with in-house prepared embryo solution (E3 1X, prepared of MilliQ distilled water, 5mM NaCl (Sigma-Aldrich, Cas #: 7647-14-5), 0.17mM KCl (Sigma-Aldrich, Cas #: 7447-40-7), 0.33mM $CaCl_2 \cdot 2H_2O$ (Sigma-Aldrich, Cas #: 10035-04-8), 0.33mM $MgSO_4 \cdot 7H_2O$ (PanReac AppliChem, Cas #: 10034-99-8), 0.1% w/v methylene blue (Supelco, Cas #: 60-56-0); pH 7.2 ± 0.2) (Westerfield, 2000)and maintained in petri dishes (Fisher Scientific, Cat #: 11309283) in a specialised incubator (Memmert, Peltier IPP110ecoplus) at 28 ± 1ºC with a 14:10 hours light:dark cycle, mimicking the light conditions in the animal facility. Approximately 4-6 hours after collection, the fertility of the collected eggs is assessed. Batches with less than 80% fertilisation are discarded. The embryos are plated at a density of 100-150 embryos per plate to allow for proper embryo development. Plates are cleaned every day, removing dead embryos and changing the media with fresh embryo solution. At 5 dpf, total mortality and aberrant phenotypes are annotated in order to evaluate the quality of the embryo batch. Criteria of exclusion include ≥20% mortality and ≥10% abnormal phenotypes. Most behavioural experiments along this thesis are performed with 5 dpf larvae, except for gastrointestinal evaluation experiments, where 7 dpf to 8 dpf larvae are used. Shortly after each experiment, unless otherwise stated, the larvae are ethically euthanised, following the appropriate guidelines.

2. Whole mount *in situ* hybridisation (WISH)

The *in situ* hybridization (ISH) is a technique that allows for precise localization of a specific segment of nucleic acid within a histologic section or using the whole larvae in our specific case of zebrafish (whole mount). It is considered a qualitative technique, given the intensity of the signal depends mostly on the exposure time rather than the quantity of detected nucleic acids. The underlying basis of ISH is that nucleic acids, if preserved adequately within a histologic specimen, can be detected through the application of a complementary strand of nucleic acid to which a reporter molecule is attached (Figure 9).

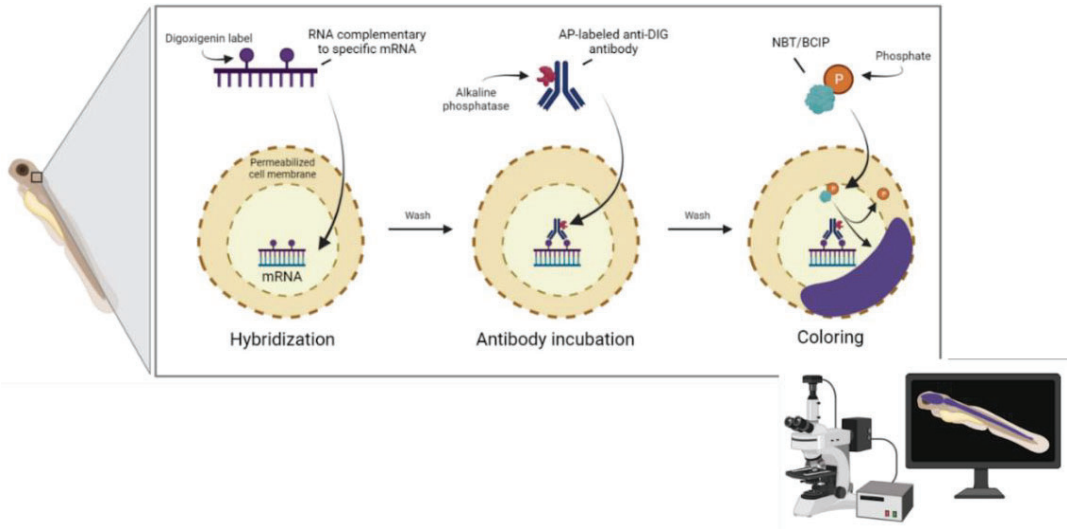

Figure 9. Schematic representation of the *in situ* hybridization protocol. Generated with BioRender online software. Adapted from Koshiba-Takeuchi, 2018 and D. Lee et al., 2013.

Visualisation of the reporter molecule allows localising DNA or RNA sequences in heterogeneous cell populations including tissue samples and environmental samples. Riboprobes also allow to localise and assess degree of gene expression. The technique is particularly useful in neuroscience.

In this project, RNA probes complementary to a mRNA sequence of interest are generated with the addition of a digoxigenin label (ATTTAGGTGACACTATAG). These riboprobes are hybridised with our mRNA of interest after permeabilization of the membranes. The digoxigenin label allows the detection of the hybridised probes through a commercial antibody that has an alkaline phosphatase attached. This alkaline phosphatase will react with NBT/BCIP reagents, which have a phosphate, resulting in a purple colouring in the locations where the riboprobe was previously hybridized and, therefore, where the mRNA of interest is expressed.

For the study of the expression of the different *grin* genes, the following primers were used to synthesise cDNA fragments:

Gene	Primer sequences
grin1a	FW – 5′-GGACGATACGAGACGCATCA-3′ RV – 5′-**ATTTAGGTGACACTATAG**AATCGCGTTGGCTTTGTGAG-3′
grin1b	FW – 5′-GCAAATCCACACTGCCACAC-3′ RV – 5′-**ATTTAGGTGACACTATAG**AAGCAACCTGGACCATTTCAG-3′
grin2Aa	FW – 5′-TCCACAGCACTACAGGGAAG-3′ RV – 5′-**ATTTAGGTGACACTATAG**TGTCAAAGGAGTGCTGACGA-3′
grin2Ab	FW – 5′-CGAGAACCTGCCACAGAAGA-3′ RV – 5′-**ATTTAGGTGACACTATAG**CCTGCCGCTCTCTGTATCAG-3′
grin2Ba	FW – 5′-AGACAAGAGTTCTGCGCTGA-3′ RV – 5′-**ATTTAGGTGACACTATAG**TGCTCATGTTCCTGTGGGTC-3′
grin2Bb	FW – 5′-GACCTTCTCCATCAGCAGGG-3′ RV – 5′-**ATTTAGGTGACACTATAG**TGTCACAATCGTACCCACCC-3′

Table 3. Primers of the different *grin* genes for *in situ* hybridization

cDNA fragments of the different genes were amplified by PCR with Phusion™ High-Fidelity DNA Polymerase (2U/µL) (ThermoFisher Scientific, #F530S) from 120hpf zebrafish wild-type larvae. The resulting cDNA probes were purified with the QIAquick Gel Extraction Kit (QIAGEN, Cat #: 28704) and subsequently transcribed *in vitro* with the DIG RNA Labelling Kit (SP6 polymerase) (Roche Diagnostics, Cat #: 11175025910) according to manufacturer's instructions.

Single whole-mount *in situ* hybridization was carried out with the generated antisense DIG-labelled RNA probes and alkaline-phosphatase coupled anti-Digoxigenin-AP antibody, and detection with NBT/BCIP according to Thisse & Thisse, 2004. During the whole procedure, 2 ml Eppendorf tubes were used with a round bottom, as the round shape is less aggressive for the embryos. Moreover, all the incubations and wash-steps were performed in mild agitation.

Larvae at different developmental stages, from 24 hpf to 120 hpf, were collected to perform the WISH. For those larvae that were still in their chorion (24 hpf and 48 hpf), a chemical dechorionation was performed. This dechorionation was performed with 1mg/ml pronase (Roche, Cat #: 10165921001) solution. Moreover, all the larvae were treated with 1X N-Phenylthiourea (PTU, stock 100 mM) (Sigma-Aldrich, Cas #: 103-85-

5) from 24hpf stages on to avoid pigmentation and facilitate the visualisation of the ISH development.

Once collected at the desired stages, all the larvae were fixed with 4% paraformaldehyde (PFA, in PBS solution) (PanReac AppliChem, Cas #: 50-00-0) overnight at 4ºC. The following day, larvae were rinsed and then washed for 5 minutes twice with PBST in order to remove all the PFA traces. Then, the larvae were dehydrated with increasing concentrations of methanol, *i.e.* 25%, 50%, 75% and 100%, with consecutive washes of 10 minutes each. Once dehydrated, larvae can be stored at -20ºC for up to 6 months.

Subsequently, the larvae were re-hydrated with increasing concentrations of methanol, from 100% to 25%, with consecutive washes of 10 minutes each. Then, larvae were washed twice for 10 minutes with PBST (1X PBS + 0.1% Tween-20 (Sigma-Aldrich, Cas #: 9005-64-5)). A digestion with proteinase K (10mg/ml stock, 1/1000 in PBST, Sigma-Aldrich, Cas #: 39450-01-6) treatment was performed to improve the penetration of the probes, optimizing the signal-to-noise ratio. The digestion times depend on developmental stage, so different incubation times were used depending on the larval stage of the samples:

- 24 hpf embryos - 8 minutes incubation
- 48 hpf embryos - 20 minutes incubation
- 72 hpf embryos - 72 minutes incubation
- 96 hpf embryos - 90 minutes incubation
- 120 hpf embryos - 120 minutes incubation

All the incubations were started at the same time and each reaction was stopped when necessary with PBST. Once all the treatments were performed, the larvae were washed for 5 minutes twice with PBST to remove all the remaining proteinase K. A post-fixation step with 4% PFA was performed for 20 minutes, followed by two more 5-minute washes in PBST.

Subsequently, the samples were pre-hybridised with the hybridisation buffer (50% Formamide (Sigma-Aldrich, Cas #: 75-12-7; 50µg/ml heparin (Merck, Cas #: 9041-08-1); 0,5 mg/ml tRNA (ribonucleic acid from torula yeast, Sigma-Aldrich, Cas #: 63231-63-0); 0,1% Tween-20; 2,5mM citric acid pH 6.0 (Sigma-Aldrich, Cas #: 77-92-9); diluted in ddH2O) for 1 hour at 70ºC. Afterwards, the previously designed and generated probes

are diluted independently in the hybridisation buffer 1:200 probe:buffer and incubated overnight at 70ºC.

The following day, the larvae were washed with different pre-warmed wash-buffers. These buffers are prepared with different concentrations of HYB-buffer (32,5 ml 100% formamide / 12,5 ml 20x SSC (Sigma-Aldrich, Cat #: S6639) / 500 ul 10% Tween-20 / 4,5 ml ddH2O) and 2X SSC (diluted in ddH2O from 20x SSC stock). The washing steps were:

- Wash 1, 75% HYB-Buffer / 25% 2X SSC: 10 minutes at 70º
- Wash 2, 50% HYB-Buffer / 50% 2X SSC: 10 minutes at 70º
- Wash 3, 25% HYB-Buffer / 75% 2X SSC: 10 minutes at 70º
- Wash 4, 2X SSC: 10 minutes at 70º
- Wash 5, 0,5X SSC: 30 minutes twice at 70º

Afterwards, all the samples were fast-washed and washed twice for 10 minutes with PBST at room temperature in order to remove all the remaining buffers and probes.

Larvae were incubated with blocking solution (2% BSA, 10% iNGS in 0,1% PBST) for at least 90 minutes at room temperature. Then, the samples were incubated with anti-Digoxigenin-AP (anti-Digoxigenin-AP, Fab fragments; Roche Diagnostics, CAS #: 11093274910) diluted 1:1000 in blocking solution overnight at 4ºC. The following day, at least 10 washes of 10 minutes each were performed with PBST in order to remove any remaining of the anti-DIG-AP to avoid interferences during the development. Afterwards, the larvae were incubated with alkaline phosphatase buffer (NTMT, 100mM Tris-HCl pH 9,5, 50mM MgCl2, 100mM NaCl, 0,1% Tween-20, 0,2% Triton X-100, in ddH2O) with at least 3 rounds of incubation of 10 minutes each.

Then, larvae were incubated with 4.5 µL/mL 4-Nitro blue tetrazolium chloride (NBT) (Roche Diagnostics, Cas #: 11585029001) and 3.5 µL/mL BCIP (5-bromo-4-chloro-3-indolyl-phosphate, Roche Diagnostics, Cas #: 11383221001) diluted in NTMT for signal development. During the incubation period, the solution was renewed when necessary. The reactions were stopped with some fast washes with PBST.

The image acquisition of the whole larvae was performed with a Nikon SMZ18 stereomicroscope equipped with a Nikon DS-Fi2 camera with digital sight.

3. CRISPR/Cas9 strategy for knockout lines generation: sgRNAs design, primers design and injections

To generate knockout lines for different candidate genes, the strategy consisted in ideally targeting the first common exon of all the different possible transcripts. With this objective, the sequences were searched and analysed using the Ensembl database (https://www.ensembl.org/index.html) and Geneious Prime (Dotmatics, New Zeland).

Once the different target regions were determined, the CRISPOR web tool (http://crispor.tefor.net/) (Concordet & Haeussler, 2018) was used to design the sgRNAs. With this online tool, different guide sequences are proposed, along with their PsAM (Protospacer Adjacent Motif) sites and the expected cleavage position located -3b 5' of the PsAM site. Moreover, different specificity scores are displayed (Hsu et al., 2013), as well as different efficiency predictions, restriction enzymes sites, the out-of-frame outcome and the possible off-targets. To select our sgRNAs of interest, the different information was evaluated, paying special attention to the specificity score and the off-target genes. All the sgRNA with identified off-targets in exons of other genes were discarded. For each gene of interest, a couple of specific sgRNA were designed in order to generate large deletions (≈200 base pairs).

All the analysis of the sequences and genotyping were performed by PCR, looking for shorter amplifications when the expected deletion was present. With this objective, specific primers flanking the sgRNA covered region were designed using the NCBI Primer-Blast tool (https://www.ncbi.nlm.nih.gov/tools/primer-blast/) and ordered from IDT (Integrated DNA Technologies, Inc.).

GRD are caused by the presence of pathogenic *de novo* genetic variants of GRIN genes and, more prevalently, by mutations affecting *GRIN1*, *GRIN2A*, and *GRIN2B* genes (García-Recio et al., 2021; J. Li et al., 2019; S. J. Myers et al., 2023; XiangWei et al., 2018).

Each of these genes have two orthologous genes in zebrafish: *grin1a* and *grin1b* for *GRIN1*, *grin2Aa* and *grin2Ab* for *GRIN2A* and *grin2Ba* and *grin2Bb* for *GRINB*. For zebrafish *grin* genes, both the sgRNAs sequences and the primer sequences obtained were ordered from IDT (Integrated DNA Technologies, Inc.).

With the designed sgRNAs, ribonucleoprotein complexes *in vitro* were generated according to IDT recommendations, formed by the sgRNA (≈240 ng) and the Cas9 protein (≈300 ng) (Alt-R® S.p. Cas9 Nuclease V3, IDT Technologies, #1081059). The designed sgRNA (20bp) were coupled to additional 16 nucleotides, generating the crRNA 36-mer molecule pairing the tracrRNA. The latter is a universal 67-mer molecule that contains proprietary chemical modifications conferring increased nuclease resistance and with the ability to activate the Cas9 endonuclease, which will produce double-stranded breaks in the region of interest, which is flanked by the designed sgRNAs. The double-stranded break will be repaired by non-homologous end joining (NHEJ). For the generation of the stable lines, only *out-of-frame* deletion in the desired location, changing the reading frame of the sequence and assuring the absence of the functional protein, were considered (Figure 10).

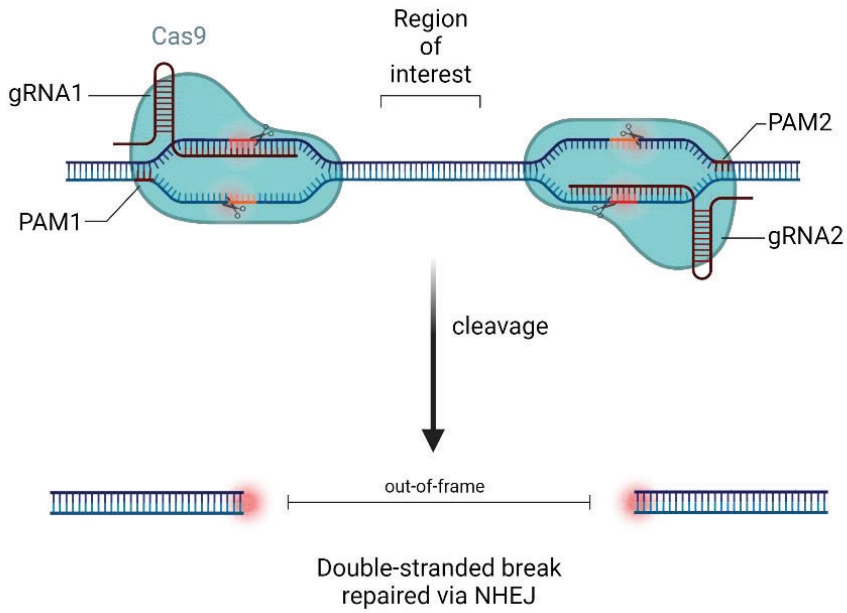

Figure 10. Schematic representation of the CRISPR/Cas9 technology and NHEJ used for stable lines generation**.** Generated with BioRender online software, adapted from CRISPR Technology template.

The sequences and targeted exon for each gene are the following:

Zebrafish gene	sgRNAs	Targeted exon
grin1a	5′-GAGCCAGAAGCGGTACGAGC-3′ 5′-GATGGCGCTGTCTGTCTGCG-3′	Exon 1
grin1b	5′-GATGGTCATTGGACTGGGGA-3′ 5′-TATCAGAATAGATGGACATG-3′	Exon 2
grin2Aa	5′-TGAAGCGGCGTACATCCTGG-3′ 5′-AGAGTTTGGCGATATCCCGG-3′	Exon 4
grin2Ab	5′-CAGGGATGGAGGCTTCTCTG-3′ 5′-AGGTGAATCAGACGGACCCA-3′	Exon 3
grin2Ba	5′-AGACGCTGATCACATCCCGG-3′ 5′-TGGTGTGGCTGTTATCGCCA -3′	Exons 1-2
grin2Bb	5′-GTGGAGGCTGACAAGCATGG-3′ 5′-GCGTCCCGATCCCACCTCCG-3′	Exon 2

Table 4. sgRNAs sequences and targeted exons for each zebrafish *grin* gene.

The generation of these knockout models has been performed in a Tg(HuC,Gal4;UAS,dsRed) background, enabling a direct detection of all neuron cell types (e.g. red fluorescence endogenous labelling) together with the Gal4/UAS control for future experimental purposes. Six single knockout models or lines have been generated by CRISPR technology: *KO-grin1a, KO-grin1b, KO-grin2Aa, KO-grin2Ab, KO-grin2Ba* and *KO-grin2Bb*. To generate the double knockout models, single models for a given human gene were outcrossed (e.g. *KO-grin1a* x *KO-grin1b*), obtaining the three double models: *KO-grin1a/b, KO-grin2Aa/b* and *KO-grin2Ba/b*.

For the generation of these models, zebrafish embryos were injected at one-cell stage with the corresponding CRISPR/Cas9 machinery mix. The injected embryos were grown to adulthood to generate stable lines.

4. Genomic DNA extraction and genotyping PCRs of the models

4.1. Genomic DNA extraction

4.1.1. Generation of the stable lines

As previously stated, when generating stable lines zebrafish embryos were injected at one-cell stage with the corresponding CRISPR/Cas9 machinery mix. The injected embryos are grown to adulthood. To establish the lines, at least one adult fish with the desired mutation in the germline is needed, which will be considered the F0 founder of the line. Once an F0 founder is identified (see section 4.1.1.1.) and isolated, it is crossed with wild-type zebrafish (in this case, Tg(HuC,Gal4;UAS,dsRed) background fish were used), and the progeny, also known as F1 generation (first filial generation), is grown to adulthood. A variable amount of the progeny will be heterozygous depending on the transmission of the mutation. The adult F1 population is genotyped (see section 4.1.1.2.), and the heterozygous adult fish are crossed to obtain the F2 generation (second filial generation). When the genetics are mendelian, the F2 generation will be constituted by 25% of wild-type fish, 50% of heterozygous fish for the desired mutation and 25% of homozygous fish for the desired mutation. The F2 generation fish can also be grown to adulthood, genotyped and segregated depending on their genotype (Figure 11).

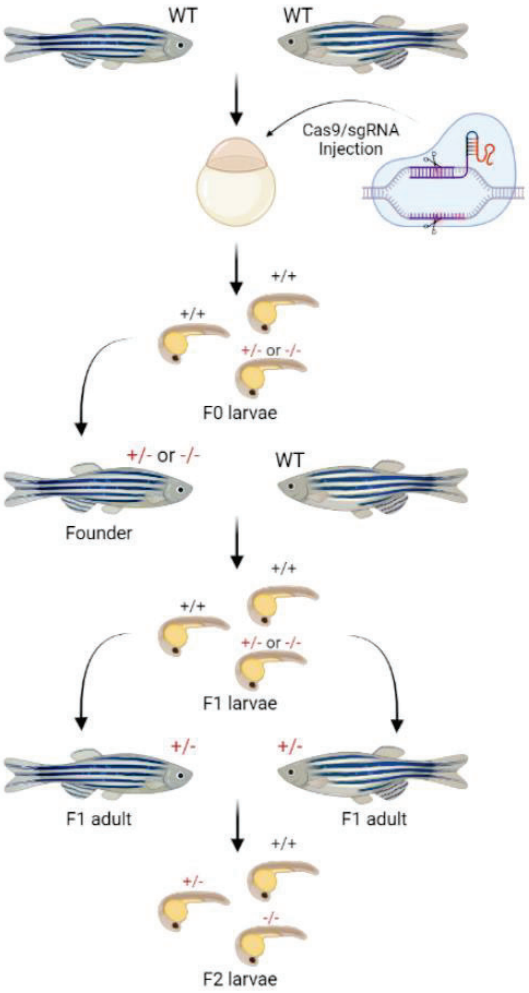

Figure 11. Schematic representation of the generation of stable lines in the Zebrafish. Wild-type fish are crossed, and the CRISPR/Cas9 machinery is injected at one-cell stage eggs. The F0 Founder, bringer of a deleterious mutation, is crossed with a wild-type fish to obtain the F1 generation. Heterozygous adult fish from the F1 generation are crossed to obtain the F2 generation, where wild-type, heterozygous and homozygous fish will be present. Generated with BioRender online software.

To generate the double knockout lines, homozygous adult animals of single knockout lines for each paralog *grin* gene were crossed, obtaining double heterozygous animals for the line. As a result of the crosses of the double heterozygous fish, the nine possible genotypes where present in the progeny. The different possible genotypes are represented in Table 5.

AaBb♂	AaBb ♀	AB	Ab	aB	ab
AB		AABB	AAbB	aABB	aAbB
Ab		AABb	AAbb	aABb	aAbb
aB		AaBB	AabB	aaBB	aabB
ab		AaBb	Aabb	aaBb	aabb

Table 5. Punnett square, representation of the possible genotypes. To facilitate the representation, paralogs *a* and *b* are represented with these letters. Uppercase letters represent wild-type alleles, while lowercase letters represent mutated alleles. Therefore, AA is wild-type for paralog *a*, Aa is heterozygous and aa is homozygous. Equivalently, BB is wild-type for paralog *b*, Bb is heterozygous and bb is homozygous. Each possible combination represents a 6.25% of the progeny. In white, the combinations resulting only in 6.25% of the progeny are represented, in light grey the combinations resulting on 12.5%, and in dark grey the only combination present in the 25% of the progeny, which is the double heterozygous AaBb.

4.1.1.1. Determination of the line founders

To generate stable lines, at least one adult fish with the desired mutation in the germline is needed, which will be considered the F0 founder of the line. To evaluate the presence or not of the mutations, the potential founders were crossed with wild-type adult zebrafish, and the obtained eggs were genotyped.

From the obtained progeny from each possible founder, pools of 20 to 30 embryos were taken, and the genomic DNA (gDNA) was extracted. Between 10 and 30µl of CoboXtract™- Quick DNA Extraction Solution (Cobo Technologies, Cas #: C20101) were used, depending on the amount of tissue to be digested. The tissue digestion was performed by a 10-minute incubation at 70ºC followed by a 10-minute incubation at 98ºC. Subsequently, 90µl of UltraPure Molecular Water (Thermo Fisher, Cas #: 10977035) was added to dilute the extracted gDNA. The extracted gDNA was stored long-term at -20ºC, or until the PCRs were performed.

After genotyping the possible founders, the mutant amplicons were purified with the QIAquick Gel Extraction Kit (QIAGEN, Cat #: 28704) and sent for sequencing with either the forward or the reverse primer, according to sample requirements, to StabVida.

The sequencing data was analysed in Geneious Prime (Dotmatics, New Zeland) (Kearse et al., 2012). As aforementioned, to consider a potential founder the founder of the line, it must have an out-of-frame deletion in the desired location, changing the reading frame of the sequence and assuring the absence of the functional protein.

4.1.1.2. gDNA extraction of adult zebrafish

To genotype the adult population of the lines (used in F1 generation and F2 generation), caudal fins of the zebrafish were clipped. Due to the regenerating capabilities of the zebrafish, the clipped fin is regenerated in a week-time. The clipped fins were used to extract gDNA using 10µl of CoboXtract™- Quick DNA Extraction Solution per individual fin, following manufacturer's instructions and the previously mentioned extraction protocol. The extracted gDNA was stored long-term at -20ºC, or until the PCRs were performed.

4.1.1.3. gDNA extraction of zebrafish larvae

The model characterisation experiments performed along this project were performed with F2 larvae, the progeny of the F1 adult heterozygous zebrafish. The genotyping of the F2 larvae was performed post hoc, after phenotypic assessment. Briefly, the larvae used were individualised, sacrificed and their gDNA was extracted using 10µl of CoboXtract™- Quick DNA Extraction Solution per larvae as described above. The extracted gDNA was stored long-term at -20ºC, or until the PCRs were performed.

4.2. Genotyping PCRs

Once the gDNA was obtained, different polymerases were used to perform the PCRs. One-Taq polymerase (OneTaq® Quick-Load® 2X Master Mix with Standard Buffer; New England BioLabs, Cas #:M0486L) was used for *grin1a*, *grin1b, grin2Aa, grin2Ab* and *grin2Bb* genes (Table 6). GoTaq polymerase (GoTaq ® G2 Flexi DNA Polymerase; Promega, Cas #: M7805) was used for *grin2Ba* gene (Table 7). With both polymerases, the reactions were prepared following the manufacturer's recommendations. The thermocycling conditions were adjusted as indicated in the manufacturer's instructions, with a specific annealing temperature for each primer-pair (Table 8).

Step		Temperature	Time
Initial Denaturation		94ºC	30 seconds
30 cycles	Denaturation	94ºC	30 seconds
	Annealing temperature	45-68ºC	30 seconds
	Extension	68ºC	1 minute per kb
Final Extension		68ºC	5 minutes
Hold		4ºC	∞

Table 6. OneTaq cycles protocol

Step		Temperature	Time
Initial Denaturation		94ºC	2 minutes
35 cycles	Denaturation	94ºC	30 seconds
	Annealing temperature	45-68ºC	30 seconds
	Extension	72-74ºC	1 minute per kb
Final Extension		72-74ºC	5 minutes
Hold		4ºC	∞

Table 7. GoTaq cycles protocol

Zebrafish gene	Primers	Annealing temperature
grin1a	FW – 5′-CAATCTCCTCCGCAAGCGAC-3′ RV – 5′-TTACCCCTCGAGCAACTTTCA-3′	60,1ºC
grin1b	FW – 5′-AGCTTGGTGGTCAAATTAAACAG-3′ RV – 5′ACAATCATGGAGGATGACCATCAG-3′	60,1ºC
grin2Aa	FW – 5′ACAGCTTCGTGGGTTGGGA-3′ RV – 5′-GGCTGTTGACAGAAAACACTCAC-3′	59ºC
grin2Ab	FW – 5′-TCCCATTCATTTACAGTCCCCG-3′ RV – 5′-ATTCCCAGTATGGGCATGGAA-3′	61,5ºC
grin2Ba	FW – 5′-TACGGGTACACCTGGATCGT-3′ RV – 5′-TCGTTGTTGTTCCCCGTCAT-3′	57ºC
grin2Bb	FW – 5′-TCAGGTCTCTTGCTGGTTTAACT-3′ RV – 5′- GGCACGTGTAGAAAGTCCTCT-3′	59ºC

Table 8. Annealing temperatures and primers of each studied gene

After each PCR, the amplified DNA products were loaded onto a 2% agarose gel with SYBR Safe DNA Gel Stain (Invitrogen, Cat #: S33102) and separated by size by electrophoresis (BioRad PowerPac Basic, Cat #: 1645050). The product of the PCR with the different amplicons was visualised by exposing the agarose gel under UV light. With this aim, the UV transilluminator Gel Doc (Bio-Rad, Molecular Imager® Gel Doc™ XR+ System, Cat #: 1708195EDU) was used.

5. Assays for phenotypic characterisation of the models and statistical analysis

5.1. Morphological analysis

To assess any morphological alteration in the different studied lines, the vertebrate automated screening technology (VAST, Union Biometrica System) was used. Each larva was analysed at 120 hpf for different morphological parameters, such as body deformity, heart oedema, yolk oedema, scoliosis, heart area, eye diameter, lateral and dorsal length and absence of the fin. Phenotypes were assessed using an ad-hoc ImageJ/FIJI plug-in for the analysis of the morphological alteration (Jarque et al., 2020). The experimental design used a 96 well plate (Clearline, Cat #: 131012C) with one larva per well. A negative control group (wild-type with the Tg(HuC,Gal4;UAS,dsRed) background, siblings or related to the studied mutants if possible) was included for each plate imaged at the VAST. This negative control group was manipulated together with the studied mutants, to minimize the possible batch effect. The experiments were arranged for all groups to be equally present in the plates to avoid variations (Q. Li et al., 2015).

5.2. Custom pipeline to evaluate GRD alterations in the zebrafish

The behaviour of GRD models was analysed by a series of different standardized paradigms, specifically selected and designed to evaluate GRD possible phenotypes. The locomotor performance of the larvae was recorded at 120 hpf using the EthoVision XT 12.0.30 software along with the DanioVision chamber (Noldus Information Technologies, Wageningen, The Netherlands). This system consists of a closed circulating water system maintained at 28ºC with a temperature sensor. The chamber has a camera placed above allowing the recording of the zebrafish larvae. Adapting to the zebrafish cycle, experiments were always performed between 10.00h and 16.00h (Padilla et al., 2011), at least 4 hours after the lights-on in the incubator. As stated with the morphological analysis, a negative control group of wild-type with the Tg(HuC,Gal4;UAS,dsRed) background, siblings or related to the studied mutants if possible was included in each plate in order to minimise the batch effect and to always be compared with. The experiments were arranged for all groups to be equally present in the plates to avoid variations (Q. Li et al., 2015).

A polarised corrector lens is used to adjust and normalise the image of the plate, allowing the recording of the whole plate equally. The threshold detection settings were optimised to correctly detect the larvae. Videos were recorded in a 1024x960 resolution and a framerate of 30fps (frames per second).

The data of the different behavioural protocols was exported from the EthoVision XT software to perform the data analysis. The different readouts vary in each behavioural paradigm, and it is stated in every corresponding sub-section. The sample size is specified in the corresponding results section.

For these experiments, 48-well plates (Thermo Scientific, Nunc, Cat #: 055431/150687) were used and placed in the chamber in line with the camera. Larvae were plated with 400µL of 1X E3 medium in each well of the 48-well plates, with only one larva per well. To allow the habituation of the larvae to the plate, they were plated at least 3h before the behavioural recording and all the tests had a 10-minute light acclimatation phase inside the recording chamber (Figure 12A).

In reference to standardised paradigms available in the literature along with the experience of the laboratory, the custom proposed and designed protocol consists of three distinct phases (Figure 12A):

- **Locomotor activity assessment in dark/light transitions**: to evaluate possible locomotion alterations. Is a standardised 25 minutes dark/light cycles paradigm (5 minutes darkness – 5 minutes light, up to 25 minutes (Peng et al., 2016).
- **Response and habituation to tactile stimuli**: to analyse the response to environmental tactile stimuli and the non-associative memory or habituation to the mentioned stimuli. In light baseline conditions, a series of 30 consecutive 1 second-spaced taps are given to the plate. The same rationale is repeated fifteen minutes after to evaluate de-habituation to the response (Best et al., 2008; McDiarmid et al., 2019; Reemst et al., 2023).
- **Light-induced epilepsy-like behaviour**: to study the presence of epilepsy-like behaviour. A set of five flashes (1 second of light-flash – 59 seconds of darkness, repeated five times) was performed to trigger epileptic behaviour in a timed-controlled manner (Turrini et al., 2022).

The recording chamber was not opened between paradigms. For each phase of the experimental design, different outputs were obtained and analysed to evaluate the different behavioural patterns of the zebrafish larvae (Figure 12B).

A

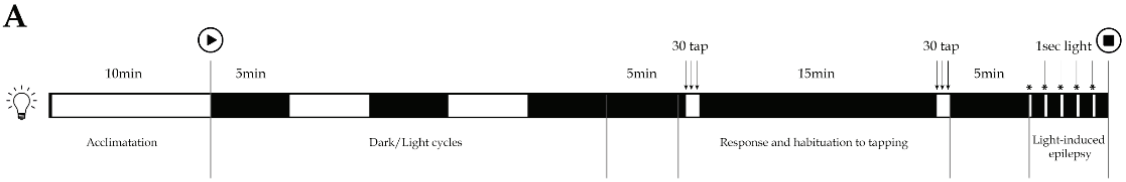

B

Data	Variable	Measurement
Dark/Light cycles	Total distance moved (mm)	Total distance travelled by each larva in the 25 minutes of the protocol
	Distance moved by 1-minute time bin (mm)	Total distance travelled by each larva every single minute of the protocol
	Percentage of time in centre/periphery areas	Percentage of time spent by each larva either in the centre area and the periphery area of each well to measure anxiety
	Dark/Light transitions	Difference between the total distance travelled the minute after and the minute before each transition
Response and habituation to tapping	Quantitative response to the first stimulus (mm)	Difference between the total distance travelled the second after and the second before the first tap of the set
	Qualitative response to the first stimulus	Percentage of larvae that responds to the first tap of the set
	Time for habituation (s)	Total time or number of taps each larvae takes to stop reacting to the tapping stimulus
Light-induced epilepsy	Maximum velocity (s)	Maximum velocity achieved by each larva within the two seconds after each light flash
	Number of angle turns	Number of big changes in the direction of the trajectory performed by each larva within the two seconds after each light flash

Figure 12. Schematic representation of the complete behavioural protocol and the evaluated parameters. A. Representation of the complete custom experimental design, which includes the dark/light transitions, the response and habituation to tapping and the light-induced epilepsy protocol. A 10 minutes acclimatation phase in light conditions is performed before the start of the recording. The different phases are divided by vertical grey lines. Each phase is separated 5 minutes from the following one. The white spaces represent periods of light, while dark spaces represent periods of darkness. Vertical arrows with arrow heads represent the tapping in the plate. Vertical arrows with star heads represent the 1 second light flashes in the darkness period. B. Table with a summary of the different readouts evaluated in the different designed phases.

5.2.1. *Locomotor activity assessment in dark/light transitions*

To evaluate possible locomotion alterations in the generated *grin* library, the standardised 25 minutes dark/light cycles paradigm (5 minutes darkness – 5 minutes light up to 25 minutes) was used, and the total distance moved (mm) was analysed.

The main readouts evaluated within these behavioural experiments are distance moved (mm) within the arena, both total and in 1-minute time bin, the percentage of time in each area of the well, centre or periphery, representing a thigmotaxis behaviour; and dark/light transitions, measured by the difference of distance moved between the last minute of one light or dark period and the first minute of the following period.

5.2.2. *Response and habituation to tactile stimuli*

To analyse the response to environmental tactile stimuli and the non-associative memory or habituation to the stimuli, the tapping system integrated in the Noldus DanioVision chamber was used. During light baseline conditions -with reduced larval movement- a series of 30 consecutive brief taps, with an inter-stimulus of 1-sec were delivered to the plate, and the movement was recorded. The data (individual trajectories, time) were exported and analysed in a 1-second time bin for a total of 40 seconds corresponding to the initial 10 seconds baseline (light without tapping stimulus) and 30 seconds where the tactile stimuli are applied.

The readouts included the response to the first stimulus, both qualitative and quantitative, and the habituation to the continuous stimuli. To analyse the response to the first stimulus, the number of larvae reacting to the stimulus are evaluated, comparing their movement after the first tap with the baseline movement, along with the quantification of this movement difference. For the analysis of the habituation, the time necessary to stop responding to the stimuli was quantified and compared between groups. For this quantification, the average movement during the baseline (10 seconds) was calculated per larva. The threshold of response was set at individual baseline values plus 0.5mm of movement (MacPhail et al., 2009).

The same rationale was repeated fifteen minutes after the first one in order to evaluate memory extinction to the response. The same parameters were evaluated and compared within the different groups in the same period of time. Moreover, the responses of the same groups in the two different sets of tapping were also compared and analysed.

5.2.3. Light-induced epilepsy behaviour

To induce seizures in zebrafish larvae, a paradigm of light-flash induced epilepsy was adapted from Koseki et al., 2014. Briefly, a set of five flashes (1 second of light-flash – 59 seconds of darkness, repeated five times) were performed to trigger epileptic behaviour in a timed-controlled manner. The five flashes were executed to perform five triggers (or replicates) for experiment. For the final analysis, the mean of the responses of the five different flashes were evaluated. For the quantification of seizures, the maximum speed (mm/s) reached by the larvae and the number of turns along 2 seconds following a light flash were analysed. Seizure events were identified by abnormal maximum velocity values and confirmed by visual inspection. Increased maximum velocity (>30mm/sec) is considered pathological, and velocities above 90mm/sec are described to be compatible with epileptic seizures (LaCoursiere, 2024).

6. Development of new tools to characterise GRD models

6.1. Visual assessment through colour preference

To evaluate the proper visual function of the *grin* models, a colour preference test was used, benefiting from the innate colour preference of the zebrafish of blue, over yellow colour (Bruzzone et al., 2020; Hagen et al., 2023). Larvae are placed in in-house created two-coloured plates (Figure 13) and recorded for 15 minutes under light conditions. 24-well plates (Thermo Scientific, Nunc, Cat #: 142475) were used and placed in the chamber in line with the camera. Larvae were plated with 2mL of 1X E3 medium in each well, with only one larva per well. Larvae were plated immediately before the behavioural recording, and all the tests had only one minute of light and one minute of dark acclimatation phase inside the recording chamber.

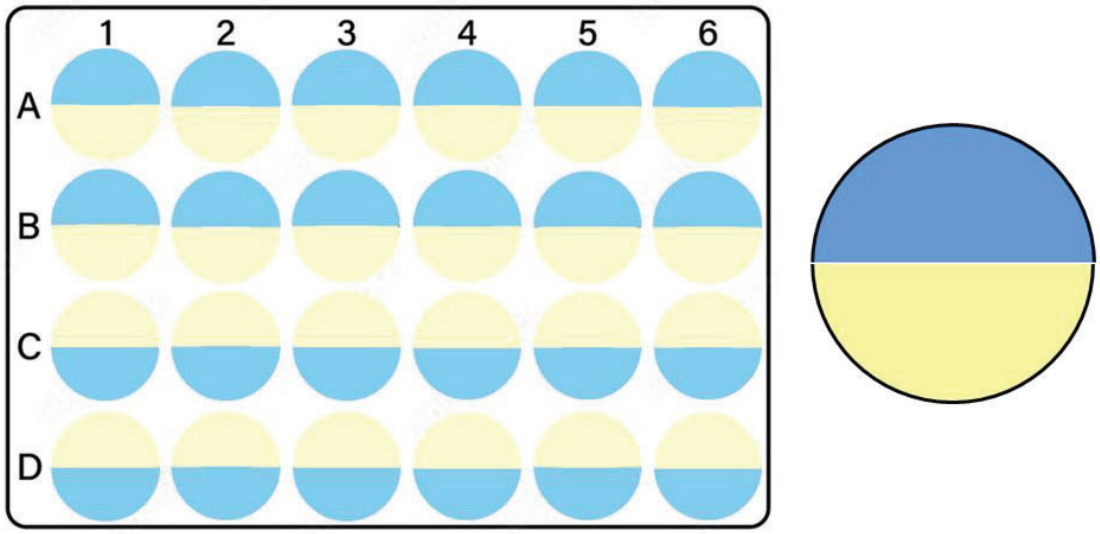

Figure 13. Schematic representation of the colour preference plate. Each well is horizontally divided in two areas, blue and yellow. The plate has a different distribution to minimise the possible bias of the top or down areas in the well.

For each larva, the colour preference was calculated as the percentage of time spent in each colour zone. Furthermore, a blue preference index (*Bpi)* was also analysed by using the following formula: $BPi = \frac{(\%B - \%Y)}{(\%B + \%Y)}$, where BPi is the blue preference index, $\%B$ is the percentage of time spent in the blue area and $\%Y$ is the time spent in the yellow area. A BPi of 0 represents no preference for any of the colours, between 0 and 1 represents a blue preference and between -1 and 0 represents a yellow preference. The blue preference index was compared between all the groups.

6.2. Gastrointestinal tract function analysis

This gastrointestinal tract (GIT) functional analysis was carried out to evaluate both the initial food intake and excretion. To address this objective, a novel in-house protocol was set-up and optimised to study gastrointestinal function, based on Cassar et al., 2018 and James et al., 2019.

For this set of experiments, zebrafish eggs were collected and plated in petri dishes, with 100-150 eggs density per plate, as before stated. When the embryos were 24 hpf were treated with PTU 1X in E3 1X. The media of the plates was renewed every 24 hours with new PTU 1X until the day of the experiment. This procedure is performed to inhibit the

pigmentation of the larvae, facilitating the gut imaging. The 7 dpf larvae embryo media was supplemented with chicken egg yolks (Sigma-Aldrich, Cas #: E0625) solution labelled with BODIPY 505/515 ($C_{13}H_{15}BF_2N_2$; Sigma-Aldrich, Cas #: 21658-70-8) allowing the food monitoring (e.g. visible in green wavelength). More precisely, the feeding solution of the egg yolks from chicken was prepared at 400mg/ml in E3 1X and gently mixed with the vortex and with a plastic pipette if needed. Once the mix was homogeneous, the BODIPY solution was added to a final concentration of 2.5X.

The day of the experiment, the 7 dpf larvae were plated in 6-well plates (ClearLine, Cat #: 131028C), with 3mL of PTU 1x in E3 1X media. Each plate also contained a negative control group, from the same batch of embryos (wild-type with the Tg(HuC,Gal4;UAS,dsRed) background, siblings or related to the studied mutants if possible) and manipulated together with the studied mutants, to minimise the possible batch effect. Furthermore, a group of larvae were treated with 4,2µM Atropine (Sigma-Aldrich, Cas #: 51-55-8) as a constipation positive control, adapting the protocol described in Cassar et al., 2018. If any other treatment was assessed, larvae were also treated at this point.

Subsequently, larvae were fed with the feeding solution, adding a ratio of 50µl/well. After 6 hours of feeding, the larvae the whole media of the plates was removed and fast-washed with fresh E3 1x media to rinse the feeding solution. Afterwards, the larvae were anesthetised with 0,28mg/ml Tricaine ($C_9H_{11}NO_2 \cdot CH_4SO_3$, CAS #: 886-86-2, Stock 4mg/ml) and plated in 96-well plates (ClearLine, Cat #: 131012C), with a final volume of 200µl in each well. The time between the tricaine application and the initiation of the imaging was never higher than 1 hour, in order to minimise the impact of the Tricaine in the gastrointestinal motility. In every analysed plate, both the negative and the positive control groups were present besides the studied mutants. The same conditions were used in all the performed experiments.

To image the GIT of the larvae, the vertebrate automated screening technology (VAST, Union Biometrica System) coupled to a Leica microscope (Leica, Cat # DFC9000GTC) was used. The plates with anesthetised larvae were disposed in the VAST and images of the larvae GIT were obtained. The 10X objective was used, and a z-stack of 500µm wide of the gastrointestinal region was obtained, both in bright field and green fluorescence. After the imaging, larvae were dispensed in a new 96-well plate (ClearLine, Cat #: 131012C) and treated with new PTU 1X in E3 1X media, 4,2µM

Atropine treatment, and with other corresponding treatments if needed. Afterwards, larvae were returned to the incubator. After 16 hours of the first imaging, larvae were anesthetised again with 200µl/well with 0,28mg/ml Tricaine and imaged again using the same VAST-Leica system.

The obtained images were analysed using ImageJ/FIJI software (Schindelin et al., 2012; Schneider et al., 2012). The mean of the fluorescence intensity in the GIT area was quantified. The raw value in the first time point after the feeding time gives the information of the amount of intake food. The ratio between the values of the two timepoints (First time point / Second time point) was calculated to estimate the digestive performance of the larvae.

7. Animal Growth studies

With the aim of describing any possible growth impairment in the *grin1* models, both *grin1a* and *grin1b* F3 fish growth was evaluated from 4 weeks old to up to 16 weeks old. To conduct the experiment F2 fish of each line were crossed. Wild-type fish were in-crossed, giving an offspring of only wild-type animals, together with homozygous siblings of these wild-type for each line, giving an offspring of only homozygous animals. With this approach, the genotype of the animals is known from the beginning.

Starting at week 4, and every two weeks, all the animals were weighed and measured individually, and the mortality of the group was also assessed. To perform the measurements, animals were anaesthetised with 0,28mg/ml Tricaine, rinsed, weighed in a precision balance (AnD Discovery Precision, Analytical balance Cat #: HR-251A) and size-measured with digital calliper (Fine Science Tools, Cat #: 30087-00). Rapidly, the animals were returned to a tank with fresh system water to recover from the anaesthesia. To minimise the bias and differences caused by food intake, the animals were always measured along the fasting phase (from 8:00 to 12:00 AM).

Besides the body length and weight growth, sexual maturation was assessed. Starting at week 12, the animals were in-crossed in massive breedings (crosses including all the tank individuals, between 10 and 30 fish involved) to assess whether they had reached sexual maturity. The fertility of the laid eggs was evaluated at least at 6 hpf.

8. Pharmacological treatments with NMDAR modulators

One antagonist of the NMDAR, the MK-801 ((+)-MK 801 maleate, Tocris, Cas #: 0924); one agonist, the D-Serine (Sigma-Aldrich, Cas #: 312-84-5) and one Positive Allosteric Modulator (PAM), the Spermine (Sigma-Aldrich, Cas #: 71-44-3) were used for the custom designed protocol evaluation.

Five different compounds recently identified as potential therapeutic molecules were used to evaluate the potential of zebrafish models. To protect their IP, the identity of the compounds will remain hidden. Therefore, the compounds will be named "Compound *N*", where *N* is a number from 1 to 5.

All the compounds were prepared with UltraPure Molecular Water (Thermo Fisher, Cas #: 10977035) to a stock concentration of 100mM, and diluted in E3 1x medium to reach the final concentration. All the compounds were manipulated under a security fume hood.

For the pharmacological screening and evaluation, the Fish Embryo Toxicity Test (FET, Guideline 236 of the OECD) was performed, which allows to determine the maximum tolerated concentration. With this aim, 96 hpf wild-type larvae were exposed to five different concentrations of the compounds for 24 hours. The larvae were plated in 96-well plates (ClearLine, Cat #: 131012C) and exposed to 200µL of the corresponding compound. At 120hpf, the toxicity of the different compounds was evaluated, considering important toxicity phenotypes, *i.e.*, scoliosis, yolk edema, heart edema and necrosis; as well as mortality.

Once the NOEC has been defined, a series of lowering concentrations have been selected and tested in wild-type animals to determine their function in basal conditions. With all the compounds, the previously described behavioural assessment was performed.

To evaluate the effect of different modulators of the NMDAR activity in behaviour, the same protocol described in section 5.2., Figure 12, used for the evaluation of a set of phenotypical paradigms in the *grin* generated models, was performed. The same conditions described in the 5.2. section were used. Furthermore, the same readouts and statistical analysis was performed for each section of the used protocol.

9. Statistical analysis

Data and statistical analysis were performed with Graphpad Prism 8.0.1 software for Windows (GraphPad Software, San Diego, California USA, www.graphpad.com). Statistical significance was evaluated using the adequate test, always comparing wild-type fish with their related homozygous fish. Comparisons between two different groups were analysed using t-test; comparison between different groups was performed using One-way-ANOVA, whereas post-hoc analysis was performed using Tukey's test. In all the analysis p-value<0.05 was set as statistically significant.

Chapter 2: A zebrafish-based platform for high-throughput epilepsy modelling and drug screening in F0

1. Zebrafish husbandry and breeding

The zebrafish were maintained as explained in Chapter 1 - Section 1 of Materials and Methods.

2. CRISPR/Cas9 strategy for lines generation: sgRNAs design, primers design and injections

The rationale of the CRISPR/Cas9 strategy has been explained in Chapter 1 – Section 4 of Materials and Methods. In this section, only the different procedure specific to the epilepsy modelling in F0 will be described. To perform this evaluation, injected F0 animals, also named "crispants", were used for all the experiments, with no generation of stable lines of the different childhood epileptic genes models.

In this chapter, the proposed approach for high-throughput epilepsy modelling and drug screening was tested on the zebrafish orthologues of six genes, whose loss-of-function has been associated with different kinds of genetic epilepsy (Table 9).

One of the epilepsy associated genes (*KCNQ2*) has two orthologues in zebrafish (*kcnq2a* and *kcnq2b*). In this case, we generated three types of crispants: two single crispants in

which only one of the two paralogues was targeted (single crispants) and a double crispant in which both paralogues were simultaneously targeted.

Human gene	Disease	Zebrafish orthologue
ADGRG1	Bilateral frontoparietal polymicrogyria (Bahi-Buisson et al., 2010)	*adgrg1*
GABRA1	Different epileptic disorders (Johannesen et al., 2016)	*gabra1*
KCNQ2	Benign familial neonatal seizures (Castaldo et al., 2002)	*kcnq2a; kcnq2b*
PCDH19	PCDH19 Epilepsy (Samanta, 2020)	*pcdh19*
SCN1A	Dravet syndrome (Depienne et al., 2008)	*scn1lab*
UBE3A	Angelman syndrome (Fang, 1999)	*ube3a*

Table 9. Candidate epilepsy-associated genes analysed in this study.

For the childhood epilepsy genes, the primer sequences obtained were ordered from IDT (Integrated DNA Technologies, Inc.), while the sgRNA already forming the ribonucleoprotein complexes were obtained from Synthego (Synthego Corporation, California, USA).

The primer and sgRNA sequences and targeted exon for each gene are the following:

Zebrafish gene	Primers	sgRNAs	Targeted exon
adgrg1	FW - 5′-GTCATTTCTGTGTGTTCTGGGAG-3′ RV - 5′-GGTGATGTTGTGATGCATGGTA-3′	5′-CGGTGCAGCAGGTTCCTTGA-3′; 5′-GTCAAAGGTGATATCATCAC-3′	Exon 2
gabra1	FW - 5′-TATTCCTTTGCACTGGCTGAGA-3′ RV - 5′-CGAACACAGACACCAACGAAAT-3′	5′-CTGCCTGAAGAACACATCTA-3′ 5′-CCCGACACGTTCTTCCACAA-3′	Exon 5
kcnq2a	FW - 5′-CCGCCAACGGGGAAGTTTA-3′ RV - 5′-AGTTTGAGCATTCTGGGCGG-3′	5′-GGTAAATGAACGCCCAGCCG-3′; 5′-TCTGGAGCGACCCCGCGGCT-3′	Exon 1
kcnq2b	FW - 5′-CCAGAACAAGTTCTCCAGGGA-3′ RV - 5′-AATTCTGCAGGCGTCGGTAA-3′	5′-TGCTCGCACCTGCTGTAGGG-3′; 5′-TTTCTCGGCCTGCGGGGCGG-3′	Exon 1
pcdh19	FW - 5′-GGACTGGAGTCGATGCCG-3′ RV - 5′-GTGTACCGAGACTGCGTTTCT-3′	5′-TAACCCGCAAATAAGGCTGT-3′; 5′-CGGTACCAGATTTCCCCTAG-3′	Exon 1
scn1lab	FW - 5′-CATCAGCTCCCAGAGTGACC-3′ RV - 5′-CCTTCAGGTAGTCCTACAGCCT-3′	5′-TGCGATGCGTTGCTCGATAG-3′; 5′-TCTCCGTAGATGAACGGCAG-3′	Exon 1
ube3a	FW - 5′-ATCACAATGTGTACGCCGCT-3′ RV - 5′-GATCCACTCGAGGGCCTTTT-3′	5′-GTTGTGGTCGCAGTACGGTG-3′; 5′-AGCTCGCTGGACTCAGGGAT-3′	Exon 2

Table 10. Sequence information for the crispants generation. Summary of the zebrafish childhood-epileptic genes, the primers sequences, the sgRNA sequences and the targeted exon of each gene.

The generation of these models was performed in a wild-type AB background zebrafish. For the generation of crispants, zebrafish embryos were injected at one-cell stage with the corresponding CRISPR/Cas9 machinery mix. As a negative control for the experiments, commercial scrambled sgRNA (5′-G*C*A*CUACCAGAGCUAACUCA-3′) were also injected in one-cell stage embryos at the same time as the other crispants. The scrambled sgRNA binds the Cas9 without targeting any sequence of the zebrafish genome, simulating the injection conditions in the embryo but not generating any indel in its DNA. When stated, tyrosinase sgRNA (5′-GGACTGGAGGACTTCTGGGG-3′) was co-injected with the sgRNAs for each target gene.

3. Rate of mutations analysis

For the evaluation of the mutagenesis ratio for each childhood epileptic crispant and assess the efficacy of co-injecting sgRNAs for our target genes and *tyr* sgRNA, 120 hpf

pigmented (low tyrosinase efficacy) and non-pigmented (high tyrosinase efficacy) larvae were selected, individualized, extracted their genomic DNA and Sanger sequenced the locus targeted by the sgRNAs of our target genes (STABvida). With the obtained individualized sequences, the mutation ratio was quantified using Synthego ICE analysis tool.

4. Morphological analysis

To assess any morphological alteration in the different crispants studied, the same equipment and analysis method described in Chapter 1 were used. The experimental design used a 96 well plate (ClearLine, Cat #: 131012C) with one larva per well, negative control group (injected with a scramble sequence) was included for each plate imaged at the VAST.

Each plate contained a scrambled control, from the same batch of embryos, injected, and manipulated together with the studied childhood epilepsy mutants, to minimise the possible batch effect.

5. Behavioural experiments

The behaviour was analysed by a series of different standardized paradigms. The performance of the injected larvae was recorded at 120 hpf using the EthoVision XT 12.0.30 software along with the DanioVision chamber (Noldus Information Technologies, Wageningen, The Netherlands). The same conditions described in the Chapter 1- Section 6.2. were used. The threshold detection settings were optimized for each experiment to identify the larvae correctly considering the pigmentation loss.

As stated with the morphological analysis, different distributions for the plates were used in the different behavioural analysis of the epilepsy-associated genes, always with a scrambled control in each plate to minimize the batch effect and to always be compared with.

5.1. Locomotion activity assessment

The dark/light paradigm used and the different analysed parameters were analogous to the described Chapter 1 – Section 5.2.

5.2. *Light-induced epilepsy behaviour*

The dark/light paradigm used was analogous to the described Chapter 1 – Section 5.2. Additionally, different parameters possibly related with an epilepsy-like behaviour were exported. The considered parameters are the following:

Variable	Description
Maximum speed (mm/s)	Maximum velocity reached by larvae in the two seconds after the light trigger in the trial
Maximum acceleration (mm/s^2)	Maximum acceleration reached by larvae in the two seconds after the light trigger in the trial
Mobility of the larvae in the area (%)	The total percentage change (in pixels) in the detected body area when compared with the previous measure after the light trigger in the trial
Mobility state	Definition of a discrete variable with three possible states, defined by different thresholds of movement. It is the calculation of the duration for which the complete area detected as animal is changing, even if the centre point remains the same
Immobile (s)	Cumulative time after the light trigger in the trial when the larvae has been immobile, below the 20% of mobility threshold
Mobile (s)	Cumulative time after the light trigger in the trial when the larvae has been immobile, below the 20% of mobility threshold
Highly mobile (s)	Cumulative time after the light trigger in the trial when the larvae has presented high mobility, above 60% of mobility threshold
Number of angle turns	Number of turns performed by larvae after the light trigger in the trial

Table 11. Description of the different kinematic variables used for epilepsy-like analysis.

These parameters were considered for the evaluation through Mahalanobis Distance calculations. Maximum velocity (mm/s) and the number of bouts the 2 seconds immediate to the flash were used for standard analysis (Chapter 1 – Section 5.2.).

5.3. *Pharmacological induced epilepsy behaviour*

To perform the experiments, PTZ (Sigma-Aldrich, Cas #: 54-95-5) was dissolved in DMSO (dimethylsulfoxide, MRI Global, Cas#: 67-68-5) to 1M stock solutions, were stored at -20^{o}C until needed and treatment solutions were freshly prepared before each experiment.

Given PTZ characteristics (Baraban et al., 2005; Dinday & Baraban, 2015; Ellis et al., 2012; Griffin et al., 2021; Tiedeken & Ramsdell, 2007), the time exposure should be limited to avoid toxicity and larvae mortality. For this reason, the larvae were exposed in an acute treatment of 180 minutes before the behavioural assay in all the experiments. Two different concentrations, 1mM as sub-optimal non-epileptic concentration, and 3mM as

pro-convulsant concentration (Baraban et al., 2005; Yang et al., 2017), were used in order to evaluate the sensitivity to its effects of the different studied crispants. The experiments were performed in 96 square well-plates (Cytiva, Cat #: 7701-1651). The used paradigm in this set of experiments was constituted by one approach to evaluate locomotor alterations and spontaneous seizures during a continuous light period. The approach consists of 15 minutes of continuous light. To allow the habituation of the larvae to the plate, they were plated at least 3 hours before the behavioural recording and all the tests had a 10-minute dark acclimatation phase inside the recording chamber.

Analogously with the previous behavioural experiments, different plate distributions were used in order to have different epilepsy-associated genes and the negative control scrambled.

6. Behavioural analysis

In light-induced behaviour experiments, locomotion during the dark and light was evaluated, and the total distance moved (mm) both cumulative along the experiment and per minute was analysed. To describe the presence of epileptic crisis, the maximum speed (mm/s) reached by the larvae and the number of turns performed the 2 seconds following a light flash were analysed. In order to obtain a complete picture of the behaviour of the studied crispants, five different light flashes were performed, distanced one minute from each other, to perform five different triggers (or replicates) per experiment. For the final analysis, the mean of the responses of the five different flashes were evaluated.

In pharmacological epilepsy behaviour experiments, the maximum speed (mm/s) reach by the larvae during the experiment was evaluated, analysing the presence of spontaneous epileptic events along the recorded time.

Statistical significance was evaluated using a one-way ANOVA comparing the different crispants with the negative control in their plate, or t-test if the comparisons were only between two conditions. The significance was considered at $p\text{-value}<0.05$.

7. Principal component analysis and Mahalanobis Distance calculations

Multivariate data analysis (principal component analysis, PCA-2D) was used to assess differences in behavioural analysis among all observations. Kinematic variables were collected from the performed behavioural experiments, after the flash-light induction, flash experiments such as maximum acceleration, maximum velocity, highly mobile, mobile, mobility body percentage, turn angle number and immobile values for each larva. PCA shows linear combinations of the variables that maximally explain the total variance of the dataset. We take only variables with a contribution above a certain threshold (squared distance of the observation to the origin, cos2 >0.75) were considered. For comparison purposes, quantile transformation was applied to filter observations below a kinematic threshold ('colMoving'). Batch effect has been tested for experiment date, replicates, flash number and other technical differences, showing no significant differences.

To measure differences in flash behaviour activity, we applied a statistical test of variance called Mahalanobis distance (MD) on the PC plot. MD measures how distant a point is from the centre of a multivariate normal distribution. Mahalanobis distances can be converted into probabilities using a chi-squared distribution and a significance level might be specified (Charu C. Aggarwal, 2017). It is commonly applied in multivariate anomaly detection by defining two parameters, a distance magnitude (MD) and a p-value as a statistical measure to validate a hypothesis (outliers, p-value < 0.05). Using a histogram of the MD values (density plot) we detect a threshold was defined between two distributions of main variances, with an MD > 2 and p value < 0.15 for the samples with the highest variance. Binomial test showed a high statistical difference between the number of crispants in the high variance region compared to scrambles (the proportion of crispants is 0.063 greater than expected for scrambles 0.04; p value < 0.001).

The R v4.2 software program was used for statistical computing and graphics.

8. Pharmacology with antiepileptic compounds

The different compounds (Topiramate (Sigma-Aldrich, Cas #: 97240-79-4), Valproic acid (Sigma-Aldrich, Cas #: 1069-66-5) and Fenfluramine (Cymit quimica, Cas #: 458-24-2) were dissolved in DMSO (dimethylsulfoxide, MRI Global, Cas #:67-68-5) to 100mM stock solutions, were stored at -20^{o}C until used and treatment solutions were freshly prepared before each experiment.

Some of the tested drugs, such as Topiramate and Valproic acid, are known to have potential teratogenic and toxic effects (DeOliveira-Mello et al., 2023; Lai et al., 2017; Rajesh et al., 2020), so the time exposure to these compounds should be limited. Different publications using the above-mentioned compounds show different concentrations and incubation times (Baraban et al., 2013; Dinday & Baraban, 2015; Grone et al., 2017; Moog & Baraban, 2022; Zhang et al., 2015). The compounds were tested only in some of the epileptic childhood crispants that showed an epileptic phenotype.

The different doses and treatment times used are the following:

- Topiramate: 50µM and 100µM, treatment 180' before the behavioural assay.
- Valproic acid: 50µM and 100µM, treatment 180' before the behavioural assay.
- Fenfluramine: 17,5µM and 35µM, treatment 24h before the behavioural assay.

9. Statistics of the pharmacology

In order to compare light flash kinematic between crispants and treated-crispant larvae samples, the binomial or Fisher's exact (smallest sample sizes) tests for binary sampling statistics were applied. Highest variance compared to low variance samples proportions based on Mahalanobis metrics was assessed for each dose and treatment between treated-crispants and crispants observations. Crispants were also tested against scrambled larvae as a reference.

Results

Chapter 1:
Generation of GRIN-related disorders models and deep endophenotypic evaluation

1. Study of *grin* genes expression pattern in the zebrafish larvae

The expression of NMDAR has been extensively studied in humans, but the knowledge in zebrafish is still limited (Cox et al., 2005; Zoodsma et al., 2020). Our first objective was to characterise *grin* genes expression patterns in this animal model. The findings will be compared to GRIN genes expression in humans. Given the main function of the NMDAR in the central nervous system (CNS), we hypothesised that the main expression in zebrafish would be also in the CNS, but also including other important tissues, as previously reported also in humans (Hogan-Cann & Anderson, 2016).

To address this objective, we characterised the spatio-temporal expression pattern of *GRIN1, GRIN2A* and *GRIN2B* zebrafish orthologs, by means of whole-mount *in situ* hybridisation using specific riboprobes. The experiments were performed along different developmental stages, from 24 hours post-fertilisation (hpf) to 120 hpf, every 24 hours (Figure 14).

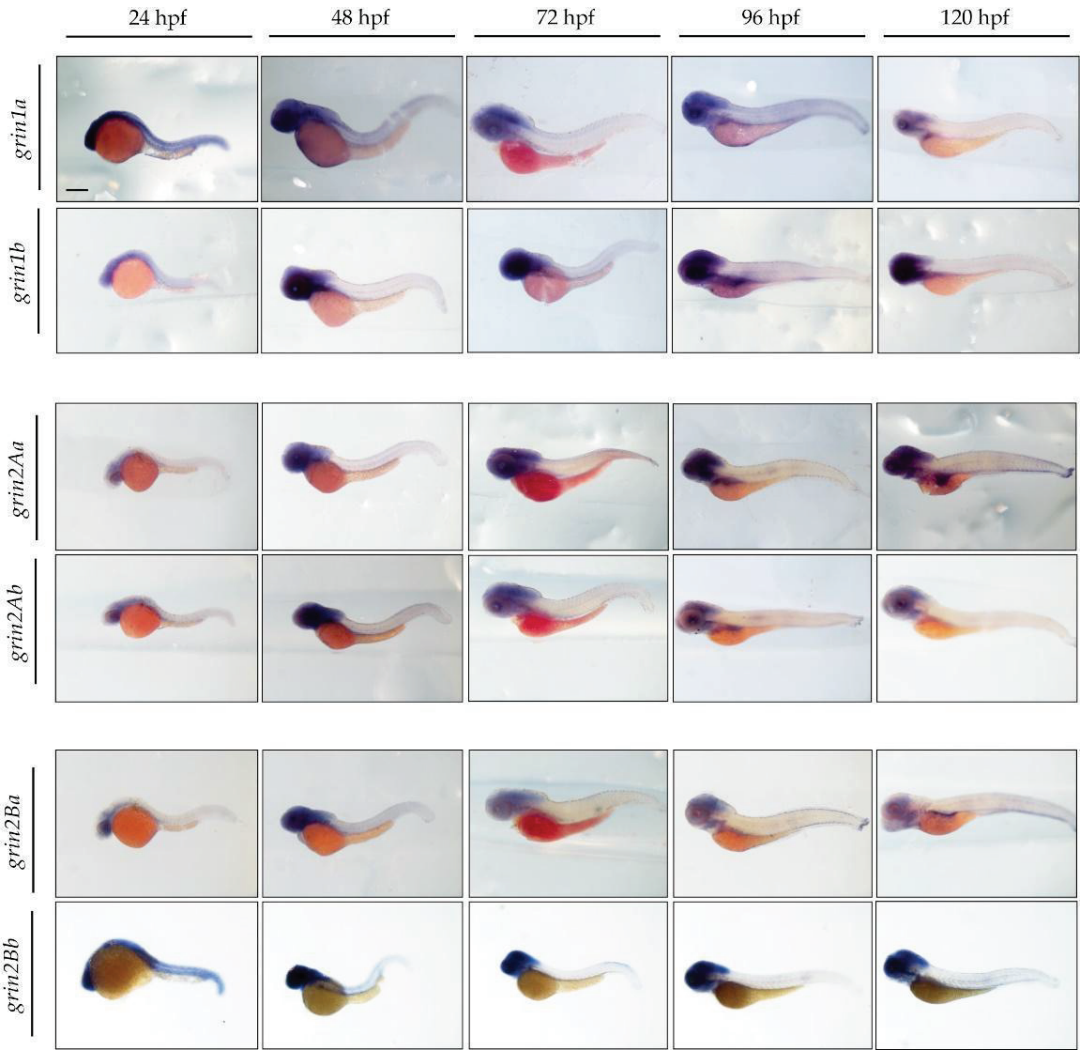

Figure 14. Zebrafish *grin* genes spatio-temporal expression. Whole-mount *in situ* hybridisation images of developmental stages from 24 hpf to 120 hpf, describing their spatio-temporal expression. Scale bar = 300µm.

Our results showed that *grin* genes are widely expressed in the CNS in early stages. Upon 48 hpf, *grin* genes expression decreases in the spinal cord, while expression in the CNS, retina and, interestingly, the gut, is increased.

Additionally, with the objective to describe more in detail the expression of *grin* genes, 120 hpf larvae were used to investigate *grin1a* and *grin1b* (encoding for the GluN1 obligatory subunit of the NMDAR) expression pattern. Using the zebrafish University College London brain map as reference (http://zebrafishucl.org/brain-regions), we observed that both *grin1a* and *grin1b* are widely expressed through the forebrain, midbrain, hindbrain and retina (Figure 15).

Specifically, despite its ubiquitous brain expression, *grin1a* (Figure 2A-C) is strongly enriched in specific forebrain areas including the olfactory bulb (OB), dorsal (D) and ventral (V) telencephalon, habenulae (Hb), thalamus (Th), prethalamus (PTh), pretectum (PrT) and hypothalamus (Hyp). The expression is also clear in midbrain areas, e.g. tegmentum (Teg), optic tectum (OT) and torus semicircularis (TS). In the hindbrain we also observe expression in the cerebellum or cerebellar plate (Ce), and milder expression in the medulla oblongata (MO).

On the other hand, *grin1b* (Figure 2D-E) is also expressed in the forebrain and midbrain areas, but with a less specific expression in the olfactory bulb and the thalamic regions. Interestingly, the expression is lower in the cerebellar plate (Ce) and there is no expression in the medulla oblongata (MO). Additionally, we also observe a mild expression of *grin1b* in the liver (L).

Furthermore, both *grin* genes are also expressed in the gastrointestinal tract (G), in accordance with what has been observed in humans. This expression could be associated with some of the gastrointestinal alterations observed in GRD patients.

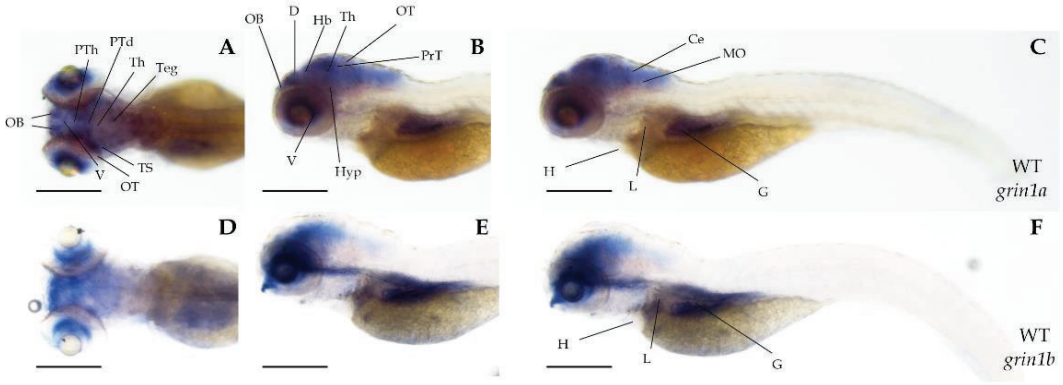

Figure 15. *grin1a* and *grin1b* expression in the CNS, in the retina and in the gut. Whole-mount *in situ* hybridisation images of 120hpf wild-type animals, illustrating the expression pattern of *grin1a* (A - dorsal, B – lateral, and C – lateral whole larvae) and *grin1b* (D - dorsal, E – lateral, and F – lateral whole larvae). Abbreviations: cerebellar plate (Ce), dorsal telencephalon/pallium (D), habenulae (Hb), hypothalamus (Hyp), olfactory bulb (OB), optic tectum (OT), pretectum (PrT), posterior tuberculum dorsal part (PTd), prethalamus (PTh), medulla oblongata (MO), tegmentum (Teg), thalamus (Th), torus semicircularis (TS), ventral telencephalon/subpallium (V), heart (H), liver (L) and gastrointestinal tract (G). Scale bars = 300µm.

In the retina (Figure 16), we observed a differential but complementary expression of both *grin* paralogs. The *in situ* images have been compared to an histological image of the retina in order to define the specific regions where the genes are expressed. Expression of *grin1a* was observed in the ciliary marginal zone (CMZ), the retinal ganglion cell layer (GCL), and in the area containing the inner plexiform layer (ipl). Interestingly, *grin1b* expression starts also in the area containing the ipl sharing expression with *grin1a*, and the inner nuclear layer (INL). *grin1a and b* expression was not observed in the lens, the outer plexiform layer (opl), the outer nuclear layer (ONL) or the retinal pigmented epithelium (RPE).

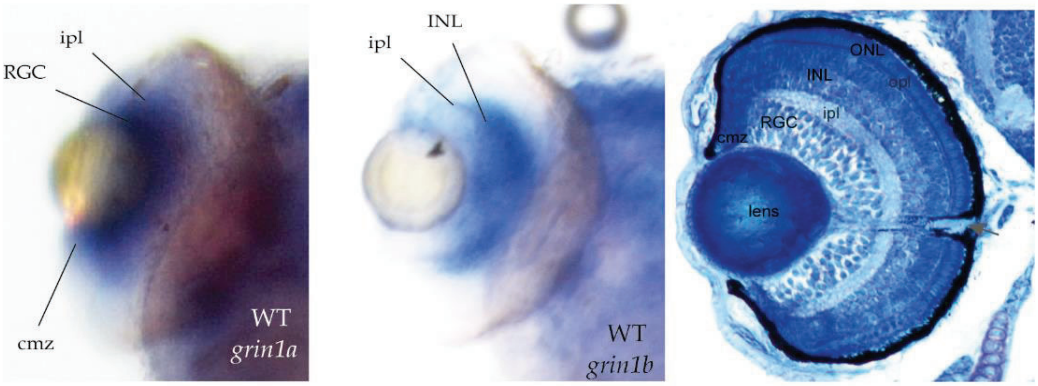

Figure 16. E**xpression of *grin1* genes in the retina**. Representative images of retina obtained from the whole mount *in situ* hybridisation samples, compared with a histology image where the different layers of the retina are represented. Reference image from zebrafish UCL brain atlas. Abbreviations: ciliary marginal zone (CMZ), retinal ganglion cell layer (GCL), inner plexiform layer (ipl), inner nuclear layer (INL), outer plexiform layer (opl), outer nuclear layer (ONL), retinal pigmented epithelium (RPE).

Both in dorsal and lateral views of 120 hpf larvae (Figure 15 and figure 16), we detected a complementary expression between *grin1a* and *grin1b* in different areas of the retina, suggesting different functions of the expressed proteins.

To summarise, our data confirms the conserved expression pattern of all the studied zebrafish *grin* genes, sharing a similar expression pattern with the human orthologs. This suggests that the function might also be conserved but divided between the two different paralogs of each *grin* gene. Therefore, both paralogs for each gene must be studied independently to better characterise their individual function.

2. Pharmacological characterisation of different NMDAR modulators to validate the experimental design

Patients with GRIN-related disorders present a wide variety of symptoms, and these may appear in a wide range of severity, including Intellectual Disability, Autism Spectrum Disorder, Cortical visual impairment, developmental delay, epilepsy, hypotonia, microcephaly, movement disorders, speech disorders and schizophrenia among others. Among these symptoms, the most prevalent ones are the developmental delay, intellectual disability, motor symptoms and epilepsy (García-Recio et al., 2021; Gjerulfsen et al., 2024; Platzer et al., 2017; Strehlow et al., 2016).

2.1. Development of experimental pipeline to evaluate GRD alterations in the zebrafish

To determine if the zebrafish is a valid animal tool to model GRD, we first designed a series of behavioural paradigms specifically adapted to the main symptoms described in patients that could be also analysed in 120 hpf zebrafish larvae. Namely, developmental delay, intellectual disability, motor symptoms and epilepsy.

In reference to standardised paradigms available in the literature, along with the experience of the laboratory, the proposed protocol to evaluate possible alterations in GRD models consists of three distinct phases: the locomotor activity assessment in dark/light transitions, the response and habituation to sensorial stimuli and the light-induced epileptic behaviour (see Materials and Methods).

The Dark/Light paradigm was employed to evaluate parameters related to the locomotion and behaviour of the larvae. The evaluated parameters were the pattern graphed by the locomotion measured by the distance moved (mm) in one-minute time bin, the difference off the distance moved (mm) in the transitions phases, changes from dark to light and vice-versa, the distance travelled (mm) in the dark and light phases separately and the total distance travelled (mm), along with the previously mentioned thigmotaxis (percentage of time in the area).

Additionally, it has been suggested that the Dark/Light cycles produce certain behaviours related with stress brought on by the changes from dark to light and vice versa (Q. Li et al., 2015). Therefore, the thigmotaxis of the larvae was also evaluated, in accordance with behaviours described in GRD patients. Thigmotaxis is described as an

index of their state of anxiety. In normal conditions, larvae tend to move more time in the outer area of the arena, close or in contact with the well walls, rather than in the central area, but with some exploration. High anxiety levels increase the time spent in the outer area of the well, while in anxiolytic behaviours the time exploring the centre of the well increases (Simon et al., 1994).

The tapping evaluation was evaluated to determine differences in habituation or non-associative learning deficits in early stages of the development. Two different responses were evaluated: the response to the first tap, both in a quantitative (mm) and a qualitative (percentage of larvae responding) manner, and the time (s) it took to every larva to habituate to the tactile stimuli. A second set of tapping, fifteen minutes apart, was also evaluated, analysing the same parameters. Finally, the response in both tapping sets was compared to understand if there was establishment/disruption of memory in a brief spaced time. To finalise, a set of light-flashes was performed with the objective to describe light-sensitivity or light-related epileptic behaviour. According to the literature, the main parameters that may be analysed related with an epilepsy-like behaviour or convulsant pattern, are the maximum speed achieved (mm/s) and the number of bouts or acute—angle turns performed, measured the two seconds immediately after the light flash (Baraban et al., 2013). A set of five different flashes was performed to increase the replicates of a short and specific paradigm. The average of the five flashes was analysed. Moreover, the existence of a habituation or desensitisation to the response was also evaluated by analysing the five flashes independently. In case of habituation to the stimulus, only the response to the first flash was considered.

2.2. *Characterisation of MK-801, a pharmacological model for GRD loss-of-function*

In the research of NMDAR, the use of the non-competitive antagonist (+) MK-801 maleate or dizocilpine, commonly named MK-801, is widely used as a pharmacological model of loss-of-function of the receptor.

In zebrafish, the MK-801 has also widely been used to model schizophrenia, as it disrupts the glutamatergic system. In 2022, R. Benvenutti elegantly reviewed the use of different NMDAR antagonists in different behavioural studies with zebrafish, where MK-801 played a significant part (Benvenutti et al., 2022).

Despite the different studies performed in mammals and in zebrafish, the dosage, timing and effect of MK-801 does not seem to be established in the latest. For this reason, we first decided to perform a Fish Embryo Toxicity Test (FET, OECD guideline 236) to determine the maximum tolerated concentration. 96 hpf larvae were treated with different concentrations of MK-801, and the mortality and toxicity were assessed at 120 hpf. The doses used were 0,1µM, 1µM, 10µM, 100µM and 1000µM. The benchmark dose (BMD) was calculated using PROAST software (National Institut for Public Health and the Environment, https://proastweb.rivm.nl/) and set at LC10, obtaining different outputs from the fitted models. Moreover, the survival rate was graphed as a survival percentage (Figure 17F). The BMD confidence interval was calculated between 34.8µM and 136µM.

According to the obtained data, and the previously published studies in zebrafish using zebrafish both in larval and adult stages, we performed a dose-response experiment with a wide range of concentrations. Furthermore, we adjusted the time of exposure at 3 hours before the behavioural assay to evaluate behavioural alterations caused by the MK-801 effect and avoid the effects caused by the possible toxicity derived from long time exposure.

With this aim, concentrations close to the calculated BMD along with saturating concentrations were used. The selected doses were 25µM, 50µM, 100µM, 200µM and 500µM, and were compared with untreated controls from the same experimental batch. After 3 hours of treatment, the custom designed protocol was used, and data were analysed and graphed using Graphpad software.

2.2.1. Evaluation of locomotor alterations upon MK-801 exposure

Inside the recording chamber, and in response to dark/light transitions, it is described in the literature that larvae should move more in dark phases, and transitions to a reduced movement in light phases, generating a cycling movement pattern (Peng et al., 2016), as can be observed in the E3 control larvae. When analysing the locomotor activity in the MK-801 treated larvae, the main alteration observed is related with the dark/light cycles and transitions. In all the concentrations and transitions, a significant impairment in the transitions was observed (Figure 17A-C). Considering the locomotion per one-minute time bin display, a lack of response to the change of cycle, both from dark to light and from light to dark, is observed in all the concentrations when compared with

the medium embryo E3 treated controls (Figure 17A). When observing these transitions in more detail, by measuring the difference of the distance moved in the transition periods, we confirm the lack of transition behaviour in a significant manner (Figure 17C). These alterations could be related with a deficit in the perception of external visual cues and/or to the motor response to those cues.

When analysing the total locomotion, hypolocomotion was observed in all the MK-801 tested concentrations (Figure 17D), manifesting a possible alteration in the signal transmission to the muscle tissue.

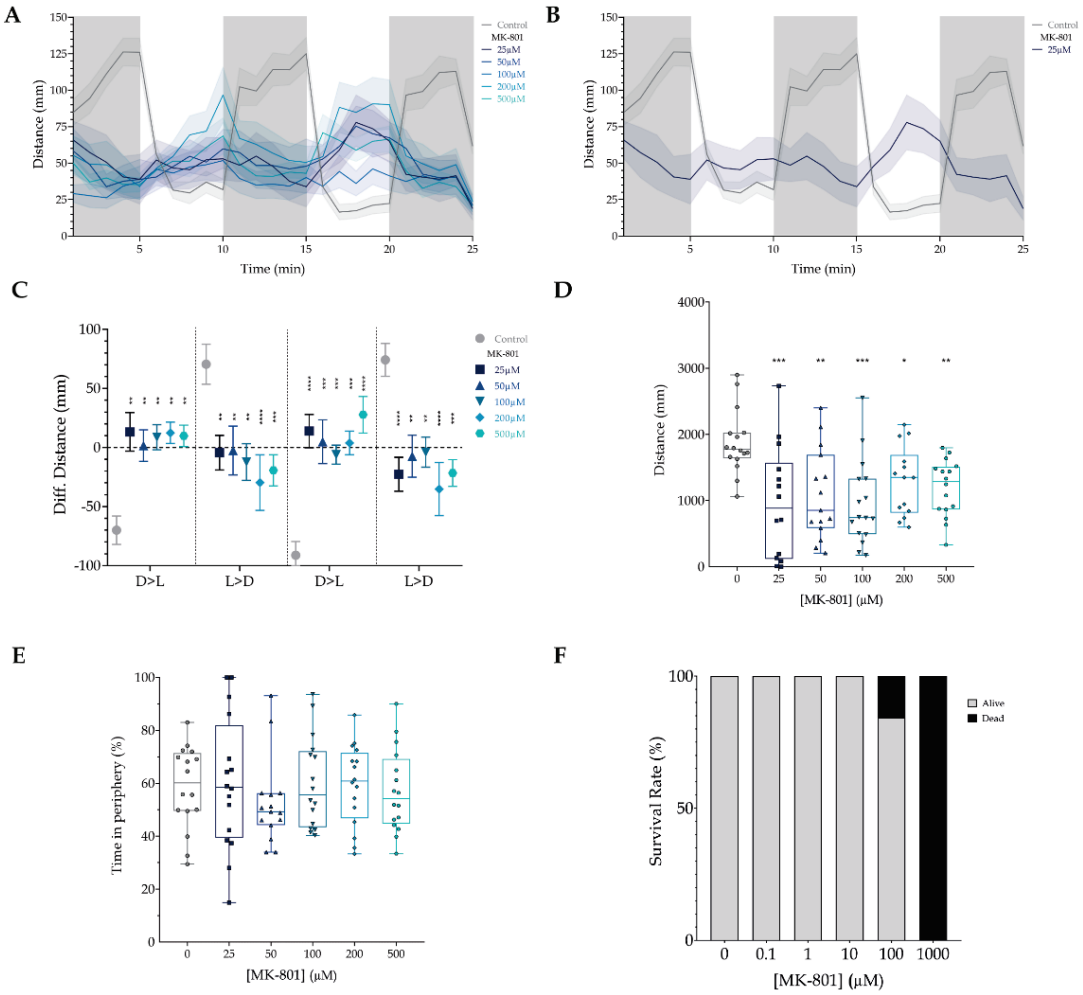

Figure 17. Evaluation of locomotor behaviour of MK-801 acute treated larvae. A. Dose-response effect of MK-801 on locomotion activity (distance travelled) in one-minute time bin. B. Graph of the distance moved in one-minute time bin of 25µM MK-801 as a representative example of the locomotion. C. Graph representing the difference in the distance moved between the different cycle changes. D. Graph of the quantification of the total distance moved (mm) during the dark/light cycles phase. E. Representation of the time (%) spent in the periphery of the well, a measurement of the thigmotaxis during the dark/light cycles. F. Graph representing the survival rate in all the tested concentrations of MK-801 in a 24-hour exposure in 96 hpf larvae. Control is represented in grey; different concentrations of MK-801 are represented in blue shades. In panels A, B and C, data is represented as mean ± SEM; in panels D and E, data is represented with box and whisker plots, showing the median, minimum and maximum, showing all points. N=16 in all groups. *p<0.05 ** p<0.01, ***p<0.001, **** p<0.0001 (One-way ANOVA with Tukey's post-hoc analysis).

In conclusion, dark/light cycles showed a significant lack of responsiveness that changed the transitions between the various phase-changes. Additionally, a generalised hypolocomotion was described in all the tested MK-801 concentrations, manifesting the effects of pharmacological inhibition of the NMDAR.

2.2.2. *Analysis of MK-801 effect on the response and habituation to tapping tactile stimuli*

To evaluate the response and habituation to external stimuli, the tapping protocol was performed. Ten seconds before the tapping stimuli starts, along with the 30 seconds of tactile stimuli, were recorded and graphed in a one-second time bin with the objective to observe the baseline movement determined in the first ten seconds, the response to the first tap, and the habituation to the consecutive tappings. All the conditions were compared with the E3 control treated larvae from the same experimental batch. The graphs allowed the description of an increased response to the tapping in all the tested MK-801 concentrations (Figure 18A-B).

To characterise these responses, the response to the initial tap was quantified by measuring the difference moved by each larva, along the interval between before and after the first tap. We performed a quantitative analysis of the response, plotting the value of the difference in the movement performed 1 second before and after the first tap stimulus (Figure 18C). Compared with control larvae, MK-801-treated larvae showed a higher distance moved to the first tap, indicative of an increased response to tactile stimulus. In terms of tap-responding larvae, MK-801-treated specimens also showed a significant increase in number, in all the tested MK-801 concentrations (Figure 18C). Therefore, the observed increase in the response to the first taping was caused by both the increase of the distance moved as a response to the stimulus, and a higher number of responding larvae.

Besides the evaluated sensory and motor immediate responses, the continuous tapping paradigm allowed to measure the habituation —a form of synaptic-plasticity induced behaviour— that was experimentally quantified as the time to recover the basal activity (*i.e.* rest, baseline), despite the presence of a continuous stimulus. Under our experimental conditions, in contrast to the habituation observed for control larvae, MK-801-treated larvae showed the lack of habituation, in agreement with the role of NMDARs functionality for synaptic plasticity mechanisms (Figure 18D).

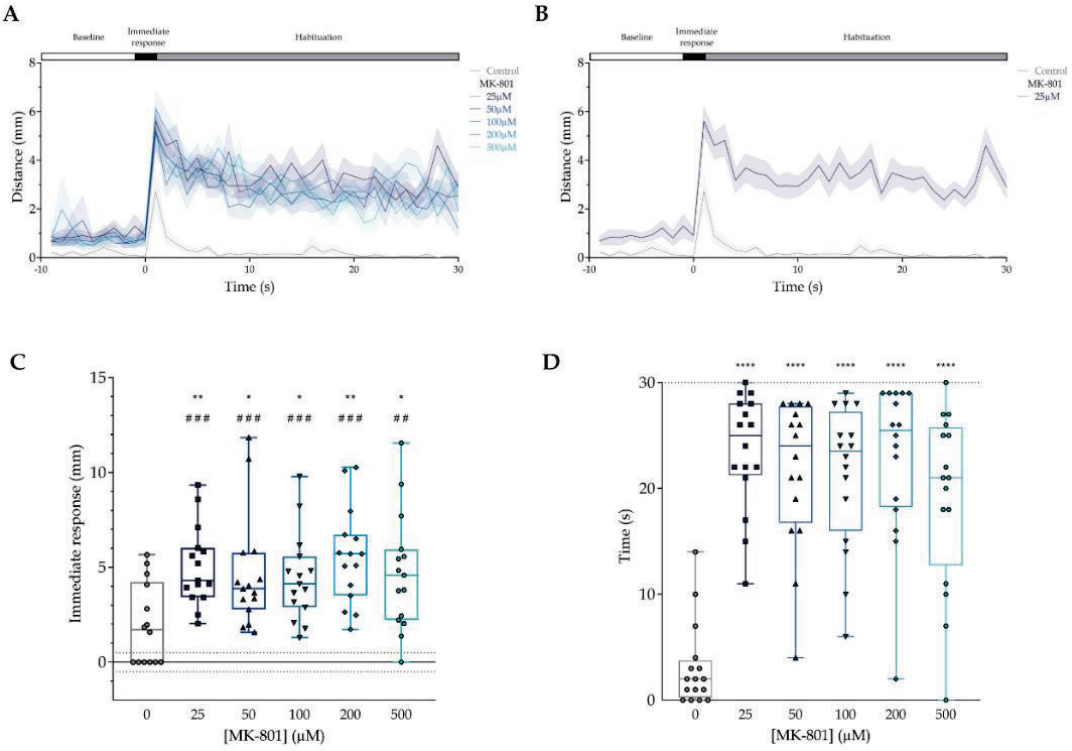

Figure 18. MK-801 exposure effects in the response and habituation to tactile stimuli. A. Dose-response effect of MK-801 on locomotor response (distance travelled) in one-second time. B. Graph of the distance moved in one-second time bin of 25µM MK-801 as a representative example of the tapping response. C. Graph representing the difference in the distance moved as a response to the first tap. Statistical analysis of the immediate response (mm) is represented with "*". Statistical analysis of the number of larvae responding (%) is represented with "#". *p<0.05, ** p<0.01 (One-way ANOVA). ##p<0.01, ###p<0.001 (Two-way ANOVA). D. Quantification of the habituation by measuring the time each larva takes to not respond to the stimulus, with a cut off at 30 seconds. In panels A and B, data is represented as mean ± SEM; in panels C and D, data is represented with box and whisker plots, showing the median, minimum and maximum, showing all points. N=16 in all groups. ****p<0.0001 (One-way ANOVA with Tukey's post-hoc analysis).

Following this initial tapping paradigm, the protocol was repeated fifteen minutes later. Similar results were observed, also describing an increased initial response to the stimulus and an impaired habituation to the continuous stimuli (Supplementary Figure 1). To evaluate an alteration in the habituation or non-associative learning between the fifteen minutes apart paradigms, all the responses were compared between the two different protocols (Supplementary Figure 2). There was no trace of habituation or learning between the first and second set of tappings, as evidenced by the lack of significant variations in any of the measures studied.

In conclusion, MK-801 caused an increased response and an impaired habituation to the tactile stimulus, while no differences in long-term habituation were detected in fifteen minutes-apart paradigms.

2.2.3. Epilepsy-like behaviour in response to light flashes upon MK-801 exposure

Application of light-flashes can trigger epilepsy in zebrafish larvae, which can be evaluated by analysing the resulting epilepsy-like behaviour. The main parameters related to epilepsy in locomotor behaviour are the maximum velocity (mm/s) achieved and the increase of sharp turns performed. Five different light-flashes were applied to increase the number of visualisations. Prior to analysing the effect of MK-801 on the response to flashes, we wanted to verify whether habituation occurred by applying five consecutive sets of flashes. No differences were observed in the maximum achieved velocity (Supplementary Figure 3) or the number of bouts (Supplementary Figure 4) in any of the MK-801 tested concentrations, describing a behaviour similar to the E3 control.

Having verified that all the larvae from each group equally behave in all the light-flashes, the different recordings were considered as different replicates. Therefore, an average of the five different measurements for each larva was calculated and compared with the other conditions. As a result, no significant differences were observed after MK-801 treatment when compared to the E3 controls (Figure 19).

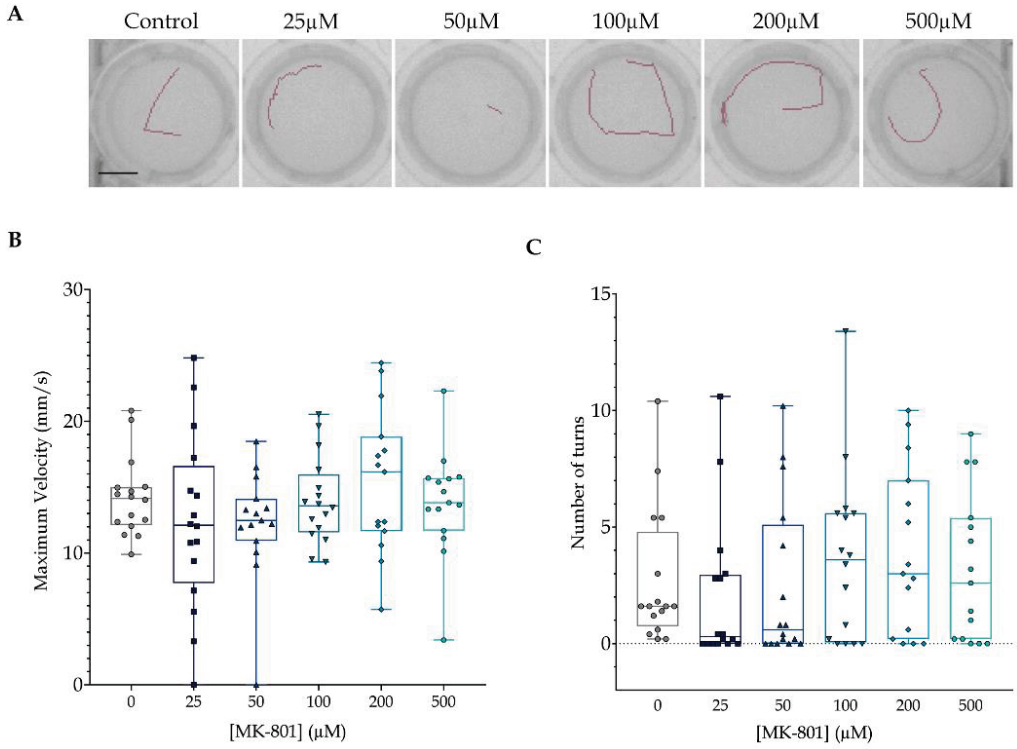

Figure 19. Evaluation of epilepsy-like behaviour of MK-801 treated larvae in response to light flashes. A. Representative images of the tracking of single larvae, recorded 2 seconds after the first applied flash. Scale bar = 6mm. B. Measurement of the maximum velocity (mm/s) achieved, the average of the five trials of all the tested MK-801 concentrations. C. Measurement of the total number of angle turns performed, comparing the average of the five trials of all the tested MK-801 concentrations. In panels B and C, data is represented with box and whisker plots, showing the median, minimum and maximum, showing all points. N=16 in all groups. (One-way ANOVA with Tukey's post-hoc analysis).

In conclusion, MK-801 treated larvae only show a mild decrease in the lower concentration, that can be classified as a lack of response, or a non-convulsant response. Overall, MK-801 treated larvae do not show an epilepsy-like behaviour in response to light flashes.

To summarise these data, the acute treatment with MK-801 showed the presence of GRD-like behavioural phenotypes, including locomotor alterations, the lack of response in the dark/light cycles suggestive of potential visual problems, and increased sensory response and decreased habituations in response to tactile stimulus. While not fully recapitulating the complexity of GRD clinical spectrum (no effects on flash induced-epilepsy), the observed GRD-like alterations supports MK-801 acute treatment of zebrafish larvae as a pharmacological model of GRD loss-of-function.

2.3. Characterisation of D-Serine effect on zebrafish larvae

D-Serine is the endogenous co-agonist of NMDA receptors, and the administration of its natural precursor L-serine has been shown by our group and others to ameliorate the clinical symptoms of patients harbouring *GRIN* loss-of-function variants (Den Hollander et al., 2023; Juliá-Palacios et al., 2024; Krey et al., 2022; Soto et al., 2019). Accordingly, we aimed to decipher the function of D-serine in zebrafish larvae and to evaluate its potential use as a pharmacological model of acute GRIN gain-of-function.

In contrast to MK-801, D-Serine effects in zebrafish have been only barely investigated. Therefore, the dosage, exposure time and effect of the compound in zebrafish larvae has not been described. For this reason, we decided to perform a Fish Embryo Toxicity Test (FET, OECD guideline 236) to determine the maximum tolerated concentration. Ninety-six hours post-fertilisation larvae were treated with 0,1µM, 1 µM, 10µM, 100µM and 1000µM D-serine, and the mortality and toxicity were assessed at 120 hpf. The BMD was calculated using PROAST software and set at LC10, obtaining different outputs from the fitted models. Moreover, the survival rate was graphed as a survival percentage (Figure 20F). Importantly, D-Serine administration showed an excellent tolerability, and the lack of mortality after 24h exposure resulted on the impossibility to calculate the BMD.

Once the toxicity assays were performed, we aimed to unveil D-Serine behavioural effects in zebrafish larvae. According to these data and previous works with mice and cellular systems, we performed a dose-response experiment using a wide range of high D-Serine concentrations (100µM, 200µM, 500µM, 1000µM and 2000µM), with a fixed exposure time of 3 hours, as for MK-801 experiments.

2.3.1. Evaluation of locomotor alterations upon D-Serine exposure

D-Serine dose-response effect on larvae locomotor activity was assessed with the dark/light test. Despite no significant alterations were detected neither along the dark/light cycles nor in the transitions (Figure 20), mild changes in the movement pattern (dark/light cycles per-minute analysis) were noticed (Figure 20A-C). Dose-response experiments showed a bell-shaped effect of D-Serine, with the locomotion activity reduced at low and high D-Serine concentrations (100µM and 2000µM), whereas intermediate D-Serine concentrations (200µM and 500µM) increased locomotion in the per-minute representation as well as in the total locomotion analysis (Figure 20D).

Besides these subtle changes, no significant differences were detected either in the transitions of the different dark and light phases (Figure 20C) or in the total locomotion quantification (Figure 20D), and thigmotaxis index was not affected by D-Serine exposure (Figure 20E).

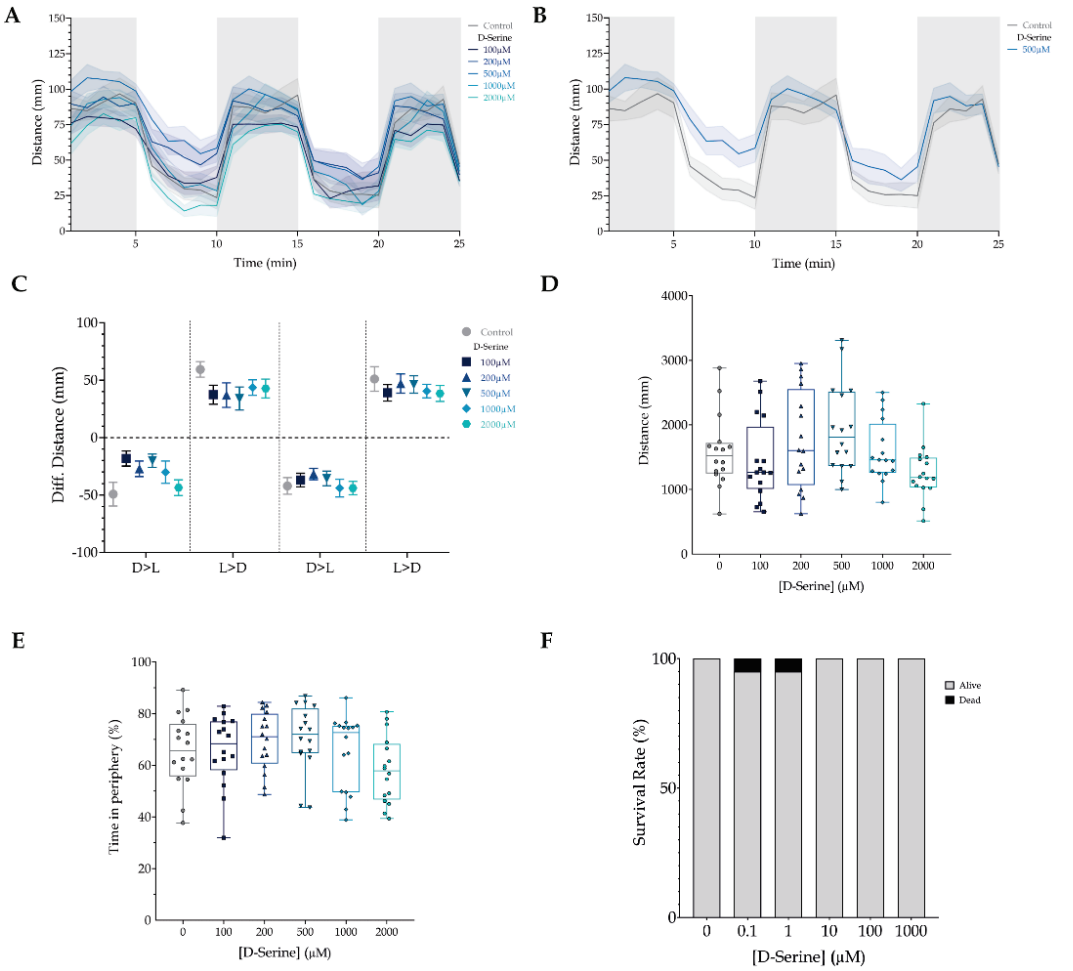

Figure 20. Evaluation of locomotor behaviour of D-Serine acute treated larvae. A. Dose-response effect of D-serine on locomotion activity (distance travelled) in one-minute time bin. B. Graph of the distance moved in one-minute time bin of 500µM D-Serine as a representative example of the locomotion. C. Graph representing the difference in the distance moved between the different cycle changes. D. Graph of the quantification of the total distance moved (mm) during the dark/light cycles phase. E. Representation of the time (%) spent in the periphery of the well, a measurement of the thigmotaxis during the dark/light cycles. F. Graph representing the survival rate in all the tested concentrations of D-Serine in a 24-hour exposure in 96 hpf larvae. Control is represented in grey; different concentrations of D-Serine are represented in blue shades. In panels A, B and C, data is represented as mean ± SEM; in panels D and E, data is represented with box and whisker plots, showing the median, minimum and maximum, showing all points. N=16 in all groups. *p<0.05 ** p<0.01, ***p<0.001, **** p<0.0001 (One-way ANOVA with Tukey's post-hoc analysis).

2.3.2. *Analysis of D-Serine exposure effect on tactile response and habituation*

As previously stated, to analyse the habituation and non-associative learning, larvae were exposed to a set of thirty consecutive taps or tactile stimuli. Similar to the dark/light results, the analysis to the response to the habituation paradigm did not show any appreciable variations in any of the tested concentrations of D-Serine (Figure 21).

After analysing both, the response to the first tap (Figure 21C), and the habituation to the continuous stimulation (Figure 21D), no differences were observed among the groups. Therefore, the administration of these doses of D-Serine did not alter the perception and habituation to external tactile stimuli.

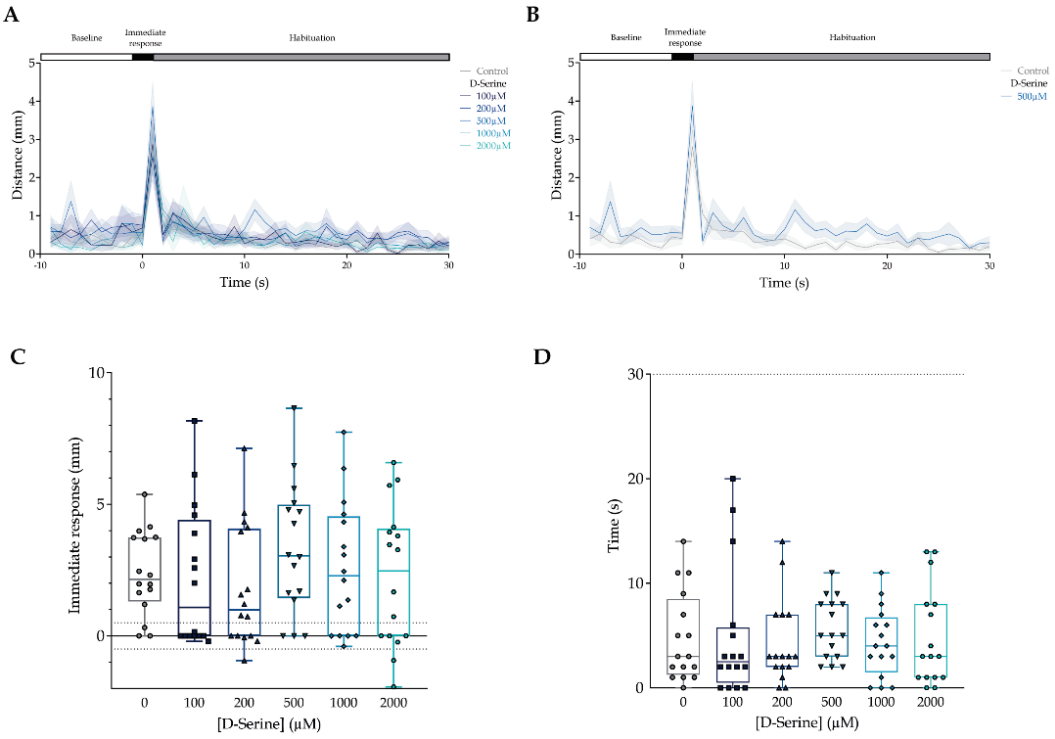

Figure 21. Response and habituation to tactile stimuli after D-Serine exposure. A. Dose-response effect of D-Serine on locomotor response (distance travelled) in one-second time. B. Graph of the distance moved in one-second time bin of 500µM D-Serine as a representative example of the tapping response. C. Graph representing the difference in the distance moved as a response to the first tap. D. Quantification of the habituation by measuring the time each larva takes to not respond to the stimulus, with a cut off at 30 seconds. In panels A, B and C, data is represented as mean ± SEM; in panels D and E, data is represented with box and whisker plots, showing the median, minimum and maximum, showing all points. N=16 in all groups. (One-way ANOVA with Tukey's post-hoc analysis).

As performed with MK-801, to determine whether the stimulus response and/or the habituation curve was maintained over time, a second set of tappings was performed 15 minutes after the initial tapping series. As for the first tapping set, no alterations were observed after D-Serine exposure (Supplementary Figure 5). Furthermore, no differences between the two paradigms were observed (Supplementary Figure 6). Overall, these findings showed that D-serine exposure do neither affect the tactile response nor the habituation to this particular sensory system.

2.3.3. D-Serine exposure effect on light flashes-induced epilepsy-like behaviour

Zebrafish larvae were exposed to D-Serine and submitted to light-induced epileptic behaviour paradigm. Compared to non-treated larvae, no differences in the maximum velocity and the number of angle turns were observed in D-Serine-treated larvae (Supplementary Figure 7 and 8, respectively). These data showed that D-Serine did not result in habituation to light flashes. Since no changes on light flashes-induced movements were observed along trials (for each experimental group), the different recordings were considered as different replicates and the average of the five measurements for each larva was calculated. Again, no differences between groups in the maximum velocity achieved and in the number of bouts were observed in response to light flashes (Figure 22). Overall, D-Serine treated larvae did not show an epilepsy-like behaviour in response to light flashes.

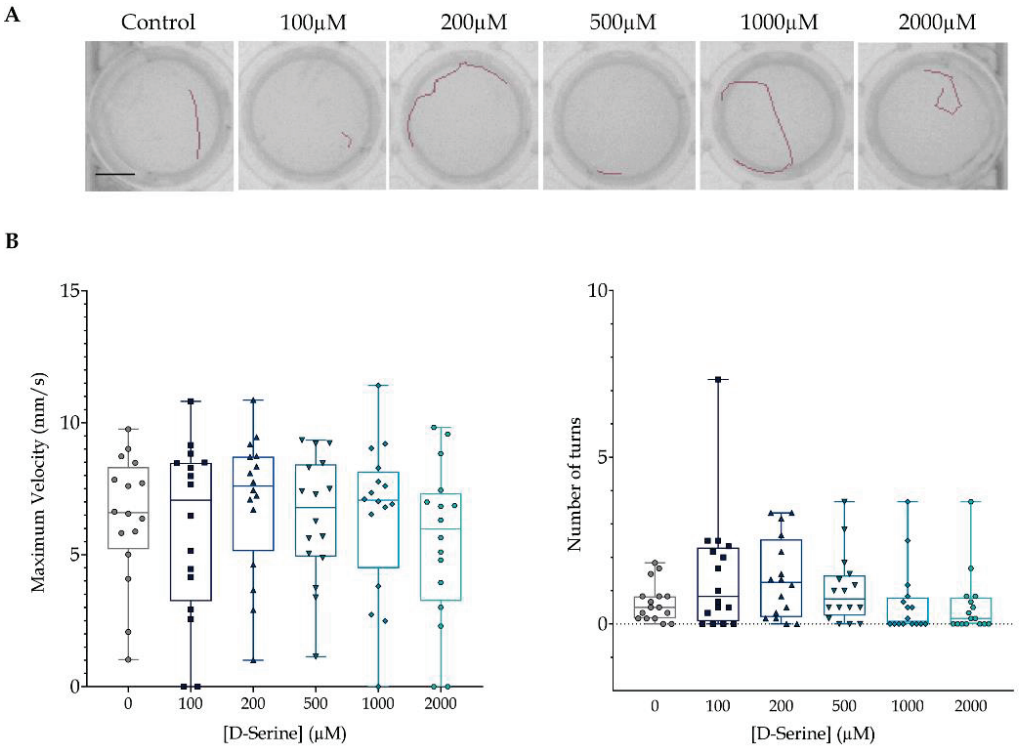

Figure 22. Light-induced epilepsy-like evaluation after D-Serine exposure. A. Representative images of the tracking of single larvae, recorded 2 seconds after the first applied flash. Scale bar = 6mm. B. Measurement of the maximum velocity (mm/s) achieved, comparing the average of the five trials of all the tested D-Serine concentrations. C. Measurement of the total number of angle turns performed, comparing the average of the five trials of all the tested D-Serine concentrations. In panels B and C, data is represented with box and whisker plots, showing the median, minimum and maximum, showing all points. N=16 in all groups. (One-way ANOVA with Tukey's post-hoc analysis).

Overall, our findings showed that D-Serine acute treatment is well tolerated and does not provoke significant changes in the activity, tactile response/habituation and epilepsy-induced paradigms. These data are in line with previous studies showing that, in a neurotypical scenario D-Serine administration does mildly enhance some neural functions, but does not generate neurotoxicity or pathogenic responses. Consequently, our results indicate that in our experimental paradigms, D-serine treatment does not represent a pharmacological model of GRD gain-of-function.

2.4. Characterisation of Spermine effect on zebrafish larvae

Likely D-Serine, the study of Spermine toxicology, metabolism and physiology is scarce in the zebrafish model. Therefore, the Fish Embryo Toxicity Test (FET, OECD guideline

236) to determine the maximum tolerated concentration was conducted. Ninety-six hours post-fertilisation larvae were treated with Spermine (0,1µM, 1 µM, 10µM, 100µM and 1000µM), and the mortality and toxicity were assessed at 120 hpf. The survival rate was graphed as a survival percentage (Figure 23F), and the calculated BMD confidence interval was between 1.08µM and 6.06µM.

According to the obtained data and the previous work with mice and cellular systems, we performed a dose-response experiment with a wide range of concentrations. Furthermore, we adjusted the time of exposure at 3 hours before the behavioural assay in accordance with and consequently to the toxicity observed in the MK-801 experiments. The objective was to observe behavioural alterations caused by the Spermine treatment and avoid the effects caused by the possible toxicity for long time exposure.

With this aim and considering the observed toxicity concentrations close to the calculated BMD and saturating concentrations were used. The selected doses were 0.1µM, 1µM, 10µM, 100µM and 200µM, and were compared with untreated controls from the same batch. After 3 hours of treatment, the custom designed protocol was performed.

2.4.1. Evaluation of Spermine exposure effects on locomotor activity

The analysis of the locomotor activity after Spermine exposure unveiled alterations in the dark/light cycles pattern, showing a sustained increase of movement in dark phases in all the concentrations except the 0.1µM. Specifically in the higher concentrations, 100µM and 200µM, a pronounced increase in locomotion was observed the first minute in dark phases. Afterwards, the locomotion decreased to control values. Contrary, in the immediate lower concentration, 10µM Spermine, this reduction of the movement was not observed, and the increased locomotion during dark phases was sustained in all the cycles (Figure 23A-B).

These differences were quantified by analysing the transitions between light phases, describing significant differences only in the transitions from dark to light in the concentrations of 10µM, 100µM and 200µM (Figure 23C).

Upon the analysis of the total locomotion during the transitions, and similarly to what was observed after D-Serine treatment, a dose-response of hyperlocomotion was

described after Spermine exposure. This dose-response effect showed an increase in total locomotion, being significative at 10µM concentration, and going back to normal values at increasing concentrations (Figure 23D).

Upon the analysis of the total locomotion during the transitions, and similarly to what was observed after D-Serine treatment, a dose-response of hyperlocomotion was described after Spermine exposure. This dose-response effect showed an increase in total locomotion in a bell-shaped manner, being significative at 10µM concentration (Figure 23D). From the results of the dark/light transitions, we confirmed that the hyperlocomotion is caused by an increase of the movement during the dark phases. At higher concentrations, despite having the peak of locomotion after the transition, did not show significant differences when compared with the E3 controls (Figure 23C).

Furthermore, a significant increase of the thigmotaxis index (indicative of an increased anxiety behaviour), was observed at 100µM and 200µM (Figure 23E). This behaviour could be related to the peak of movement after the transitions from light to dark.

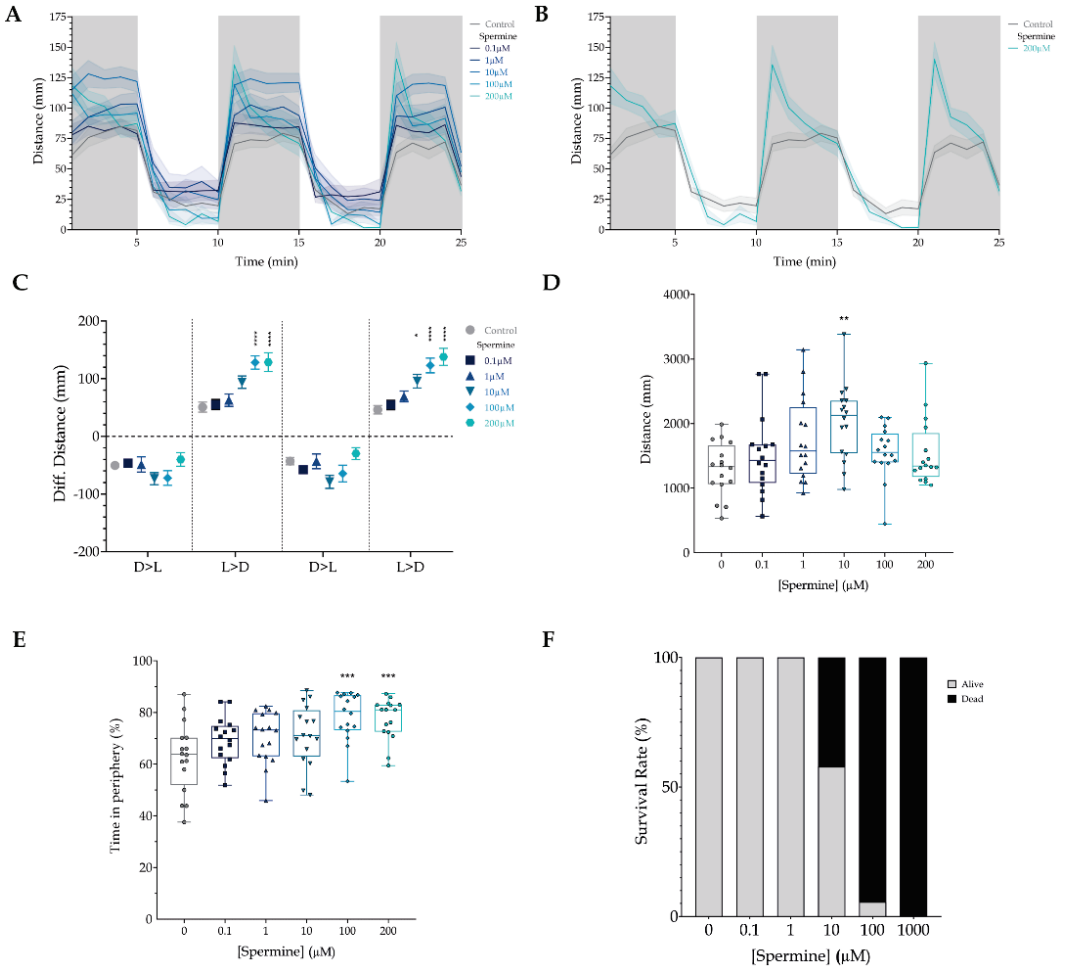

Figure 23. Analysis of the Dark/Light transitions observed after Spermine exposure. A Dose-response effect of Spermine on locomotion activity (distance travelled) in one-minute time bin. B. Graph of the distance moved in one-minute time bin of 200µM Spermine as a representative example of the locomotion. C. Graph representing the difference in the distance moved between the different cycle changes. D. Graph of the quantification of the total distance moved (mm) during the dark/light cycles phase. E. Representation of the time (%) spent in the periphery of the well, a measurement of the thigmotaxis during the dark/light cycles. F. Graph representing the survival rate in all the tested concentrations of Spermine in a 24-hour exposure in 96 hpf larvae. Control is represented in grey; different concentrations of Spermine are represented in blue shades. In panels A, B and C, data is represented as mean ± SEM; in panels D and E, data is represented with box and whisker plots, showing the median, minimum and maximum, showing all points. N=16 in all groups. *p<0.05 ** p<0.01, ***p<0.001, **** p<0.0001 (One-way ANOVA with Tukey's post-hoc analysis).

To conclude, we observed an increased mortality rate after 24 hours of Spermine treatment. After the adjustment of the doses and the dose exposure time, we observed alterations in the locomotion in a dose-related manner. Moreover, a disruption in the dark/light transitions from light to dark was described at 100µM and 200µM concentrations. Increased anxiety levels were also present in these concentrations. Overall, spermine exposure resulted in anxiety-related alterations of locomotion.

2.4.2. *Analysis of Spermine effect on tactile response and habituation*

The response to external tactile stimuli was evaluated using the tapping protocol. While low spermine concentrations did not affect the response to external tactile stimulus, high spermine concentrations (200µM) significantly disrupted tapping habituation (Figure 24A-B). More precisely, despite no differences of the distance moved and the number of responding larvae (Figure 24C), a significant increase in the habituation time was observed following 200µM Spermine treatment (Figure 24D). These data showed that, despite Spermine does not affect tactile sensitivity, high Spermine concentration alters habituation to tactile stimulation, a form of non-associative learning. Upon the second set of tapping (15 minutes later), similar results were observed (Supplementary Figure 9). In line with the previous results, a significant increase in the time responding to the tap was described at high spermine concentration, while no inter-series differences were detected (Supplementary Figure 10).

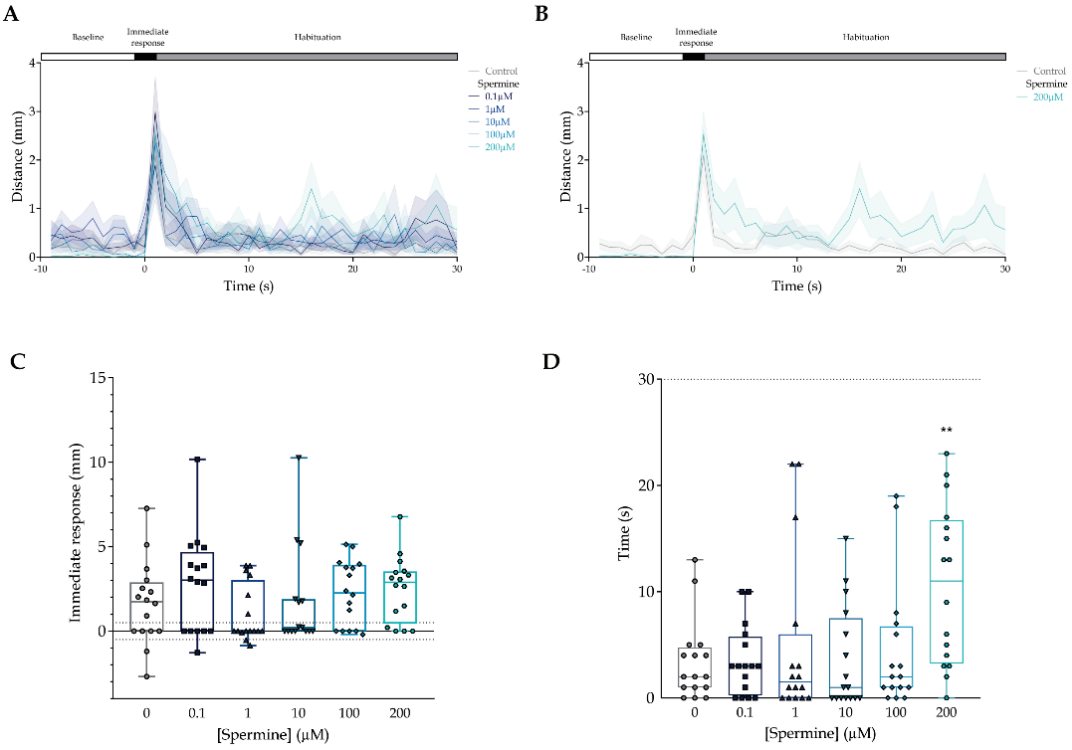

Figure 24. Response and habituation to tactile stimuli after Spermine exposure. A. Dose-response effect of Spermine on locomotor response (distance travelled) in one-second time. B. Graph of the distance moved in one-second time bin of 500µM D-Serine as a representative example of the tapping response. C. Graph representing the difference in the distance moved as a response to the first tap. D. Quantification of the habituation by measuring the time each larva takes to not respond to the stimulus, with a cut off at 30 seconds. In panels A, B and C, data is represented as mean ± SEM; in panels D and E, data is represented with box and whisker plots, showing the median, minimum and maximum, showing all points. N=16 in all groups. **p<0.01 (One-way ANOVA with Tukey's post-hoc analysis).

2.4.3. *Spermine exposure effect on light flashes-induced epilepsy-like behaviour*

The effects of Spermine treatment were also investigated on light flash-induced epilepsy behaviour. The comparative analysis between Spermine-treated and control larvae showed the absence of changes in maximum velocity (Supplementary Figure 11) and the angle turns number (Supplementary Figure 12). The analysis of the average response to light flashes showed an increased maximum velocity in the larvae treated with 0.1, 1 and 10µM (Figure 25B), together with an increase in the number of bouts (10µM spermine-treated larvae, Figure 25C).

Despite being significantly different to the E3 control and indicating an increased sensitivity and response to the stimulus, the values were not pathogenic (<30mm/s). Therefore, we could not state specifically an epileptic pattern of convulsions. However, it could be considered an impaired response to light flashes.

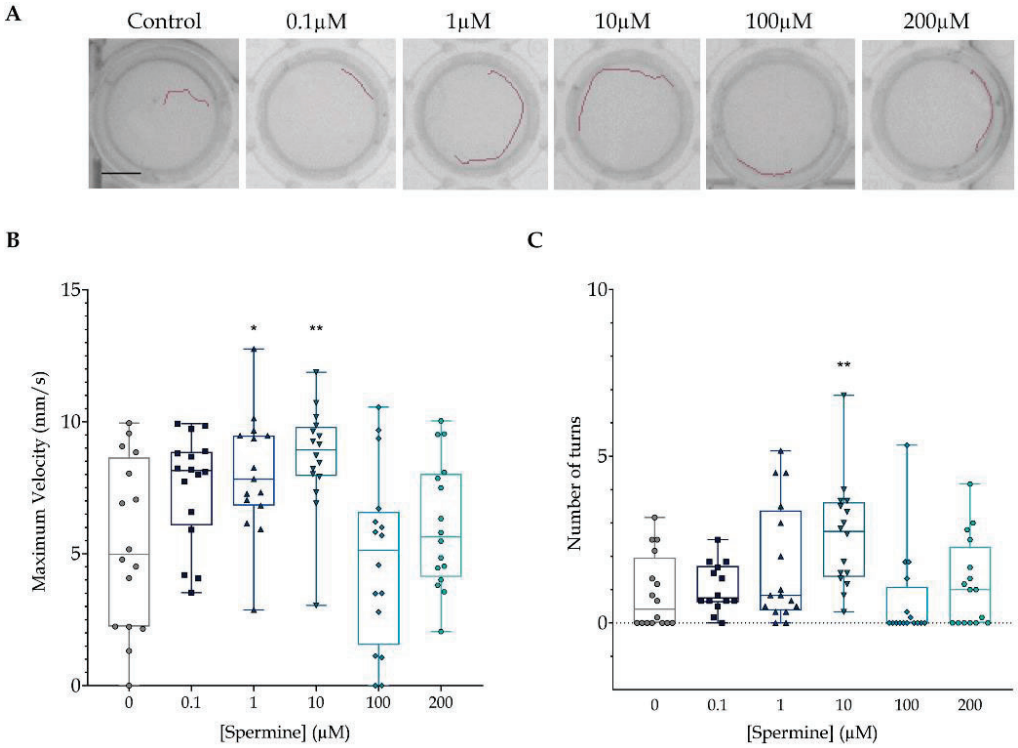

Figure 25. Light-induced epilepsy-like evaluation after Spermine exposure. A. Representative images of the tracking of single larvae, recorded 2 seconds after the first applied flash. Scale bar = 6mm. B. Measurement of the maximum velocity (mm/s) achieved, comparing the average of the five trials of all the tested Spermine concentrations. C. Measurement of the total number of angle turns performed, comparing the average of the five trials of all the tested Spermine concentrations. In panels B and C, data is represented with box and whisker plots, showing the median, minimum and maximum, showing all points. N=16 in all groups. (One-way ANOVA with Tukey's post-hoc analysis).

Interestingly, the behaviour of Spermine, a gain-of-function treatment, was similar to the observed after the treatment of MK-801, a loss-of-function compound, but milder. In accordance with what is observed in GRD patients, the dysregulation of the NMDAR, both with a gain-of-function and loss-of-function, similar behavioural outcomes may appear as a consequence of the disruption of the glutamatergic neurotransmission. D-

Serine did not have any effect on control animals, similar to what has already been observed by Dr. Xavier Altafaj's group (Soto et al., 2019).

In conclusion, the pharmacological interventions of wild-type zebrafish larvae with formerly described NMDAR activity modulators (MK-801, D-Serine, Spermine) have shown striking GRD-like phenotypes. Interestingly, while D-Serine does not show a significant effect in the test performed, the exposure of zebrafish larvae to MK-801 or to Spermine (putative loss- and gain-of-function models, respectively), resulted in similar sensory, motor, cognitive and epilepsy behavioural phenotypes (see Table 12), mimicking GRD phenotypes. Importantly, beyond the intrinsic pharmacological insights, these data validated the behavioural tests battery established, towards the evaluation of the novel genetic zebrafish models of GRD developed along this Thesis.

Paradigm	Variable	MK-801	D-Serine	Spermine
Dark/Light cycles	Total distance (mm)	↓↓↓	↑	↑↑
	Percentage of time in periphery area	=	=	↑↑
	Dark/Light transitions	↓↓↓	=	↑↑↑
Response and habituation to tapping	Quantitative response to the first stimulus (mm)	↑↑↑	=	=
	Qualitative response to the first stimulus (%)	↑↑↑	=	=
	Time for habituation (s)	↑↑↑	=	↑↑
Light-induced epilepsy	Maximum velocity (s)	=	=	↑↑
	Number of angle turns	=	=	↑↑

Table 12. Summary of the described behaviours in the different studied paradigms. A code of arrows is used to simplify the observed results in all the concentrations. Up arrows refer to an increase in the response compared with the control group. Down arrows refer to a decrease in the response compared with the control group. Equal sign refers to no changes in the response compared with the control group. The number of arrows refers to the magnitude of the observed changes and its significance.

3. Generation and characterisation of ZeGRIN models

3.1. Generation and characterisation of grin1 knockout zebrafish models

3.1.1. Generation of grin1 models: knockout strategy

After our characterisation of the spatio-temporal expression of the *grin1* genes in the zebrafish larvae and observing the different but complementary expression of the two paralogs, we hypothesised that the zebrafish loss-of-function model may present some of the alterations observed in LOF GRIN-related disorders patients. To validate our hypothesis, we used the CRISPR/Cas9 technology to generate loss-of-function knockout lines of the *grin1* paralogs (*grin1a* and *grin1b*) as well as the double mutant *grin1a-grin1b* to recapitulate the complete loss-of-function of the *grin1* genes.

Technically, our main strategy consisted into knocking out "*grin*-X" genes by targeting the initial and accessible exon conserved across the described *grin*-X isoforms. In the different loci, we ought to generate large deletions that result in an out-of-frame result, completely disrupting the translated protein and ideally generating early STOP codons which would ultimately disrupt the formation of surface trafficking NMDARs and provoke a loss-of-function.

With this aim, we designed two different sgRNAs per gene to target the first possible exon shared with all the isoforms: exon 1 for *grin1a* (Figure 26A-C) and exon 2 for *grin1b* (Figure 26D-F). In both genes, we were able to generate out-of-frame deletions, changing the ORF and disrupting the protein, leading to a premature STOP codon. For *grin1a*, a deletion of 130 nucleotides in the exon 1 was generated (Figure 26B), disrupting the ORF and leading to a premature STOP codon after 27 amino acid translation (Figure 26C). Similarly, for *grin1b* an 89-nucleotide deletion was generated in exon 2 (Figure 26E), disrupting the ORF and leading to a premature STOP codon after 3 amino acid translation (Figure 26F).


A
Forward strand
grin1a
11.47Mb
11.48Mb
11.49Mb
11.50Mb
grin1a-201 - ENSDART00000041869 >
protein coding
grin1a-202 - ENSDART00000102368 >
protein coding
grin1a-204 - ENSDART00000129744 >
protein coding
grin1a-203 - ENSDART00000126045 >
protein coding
B
sgRNA1
PAM
ENSDARG00000027828.10 gene
sgRNA2
PAM
WT
MUT
C
WT
MUT
STOP
D
Reverse strand
grin1b
< grin1b-202 - ENSDART00000161250
protein coding
< grin1b-201 - ENSDART00000034849
protein coding
29.60Mb
29.61Mb
29.62Mb
29.63Mb
29.64Mb
E
Reverse complement
PAM
sgRNA1
PAM
sgRNA2
ENSDARG00000025728.11 gene
WT
MUT
F
Reverse complement
WT
MUT
STOP

Figure 26. Schematic representation of the knockout strategy for *grin1a* and *grin1b* zebrafish genes. A. D. Schematic representation of *grin1a* (A) and *grin1b* (D) loci in the zebrafish genome. Adapted from Ensembl database (https://www.ensembl.org/). The different transcripts of the gene are displayed, and the targeted exons for the CRISPR/Cas9 strategy are highlighted. B. E. Representative images of the CRISPR/Cas9-modified regions, the localisation of the sgRNA used (in blue) and their respective protospacer adjacent motifs (PsAMs) in *grin1a* (B) and *grin1b* (E). Top sequences represent the wild-type reference sequence, and bottom sequences correspond to the mutated sequences. The alignment graph is displayed in-between. The deletions represented as a red dotted line in all the positions where there was any alignment. The deleted or changed nucleotides are coloured, in contraposition of the conserved nucleotides which remain uncoloured. C. F. Enlarged fragments of the CDS and aminoacidic sequence surrounding the deletion localisation of the gene in *grin1a* (C) and *grin1b* (F). The specific deletion point is highlighted with a vertical arrow and a red dotted line. The premature STOP codon is represented with a black asterisk. Images generated using Geneious Prime software.

The generation of the single knockouts for each zebrafish paralog (*grin1a* and *grin1b*) was confirmed by Sanger sequencing, and resulted on viable zebrafish lines. Finally, in order to generate the *grin1* double mutant, the homozygous animals of both lines ($grin1a^{-/-}$ and $grin1b^{-/-}$) were crossed, obtaining the double heterozygous mutants $grin1a^{+/-}$ - $grin1b^{+/-}$.

3.1.2. Morphological analysis of grin1 GRD models

The clinical examination of GRD patients revealed that the developmental alterations are accompanied by the presence of morphological changes, including facial dysmorphism, microcephaly, and slim body, among others (García-Recio et al., 2021). Using the VAST System (Union Biometrica), we evaluated the potential morphological changes of zebrafish larvae *grin* models. Images of 120 hpf larvae of both lines *grin1a* and *grin1b* were performed (Figure 27A-B). Images of 168 hpf (7 dpf) from the double mutant line *grin1a-grin1b* were also obtained (Figure 27C). Larvae were obtained crossing heterozygous $grin1a^{+/-}$ or $grin1b^{+/-}$ for the single mutant lines, or double heterozygous $grin1a^{+/-}$ - $grin1b^{+/-}$ for the double mutant line. The heterozygous and homozygous larvae from the progeny were always compared with their wild-type siblings from the same batch. The different morphometric phenotypes were analysed using an in-house developed tool (Jarque et al., 2020), and revealed the absence of significant differences were observed in any of the studied morphological traits (Figure 27).

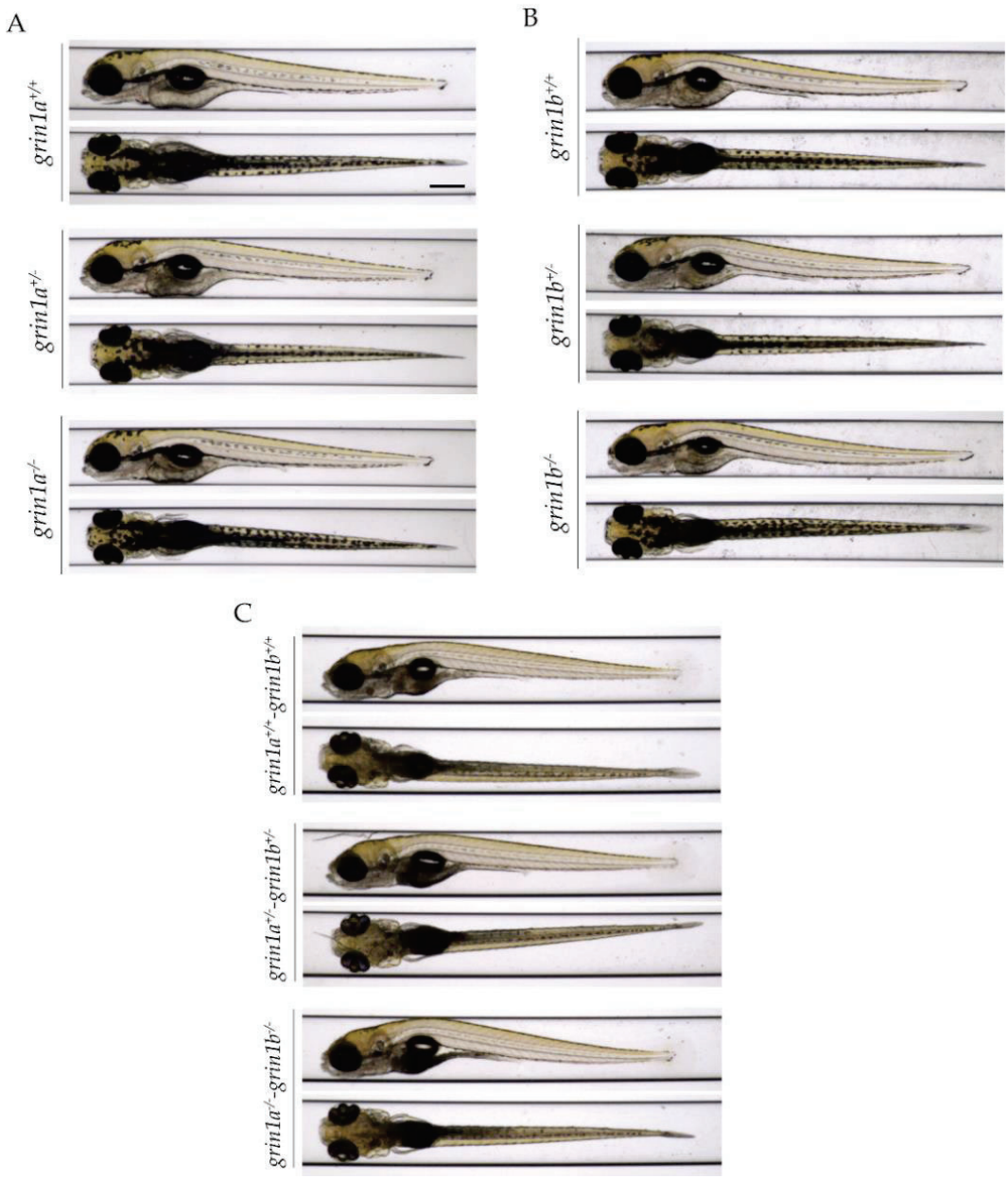

Figure 27. Representative images of the generated *grin1* ZebraGRIN lines. A. Dorsal (lower panels) and lateral (upper panels) images of *grin1a*$^{+/+}$, *grin1a*$^{+/-}$ and *grin1a*$^{-/-}$ 120 hpf larvae. B. Dorsal (lower panels) and lateral (upper panels) images of *grin1b*$^{+/+}$, *grin1b*$^{+/-}$ and *grin1b*$^{-/-}$ 120 hpf larvae. A. Dorsal (lower panels) and lateral (upper panels) images of *grin1a*$^{+/+}$ - *grin1b*$^{+/+}$, *grin1a*$^{+/-}$ - *grin1b*$^{+/-}$ and *grin1a*$^{-/-}$ - *grin1b*$^{-/-}$ 168 hpf larvae. Scale bar = 300µm

3.1.3. Behavioural analysis of grin1 models

Our experimental design to study the different *grin* genes consisted of crossing F1 heterozygous adult animals to putatively obtain all genotype combinations. For the characterisation of the double *grin1* line, double heterozygous *grin1a*$^{+/-}$ - *grin1b*$^{+/-}$ F2 adult zebrafish were crossed. As a result of the crosses of the double heterozygous progenitors, all the possible genotypes were also present in the F3 progeny. Importantly, this breeding design allowed direct comparison between different knockout genotypes against their wild-type siblings, providing a homogenous genetic background and devoid of a batch effect.

In all the experiments, for both *grin1a* and *grin1b* single knockout lines, and *grin1a-grin1b* double knockout lines, the progeny followed mendelian proportions, not showing a mortality at larval stages of any genotype. Noteworthy, a recent work from Wollmuth's group showed that *grin1a*$^{-/-}$*-grin1b*$^{-/-}$double homozygous mutants are lethal at 12 dpf (Zoodsma et al., 2020). In our generated models, these results were confirmed in the progeny of the double heterozygous *grin1a*$^{+/-}$*-grin1b*$^{+/-}$ (survival rate studies until 15 dpf), with the detection a mortality between dpf10 and dpf13 and no survival of the double homozygous *grin1a*$^{-/-}$*-grin1b*$^{-/-}$ in the adult stage (data not shown).

A summary table of the behavioural findings is available at the end of the section (Table 13).

3.1.3.1. Assessment of motor phenotypes in grin1 knockout lines

To analyse possible locomotor alterations (activity, thigmotaxis), the dark/light cycles paradigm was performed, using the parameters identified along the pharmacological models.

When analysing the dark/light cycles, not only the characteristic movement pattern was evaluated, but importantly the movement differences in the light transitions. With the objective of better study and obtaining more relevant information from the analysed data, a distinction of independent locomotion analysis in the light and dark periods was also performed.

In *grin1a* mutant zebrafish larvae (heterozygous and homozygous), no major locomotor alterations were observed (Figure 28). Interestingly, only a significant alteration in the thigmotaxis index of heterozygous *grin1a*+/- larvae was observed (p-value=0.0364;

Figure 28D). Specifically, a decrease in the time spent in the periphery area was described, indicating an anxiolytic behaviour, with less thigmotactic response and a higher exploration of the central area of the well.

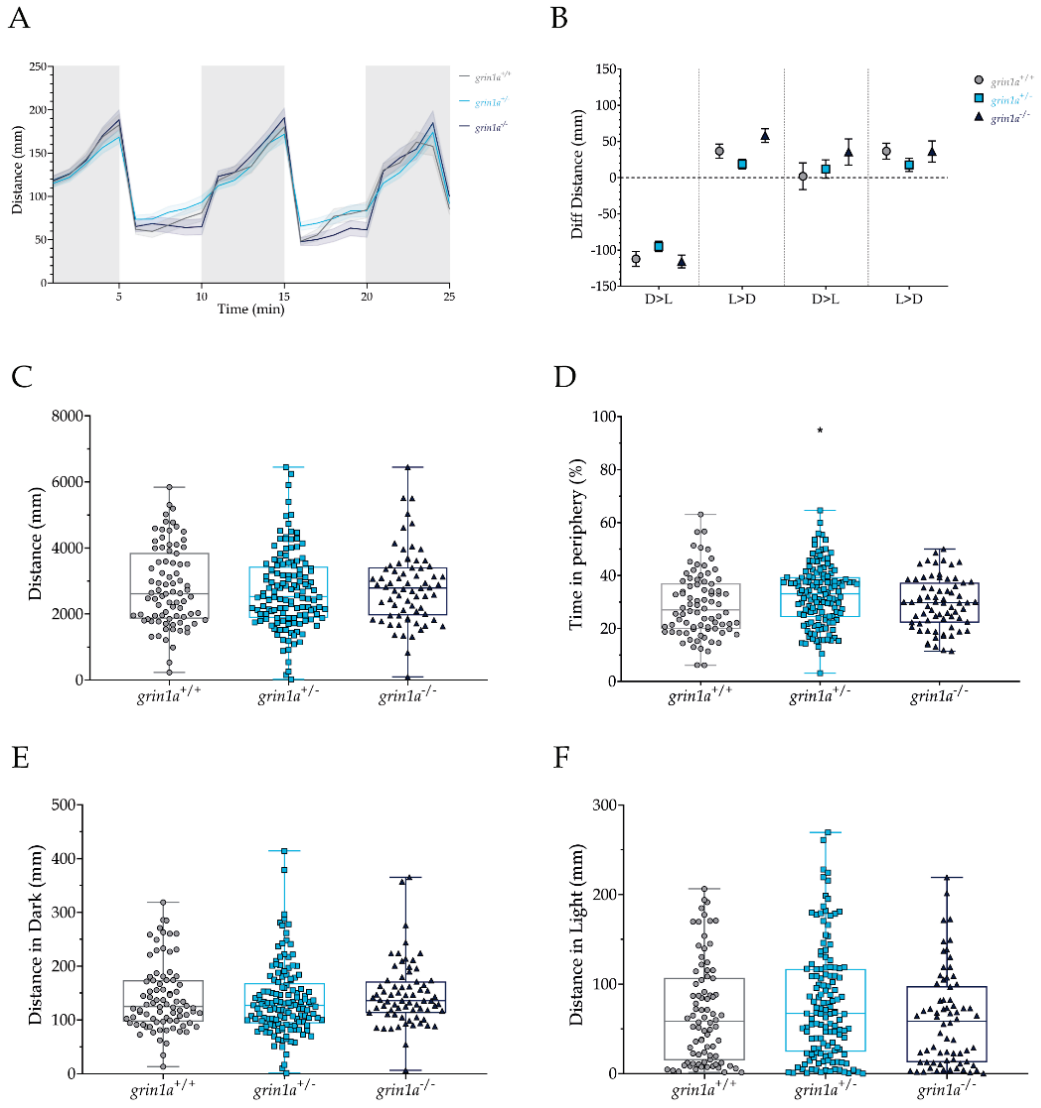

Figure 28. Analysis of the locomotor performance of *grin1a* mutant zebrafish larvae. A. Representation of the distance moved by one-minute time bin during the 25-minute dark/light cycles. Dark cycles are annotated as grey vertical lines for better visualisation. B. Representation of the difference of the distance moved in the transitions from dark to light (D>L) and from light to dark (L>D). C. Graph of the total distance moved (mm) of the larvae in the complete 25-minute protocol. D. Analysis of the average percentage of time spent in the peripherical area of the well. E. Graph of the total distance moved (mm) only in the dark phases of the dark/light cycle protocol. F. Graph of the total distance moved (mm) only in the light phases of the dark/light cycle protocol. In panels A and B, data is represented as mean ± SEM; in panels C to F, data is represented with box and whisker plots, showing the median, minimum and maximum, showing all points. Wild-type *grin1a*$^{+/+}$ larvae are represented in grey (N=82), heterozygous *grin1a*$^{+/-}$ in light blue (N=136) and homozygous *grin1a*$^{-/-}$ in dark blue (N=70). *p<0.05 (One-Way ANOVA with Tukey's post-hoc analysis).

Similarly, in *grin1b* mutant zebrafish larvae (heterozygous and homozygous) no locomotor alterations were detected (Figure 29). However, a mild but not significant hypolocomotion was observed in the homozygous *grin1b*$^{-/-}$, both in the dark/light cycles (Figure 29A) and in the locomotion analysis only in the light phases (Figure 29F). No significant differences were observed during the dark phases (Figure 29E).

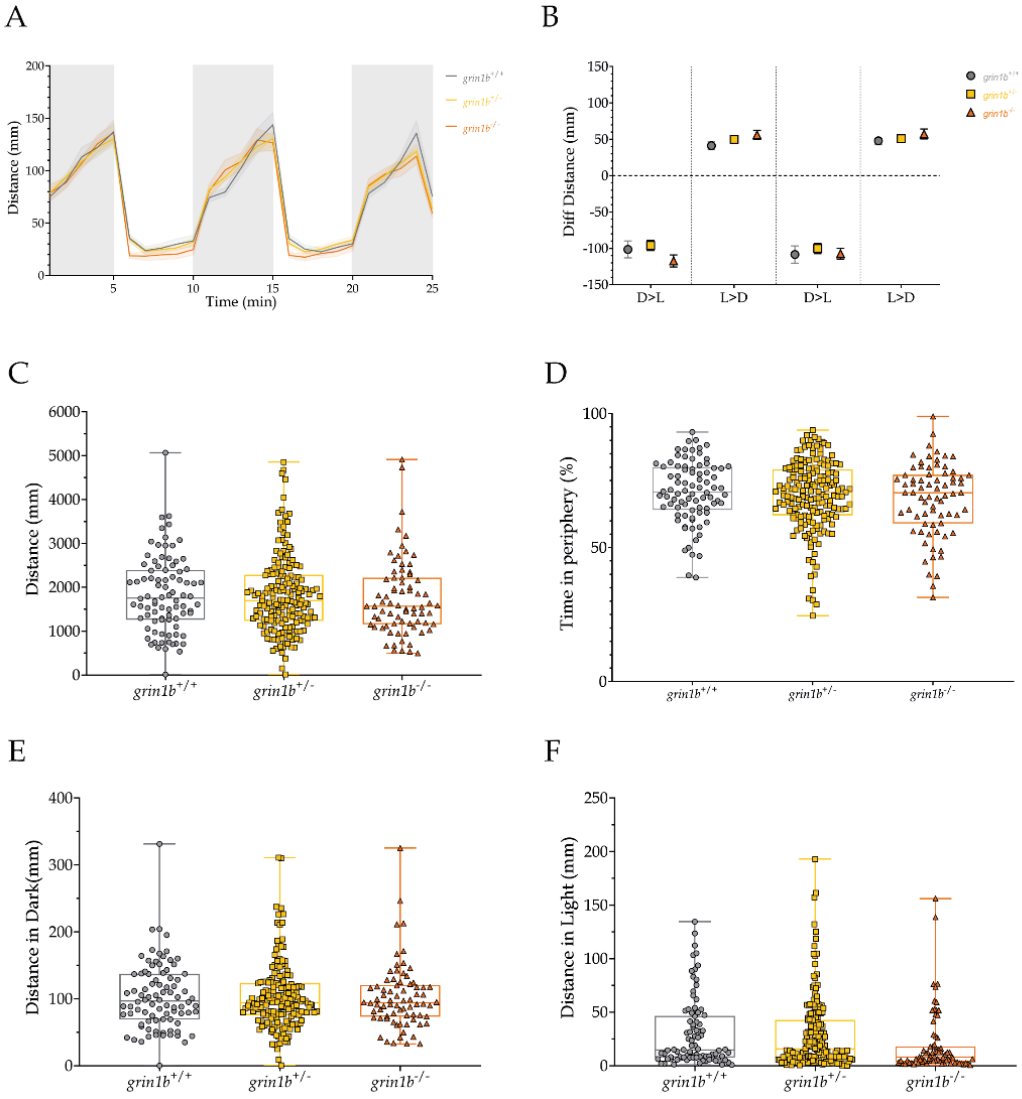

Figure 29. Analysis of the locomotor performance of *grin1b* mutant zebrafish larvae. A. Representation of the distance moved by one-minute time bin during the 25-minute dark/light cycles. Dark cycles are annotated as grey vertical lines for better visualisation. B. Representation of the difference of the distance moved in the transitions from dark to light (D>L) and from light to dark (L>D). C. Graph of the total distance moved (mm) of the larvae in the complete 25-minute protocol. D. Analysis of the average percentage of time spent in the peripheral area of the well. E. Graph of the total distance moved (mm) only in the dark phases of the dark/light cycle protocol. F. Graph of the total distance moved (mm) only in the light phases of the dark/light cycle protocol. In panels A and B, data is represented as mean ± SEM; in panels C to F, data is represented with box and whisker plots, showing the median, minimum and maximum, showing all points. Wild-type *grin1b*$^{+/+}$ larvae are represented in grey (N=86), heterozygous *grin1b*$^{+/-}$ in yellow (N=176) and homozygous *grin1b*$^{-/-}$ in orange (N=74). (One-Way ANOVA with Tukey's post-hoc analysis).

For the study of the double KO line, double heterozygous *grin1a*$^{+/-}$ - *grin1b*$^{+/-}$ adult fish were crossed to obtain a complete loss of *grin1* activity, as well as to compare wild-type larvae with all the possible mutant genotypes siblings in a single experiment. Considering the coexistence of nine different genotypes in these experiments, the display of the results of the dark/light cycles was divided into three different sets of graphs: representation of only the single knockouts of *grin1a* (Figure 30A-B), preserving the previously used blue colour palette; representation of only the single knockouts of *grin1b* (Figure 30C-D), preserving the orange shades; and representation of the double knockout larvae: double heterozygous, *grin1a*$^{+/-}$ - *grin1b*$^{+/-}$; homozygous for *grin1a* and heterozygous for *grin1b, grin1a*$^{-/-}$ - *grin1b*$^{+/-}$; heterozygous for *grin1a* and homozygous for *grin1b*, *grin1a*$^{+/-}$ - *grin1b*$^{-/-}$; and the double homozygous *grin1a*$^{-/-}$ - *grin1b*$^{-/-}$, represented in a green palette (Figure 30E-F).

After the analysis of the locomotion, some differences were observed in the dark/light cycles characteristic pattern (Figure 30A,C,E). These differences in the pattern were quantified in the dark/light transitions, unveiling significant alterations in the transitions from dark to light in homozygous *grin1a*$^{-/-}$ and the double mutants *grin1a*$^{-/-}$ - *grin1b*$^{+/-}$ and *grin1a*$^{+/-}$ - *grin1b*$^{-/-}$ (Figure 30B,D,F).

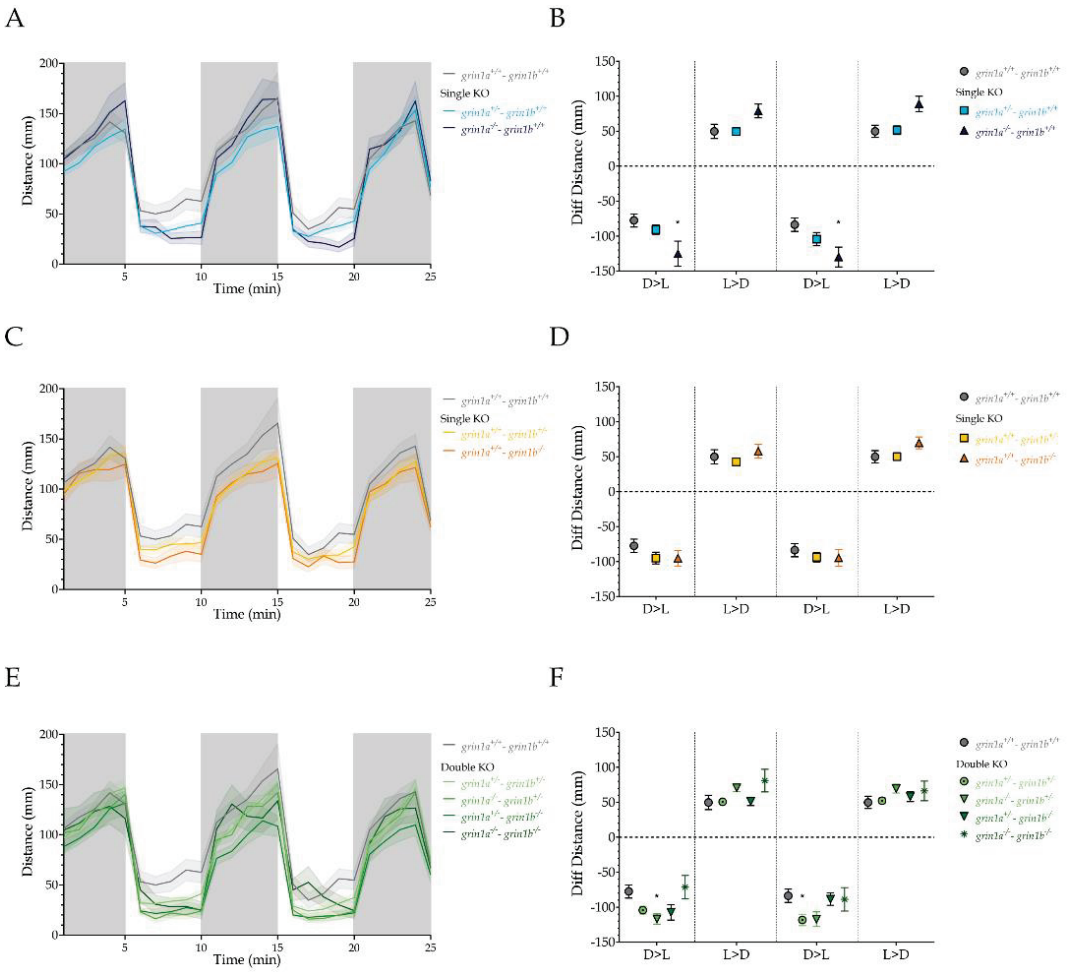

Figure 30. Analysis of locomotion in the dark/light cycles of *grin1a-grin1b* double mutant zebrafish larvae. A, C, E. Representation of the distance moved by one-minute time bin during the 25-minute dark/light cycles. Dark cycles are annotated as grey vertical lines for better visualisation. The data was divided into different panels: *grin1a* single knockouts (A), *grin1b* single knockouts (C) and double knockouts (E). B, D, F Representation of the difference of the distance moved in the transitions from dark to light (D>L) and from light to dark (L>D). The data was divided into different panels: *grin1a* single knockouts (B), *grin1b* single knockouts (D) and double knockouts (F). Data is represented as mean ± SEM. Wild-type *grin1a*$^{+/+}$-*grin1b*$^{+/+}$ larvae are represented in grey (N=41), heterozygous *grin1a*$^{+/-}$ in light blue (N=91), homozygous *grin1a*$^{-/-}$ in dark blue (N=36), heterozygous *grin1b*$^{+/-}$ in yellow (N=68), homozygous *grin1b*$^{-/-}$ in orange (N=37), double heterozygous *grin1a*$^{+/-}$-*grin1b*$^{+/-}$ in lime (N=138), homozygous for *grin1a* and heterozygous for *grin1a, grin1a*$^{-/-}$-*grin1b*$^{+/-}$ in light green (N=70), heterozygous for *grin1a* and homozygous for *grin1b*, *grin1a*$^{+/-}$-*grin1b*$^{-/-}$ in green (N=65), and the double homozygous *grin1a*$^{-/-}$-*grin1b*$^{-/-}$, in dark green (N=28). *p<0.05 (One-Way ANOVA with Tukey's post-hoc analysis).

Furthermore, a generalised hypolocomotion was observed in the double mutants *grin1a*$^{-/-}$ - *grin1b*$^{+/-}$, *grin1a*$^{+/-}$ - *grin1b*$^{-/-}$ and *grin1a*$^{-/-}$ - *grin1b*$^{-/-}$, but not in any of the single mutant larvae or the double heterozygous *grin1a*$^{+/-}$ - *grin1b*$^{+/-}$ (Figure 31A), confirming previous results. When dissecting the analysis of the locomotion upon light conditions, we adscribed the hypolocomotion to a specific hypoactivity along the light phase (Figure 19D), with no changes during the dark phase (Figure 31C).

Interestingly, in light phases we also observed a significant hypolocomotion also in the heterozygous *grin1a*$^{+/-}$ larvae, heterozygous *grin1b*$^{+/-}$ larvae, homozygous *grin1b*$^{-/-}$ larvae, and all the double mutants: double mutants, *grin1a*$^{+/-}$*-grin1b*$^{+/-}$, *grin1a*$^{-/-}$*-grin1b*$^{+/-}$, *grin1a*$^{+/-}$*-grin1b*$^{-/-}$, and the double homozygous *grin1a*$^{-/-}$*-grin1b*$^{-/-}$ (Figure 31D). These differences in the locomotion in light phases were causing the increase in the difference of the distance moved when measuring the dark/light transitions.

In reference to the thigmotaxic index, a mild decrease in the periphery exploration was described for homozygous *grin1b*$^{-/-}$ larvae, homozygous for *grin1a* and heterozygous for *grin1b*, *grin1a*$^{-/-}$*-grin1b*$^{+/-}$ larvae, and heterozygous for *grin1a* and homozygous for *grin1b*, *grin1a*$^{+/-}$*-grin1b*$^{-/-}$ larvae, but surprisingly not in the double homozygous mutant larvae. As observed in previous experiments, the values are not pathological despite being significant, but should be equally considered as a mild alteration in the anxiety behaviour (Figure 31B).

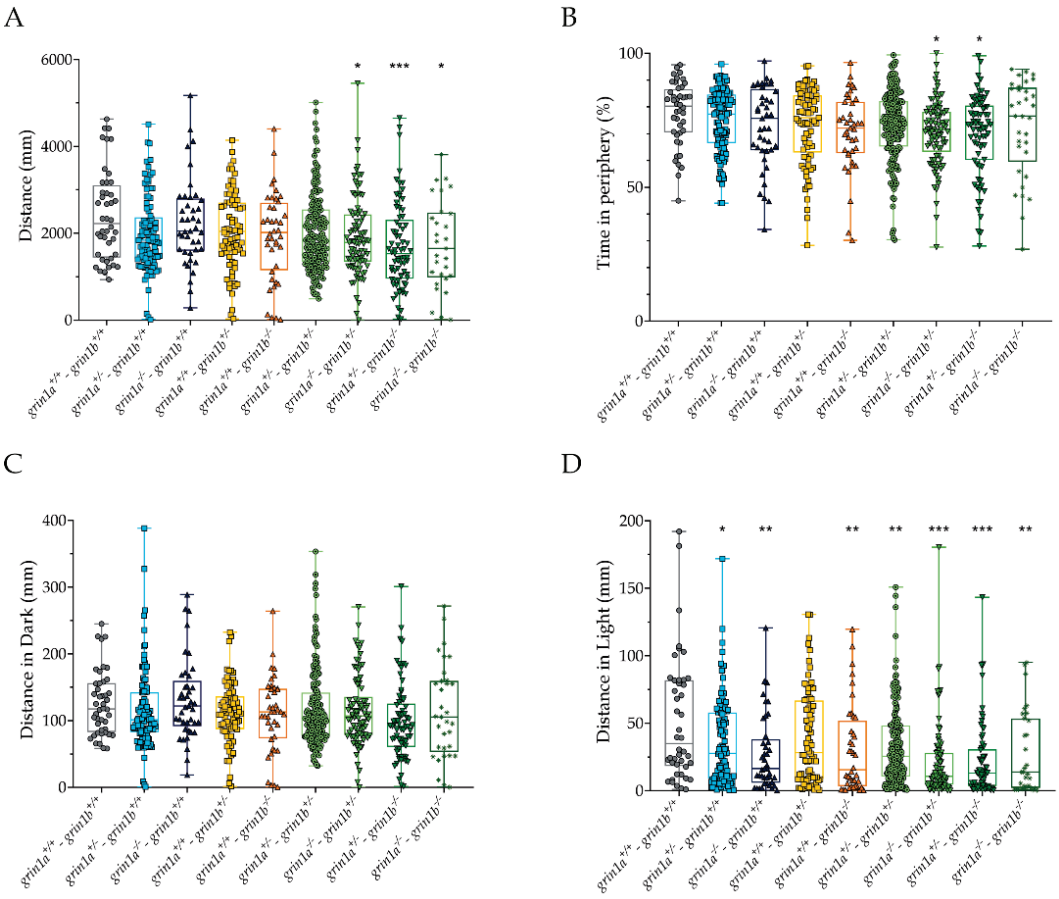

Figure 31. Analysis of the locomotor performance of *grin1* double knockout line. A. Graph of the total distance moved (mm) of the larvae in the complete 25-minute protocol. B. Analysis of the average percentage of time spent in the peripherical area of the well. C. Graph of the total distance moved (mm) only in the dark phases of the dark/light cycle protocol. D. Graph of the total distance moved (mm) only in the light phases of the dark/light cycle protocol. Data is represented with box and whisker plots, showing the median, minimum and maximum, showing all points. Wild-type *grin1a*$^{+/+}$-*grin1b*$^{+/+}$ larvae are represented in grey (N=41), heterozygous *grin1a*$^{+/-}$ in light blue (N=91), homozygous *grin1a*$^{-/-}$ in dark blue (N=36), heterozygous *grin1b*$^{+/-}$ in yellow (N=68), homozygous *grin1b*$^{-/-}$ in orange (N=37), double heterozygous *grin1a*$^{+/-}$-*grin1b*$^{+/-}$ in lime (N=138), homozygous for *grin1a* and heterozygous for *grin1a, grin1a*$^{-/-}$-*grin1b*$^{+/-}$ in light green (N=70), heterozygous for *grin1a* and homozygous for *grin1b*, *grin1a*$^{+/-}$-*grin1b*$^{-/-}$ in green (N=65), and the double homozygous *grin1a*$^{-/-}$-*grin1b*$^{-/-}$, in dark green (N=28). *p<0.05, **p<0.01, ***p<0.001, ****p<0.0001 (One-Way ANOVA with Tukey's post-hoc analysis).

When comparing the data obtained with mutant larvae from double heterozygous parents *vs.* previous data of larvae from single heterozygous parents, some different outcomes were observed. These results suggest that a genetic compensation might occur when the two paralogs of *grin1* are mutated. Moreover, the discordant results of the single knockout larvae from single heterozygous parents *vs.* double heterozygous parents also were in line with the hypothesis of a compensation mechanism occurring in larval stages, given the absence of phenotypes.

3.1.3.2. Analysis of grin1 models' response and habituation to tactile stimuli

Patient's awareness of their surroundings can be altered, producing changes in how they respond to different stimuli. Depending on the mutated subunit, the domain and the functional outcome of the mutation, the response can vary from a lack of response to an increased response and lack of habituation. With the proposed tapping paradigm, applying an external tactile stimulus, we ought to describe any of the possible outcomes in the generated GRD models.

When applying an external tactile stimulus, an increased response to the first tap was observed both in heterozygous *grin1a*$^{+/-}$ and in homozygous *grin1a*$^{-/-}$ (Figure 32A). Subsequently, the quantification of the response to the stimulus revealed that the increased response observed was given by an increased number of larvae responding, but not a significant increase in the distance moved for each responding larva (Figure 32B). Regarding tapping habituation, no differences were observed in *grin1a* genetic models (Figure 32C).

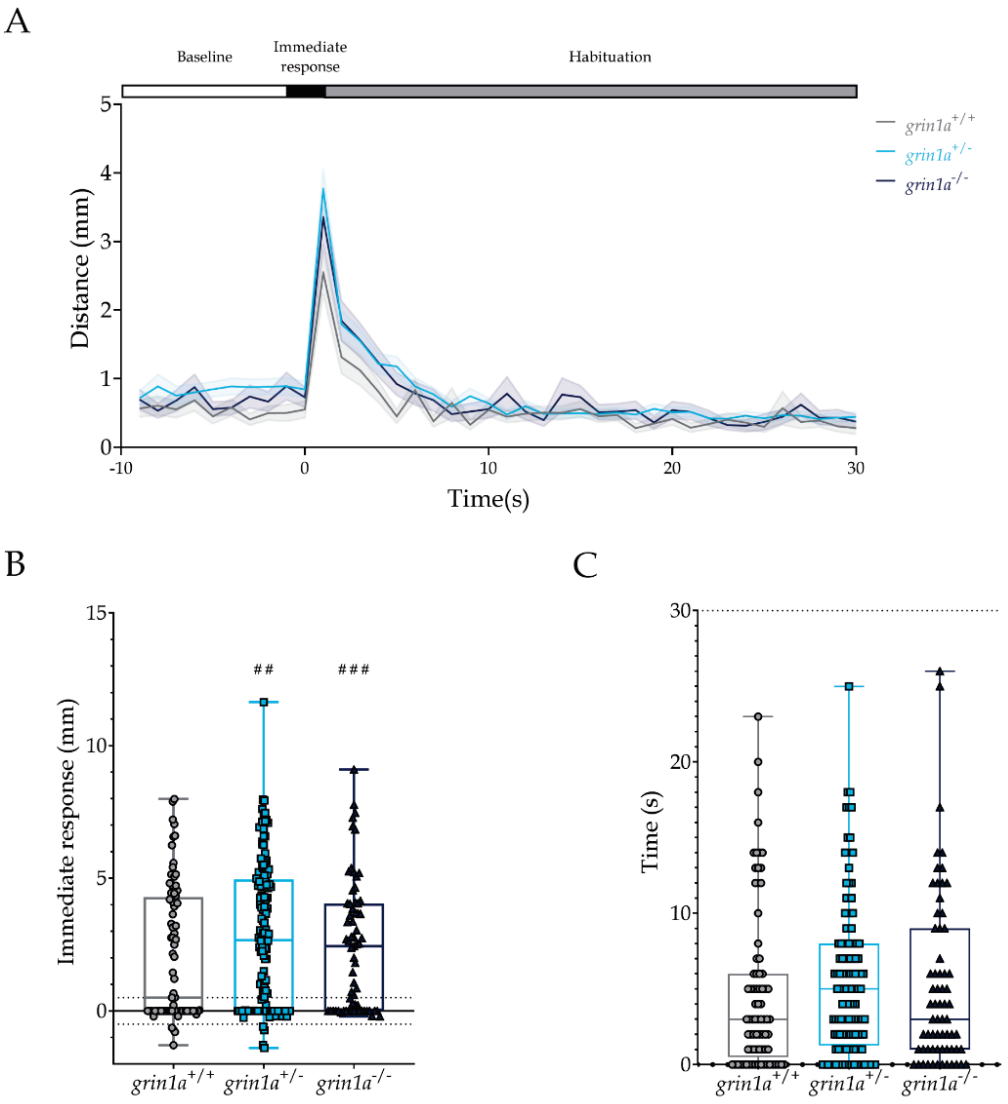

Figure 32. Evaluation of *grin1a* mutant larvae immediate response and habituation to tapping. A. Graph of the distance moved in 1-sec time bin. B. Graph representing the difference in the distance moved as a response to the first tap. Statistical analysis of the immediate response (mm) is represented with "*" symbols. Statistical analysis of the number of larvae responding (%) is represented with "#" symbols. C. Quantification of the habituation by measuring the time each larva lasts to recover baseline levels, with a cut off at 30 seconds. In panel A, data is represented as mean ± SEM; in panels B and C, data is represented with box and whisker plots, showing the median, minimum and maximum, showing all points. Wild-type (*grin1a*$^{+/+}$) larvae are represented in grey (N=77), heterozygous *grin1a*$^{+/-}$ in light blue (N=128) and homozygous *grin1a*$^{-/-}$ in dark blue (N=66). ## p<0.01, ### p<0.001 (Two-way ANOVA with Sidak's multiple comparisons test).

The performance of the larvae in the second set of tappings was equivalent to the first one, with no differences between both sets described (data not shown). Therefore, no alterations in the possible learning between the two sets were observed.

The analysis of *grin1b* single knockout lines performance did reveal a mild increase in the time to habituate to the stimulus (Figure 33C), but not in the other analysed parameters (Figure 33B-C). The increase in the time could be indicative of a deficit in the capacity to recognise previous stimulus and to adapt to the environment.

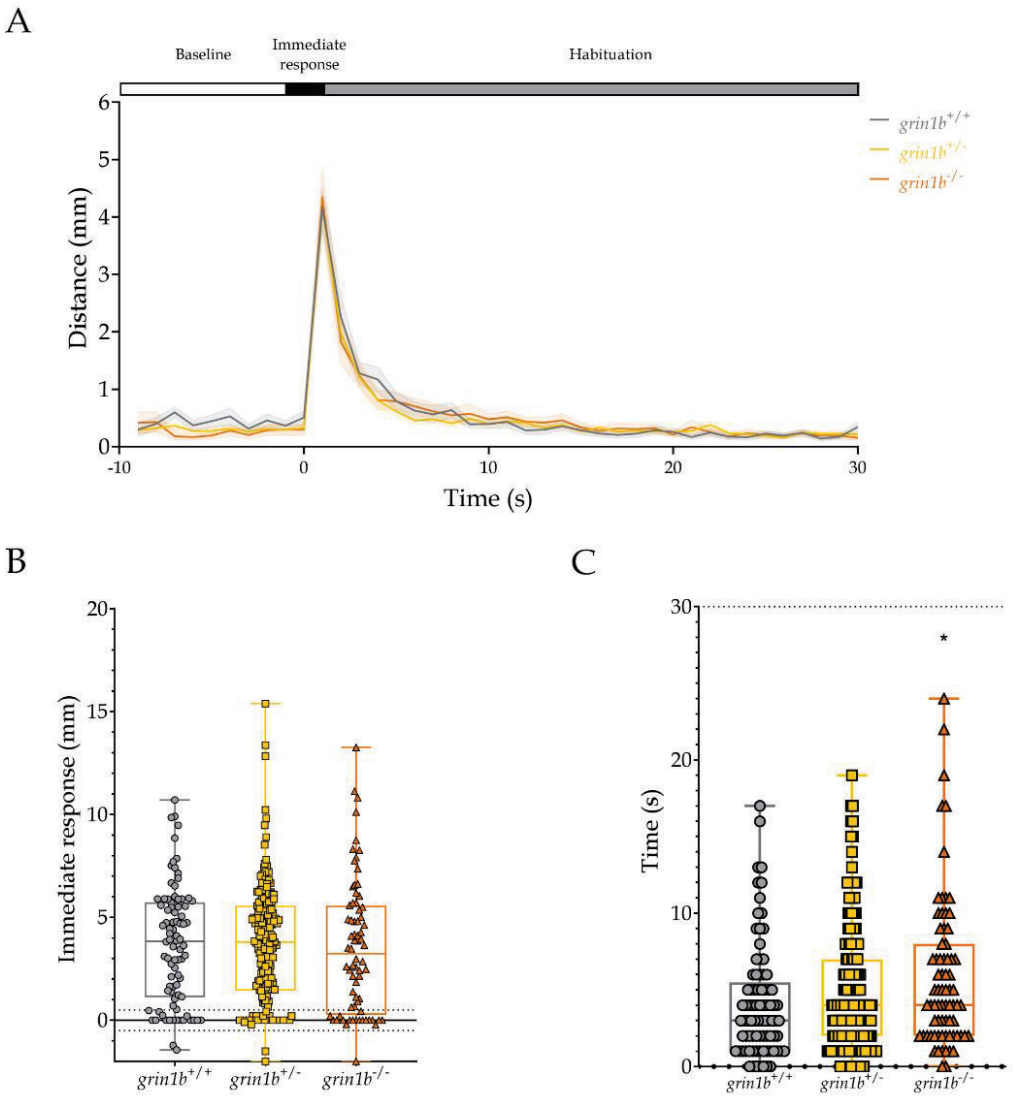

Figure 33. Evaluation of *grin1b* mutant larvae immediate response and habituation to tapping. A. Graph of the distance moved in 1-sec time bin. B. Graph representing the difference in the distance moved as a response to the first tap. Statistical analysis of the immediate response (mm) is represented with "*" symbols. C. Quantification of the habituation by measuring the time each larva lasts to recover baseline levels, with a cut off at 30 seconds. In panel A, data is represented as mean ± SEM; in panels B and C, data is represented with box and whisker plots, showing the median, minimum and maximum, showing all points. Wild-type *grin1b*$^{+/+}$ larvae are represented in

grey (N=86), heterozygous *grin1b*$^{+/-}$ in yellow (N=176) and homozygous *grin1b*$^{-/-}$ in orange (N=74). *p<0.05 (One-Way ANOVA with Tukey's post-hoc analysis)

Similarly to *grin1a* mutant and the pharmacological model findings, the response to the second set of tapping was equivalent, showing no significant differences in the response to the first tap, but describing an increase in the time needed to habituate to the consecutive application of the stimulus (data not shown).

Despite these phenotypes were mild, the complementarity of the results was considered relevant: *grin1a* mutant larvae presented an alteration in the response to the first tap, while *grin1b* mutant larvae did not present that impairment, but displayed a deficit in the habituation to the continuous stimulus. These results, in accordance with the *in situ* hybridisation results, reinforce the hypothesis of complementary functions of *grin1a* and *grin1b* genes.

In the analysis of the tapping response of the double *grin1* mutants, the tapping graphs were divided into three different sets of graphs representation of the single knockout *grin1a* and *grin1b* larvae (Figure 34A and B, respectively), and the double knockout *grin1a - grin1b* larvae (Figure 34C). The analysis showed that only the double mutant larvae in homozygous state (*grin1a*$^{-/-}$ *- grin1b*$^{-/-}$) displayed an impairment of the tapping response. No statistical differences were observed in the other genotypes. We confirmed that both analysed parameters were altered in the *grin1a*$^{-/-}$ *- grin1b*$^{-/-}$ mutants: an increase in the response to the first tap (Figure 34D), with a strong increase of the velocity (Figure 34C) and an increase in the time needed to habituate to the continuous stimulation (Figure 34E). No differences were observed in the relative number of larvae responding to the first tap.

A

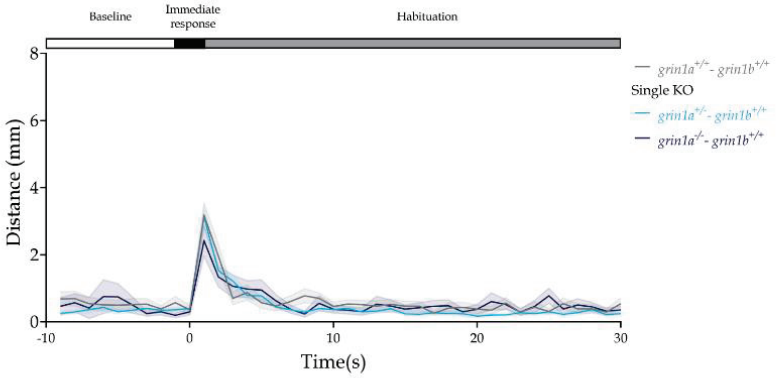
Baseline
Immediate response
Habituation
Distance (mm)
Time(s)
Single KO

B

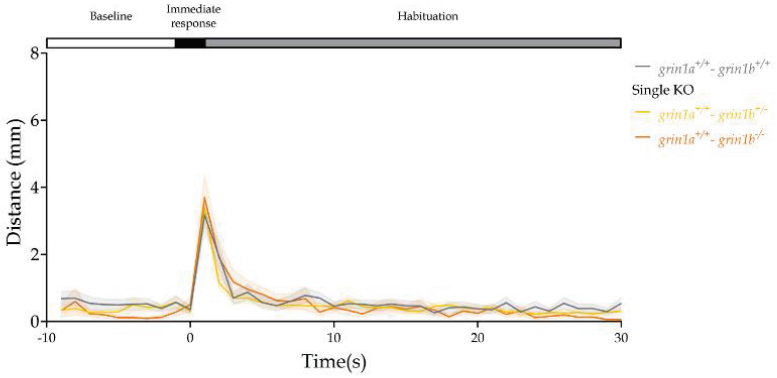
Baseline
Immediate response
Habituation
Distance (mm)
Time(s)
Single KO

C

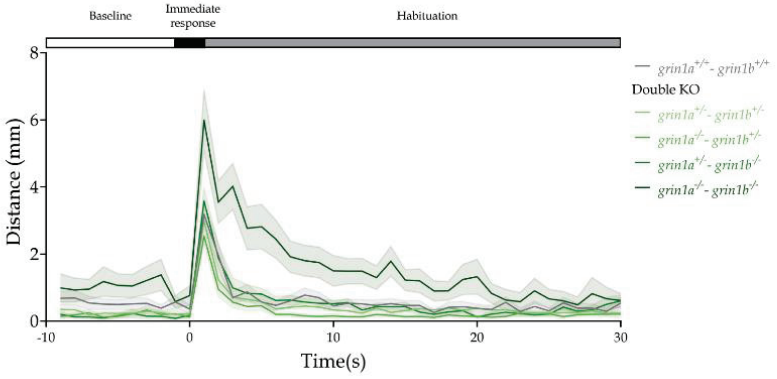
Baseline
Immediate response
Habituation
Distance (mm)
Time(s)
Double KO

D

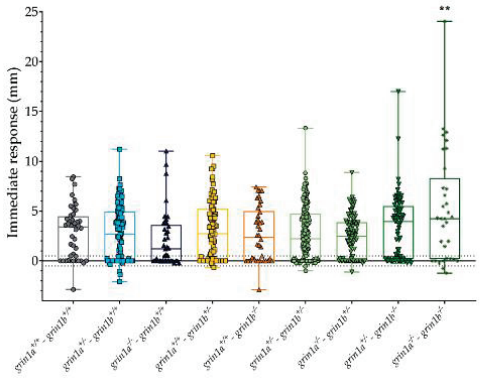
Immediate response (mm)

E

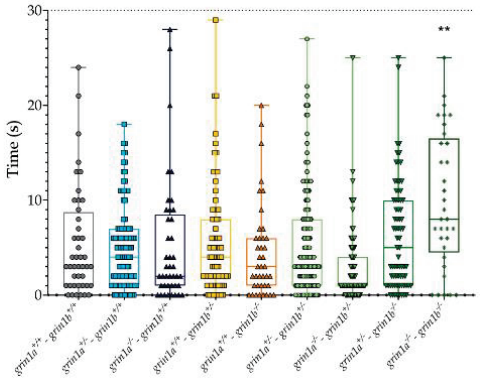
Time (s)

Figure 34. Evaluation to the immediate response and habituation to tapping in in *grin1a-grin1b* double mutant larvae. A, B, C. Representation of the distanced moved in one-minute time bin, showing a characteristic response pattern. The data was divided into different panels: *grin1a* single knockouts (A), *grin1b* single knockouts (B) and double knockouts (C). D. Graph representing the difference in the distance moved as a response to the first tap. Statistical analysis of the immediate response (mm) is represented with "*". Statistical analysis of the number of larvae responding (%) is represented with "#". E. Quantification of the habituation by measuring the time each larva takes to not respond to the stimulus, with a cut off at 30 seconds. In panels A to C, data is represented as mean ± SEM; in panels D and E, data is represented with box and whisker plots, showing the median, minimum and maximum, showing all points. Wild-type *grin1a*$^{+/+}$-*grin1b*$^{+/+}$ larvae are represented in grey (N=44), heterozygous *grin1a*$^{+/-}$ in light blue (N=104), homozygous *grin1a*$^{-/-}$ in dark blue (N=41), heterozygous *grin1b*$^{+/-}$ in yellow (N=78), homozygous *grin1b*$^{-/-}$ in orange (N=40), double heterozygous *grin1a*$^{+/-}$-*grin1b*$^{+/-}$ in lime (N=171), homozygous for *grin1a* and heterozygous for *grin1a, grin1a*$^{-/-}$-*grin1b*$^{+/-}$ in light green (N=88), heterozygous for *grin1a* and homozygous for *grin1b*, *grin1a*$^{+/-}$-*grin1b*$^{-/-}$ in green (N=73), and the double homozygous *grin1a*$^{-/-}$-*grin1b*$^{-/-}$, in dark green (N=33). **p<0.01 (One-Way ANOVA with Tukey's post-hoc analysis).

These findings are in accordance with the symptoms observed in some GRD patients, where more reactivity and less habituation to external stimuli can be observed.

As stated in the single models, similar results were observed in the second set of tappings performed fifteen minutes after the first set (data not shown). In consequence, no significant differences between the two sets of tapping were detected.

In the mutant coming from heterozygous parents, we did observe an increase in the larva responding to the first tap in *grin1a* mutant larvae, and an increase in the time to habituate to the stimulus in homozygous *grin1b*$^{-/-}$ larvae. To our surprise, and in accordance with the observations in the dark/light locomotion analysis, these results were not replicated with the genetically equivalent larvae coming from double heterozygous parents. In the latest, we did only observe defects or alterations in the double homozygous mutant larvae. In accordance with the results described from the dark/light cycles analysis, some compensation or modification might be happening in the larvae coming from double heterozygous parents that is altering the outcome observed. Further studies should be performed to better understand the underlying mechanisms covering the possible phenotypes.

3.1.3.3. Study of epilepsy-like responses to light flashes of grin1 models

To study epilepsy-like behaviour, we analysed two of the most relevant parameters as a response to a light-flash that are known to trigger an epilepsy-like response. Specifically, the maximum achieved velocity (mm/s) and the number of acute turns performed the two seconds immediately after the light stimulus were analysed. In *grin1a* mutant larvae, no epilepsy-like response was observed after the light flashes. The fractioned analysis of the independent series of five consecutive flashes showed no habituation to the light flashes in *grin1a* (*grin1a*$^{+/-}$ and *grin1a*$^{-/-}$) models, similarly to wild-type larvae (Supplementary Figure 13). Therefore, every flash response was considered as an independent replicate and we averaged the responses (Figure 35B-C). Moreover, to compare the results with the other mutant larvae, the independent analysis of the response to the first flash was also performed (Figure 35D-E). No significant differences were observed when comparing the *grin1a* mutants *grin1a*$^{+/-}$ and *grin1a*$^{-/-}$ to their wild-type relatives *grin1a*$^{+/+}$.

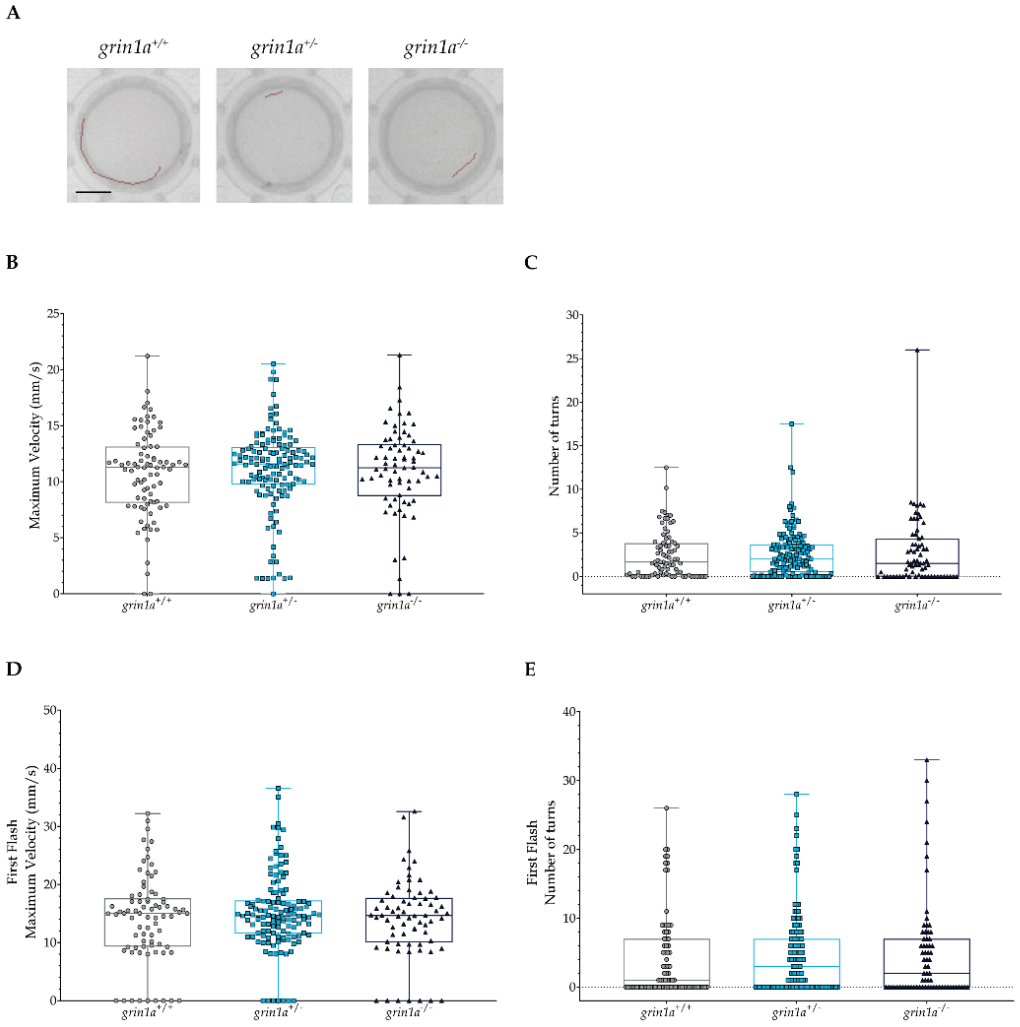

Figure 35. Light-induced epilepsy-like response evaluation in *grin1a* mutant larvae. A. Representative images of the tracking of single larvae, recorded 2 seconds after the first applied flash. Scale bar = 6mm. B. Measurement of the maximum velocity (mm/s) achieved, comparing the average of the five trials. C. Measurement of the total number of angle turns performed, comparing the average of the five trials. D. Measurement of the maximum velocity (mm/s) achieved, comparing five trials angle turn performed. C. Measurement of the total number of angle turns performed, comparing only the response to the first flash. The data is represented with box and whisker plots, showing the median, minimum and maximum, showing all points. Wild-type *grin1a*$^{+/+}$ larvae are represented in grey (N=82), heterozygous *grin1a*$^{+/-}$ in light blue (N=136) and homozygous *grin1a*$^{-/-}$ in dark blue (N=70).

Interestingly, we did observe an epilepsy-like response when analysing the behaviour of *grin1b* line. Equally to the previous analysis, our first analysis was to compare the response of the larvae to the five different consecutive light-flashes. We did observe a clear and significant habituation pattern in both maximum velocity (mm/s) and number of angle turns in both *grin1b* mutants, heterozygous *grin1b*$^{+/-}$ and homozygous *grin1b*$^{-/-}$ (Figure 36). A significant decrease in the responses to the light-flash was observed in all the flashes compared with the first one, showing a habituation to the light stimulus. This habituation would bias the results if we considered the average of the responses across all flashes, diluting the potential effect they may cause. Therefore, we considered most appropriate to focus only the first flash.

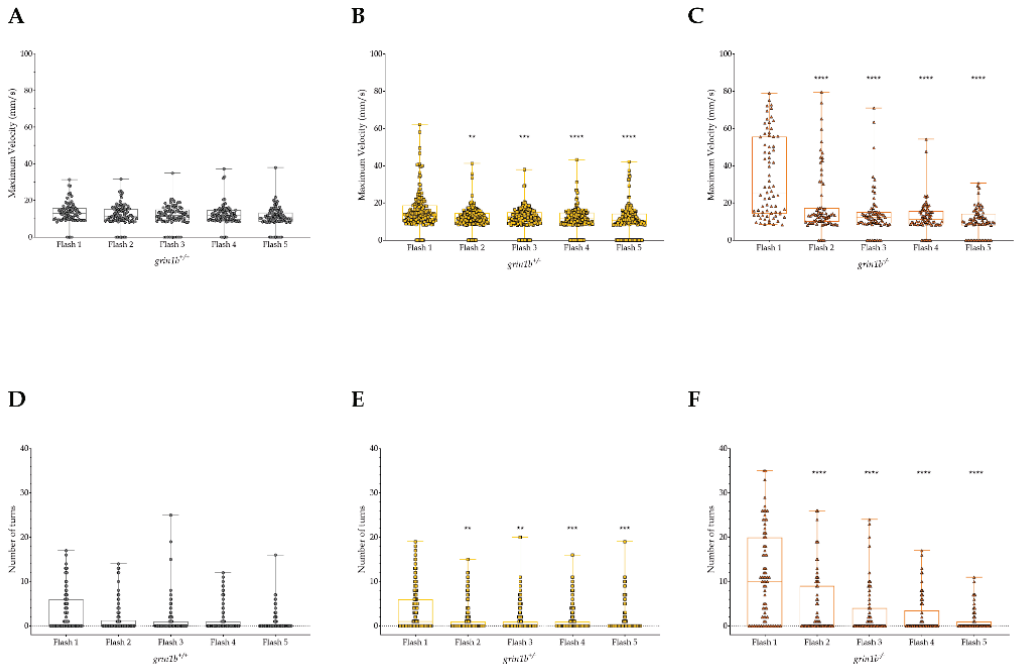

Figure 36. Analysis of maximum velocity and angle turns of independent flashes response of *grin1b* larvae. A. B. C. Measurement of the maximum velocity (mm/s) achieved, comparing the different responses to each flash of wild-type larvae (A), heterozygous *grin1b*$^{+/-}$ (B) and homozygous *grin1b*$^{-/-}$ (C). D. E. F. Measurement of the number of angle turns performed, comparing the different responses to each flash of wild-type larvae (D), heterozygous *grin1b*$^{+/-}$ (E) and homozygous *grin1b*$^{-/-}$ (F). The data is represented with box and whisker plots, showing the median, minimum and maximum, showing all points. Wild-type *grin1b*$^{+/+}$ larvae are represented in grey, heterozygous *grin1b*$^{+/-}$ in yellow and homozygous *grin1b*$^{-/-}$ in orange. **p<0.01, ***p<0.001, ****p<0.0001 (One-way ANOVA with Tukey's post-hoc analysis).

However, and despite this dilution of the response, we also performed the analysis considering the different flashes as replicates, ignoring the habituation to the stimulus. Given the magnitude of the response, and despite the habituation, we still observed significant differences in the homozygous *grin1b*$^{-/-}$ larvae, describing an increase in the response to the light flashes compatible with an epilepsy-like behaviour (Figure 37B-C).

Nevertheless, we did consider that this habituation effect should be taken into account, thus in order to compare the entire response to the light stimulus and more accurately describe the phenotype of the models, only the response to the first flash should be taken into account. When only considering the response to the first flash, a significant increase in the response in both studied parameters is observed in the homozygous *grin1b*$^{-/-}$ larvae (Figure 37D-E). Therefore, we confirmed the existence of a response compatible with an epileptic behaviour when light-flashes were applied. The epilepsy-like motor response was also evidenced when observing the tracking of the larvae after the light-flashes (Figure 37A).

The results obtained for *grin1b* genetic models can be contextualized with former data obtained by Baraban laboratory, regarding the relationship between *grin1b* mutations and epilepsy in zebrafish (Griffin et al., 2021). Our behavioural characterisation confirms that the disruption of *grin1b* causes epilepsy-like behaviour in zebrafish. This phenotype is also in accordance with the pathological epileptic behaviour observed in some GRD patients, particularly in individuals harbouring *GRIN1* disease-associated variants.

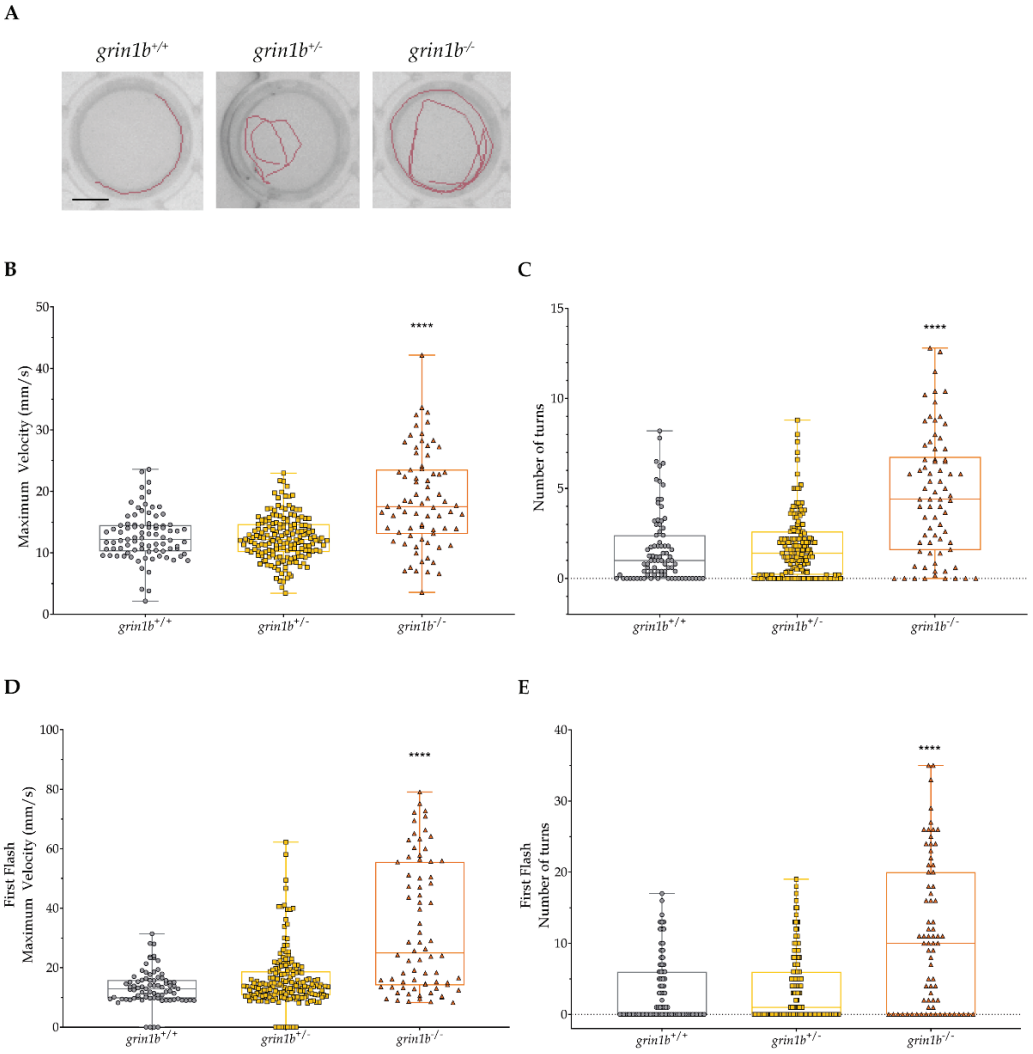

Figure 37. Light-induced epilepsy-like response evaluation in *grin1b* mutant larvae. A. Representative images of the tracking of single larvae, recorded 2 seconds after the first applied flash. Scale bar = 6mm. B. Measurement of the maximum velocity (mm/s) achieved, comparing the average of the five trials. C. Measurement of the total number of angle turns performed, comparing the average of the five trials. D. Measurement of the maximum velocity (mm/s) achieved, comparing only the response to the first flash. C. Measurement of the total number of angle turns performed, comparing only the response to the first flash. The data is represented with box and whisker plots, showing the median, minimum and maximum, showing all points. Wild-type *grin1b*$^{+/+}$ larvae are represented in grey (N=86), heterozygous *grin1b*$^{+/-}$ in yellow (N=176) and homozygous *grin1b*$^{-/-}$ in orange (N=74). ****p<0.0001 (One-way ANOVA with Tukey's post-hoc analysis).

After the characterisation of epilepsy-like behaviour in the single models of *grin1*, we proceeded with the double mutants. As with the other paradigms described before, the single mutants' response differed when analysing the progenies of the double heterozygous fishes.

The first verification was the study of a habituation to the flashes when applying five consecutive flashes. The previously observed phenomenon of habituation was only described in the maximum velocity achieved by the double mutant larvae *grin1a*$^{-/-}$ - *grin1b*$^{+/-}$, *grin1a*$^{+/-}$ - *grin1b*$^{-/-}$ and *grin1a*$^{-/-}$ - *grin1b*$^{-/-}$, but not in the single *grin1b*$^{-/-}$ knockout larvae, as previously described. No differences were observed in the number of bouts performed in the different flashes (Supplementary Figures 14 and 15). Since not all the models behaved equally, and following the previous studies, both the analysis of the average of the five flashes and only the first flash was considered.

Nevertheless, in the two different analyses of the maximum velocity achieved (mm/s), a significant increase in the response was observed only in *grin1a*$^{+/-}$ - *grin1b*$^{-/-}$ and *grin1a*$^{-/-}$ - *grin1b*$^{-/-}$ larvae (Figure 38B and Figure 38D). However, the results were more consistent when only analysing the first flash, since the habituation to the response was not interfering with the final observations. No significant differences were observed in the number of bouts performed after the light flashes (Figure 38C and Figure 38E). As observed in the *grin1b* single knockout models, the presence of an epilepsy-like behaviour was also detected when analysing the tracking of the larvae after the light-flashes (Figure 38A).

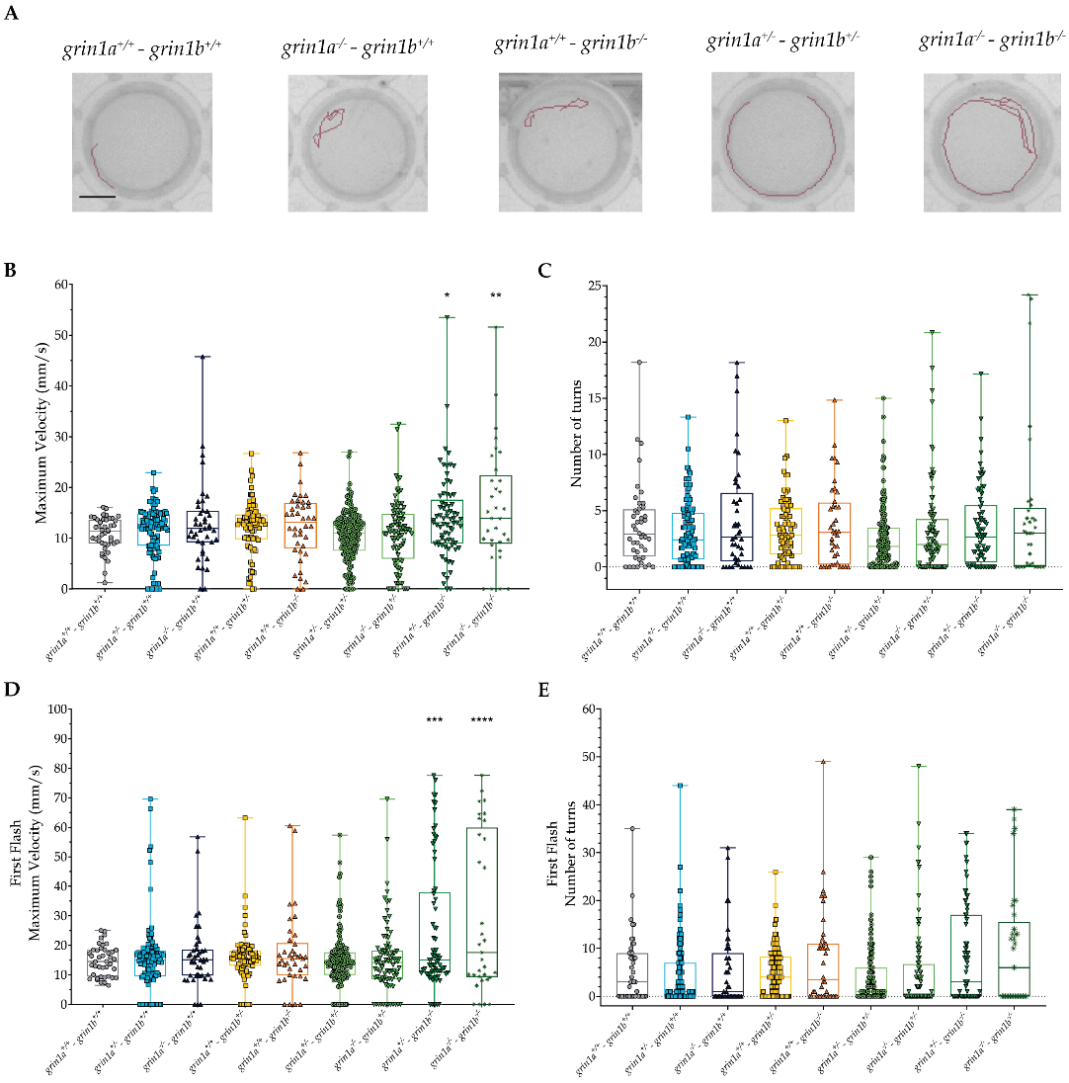

Figure 38. Light-induced epilepsy-like response evaluation in double *grin1a* – *grin1b* mutant larvae. A. Representative images of the tracking of single larvae, recorded 2 seconds after the first applied flash. Scale bar = 6mm. B. Measurement of the maximum velocity (mm/s) achieved, comparing the average of the five trials. C. Measurement of the total number of angle turns performed, comparing the average of the five trials. D. Measurement of the maximum velocity (mm/s) achieved, comparing only the response to the first flash. C. Measurement of the total number of angle turns performed, comparing only the response to the first flash. The data is represented with box and whisker plots, showing the median, minimum and maximum, showing all points. Wild-type grin1a+/+-grin1b+/+ larvae are represented in grey (N=43), heterozygous grin1a+/- in light blue (N=104), homozygous grin1a-/- in dark blue (N=41), heterozygous grin1b+/- in yellow (N=78), homozygous grin1b-/- in orange (N=40), double heterozygous grin1a+/--grin1b+/- in lime (N=171), homozygous for grin1a and heterozygous for grin1a, grin1a-/--grin1b+/- in light green (N=88), heterozygous for grin1a and homozygous for grin1b, grin1a+/--grin1b-/- in green (N=73), and the double homozygous grin1a-/--grin1b-/-, in dark green (N=33). *p<0.05, **p<0.01, ***p<0.001, ****p<0.0001 (One-way ANOVA with Tukey's post-hoc analysis).

Summary of the grin1 phenotypic characterisation

Paradigm	Variable	*grin1a*		*grin1b*		*grin1a – grin1b*			
		grin1a$^{+/-}$	*grin1a*$^{-/-}$	*grin1b*$^{+/-}$	*grin1b*$^{-/-}$	*grin1a*$^{-/-}$-*grin1b*$^{+/+}$	*grin1a*$^{+/-}$ - *grin1b*$^{+/-}$	*grin1a*$^{+/-}$ - *grin1b*$^{-/-}$	*grin1a*$^{-/-}$ - *grin1b*$^{-/-}$
Dark/Light cycles	Total distance (mm)	ns (p-value=0.7132)	ns (p-value>0.9999)	ns (p-value=0.9821)	ns (p-value=0.7302)	ns (p-value=0.9429)	ns (p-value=0.1213)	ns (p-value=0.0929)	* (p-value=0.0178)
	Total distance in Dark (mm)	ns (p-value=0.7834)	ns (p-value=0.8159)	ns (p-value=0.9898)	ns (p-value=0.9900)	ns (p-value=0.9968)	ns (p-value=0.6179)	ns (p-value=0.9308)	ns (p-value=0.8945)
	Total distance in Light (mm)	ns (p-value=0.3950)	ns (p-value=0.6087)	ns (p-value=0.9703)	ns (p-value=0.0822)	** (p-value=0.0017)	** (p-value=0.0089)	** (p-value=0.0011)	** (p-value=0.0049)
	Percentage of time in periphery area	* (p-value=0.0347)	ns (p-value=0.9397)	ns (p-value=0.6317)	ns (p-value=0.2980)	ns (p-value=0.3904)	ns (p-value=0.1025)	ns (p-value=0.2054)	ns (p-value=0.3937)
	Dark/Light transitions	ns (p-value=0.4238; 0.3987; 0.7398; 0.1123)	ns (p-value=0.9727; 0.3808; 0.1123; 0.9996)	ns (p-value=0.8055; 0.5851; 0.5950: 0.9290)	ns (p-value=0.3075; 0.3550; 0.9938; 0.6385)	*/ns (p-value=0.0149; 0.2684; 0.0212; 0.0671)	ns (p-value=0.7625; 0.9944; 0.9708; 0.6646)	*/ns (p-value=0.1403; 0.9999; 0.0316; 0.9997)	ns (p-value=0.9994; 0.2603; 0.9994; 0.8420)
Response and habituation to tapping	Quantitative response to the first stimulus (mm)	ns (p-value= 0.565)	ns (p-value=0.5611)	ns (p-value=0.9987)	ns (p-value=0.9219)	ns (p-value=0.7808)	ns (p-value=0.9996)	ns (p-value=0.9999)	** (p-value=0.0028)
	Qualitative response to the first stimulus (%)	## (p-value=0.0015)	### (p-value=0.0006)	ns (p-value=0.9844)	ns (p-value=0.4872)	ns (p-value>0.9999)	ns (p-value>0.9999)	ns (p-value>0.9999)	ns (p-value>0.9999)
	Time for habituation (s)	ns (p-value=0.5869)	ns (p-value=0.8412)	ns (p-value=0.6158)	* (p-value 0.0243)	ns (p-value=0.9997)	ns (p-value=0.9629)	ns (p-value=0.9996)	** (p-value=0.0016)
Light-induced epilepsy	Maximum velocity (s)	ns (p-value=0.7847)	ns (p-value=0.9074)	ns (p-value=0.8516)	**** (p-value<0.0001)	ns (p-value=0.4878=	ns (p-value=0.7818)	ns (p-value=0.9994)	** (p-value=0.0023)
	Number of angle turns	ns (p-value=0.8964)	ns (p-value=0.6948)	ns (p-value=0.9691)	**** (p-value<0.0001)	ns (p-value=0.9511)	ns (p-value>0.9999)	ns (p-value=0.1660)	ns (p-value=0.6239)

Table 13. Summary of the readouts of the *grin1* model's characterisation. The significance and p-value of all the readouts are represented. To summarise the data, only the single homozygous, double heterozygous and double homozygous mutants were represented in the double mutant line. Significant increased parameters are highlighted in green, while significant decreased parameters are highlighted in red

3.2. Generation and characterisation of grin2A knockout zebrafish models

3.2.1. Generation of grin2A models: knockout strategy

As for the generation of *grin1* models, CRISPR/Cas9 technology was employed to generate loss-of-function knockout lines of the *grin2A* paralogs, namely *grin2Aa* and *grin2Ab* genes. To obtain the double mutant *grin2Aa-grin2Ab* knockout line, single mutant lines were crossed to recapitulate the complete loss-of-function of the *grin2A* genes. Briefly, we designed two different sgRNAs per gene to target the first possible exon shared with all the isoforms: exon 4 for *grin2Aa* (Figure 39A-C) and exon 3 for *grin2Ab* (Figure 39D-F). For *grin2Aa*, a deletion of 226 nucleotides in the exon 4 was generated (Figure 39B). After the deletion, the codon reading frame was disrupted, and a premature STOP codon appears after twenty-four amino acid translation (Figure 39C). Following the same strategy, in *grin2Ab*, a 136-nucleotide deletion was generated in exon 3 (Figure 39E). The codon reading frame was also disrupted, generating a premature STOP codon forty-nine amino-acids after the deletion region (Figure 39F).


A
grin2Aa
Forward strand
B
WT
MUT
C
WT
MUT
STOP
D
grin2Ab
Reverse strand
E
Reverse complement
WT
MUT
F
Reverse complement
WT
MUT
STOP

Figure 39. Schematic representation of the knockout strategy for *grin2Aa* and *grin2Ab* zebrafish genes. A. D. Schematic representation of *grin2Aa* (A) and *grin2Ab* (D) loci in the zebrafish genome. Adapted from Ensembl database (https://www.ensembl.org/). The different transcripts of the gene are displayed, and the targeted exons for the CRISPR/Cas9 strategy are highlighted. B. E. Representative images of the CRISPR/Cas9-modified regions, the localisation of the sgRNA used (in blue) and their respective protospacer adjacent motifs (PsAMs) in *grin2Aa* (B) and *grin2Ab* (E). Top sequences represent the wild-type reference sequence, and bottom sequences correspond to the mutated sequences. The alignment graph is displayed in-between. The deletions represented as a red dotted line in all the positions where there was any alignment. The deleted or changed nucleotides are coloured, in contraposition of the conserved nucleotides which remain uncoloured. C. F. Enlarged fragments of the CDS and aminoacidic sequence surrounding the deletion localisation of the gene in *grin2Aa* (C) and *grin2Ab* (F). The specific deletion point is highlighted with a vertical arrow and a red dotted line. The premature STOP codon is represented with a black asterisk. Images generated using Geneious Prime software.

After the generation of the single knockouts for each zebrafish paralog, *grin2Aa* and *grin2Ab*, adult homozygous *grin2Aa*$^{-/-}$ and *grin2Ab*$^{-/-}$ fishes were crossed, obtaining the double heterozygous mutants *grin2Aa*$^{+/-}$ - *grin2Ab*$^{+/-}$.

In conclusion, we successfully generated *grin2Aa* and *grin2Ab* knockouts by inducing out-of-frame big deletions. These resulted in a disruption of the codon open reading frame and the generation of premature STOP codons, causing *grin2A* loss-of-function.

3.2.2. Morphological analysis of grin2A GRD models

The morphological characterisation of potential developmental alterations in *grin2A* models was performed using the VAST System (Union Biometrica). Images of 120 hpf larvae of both lines *grin2Aa* and *grin2Ab* were obtained (Figure 40A-B), while images of 168 hpf (7 dpf) from the double mutant line *grin2Aa-grin2Ab* were analysed (Figure 40C). The heterozygous and homozygous larvae from the progeny were always compared with their wildtype siblings from the same batch. The morphometric analysis was conducted using an in-house developed tool (Jarque et al., 2020), with no significant differences observed for these genetic models, in any of the evaluated morphological parameters (Figure 40).

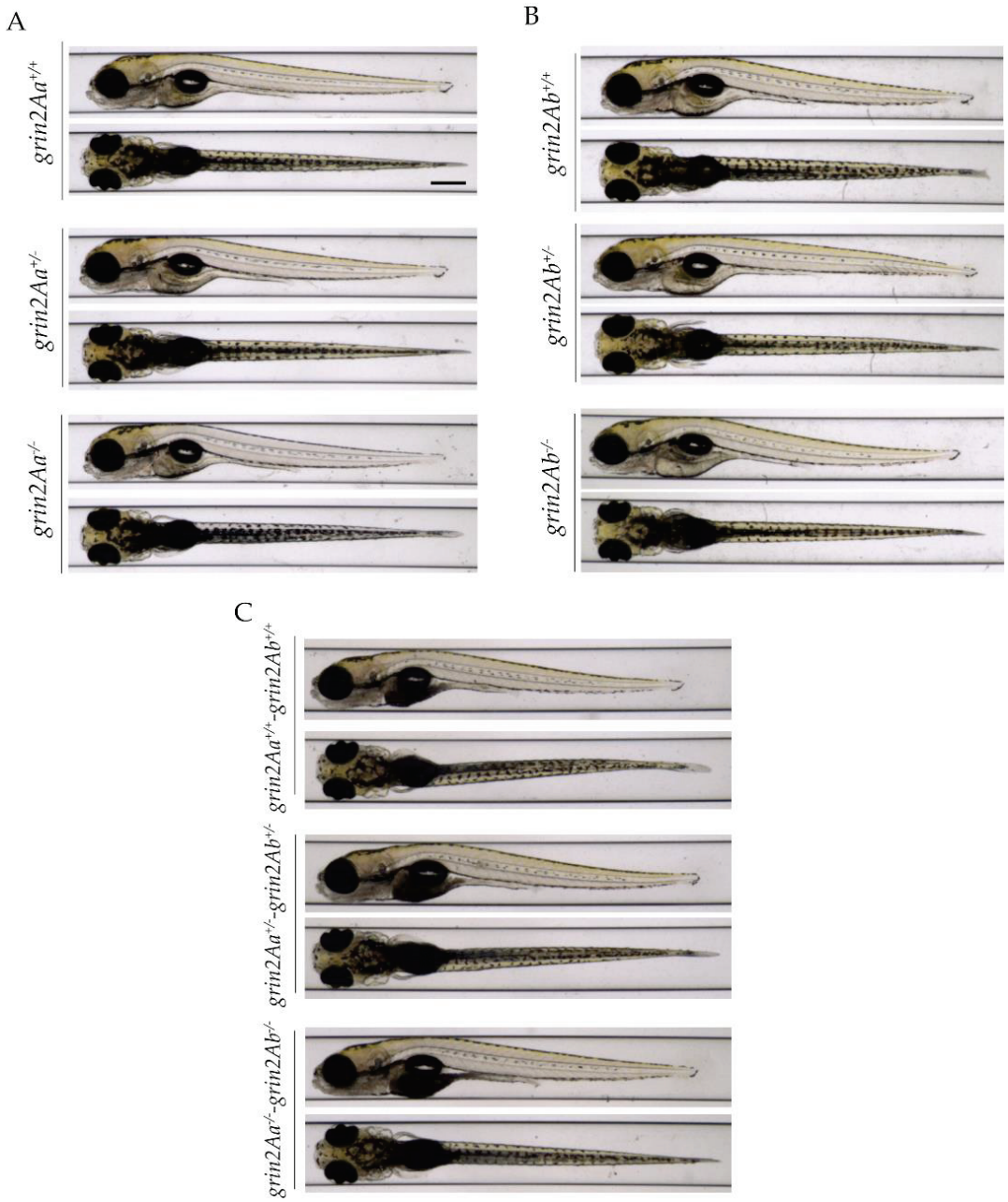

Figure 40. Representative images of the generated *grin2A* ZebraGRIN lines. A. Dorsal (lower panels) and lateral (upper panels) images of *grin2Aa*$^{+/+}$, *grin2Aa*$^{+/-}$ and *grin2Aa*$^{-/-}$ 120 hpf larvae. B. Dorsal (lower panels) and lateral (upper panels) images of *grin2Ab*$^{+/+}$, *grin2Ab*$^{+/-}$ and *grin2Ab*$^{-/-}$ 120 hpf larvae. A. Dorsal (lower panels) and lateral (upper panels) images of *grin2Aa*$^{+/+}$ - *grin2Ab*$^{+/+}$, *grin2Aa*$^{+/-}$ - *grin2Ab*$^{+/-}$ and *grin2Aa*$^{-/-}$ - *grin2Ab*$^{-/-}$ 168 hpf larvae. Scale bar = 300µm

3.2.3. Behavioural analysis of grin2A models

The same experimental design used to characterise the behaviour of *grin1* GRD models was applied for the phenotypic assessment of *grin2A* models. Briefly, heterozygous adult F1 generation fishes were crossed to obtain a progeny with a potential combinatorial presence of all *grin2A* possible genotypes. In all the experiments, for both *grin2Aa* and *grin2Ab* single knockout lines, and *grin2Aa-grin2Ab* double knockout lines, the progeny followed mendelian proportions and none of the phenotypes was associated with mortality at larval stages. The maintenance of these larvae to adult stages and their genotyping showed that none of the genotypes was lethal (data not shown).

A summary table of the behavioural findings is available at the end of the section (Table 14).

3.2.3.1. Assessment of motor phenotypes in grin2A knockout lines

To analyse possible locomotor alterations, along with thigmotaxis evaluation to describe anxiety susceptibility behaviours, the dark/light cycles paradigm was performed. The evaluation of the locomotion of *grin2Aa* mutant zebrafish larvae did not unveil major locomotor alterations (Figure 41). In the anxiety analysis, a decrease in the time spent in the periphery of the well was observed in the *grin2Aa*$^{-/-}$ homozygous larvae (Figure 41D). This result suggests a decrease in anxiety, promoting the exploration to the centre of the well. Similar behaviours have been observed in GRD patients, with an increased motivation for exploration of new spaces, along with the sensation of inhibition of fear to novelty (Bermudo-Soriano et al., 2012).

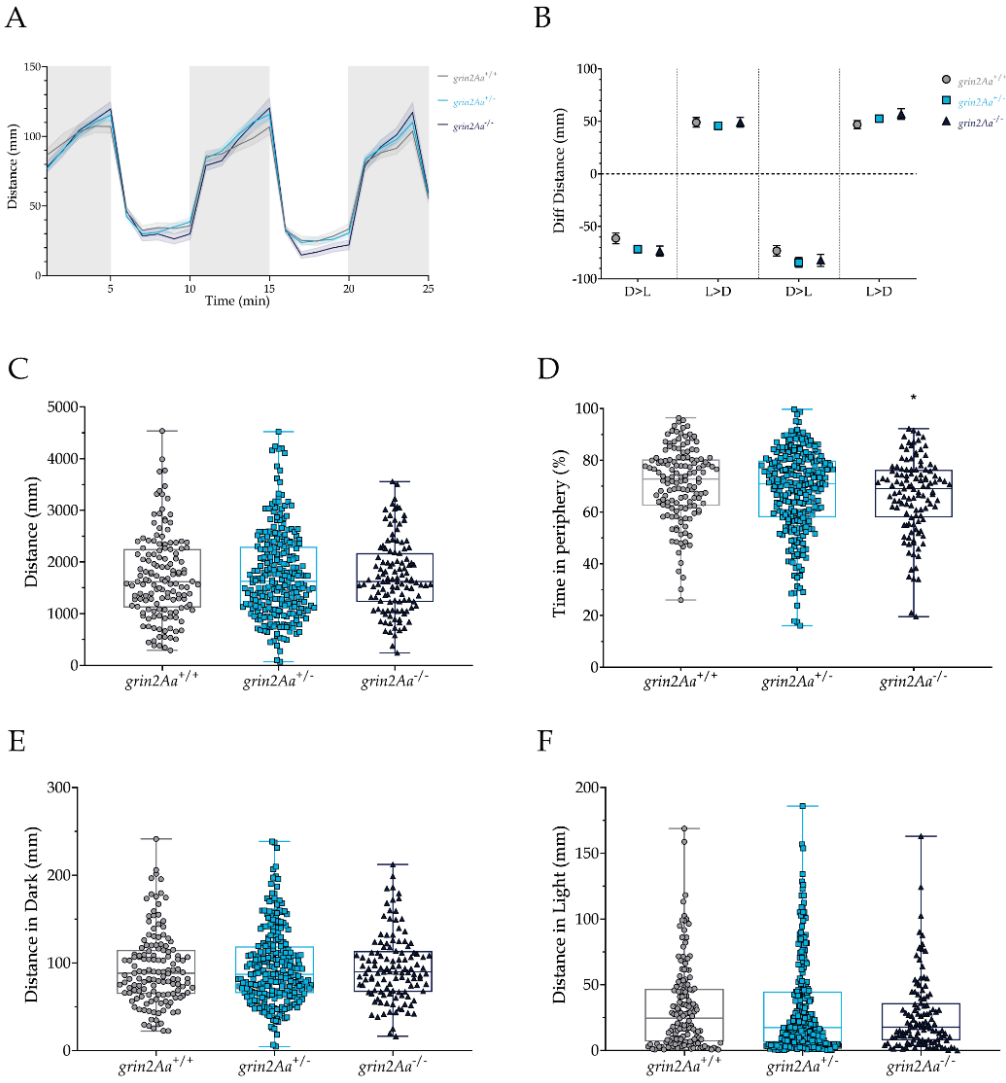

Figure 41. Analysis of the locomotor performance of *grin2Aa* mutant zebrafish larvae. A. Representation of the distance moved by one-minute time bin during the 25-minute dark/light cycles. Dark cycles are annotated as grey vertical lines for better visualisation. B. Representation of the difference of the distance moved in the transitions from dark to light (D>L) and from light to dark (L>D). C. Graph of the total distance moved (mm) of the larvae in the complete 25-minute protocol. D. Analysis of the average percentage of time spent in the peripherical area of the well. E. Graph of the total distance moved (mm) only in the dark phases of the dark/light cycle protocol. F. Graph of the total distance moved (mm) only in the light phases of the dark/light cycle protocol. In panels A and B, data is represented as mean ± SEM; in panels C to F, data is represented with box and whisker plots, showing the median, minimum and maximum, showing all points. Wild-type *grin2Aa*$^{+/+}$ larvae are represented in grey (N=141), heterozygous *grin2Aa*$^{+/-}$ in light blue (N=266) and homozygous *grin2Aa*$^{-/-}$ in dark blue (N=119). *p<0.05 (One-Way ANOVA with Tukey's post-hoc analysis).

For the *grin2Ab* model, neither major alterations in general locomotion nor changes on the anxiety behaviour were noticed (Figure 42). Interestingly, when dissecting the activity along light or dark conditions, homozygous *grin2Ab*$^{-/-}$ larvae displayed a significant increase during light phases (Figure 42F). Altogether, the genetic models effects on locomotor activity are recapitulating the clinical phenotypic heterogeneity displayed by GRD patients, where movement disorders are frequently present but clinically manifested in different forms (hypolocomotion, hyperkinesia (García-Recio et al., 2021).

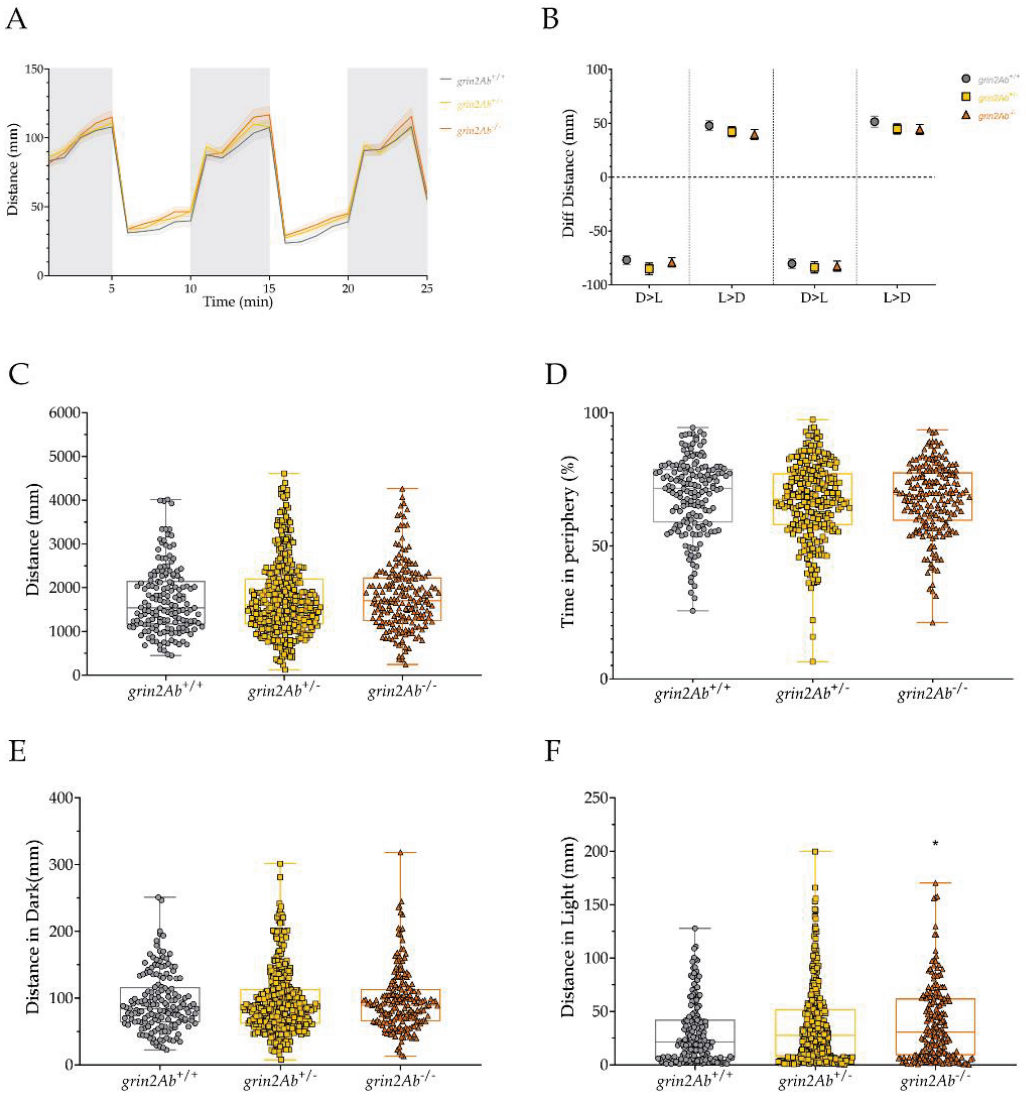

Figure 42. Analysis of the locomotor performance of *grin2Ab* mutant zebrafish larvae. A. Representation of the distance moved by one-minute time bin during the 25-minute dark/light cycles. Dark cycles are annotated as grey vertical lines for better visualisation. B. Representation of the difference of the distance moved in the transitions from dark to light (D>L) and from light to dark (L>D). C. Graph of the total distance moved (mm) of the larvae in the complete 25-minute protocol. D. Analysis of the average percentage of time spent in the

peripherical area of the well. E. Graph of the total distance moved (mm) only in the dark phases of the dark/light cycle protocol. F. Graph of the total distance moved (mm) only in the light phases of the dark/light cycle protocol. In panels A and B, data is represented as mean ± SEM; in panels C to F, data is represented with box and whisker plots, showing the median, minimum and maximum, showing all points. Wild-type *grin2Ab*$^{+/+}$ larvae are represented in grey (N=166), heterozygous *grin2Ab*$^{+/-}$ in yellow (N=353) and homozygous *grin1b*$^{-/-}$ in orange (N=198). *p<0.05 (One-Way ANOVA with Tukey's post-hoc analysis).

When analysing the locomotion of the progeny of the double heterozygous *grin2Aa*$^{+/-}$-*grin2Ab*$^{+/-}$ line, we did observe an analogous situation to *grin1* double mutant results. Alterations observed in the single *grin2Aa* or *grin2Ab* single models were not present in larvae with the same genotype with double heterozygous parents (Table 14). These observations support the hypothesis that compensatory mechanisms (*e.g.* gene expression alteration, maternal contribution) may obscure the loss-of-function effects caused by gene disruption.

Analysing the data in detail, an increase in the distance moved during the dark/light cycles was described for *grin2Aa*$^{-/-}$ single homozygous larvae, but not for *grin2Ab*$^{-/-}$ (Figure 43A-B and Figure 44A-C). The increase in *grin2Aa*$^{-/-}$ locomotion is caused by a significant increase in dark phases (Figure 44C) and a mild but not significant increase also in light phases (Figure 44D). Moreover, a significant increase in total locomotion was also observed in the double heterozygous *grin2Aa*$^{+/-}$ - *grin2Ab*$^{+/-}$ larvae. However, only the increase in *grin2Aa*$^{-/-}$ was also reflected in the dark/light transition analysis (Figure 43B). The other *grin2Aa* – *grin2Ab* mutant larvae did not present locomotor alterations.

Another important result was the decrease of the time in the periphery observed only in the double homozygous *grin2Aa*$^{-/-}$ - *grin2Ab*$^{-/-}$ larvae, meaning a decrease in thigmotaxic index and an increase in the exploration of the centre of the well (Figure 44B). This result goes in accordance with the behaviour described in *grin2Aa*$^{-/-}$ larvae from single heterozygous parents. Subsequently, this result also goes in line with the traits observed in GRD patients.

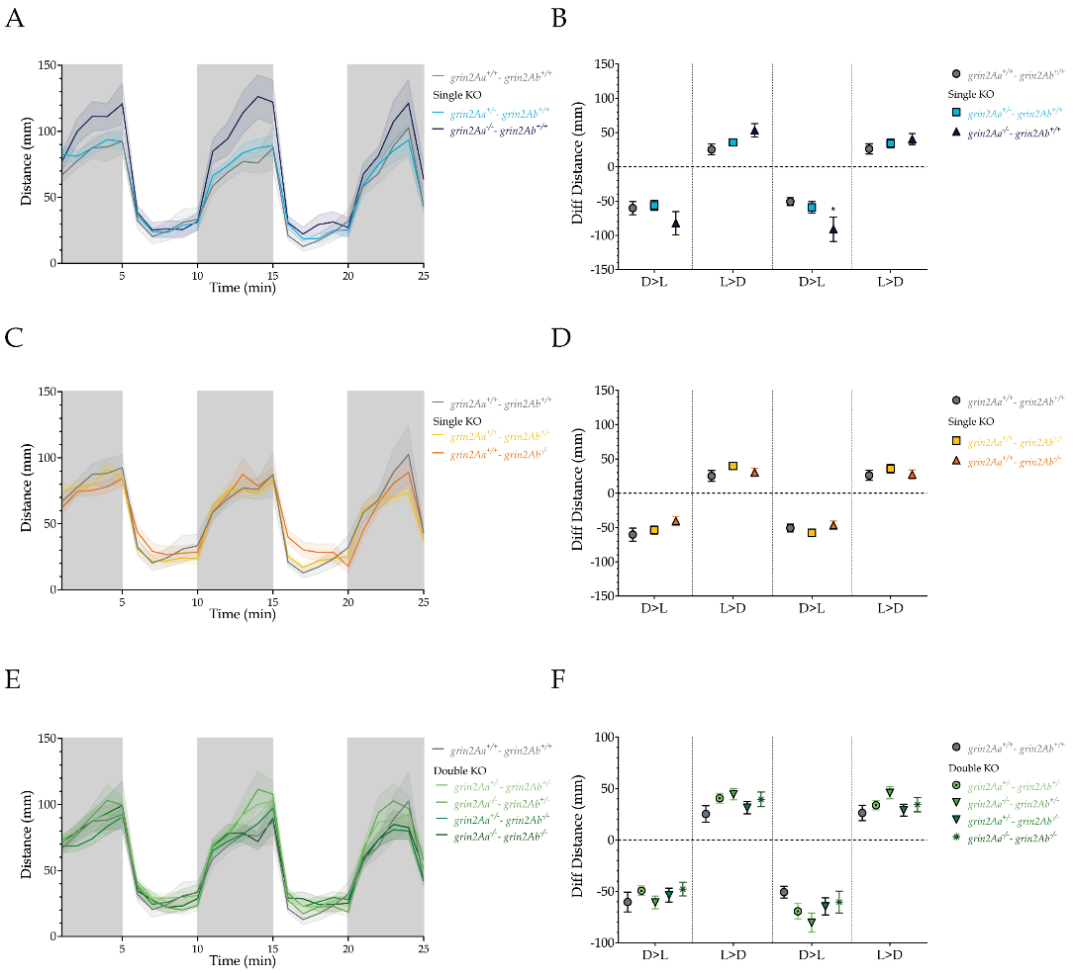

Figure 43. Analysis of locomotion in the dark/light cycles of *grin2Aa-grin2Ab* double mutant zebrafish larvae. A, C, E. Representation of the distance moved by one-minute time bin during the 25-minute dark/light cycles. Dark cycles are annotated as grey vertical lines for better visualisation. The data was divided into different panels: *grin2Aa* single knockouts (A), *grin2Ab* single knockouts (C) and double knockouts (E). B, D, F. Representation of the difference of the distance moved in the transitions from dark to light (D>L) and from light to dark (L>D). The data was divided into different panels: *grin2Aa* single knockouts (B), *grin2Ab* single knockouts (D) and double knockouts (F). Data is represented as mean ± SEM. Wild-type *grin2Aa*$^{+/+}$-*grin2Ab*$^{+/+}$ larvae are represented in grey (N=31), heterozygous *grin2Aa*$^{+/-}$ in light blue (N=66), homozygous *grin2Aa*$^{-/-}$ in dark blue (N=36), heterozygous *grin2Ab*$^{+/-}$ in yellow (N=67), homozygous *grin2Ab*$^{-/-}$ in orange (N=38), double heterozygous *grin2Aa*$^{+/-}$-*grin2Ab*$^{+/-}$ in lime (N=143), homozygous for *grin2Aa* and heterozygous for *grin2Aa, grin2Aa*$^{-/-}$-*grin2Ab*$^{+/-}$ in light green (N=78), heterozygous for *grin2Aa* and homozygous for *grin2Ab*, *grin2Aa*$^{+/-}$-*grin2Ab*$^{-/-}$ in green (N=70), and the double homozygous *grin2Aa*$^{-/-}$-*grin2Ab*$^{-/-}$, in dark green (N=42). *p<0.05 (One-way ANOVA with Tukey's post-hoc analysis).

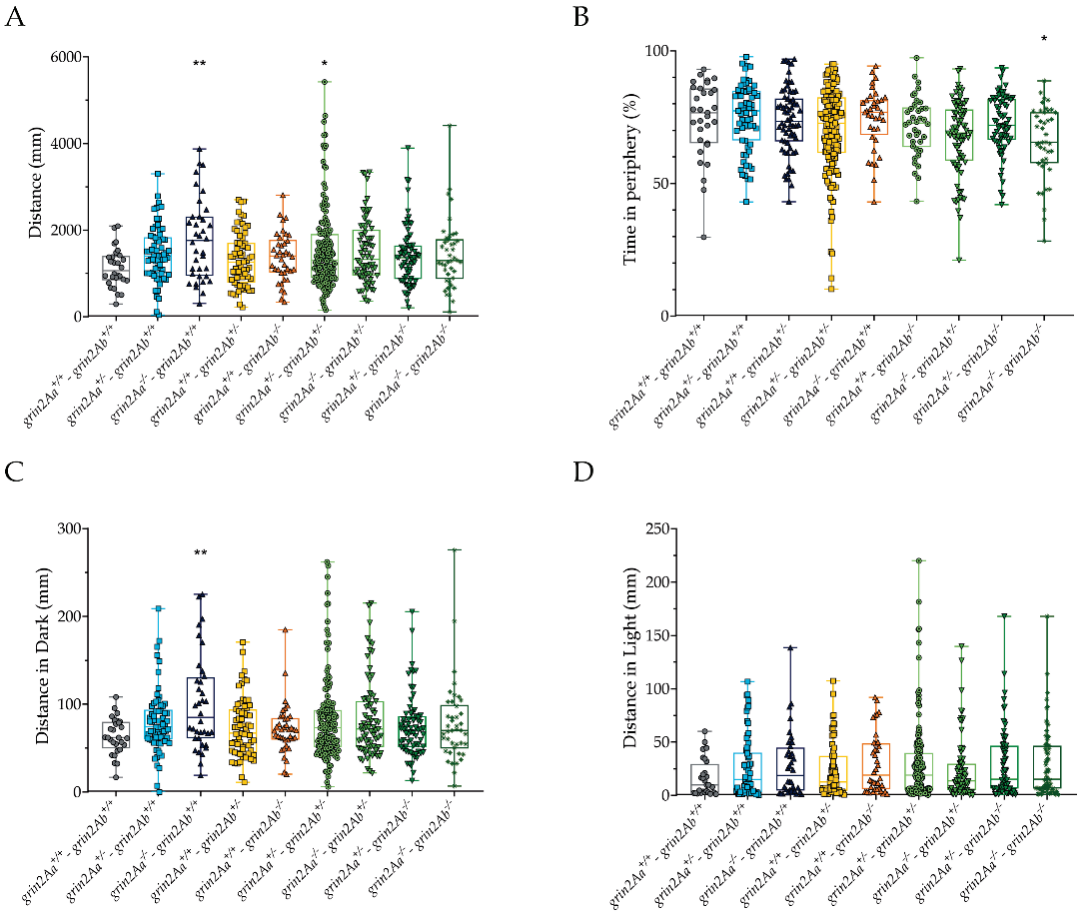

Figure 44. Analysis of the locomotor performance of *grin1* double knockout line. A. Graph of the total distance moved (mm) of the larvae in the complete 25-minute protocol. B. Analysis of the average percentage of time spent in the peripherical area of the well. C. Graph of the total distance moved (mm) only in the dark phases of the dark/light cycle protocol. D. Graph of the total distance moved (mm) only in the light phases of the dark/light cycle protocol. Data is represented with box and whisker plots, showing the median, minimum and maximum, showing all points. Wild-type *grin2Aa*$^{+/+}$-*grin2Ab*$^{+/+}$ larvae are represented in grey (N=31), heterozygous *grin2Aa*$^{+/-}$ in light blue (N=66), homozygous *grin2Aa*$^{-/-}$ in dark blue (N=36), heterozygous *grin2Ab*$^{+/-}$ in yellow (N=67), homozygous *grin2Ab*$^{-/-}$ in orange (N=38), double heterozygous *grin2Aa*$^{+/-}$-*grin2Ab*$^{+/-}$ in lime (N=143), homozygous for *grin2Aa* and heterozygous for *grin2Aa*, *grin2Aa*$^{-/-}$-*grin2Ab*$^{+/-}$ in light green (N=78), heterozygous for *grin2Aa* and homozygous for *grin2Ab*, *grin2Aa*$^{+/-}$-*grin2Ab*$^{-/-}$ in green (N=70), and the double homozygous *grin2Aa*$^{-/-}$-*grin2Ab*$^{-/-}$, in dark green (N=42). *p<0.05, **p<0.01, (One-way ANOVA with Tukey's post-hoc analysis).

3.2.3.2. *Analysis of grin2A models' response and habituation to tactile stimuli*

The habituation and non-associative learning were explored, by means of the tapping paradigm, in *grin2A* models. In *grin2Aa* models (heterozygous and homozygous), no differences in the response to the first tapping stimulus were detected (Figure 45B). Interestingly, a faster habituation was observed both in heterozygous *grin2Aa*$^{+/-}$ and homozygous *grin2Aa*$^{-/-}$ larvae (Figure 45C). This accelerated response was more pronounced in the homozygous *grin2Aa*$^{-/-}$ larvae and might be related to a freezing response (Loganathan et al., 2023; Rennekamp, 2018). Importantly, this increased response to the stimulus also goes in line with GRD patients' behaviour.

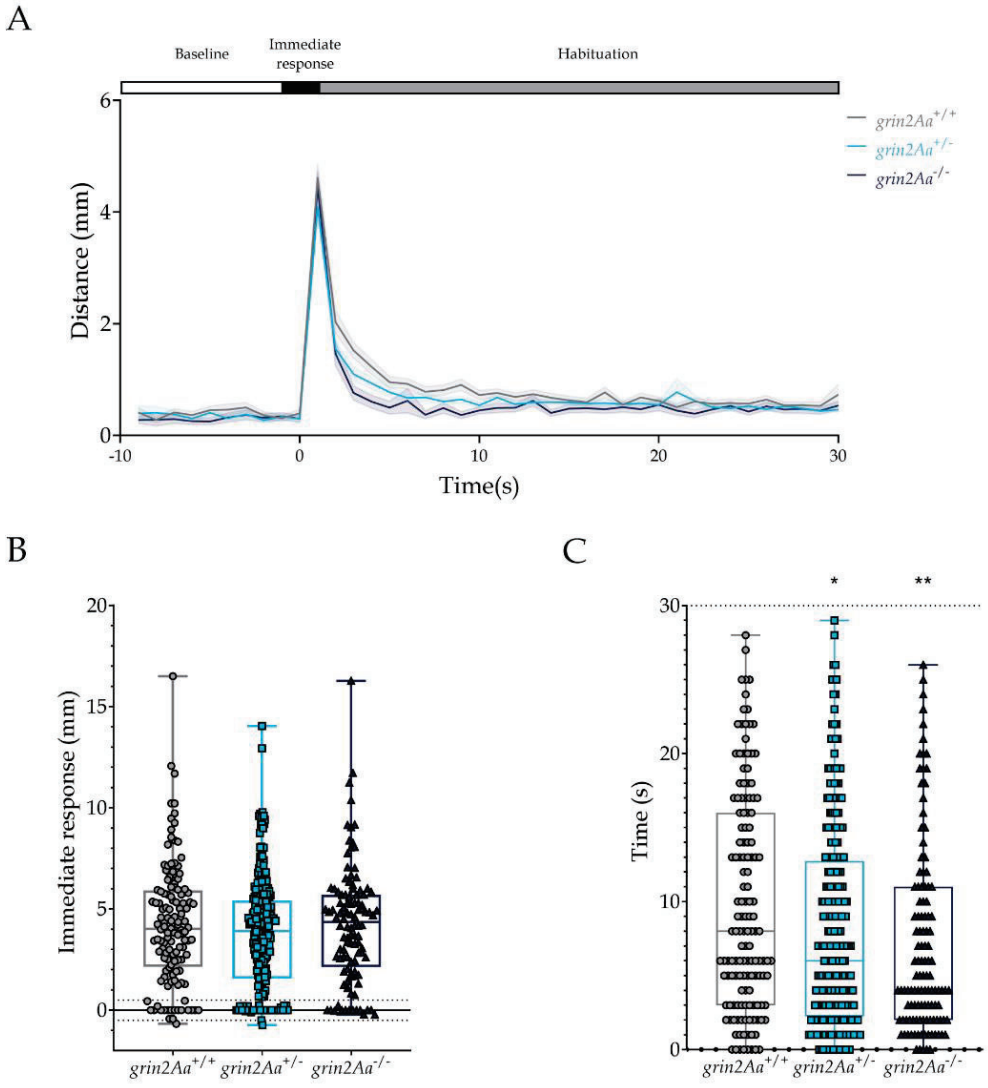

Figure 45. Evaluation to the immediate response and habituation to tapping in *grin2Aa* mutant larvae. A. Graph of the distanced moved in one-second time bin. B. Graph representing the difference in the distance moved as a response to the first tap. Statistical analysis of the immediate response (mm) is represented with "*". Statistical analysis of the number of larvae responding (%) is represented with "#". C. Quantification of the

habituation by measuring the time each larva takes to not respond to the stimulus, with a cut off at 30 seconds. In panel A, data is represented as mean ± SEM; in panels B and C, data is represented with box and whisker plots, showing the median, minimum and maximum, showing all points. Wild-type *grin2Aa*$^{+/+}$ larvae are represented in grey (N=141), heterozygous *grin2Aa*$^{+/-}$ in light blue (N=264) and homozygous *grin2Aa*$^{-/-}$ in dark blue (N=119). * $p<0.05$, ** $p<0.01$ (One-way ANOVA with Tukey's post-hoc analysis).

Interestingly, tapping test results for *grin2Ab* paralogue single homozygous line were the opposite of those detected for *grin2Aa*, and consisted of a significant increase of time to habituate to the continuous stimulation (with unaltered initial response), displayed by both heterozygous *grin2Ab*$^{+/-}$ and homozygous *grin2Ab*$^{-/-}$ larvae (Figure 46). This phenotype is similar to *grin1* larvae's tapping alterations, but strikingly is the opposite of *grin2Aa* response. It is remarkable that the loss-of-function of two paralog genes with high homology present opposite behaviours.

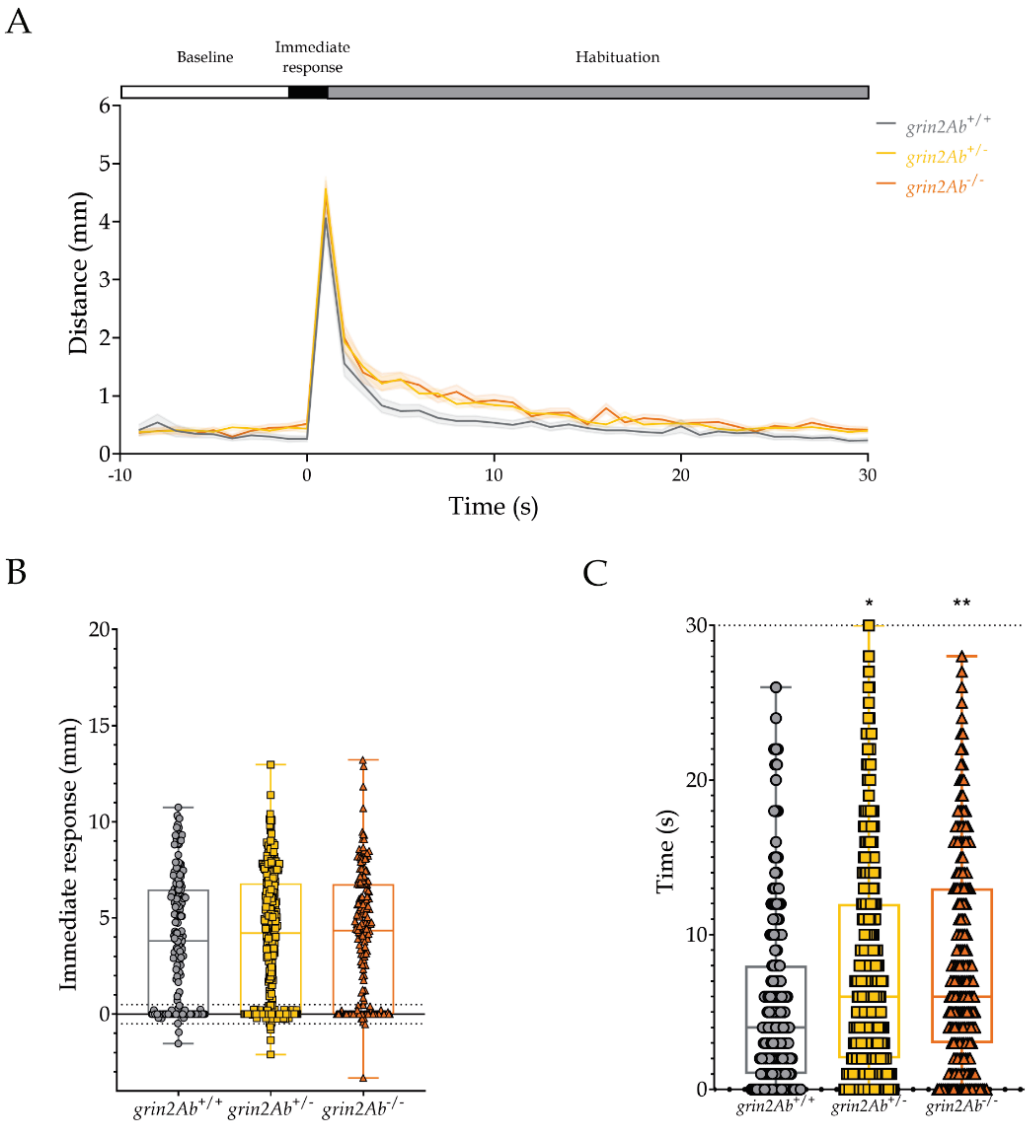

Figure 46. Evaluation to the immediate response and habituation to tapping in *grin2Ab* mutant larvae. A. Graph of the distanced moved in one-second time bin. B. Graph representing the difference in the distance moved as a response to the first tap. Statistical analysis of the immediate response (mm) is represented with "*". Statistical analysis of the number of larvae responding (%) is represented with "#". C. Quantification of the habituation by measuring the time each larva takes to not respond to the stimulus, with a cut off at 30 seconds. . In panel A, data is represented as mean ± SEM; in panels B and C, data is represented with box and whisker plots, showing the median, minimum and maximum, showing all points. Wild-type *grin2Ab*$^{+/+}$ larvae are represented in grey (N=166), heterozygous *grin2Ab*$^{+/-}$ in yellow (N=353) and homozygous *grin2Ab*$^{-/-}$ in orange (N=198). * $p<0.05$, ** $p<0.01$ (One-way ANOVA with Tukey's post-hoc analysis).

Finally, we performed the same paradigm with the double *grin2Aa* – *grin2Ab* line. In agreement with the results obtained for the single knockout lines, no differences were observed in the immediate response to tactile stimulus (Figure 47D). However, we observed a decrease in the time to habituate to the stimulus in *grin2Aa*$^{-/-}$ larvae. In contrast, the heterozygous *grin2Aa*$^{+/-}$ larvae did not present any alteration, and the observed behaviour was milder (Figure 47E). Additionally, a decrease in the time to habituate was also observed in the double mutant larvae *grin2Aa*$^{-/-}$ - *grin2Ab*$^{+/-}$. In contrast, double homozygous *grin2Aa*$^{-/-}$ - *grin2Ab*$^{-/-}$ larvae did not present any alteration in the habituation behaviour, reinforcing the hypothesis that genetic compensation might be playing a role to modulate the presence of *grin2A* loss-of-function in the progenitors.

A

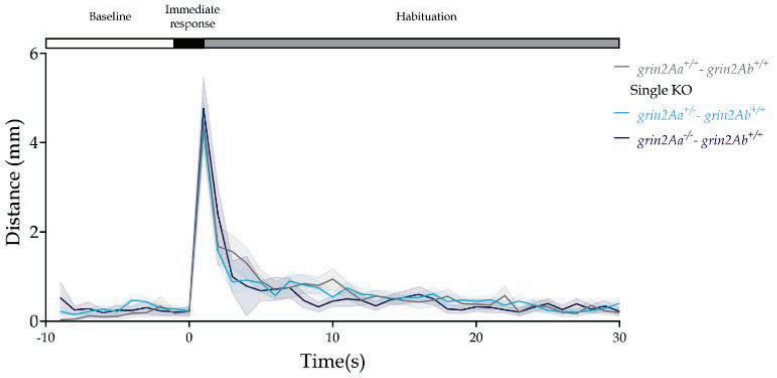
Baseline
Immediate response
Habituation
Distance (mm)
Time(s)
Single KO

B

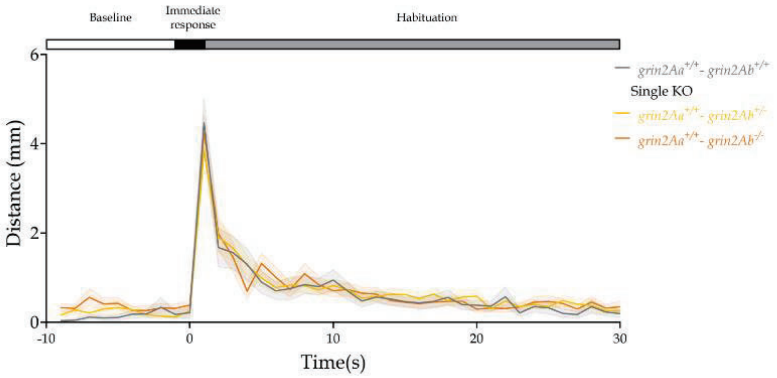
Baseline
Immediate response
Habituation
Distance (mm)
Time(s)
Single KO

C

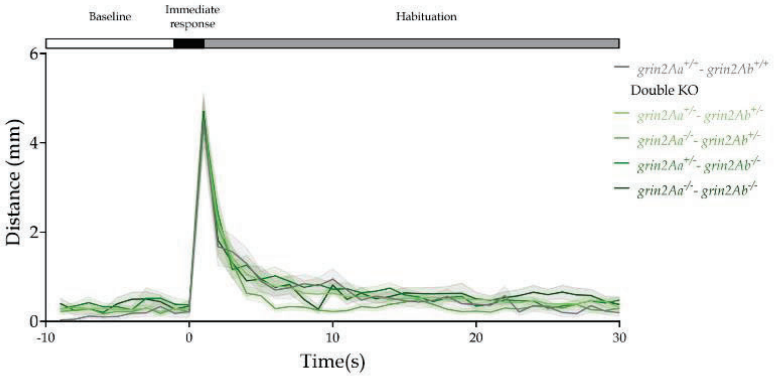
Baseline
Immediate response
Habituation
Distance (mm)
Time(s)
Double KO

D

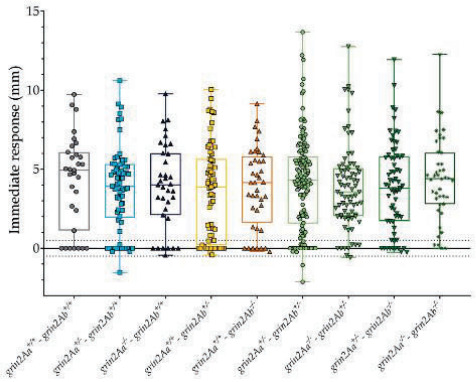
Immediate response (mm)

E

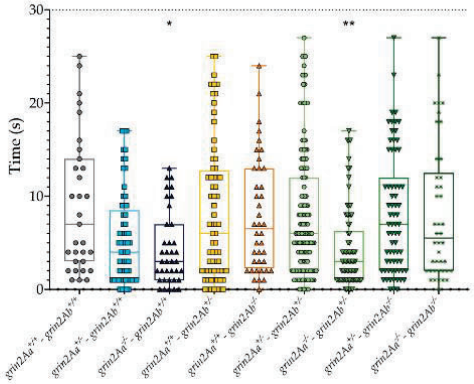
Time (s)

Figure 47. Evaluation to the immediate response and habituation to tapping in in *grin2Aa-grin2Ab* double mutant larvae. A, B, C. Representation of the distanced moved in one-minute time bin, showing a characteristic response pattern. The data was divided into different panels: *grin2Aa* single knockouts (A), *grin2Ab* single knockouts (B) and double knockouts (C). D. Graph representing the difference in the distance moved as a response to the first tap. Statistical analysis of the immediate response (mm) is represented with "*". Statistical analysis of the number of larvae responding (%) is represented with "#". E. Quantification of the habituation by measuring the time each larva takes to not respond to the stimulus, with a cut off at 30 seconds. In panels A to C, data is represented as mean ± SEM; in panels D and E, data is represented with box and whisker plots, showing the median, minimum and maximum, showing all points. Wild-type *grin2Aa*$^{+/+}$-*grin2Ab*$^{+/+}$ larvae are represented in grey (N=31), heterozygous *grin2Aa*$^{+/-}$ in light blue (N=66), homozygous *grin2Aa*$^{-/-}$ in dark blue (N=37), heterozygous *grin2Ab*$^{+/-}$ in yellow (N=68), homozygous *grin2Ab*$^{-/-}$ in orange (N=40), double heterozygous *grin2Aa*$^{+/-}$-*grin2Ab*$^{+/-}$ in lime (N=144), homozygous for *grin2Aa* and heterozygous for *grin2Aa*, *grin2Aa*$^{-/-}$-*grin2Ab*$^{+/-}$ in light green (N=78), heterozygous for *grin2Aa* and homozygous for *grin2Ab*, *grin2Aa*$^{+/-}$-*grin2Ab*$^{-/-}$ in green (N=70), and the double homozygous *grin2Aa*$^{-/-}$-*grin2Ab*$^{-/-}$, in dark green (N=42). *p<0.05, **p<0.01 (One-way ANOVA with Tukey's post-hoc analysis).

3.2.3.3. Study of epilepsy-like responses to light flashes of grin2A models

In the *grin2Aa* line, the tracking of the larval movement after the flashes was not differing from wild-type siblings (Figure 48A). No significant habituation was observed in wild-type *grin2Aa*$^{+/+}$ larvae, in the heterozygous *grin2Aa*$^{+/-}$ or homozygous *grin2Aa*$^{-/-}$ larvae (Supplementary Figure 16). Similar responses to the different flashes were observed. Accordingly, every flash response was considered as an independent replicate and the average response was quantified (Figure 48B-C). Moreover, to compare the results with the other mutant larvae, the independent analysis of the response to the first flash was also performed (Figure 48D-E). No significant differences were observed when comparing the *grin2Aa* mutants *grin2Aa*$^{+/-}$ and *grin2Aa*$^{-/-}$ to their wildtype siblings *grin2Aa*$^{+/+}$. Overall, these data showed that *grin2Aa* loss-of-function does not alter the sensitivity to develop seizure-like responses triggered by light flashes.

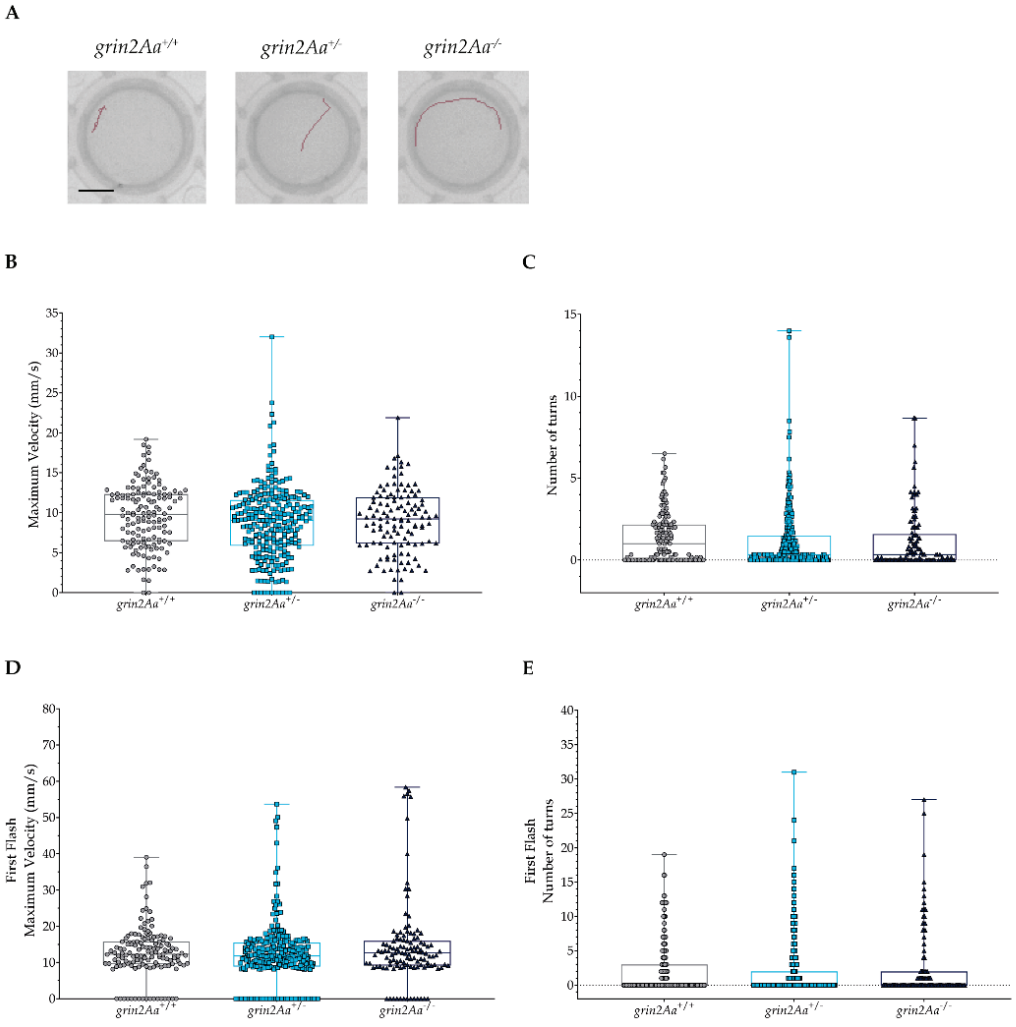

Figure 48. Light-induced epilepsy-like response evaluation in *grin2Aa* mutant larvae. A. Representative images of the tracking of single larvae, recorded 2 seconds after the first applied flash. Scale bar = 6mm. B. Measurement of the maximum velocity (mm/s) achieved, comparing the average of the five trials. C. Measurement of the total number of angle turns performed, comparing the average of the five trials. D. Measurement of the maximum velocity (mm/s) achieved, comparing only the response to the first flash. C. Measurement of the total number of angle turns performed, comparing only the response to the first flash. The data is represented with box and whisker plots, showing the median, minimum and maximum, showing all points. Wild-type *grin2Aa*$^{+/+}$ larvae are represented in grey (N=142), heterozygous *grin2Aa*$^{+/-}$ in light blue (N=266) and homozygous *grin2Aa*$^{-/-}$ in dark blue (N=117).

Regarding *grin2Ab* lines, both the heterozygous *grin2Ab*$^{+/-}$ and homozygous *grin2Ab*$^{-/-}$ displayed a habituation to the light stimulation (Supplementary Figure 17). Therefore, the response to the light stimulation was analysed *i*) using the average of the five flashes and *ii*) only considering the first flash. In both analyses similar results were obtained. A mild but not significant increase in the response was observed in heterozygous *grin2Ab*$^{+/-}$ larvae, but only in the maximum velocity achieved. Importantly, a significant epilepsy-like behaviour was observed in homozygous *grin2Ab*$^{-/-}$ larvae, both measuring the velocity and the number of turns. The epilepsy-like behaviour was also evident when considering the tracking of the larvae right after the light-flashes (Figure 49).

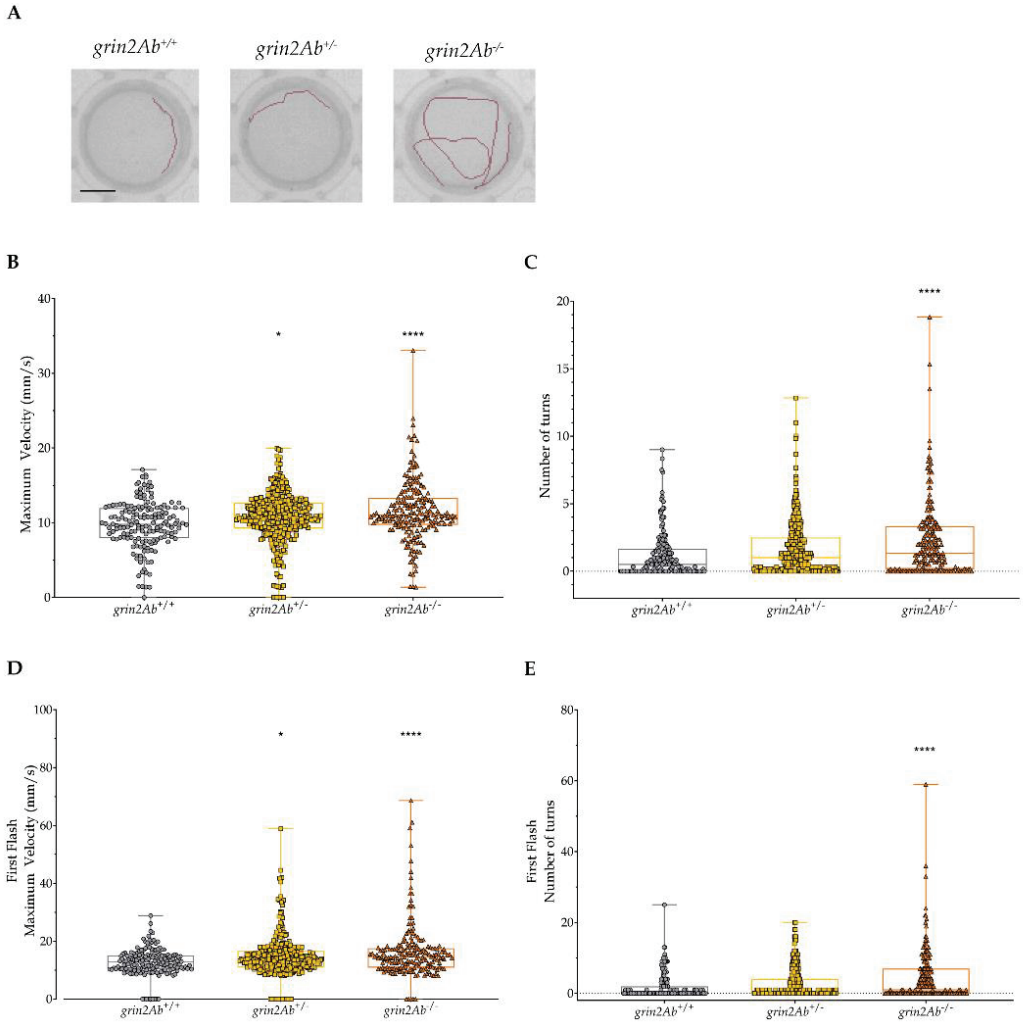

Figure 49. Light-induced epilepsy-like response evaluation in *grin2Ab* mutant larvae. A. Representative images of the tracking of single larvae, recorded 2 seconds after the first applied flash. Scale bar = 6mm. B. Measurement of the maximum velocity (mm/s) achieved, comparing the average of the five trials. C. Measurement of the total number of angle turns performed, comparing the average of the five trials. D. Measurement of the maximum velocity (mm/s) achieved, comparing only the response to the first flash. C. Measurement of the total number of angle turns performed, comparing only the response to the first flash. The data is represented with box and whisker plots, showing the median, minimum and maximum, showing all points. Wild-type *grin2Ab*$^{+/+}$ larvae are represented in grey (N=166), heterozygous *grin2Ab*$^{+/-}$ in yellow (N=353) and homozygous *grin2Ab*$^{-/-}$ in orange (N=198). *p<0.05, ****p<0.0001 (One-way ANOVA with Tukey's post-hoc analysis).

When analysing the response to light-flashes in the double mutant *grin2Aa – grin2Ab* larvae, interestingly we did not observe a significant response in any of the studied mutant larvae (Figure 50, Supplementary Figures 18 and 19). In accordance with previous results, the absence of phenotypes in the double mutant larvae reinforced the hypothesis of compensatory mechanisms activation.

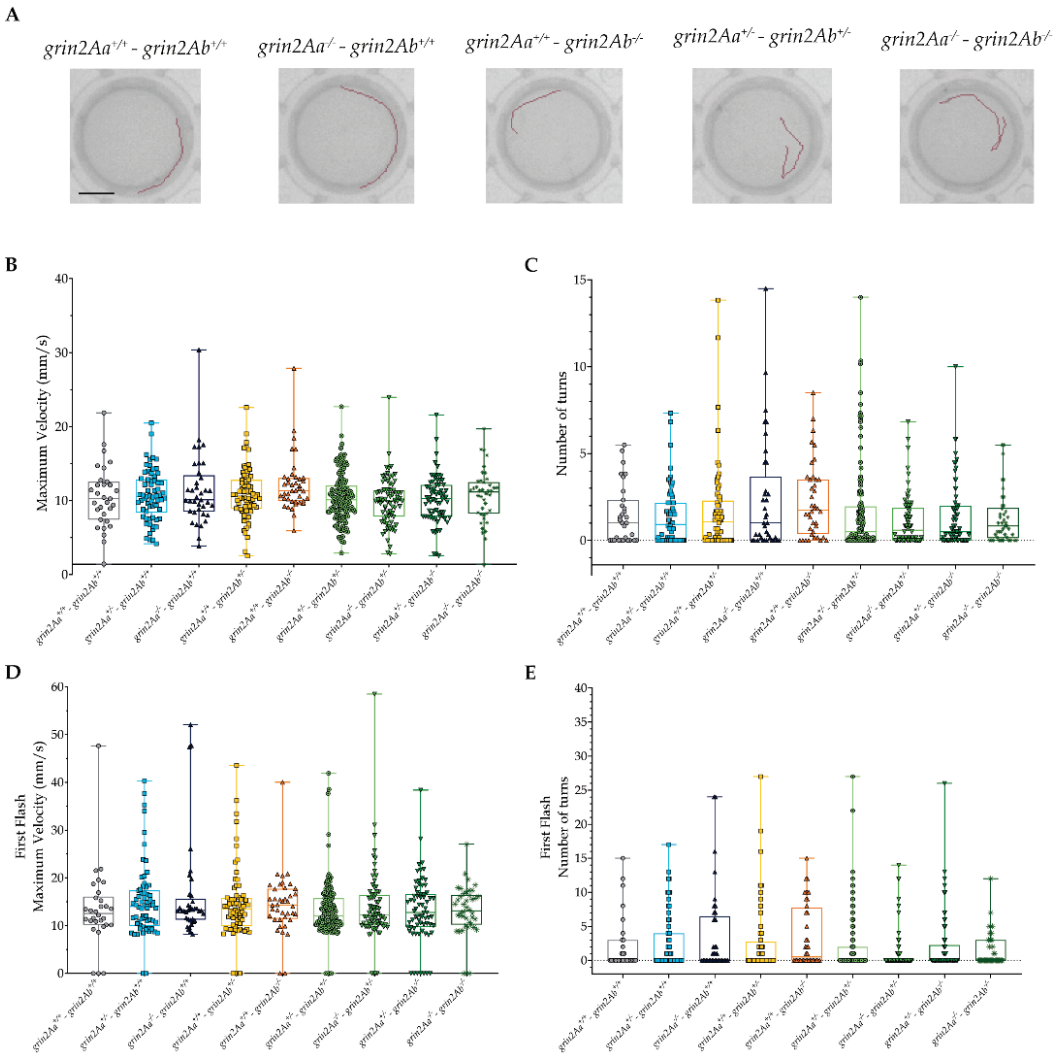

Figure 50. Light-induced epilepsy-like response evaluation in double *grin2Aa – grin2Ab* mutant larvae. A. Representative images of the tracking of single larvae, recorded 2 seconds after the first applied flash. Scale bar = 6mm. B. Measurement of the maximum velocity (mm/s) achieved, comparing the average of the five trials. C. Measurement of the total number of angle turns performed, comparing the average of the five trials. D. Measurement of the maximum velocity (mm/s) achieved, comparing only the response to the first flash. C. Measurement of the total number of angle turns performed, comparing only the response to the first flash. The data is represented with box and whisker plots, showing the median, minimum and maximum, showing all points. Wild-type *grin2Aa*$^{+/+}$-*grin2Ab*$^{+/+}$ larvae are represented in grey (N=31), heterozygous *grin2Aa*$^{+/-}$ in light blue (N=66), homozygous *grin2Aa*$^{-/-}$ in dark blue (N=37), heterozygous *grin2Ab*$^{+/-}$ in yellow (N=68), homozygous

grin2Ab$^{-/-}$ in orange (N=40), double heterozygous *grin2Aa*$^{+/-}$-*grin2Ab*$^{+/-}$ in lime (N=144), homozygous for *grin2Aa* and heterozygous for *grin2Aa, grin2Aa*$^{-/-}$-*grin2Ab*$^{+/-}$ in light green (N=78), heterozygous for *grin2Aa* and homozygous for *grin2Ab*, *grin2Aa*$^{+/-}$-*grin2Ab*$^{-/-}$ in green (N=70), and the double homozygous *grin2Aa*$^{-/-}$-*grin2Ab*$^{-/-}$, in dark green (N=42). *p<0.05, **p<0.01, ***p<0.001, ****p<0.0001 (One-way ANOVA).

The behavioural characterisation of *grin2A* models revealed the presence of genotype-dependent alterations of locomotor, anxiety, habituation and epilepsy-like phenotypes that are summarized in the table below.

Summary of the grin2A phenotypic characterisation

Paradigm	Variable	*grin2Aa*		*grin2Ab*		*grin2Aa – grin2Ab*			
		grin2Aa$^{+/-}$	*grin2Aa*$^{-/-}$	*grin2Ab*$^{+/-}$	*grin2Ab*$^{-/-}$	*grin2Aa*$^{-/-}$ - *grin2Ab*$^{+/+}$	*grin2Aa*$^{+/+}$ - *grin2Ab*$^{-/-}$	*grin2Aa*$^{+/-}$ - *grin2Ab*$^{+/-}$	*grin2Aa*$^{-/-}$ - *grin2Ab*$^{-/-}$
Dark/Light cycles	Total distance (mm)	ns (p-value=0.9056)	ns (p-value>0.9942)	ns (p-value=0.6686)	ns (p-value=0.5747)	** (p-value=0.0044)	ns (p-value=0.5786)	* (p-value=0.0479)	ns (p-value=0.3640)
	Total distance in Dark (mm)	ns (p-value=0.8773)	ns (p-value=0.9474)	ns (p-value=0.9228)	ns (p-value=0.7557)	** (p-value=0.0029)	ns (p-value=0.9096)	ns (p-value=0.1643)	ns (p-value=0.4968)
	Total distance in Light (mm)	ns (p-value=0.9005)	ns (p-value=0.2502)	ns (p-value=0.1270)	* (p-value=0.0298)	ns (p-value=0.3815)	ns (p-value=0.2832)	ns (p-value=0.1574)	ns (p-value=0.2564)
	Percentage of time in periphery area	ns (p-value=0.1124)	* (p-value=0.0308)	ns (p-value=0.1883)	ns (p-value=0.4570)	ns (p-value=0.9998)	ns (p-value=0.9483)	ns (p-value=0.5111)	* (p-value=0.0460)
	Dark/Light transitions	ns (p-value=0.1575; 0.8107; 0.1152; 0.5378)	ns (p-value=0.1602; 0.9999; 0.3326; 0.2708)	ns (p-value=0.3723; 0.6037; 0.8274; 0.4974)	ns (p-value=0.9275; 0.3734; 0.9190; 0.4537)	*/ns (p-value=0.4292; 0.2120; 0.0279; 0.8209)	ns (p-value=0.5256; 0.9994; 0.9995; 0.9999)	ns (p-value=0.8484; 0.5768; 0.3941; 0.9738)	ns (p-value=0.8759; 0.7945; 0.9627; 0.9867)
Response and habituation to tapping	Quantitative response to the first stimulus (mm)	ns (p-value= 0.2007)	ns (p-value>0.9999)	ns (p-value=0.7769)	ns (p-value=0.8833)	ns (p-value=0.9971)	ns (p-value=0.9868)	ns (p-value=0.9995)	ns (p-value=0.9997)
	Qualitative response to the first stimulus (%)	ns (p-value=0.6715)	ns (p-value=0.9801)	ns (p-value>0.9999)	ns (p-value=0.9705)	ns (p-value>0.9999)	ns (p-value>0.9999)	ns (p-value>0.9999)	ns (p-value>0.9999)
	Time for habituation (s)	* (p-value=0.0342)	** (p-value=0.0037)	* (p-value=0.0122)	** (p-value=0.0010)	* (p-value=0.0134)	ns (p-value=0.9485)	ns (p-value=0.8004)	ns (p-value=0.9835)
Light-induced epilepsy	Maximum velocity (s)	ns (p-value=0.0922)	ns (p-value=0.4224)	* (p-value=0.0135)	**** (p<0.0001)	ns (p-value=0.8126)	ns (p-value=0.2022)	ns (p-value=0.9997)	ns (p-value=0 9997)
	Number of angle turns	ns (p-value=0.2361)	ns (p-value=0.4675)	ns (p-value=0.0819)	**** (p-value<0.0001)	ns (p-value=0.3208)	ns (p-value=0.4021)	ns (p-value=0.9998)	ns (p-value=0.9977)

Table 14. Summary of the readouts of the *grin2A* model's characterisation. The significance and p-value of all the readouts are represented. To summarise the data, only the single homozygous, double heterozygous and double homozygous mutants were represented in the double mutant line. Significant increased parameters are highlighted in green, while significant decreased parameters are highlighted in red

3.3. Generation and characterisation of grin2B knockout zebrafish models

3.3.1. Generation of grin2B models: knockout strategy

Finally, for the generation of *grin2B* models we also used the CRISPR/Cas9 technology to generate loss-of-function knockout lines. To obtain the double mutant *grin2Ba-grin2Bb* knockout line, single mutant lines were crossed to recapitulate the complete loss-of-function of the *grin2B* genes. As before, the strategy was to knockout these genes in the first possible exon common to all reported *grin2B* isoforms, introducing nonsense mutations to disrupt the ORF and leading to the presence of early STOP codons. e designed two different sgRNAs per gene to target the first possible exon shared with all the isoforms: between exons 1 and 2 for *grin2Ba* (Figure 51A-C) and exon 2 for grin2Bb (Figure 51D-F). In both genes, we inserted out-of-frame deletions, changing the coding lecture and disrupting the protein, leading to a premature STOP codon.

It is crucial to note that, for the generation of *grin2Ba*, the annotated Ensembl sequence led to confusion. The annotation of the specific gene region was disorganised and presented multiple nonsense codons. Moreover, the different domains and conserved regions could not be found following the given sequence. Thanks to the collaboration with Dr. Mireia Olivella, a close academic collaborator from the University of Vic, and taking the whole *Danio rerio* chromosome 3 sequence, we identified the sequence corresponding to *grin2Ba*. Along with some genetic annotations, we finally obtained a corrected *grin2Ba* sequence version, for further genome editing.

In *grin2Ba*, a deletion of 206 nucleotides in exons 1 and 2 was generated (Figure 51B). After the deletion, the codon reading frame was disrupted, and a premature STOP codon appears after seventeen amino-acid translation (Figure 51C). Following the same strategy, in *grin2Bb*, a 115-nucleotide deletion was generated in exon 2 (Figure 51E). The codon reading frame was also disrupted, generating a premature STOP codon eight amino-acids after the deletion region (Figure 51F).

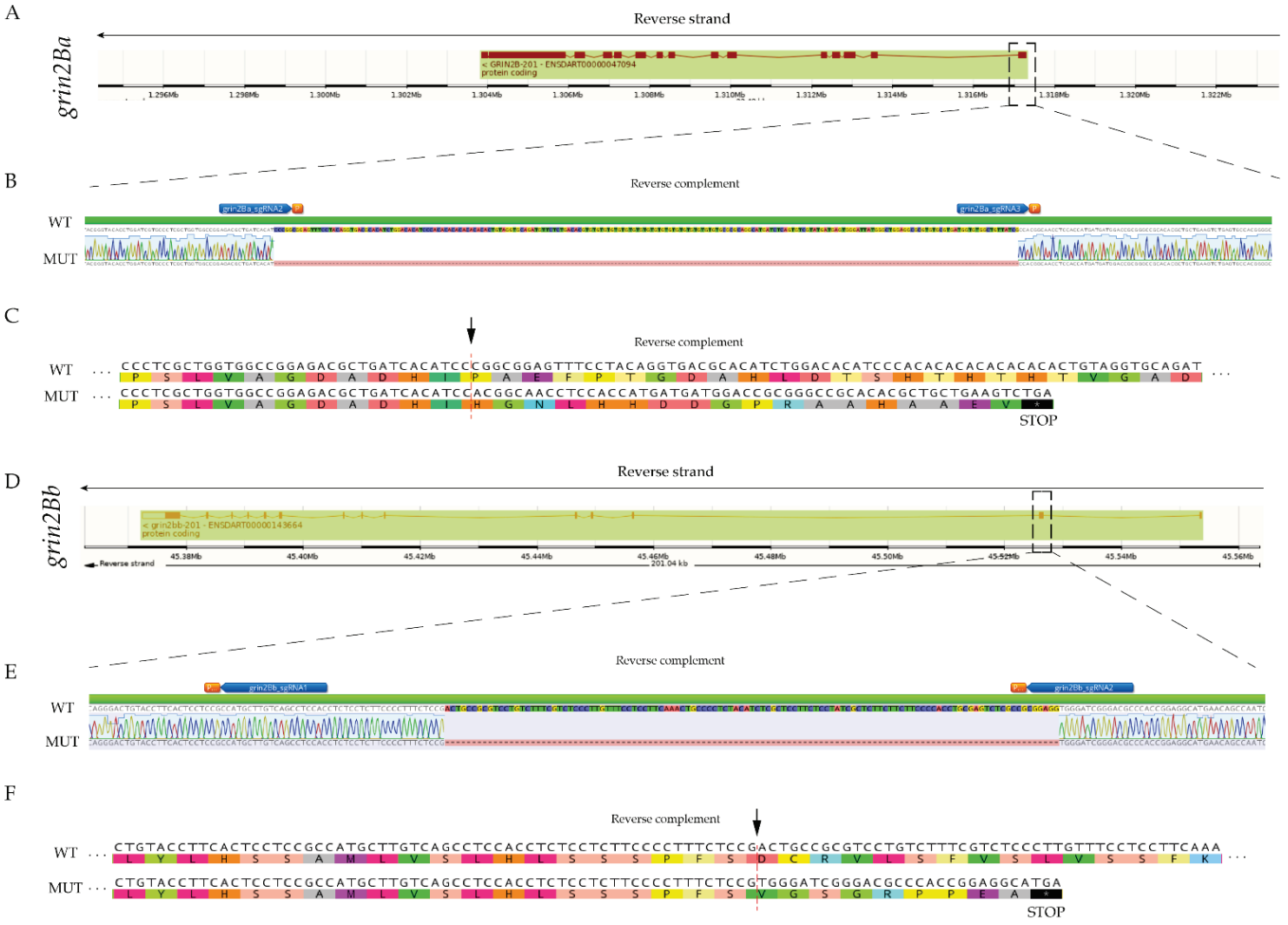
A
grin2Ba
Reverse strand
< GRIN2B-201 - ENSDART00000047094
protein coding
1.296Mb
1.298Mb
1.300Mb
1.302Mb
1.304Mb
1.306Mb
1.308Mb
1.310Mb
1.312Mb
1.314Mb
1.316Mb
1.318Mb
1.320Mb
1.322Mb
B
Reverse complement
grin2Ba sgRNA2
grin2Ba sgRNA3
WT
MUT
C
Reverse complement
WT
MUT
STOP
D
grin2Bb
Reverse strand
< grin2bb-201 - ENSDART00000143664
protein coding
45.38Mb
45.40Mb
45.42Mb
45.44Mb
45.46Mb
201.04 kb
45.48Mb
45.50Mb
45.52Mb
45.54Mb
45.56Mb
Reverse strand
E
Reverse complement
grin2Bb sgRNA1
grin2Bb sgRNA2
WT
MUT
F
Reverse complement
WT
MUT
STOP

Figure 51. Schematic representation of the knockout strategy for *grin2Ba* and *grin2Bb* zebrafish genes. A. D. Schematic representation of *grin2Ba* (A) and *grin2Bb* (D) loci in the zebrafish genome. Adapted from Ensembl database (https://www.ensembl.org/). The different transcripts of the gene are displayed, and the targeted exons for the CRISPR/Cas9 strategy are highlighted. B. E. Representative images of the CRISPR/Cas9-modified regions, the localisation of the sgRNA used (in blue) and their respective protospacer adjacent motifs (PsAMs) in *grin2Ba* (B) and *grin2Bb* (E). Top sequences represent the wild-type reference sequence, and bottom sequences correspond to the mutated sequences. The alignment graph is displayed in-between. The deletions represented as a red dotted line in all the positions where there was any alignment. The deleted or changed nucleotides are coloured, in contraposition of the conserved nucleotides which remain uncoloured. C. F. Enlarged fragments of the CDS and aminoacidic sequence surrounding the deletion localisation of the gene in *grin2Ba* (C) and *grin2Bb* (F). The specific deletion point is highlighted with a vertical arrow and a red dotted line. The premature STOP codon is represented with a black asterisk. Images generated using Geneious Prime software.

3.3.2. Morphological analysis of grin2B GRD models

We analysed defective morphometric phenotypes to understand if *grin2B* mutants displayed any potential developmental delay through the same methodologies previously described.

Images of 120 hpf larvae of both lines *grin2Ba* and *grin2Bb* were performed and analysed, and no significant differences were observed in any of the evaluated morphological phenotypes (Figure 52).

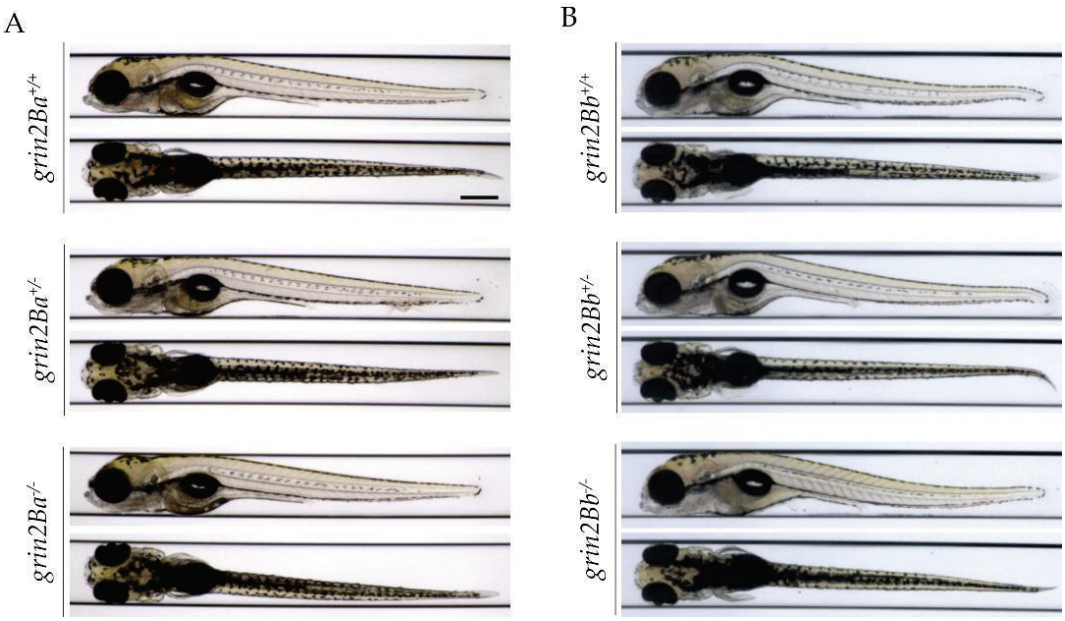

Figure 52. Representative images of the generated *grin2B* ZebraGRIN lines. A. Dorsal (lower panels) and lateral (upper panels) images of *grin2Ba*$^{+/+}$, *grin2Ba*$^{+/-}$ and *grin2Ba*$^{-/-}$ 120 hpf larvae. B. Dorsal (lower panels) and lateral (upper panels) images of *grin2Bb*$^{+/+}$, *grin2Bb*$^{+/-}$ and *grin2Bb*$^{-/-}$ 120 hpf larvae. Scale bar = 300µm

Due to unforeseen delays in the generation of the *grin2B* zebrafish models (*i.e.* annotation inaccuracies of *grin2Ba* gene), it was not possible to include this aspect in this Thesis. Future studies will aim to incorporate this model for a more comprehensive analysis.

3.3.3. Behavioural analysis of grin2B models

We followed the same experimental design used to characterise the behaviour of *grin1* and *grin2A* GRD models. Heterozygous adult animals from the F1 generation were crossed to obtain a progeny where all the possible genotypes were present. In all the experiments, for both *grin2Ba* and *grin2Bb* single knockout lines, the progeny followed mendelian proportions, not showing a mortality at larval stages of any genotype (data not shown).

A summary table of the behavioural findings is available at the end of the section (Table 15).

3.3.3.1. Assessment of motor phenotypes in grin2B knockout lines

To analyse possible locomotor alterations, along with thigmotaxis evaluation to describe anxious behaviours, the dark/light cycles paradigm was performed. The evaluation of the locomotion of *grin2Ba* mutant zebrafish larvae did not unveil locomotor alterations (Figure 53). A mild increase of locomotion activity, principally in light phases, was observed in heterozygous *grin2Ba*$^{+/-}$ larvae, but not in the homozygous *grin2Ba*$^{-/-}$ models (Figure 53A,C and E).

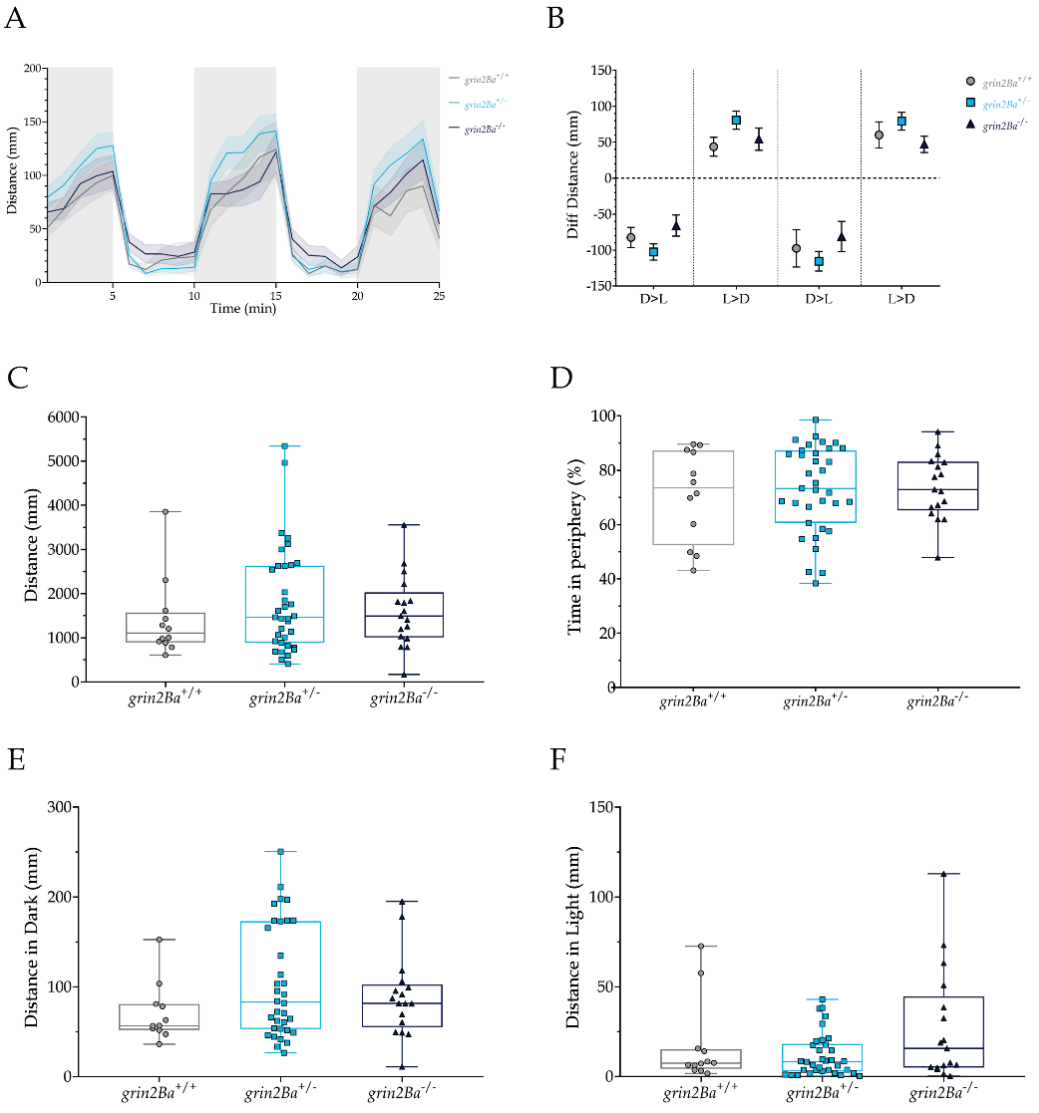

Figure 53. Analysis of the locomotor performance of *grin2Ba* mutant zebrafish larvae. A. Representation of the distance moved by one-minute time bin during the 25-minute dark/light cycles. Dark cycles are annotated as grey vertical lines for better visualisation. B. Representation of the difference of the distance moved in the transitions from dark to light (D>L) and from light to dark (L>D). C. Graph of the total distance moved (mm) of the larvae in the complete 25-minute protocol. D. Analysis of the average percentage of time spent in the peripherical area of the well. E. Graph of the total distance moved (mm) only in the dark phases of the dark/light cycle protocol. F. Graph of the total distance moved (mm) only in the light phases of the dark/light cycle protocol. In panels A and B, data is represented as mean ± SEM; in panels C to F, data is represented with box and whisker plots, showing the median, minimum and maximum, showing all points. Wild-type *grin2Ba*$^{+/+}$ larvae are represented in grey (N=12), heterozygous *grin2Ba*$^{+/-}$ in light blue (N=35) and homozygous *grin2Ba*$^{-/-}$ in dark blue (N=17). *p<0.05 (One-Way ANOVA with Tukey's post-hoc analysis).

The analysis of the *grin2Bb* knockout line revealed a hypolocomotion pattern in the homozygous *grin2Bb*$^{-/-}$ larvae. This hypolocomotion was detected when analysing the dark/light cycles pattern (Figure 54A). This locomotor alteration was quantified and verified through the analysis of general locomotion, unveiling a decrease in the distance moved during the protocol (Figure 54C). The locomotion analysis divided in movement in dark or in light showed a significant decrease in locomotion in both phases (Figure 54E-F). Therefore, the decrease in locomotion was generalised and not only in one of the dark/light phases. No significant differences were observed in the thigmotaxis analysis. (Figure 54D).

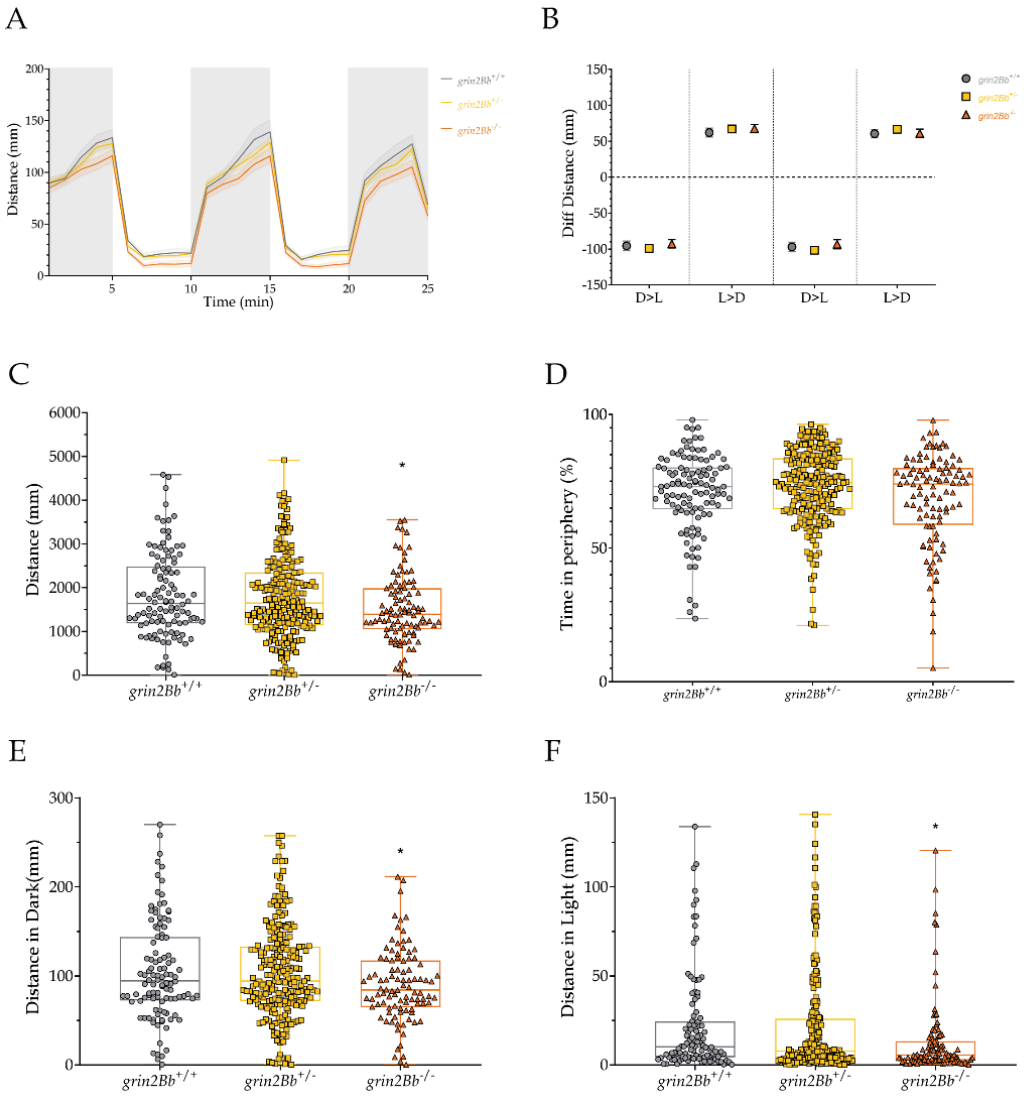

Figure 54. Analysis of the locomotor performance of *grin2Bb* mutant zebrafish larvae. A. Representation of the distance moved by one-minute time bin during the 25-minute dark/light cycles. Dark cycles are annotated as grey vertical lines for better visualisation. B. Representation of the difference of the distance moved in the transitions from dark to light (D>L) and from light to dark (L>D). C. Graph of the total distance moved (mm) of the larvae in the complete 25-minute protocol. D. Analysis of the average percentage of time spent in the peripherical area of the well. E. Graph of the total distance moved (mm) only in the dark phases of the dark/light cycle protocol. F. Graph of the total distance moved (mm) only in the light phases of the dark/light cycle protocol. In panels A and B, data is represented as mean ± SEM; in panels C to F, data is represented with box and whisker plots, showing the median, minimum and maximum, showing all points. Wild-type *grin2Bb*$^{+/+}$ larvae are represented in grey (N=109), heterozygous *grin2Bb*$^{+/-}$ in yellow (N=222) and homozygous *grin2Bb*$^{-/-}$ in orange (N=100). *p<0.05 (One-Way ANOVA with Tukey's post-hoc analysis).

To summarise, locomotor alterations were observed in both *grin2B* generated models. Nevertheless, the observed alterations were opposites, since hyperlocomotion was observed in *grin2Ba* heterozygous model, while the alterations in *grin2Bb* models were hypolocomotion in homozygosis. We could not observe significant alterations in the anxiety levels in the *grin2B* zebrafish models.

3.3.3.2. Analysis of grin2B models' response and habituation to tactile stimuli

The analysis of the immediate response to tapping of single *grin2Ba* knockout line revealed an impairment in heterozygous *grin2Ba*$^{+/-}$ larvae. A significant decrease in the number of larvae responding was observed (Figure 55A-B). Interestingly, this reduction of the response was not observed in homozygous *grin2Ba*$^{-/-}$ larvae. When analysing the habituation to the continuous tactile stimulation, a faster habituation was observed in homozygous *grin2Ba*$^{-/-}$ larvae (Figure 55A,C).

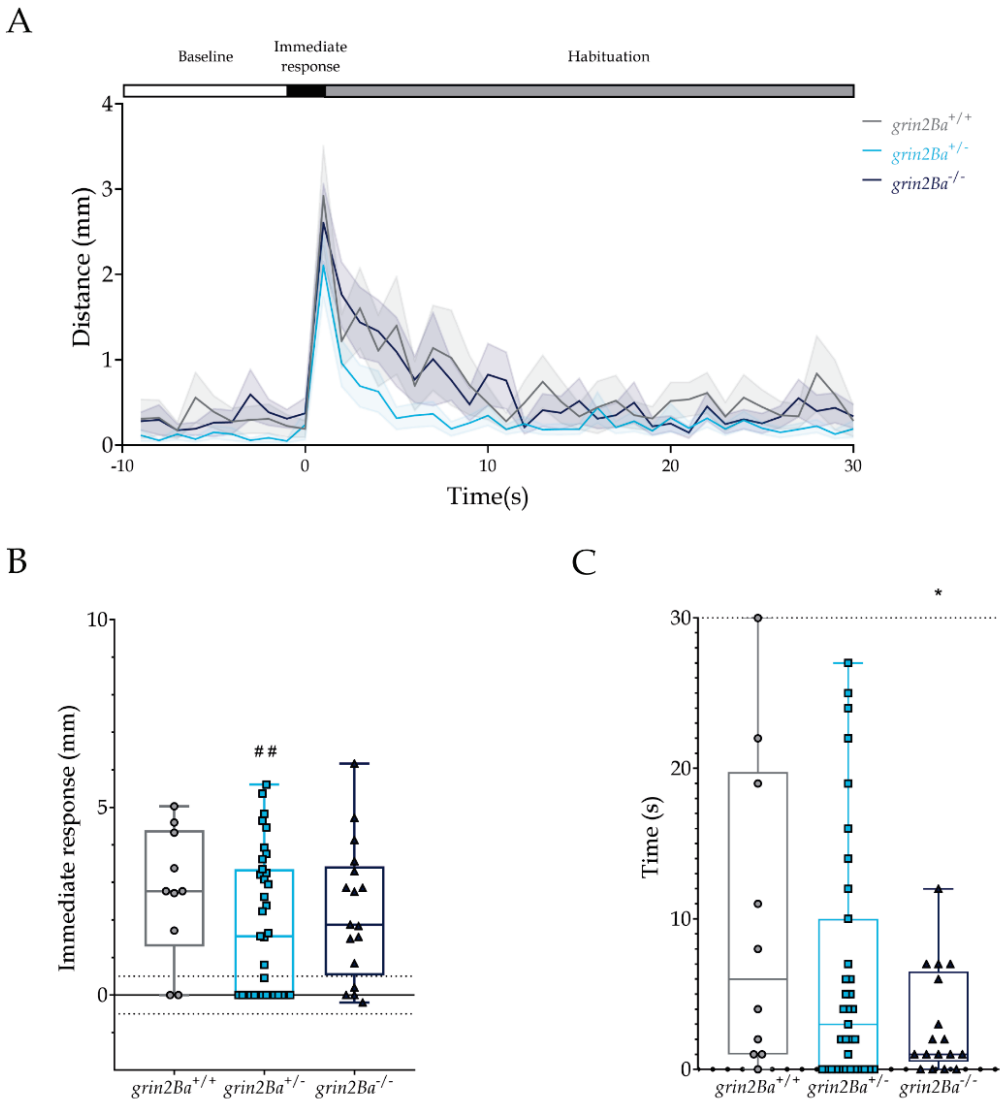

Figure 55. Evaluation to the immediate response and habituation to tapping in *grin2Ba* mutant larvae. A. Graph of the distanced moved in one-second time bin. B. Graph representing the difference in the distance moved as a response to the first tap. Statistical analysis of the immediate response (mm) is represented with "*". Statistical analysis of the number of larvae responding (%) is represented with "#". C. Quantification of the habituation by measuring the time each larva takes to not respond to the stimulus, with a cut off at 30 seconds. In panel A, data is represented as mean ± SEM; in panels B and C, data is represented with box and whisker plots, showing the median, minimum and maximum, showing all points. Wild-type *grin2Ba*$^{+/+}$ larvae are represented in grey (N=10), heterozygous *grin2Ba*$^{+/-}$ in light blue (N=35) and homozygous *grin2Ba*$^{-/-}$ in dark blue (N=17). * $p<0.05$ (One-way ANOVA with Tukey's post-hoc analysis); ## $p<0.01$ Two-way ANOVA with Sidak's multiple comparisons test).

The analysis of the response to external tactile stimuli of the *grin2Bb* models did not reveal any alteration, either in the response amplitude or the number of individuals responding (Figure 56A-B). However, when analysing the habituation to the continuous stimulation, a faster habituation was observed in the homozygous *grin2Bb*$^{-/-}$ model (Figure 56C).

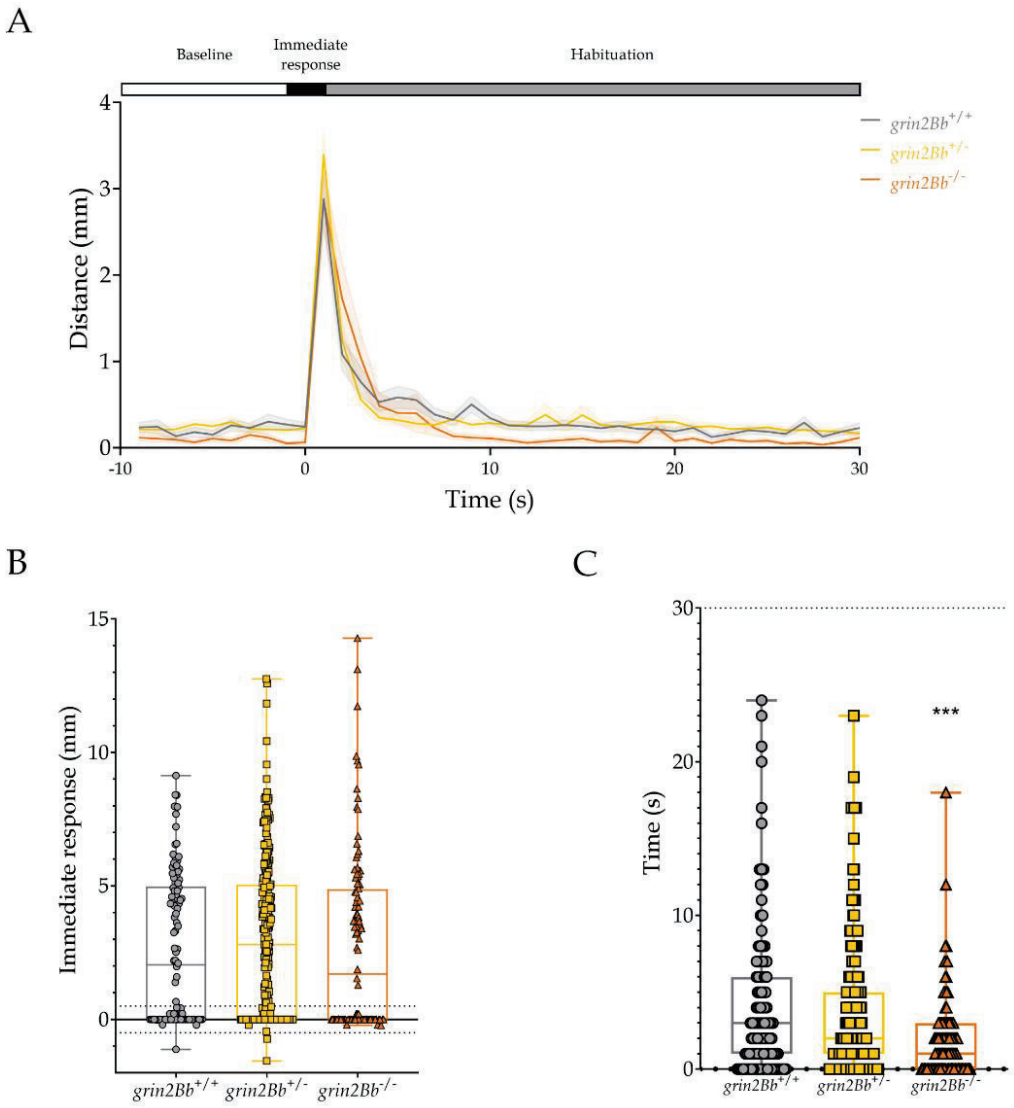

Figure 56. Evaluation to the immediate response and habituation to tapping in *grin2Bb* mutant larvae. A. Graph of the distanced moved in one-second time bin. B. Graph representing the difference in the distance moved as a response to the first tap. Statistical analysis of the immediate response (mm) is represented with "*". Statistical analysis of the number of larvae responding (%) is represented with "#". C. Quantification of the habituation by measuring the time each larva takes to not respond to the stimulus, with a cut off at 30 seconds. Wild-type *grin2Bb*$^{+/+}$ larvae are represented in grey (N=107), heterozygous *grin2Bb*$^{+/-}$ in yellow (N=225) and homozygous *grin2Bb*$^{-/-}$ in orange (N=100). * p<0.05, ** p<0.01 (One-way ANOVA with Tukey's post-hoc analysis).

In conclusion, an impairment in the immediate first response to the tapping stimulus was observed only in heterozygous *grin2Ba*$^{+/-}$ larvae. The analysis of the habituation to the tap stimulus revealed a faster habituation in both models in homozygosis, *grin2Ba*$^{-/-}$ and *grin2Bb*$^{-/-}$.

3.3.3.3. Study of epilepsy-like responses to light flashes of grin2B models

In *grin2Ba* mutant larvae, the tracking of the movement after the flashes showed the absence of seizure-like responses (Figure 57A). Since no significant differences were observed in the response to iterative light flashes for any of the experimental groups (Supplementary Figure 20), we considered each flash response as an independent replicate, and averaged the responses (Figure 57B-C). Furthermore, to compare the results with the other mutant larvae, the independent analysis of the response *vs.* the first flash was also performed (Figure 57D-E). No significant differences were observed when comparing *grin2Ba* mutants (*grin2Ba*$^{+/-}$ and *grin2Ba*$^{-/-}$) to their wildtype siblings.

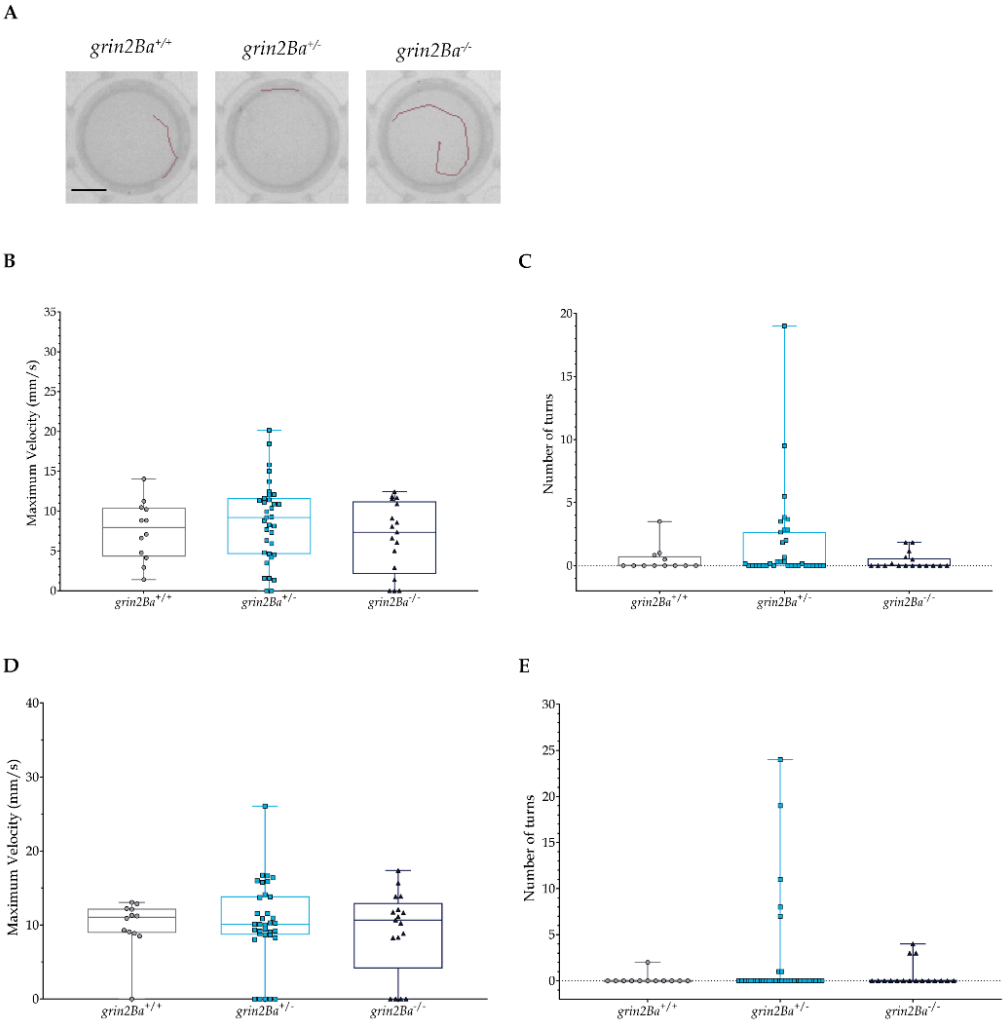

Figure 57. Light-induced epilepsy-like response evaluation in *grin2Ba* mutant larvae. A. Representative images of the tracking of single larvae, recorded 2 seconds after the first applied flash. Scale bar = 6mm. B. Measurement of the maximum velocity (mm/s) achieved, comparing the different average of the five flashes performed. C. Measurement of the total number of angle turns performed, comparing the different average of five flashes performed. D. Measurement of the maximum velocity (mm/s) achieved, comparing only the response to the first flash. C. Measurement of the total number of angle turns performed, comparing only the response to the first flash. The data is represented with box and whisker plots, showing the median, minimum and maximum, showing all points. Wild-type *grin2Ba*$^{+/+}$ larvae are represented in grey (N=12), heterozygous *grin2Ba*$^{+/-}$ in light blue (N=35) and homozygous *grin2Ba*$^{-/-}$ in dark blue (N=17).

The analysis of the habituation to the light-flash stimulus was statistically significant in both heterozygous *grin2Bb*$^{+/-}$ and *grin2Bb*$^{-/-}$ models (Supplementary Figure 21). Therefore, the proper analysis would be considering only the first flash response. Besides this measurement, and towards the comparison with the other models, we performed the analysis considering each flash as an independent observation.

When neglecting the habituation, a significant decrease in the maximum velocity achieved by the heterozygous *grin2Bb*$^{+/-}$ larvae was observed (Figure 58B). Nevertheless, these differences could be related to the habituation and the decrease in the response in the consecutive flashes. In fact, this decrease was not observed when only considering the response to the first flash (Figure 58D). On the contrary, a significant increase in the maximum velocity achieved as a response to the flashes was observed in the homozygous *grin2Bb*$^{-/-}$ generated model. Again, this excessive response was only detected when only considering the first flash. The epilepsy-like behaviour was not visible when considering all the flashes due to a dilution of the response in the analysis. In both types of analysis, no differences were observed in the number of bouts detected (Figure 58C,E).

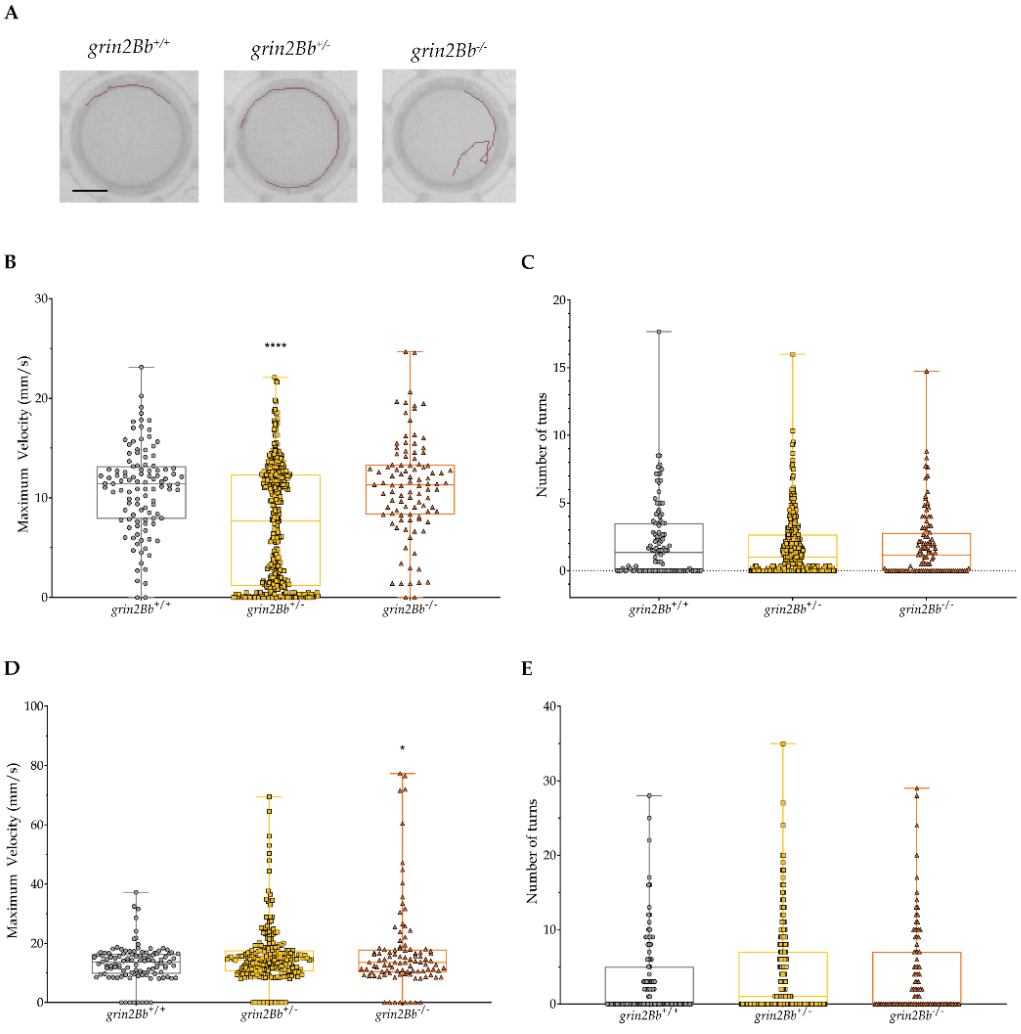

Figure 58. Light-induced epilepsy-like response evaluation in *grin2Bb* mutant larvae. A. Representative images of the tracking of single larvae, recorded 2 seconds after the first applied flash. Scale bar = 6mm. B. Measurement of the maximum velocity (mm/s) achieved, comparing the different average of the five flashes performed. C. Measurement of the total number of angle turns performed, comparing the different average of five flashes performed. D. Measurement of the maximum velocity (mm/s) achieved, comparing only the response to the first flash. C. Measurement of the total number of angle turns performed, comparing only the response to the first flash. The data is represented with box and whisker plots, showing the median, minimum and maximum, showing all points. Wild-type *grin2Bb*$^{+/+}$ larvae are represented in grey (N=109), heterozygous *grin2Bb*$^{+/-}$ in yellow (N=353) and homozygous *grin2Bb*$^{-/-}$ in orange (N=100). *p<0.05, ****p<0.0001 (One-way ANOVA).

To conclude, an increase in the response to light flashes was observed only in homozygous *grin2Bb*$^{-/-}$ larvae, and only in the maximum velocity measurements when considering the response to the first flash. When no epilepsy-like responses were present, habituation to the light flashes was not observed. Conversely, habituation to the stimulus was evident when an increased response to the light was detected.

The behavioural characterization of *grin2B* models revealed genotype-dependent alterations in locomotion, anxiety, habituation, and epilepsy-like phenotypes, as summarized in the table below.

Summary of the grin2B phenotypic characterisation

Paradigm	Variable	*grin2Ba*		*grin2Bb*	
		grin2Ba$^{+/-}$	*grin2Ba*$^{-/-}$	*grin2Bb*$^{+/-}$	*grin2Bb*$^{-/-}$
Dark/Light cycles	Total distance (mm)	ns (p-value=0.3742)	ns (p-value=0.8320)	ns (p-value=0.9147)	* (p-value=0.0348)
	Total distance in Dark (mm)	ns (p-value=0.1308)	ns (p-value=0.5884)	ns (p-value=0.9784)	* (p-value=0.0470)
	Total distance in Light (mm)	ns (p-value=0.6648)	ns (p-value=0.3206)	ns (p-value=0.8979)	* (p-value=0.0385)
	Percentage of time in periphery area	ns (p-value=0.8469)	ns (p-value=0.8008)	ns (p-value=0.3262)	ns (p-value=0.3596)
	Dark/Light transitions	ns (p-value=0.5679; 0.1873; 0.6399; 0.5970)	ns (p-value=0.7314; 0.8756; 0.7345; 0.8178)	ns (p-value=0.8453; 0.7088; 0.7521; 0.6252)	ns (p-value=0.9236; 0.7517; 0.8824; 0.9988)
Response and habituation to tapping	Quantitative response to the first stimulus (mm)	ns (p-value=0.3030)	ns (p-value=0.6903)	ns (p-value=0.4112)	ns (p-value=0.8576)
	Qualitative response to the first stimulus (%)	## (p-value=0.0019)	ns (p-value=0.9636)	ns (p-value=0.6257)	ns (p-value=0.2687)
	Time for habituation (s)	ns (p-value=0.3271)	* (p-value=0.0417)	ns (p-value=0.2183)	*** (p-value=0.0002)
Light-induced epilepsy	Maximum velocity (s)	ns (p-value=0.6571)	ns (p-value=0.8168)	**** (p-value<0.0001)	ns (p-value=0.9442)
	Number of angle turns	ns (p-value=0.3091)	ns (p-value=0.9883)	ns (p-value=0.2042)	ns (p-value=0.6296)

Table 15. Summary of the readouts of the *grin2A* model's characterisation. The significance and p-value of all the readouts are represented. To summarise the data, only the single homozygous, double heterozygous and double homozygous mutants were represented in the double mutant line. Significant increased parameters are highlighted in green, while significant decreased parameters are highlighted in red

4. Design, development and validation of novel techniques to evaluate GRD-like alterations in zebrafish larvae

4.1. Functional assessment of gastrointestinal function in zebrafish larvae

Gastrointestinal (GI) alterations are commonly neglected or unconsidered when characterising neurodevelopmental conditions, in part due to the severity of primary CNS-related disorders (e.g. cognition, communication, epilepsy). However, our recent clinical findings in GRD patients showed that gastrointestinal distress is very frequent and represents a daily burden for GRD patients.

Considering some of the characteristics that make zebrafish an innovative model, such as the fast development of their systems and their transparency during the development, we decided to develop a new set of in vivo-based assays to investigate the gastrointestinal function. Physiologically, the zebrafish gastrointestinal tract matures and is functional (active food intake and gastrointestinal motility) at 6-7 dpf. Accordingly, GI experiments were performed with 7 dpf larvae, assuring the proper maturation and functionality of the GI system. Technically, we used the anticholinergic compound Atropine (4.2µM, co-applied with fluorescent food) as a positive control of drug-induced constipation without affecting food intake. Since *grin1* genes encode for the NMDAR obligatory subunit, we set-up and optimised the gastrointestinal analysis tools using the *grin1* generated mutants.

For the quantification of the GI function, two different readouts frequently altered in GRD patients were evaluated in zebrafish larvae: the ability to ingest the available food and the transit time, defined as the time from food ingestion to the excretion of non-absorbed organic material. For the first readout, monitoring of food-conjugated fluorescence in the larvae body was performed immediately after 6 hours of food administration. To compare the data, all the values were normalised to wildtype larvae average food intake. For the evaluation of the digestive performance, a second image was obtained sixteen hours after the image of the initial intake. The ratio between the fluorescence intensity at these time-points was indicative of the motility speed for non-digested food excretion. Thus, low ratios were indicative of constipation, while high ratios were related with a faster food excretion.

To address both phenotypes, and benefiting from the VAST imaging technology, we designed a two-timepoint protocol in which both parameters could be evaluated. For this procedure we needed a food that could be consumed by 7 dpf larvae. The ingested food can easily be detected in the larval zebrafish gut, with an obscure aspect. However, and besides being evident, this was not quantifiable. Therefore, we needed a different approach that allowed a quantitative analysis. For this reason, we decided to combine the lipidic feeding of the chicken egg yolk, compatible in size with larval intake, and the binding to free lipids of the BODIPY dye. By combining these two elements, we obtained a fluorescent food of the proper size to be recognised and eaten by larvae, and at the same time could be quantified by fluorescence intensity (Figure 59).

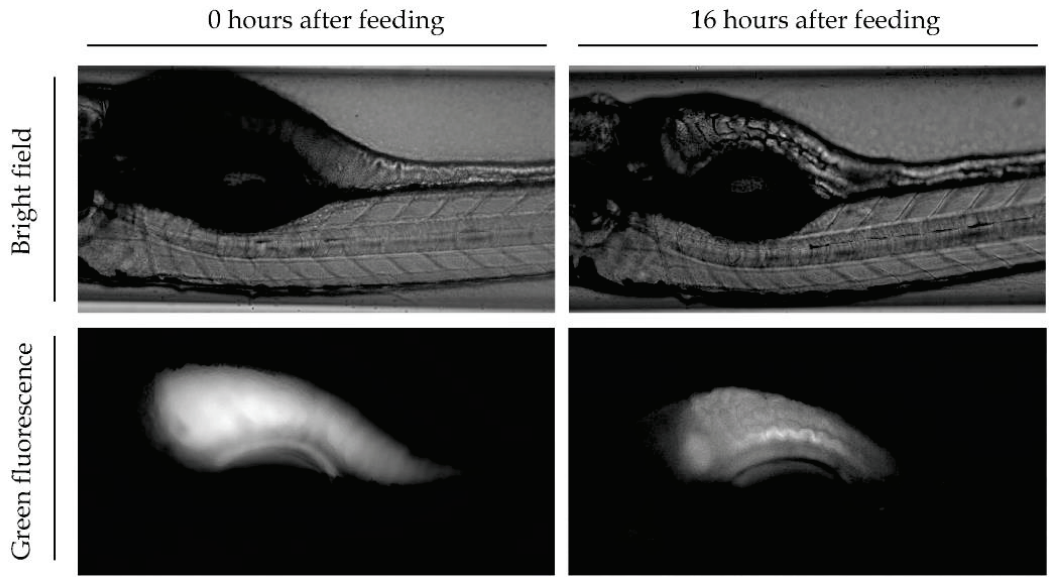

Figure 59. Representation of the larval food observed in the zebrafish gastrointestinal tract. Representative images of 7 dpf larvae at the different time points used for GI function analysis. Bright field (top) and green fluorescence (bottom) z-stack images were obtained.

In *grin1a* single models, food intake of homozygous *grin1a*$^{-/-}$ larvae was normal (Figure 60A). Homozygous *grin1a*$^{-/-}$ larvae exhibited a decreased motility (similar to atropine-treated larvae) indicative of constipation (Figure 60B). Surprisingly, the results were opposite in homozygous *grin1b*$^{-/-}$ larvae that displayed a significantly decreased food intake (Figure 60C) but not disturbed gastrointestinal motility (Figure 60D).

In relation with the double mutants study, the offspring of double heterozygous *grin1a*$^{+/-}$ - *grin1b*$^{+/-}$ parents showed normal GI function, with the exception of the *grin1a*$^{+/-}$ - *grin1b*$^{-/-}$ and double homozygous *grin1a*$^{-/-}$ - *grin1b*$^{-/-}$ showed a reduction of food intake and the evacuation ratio. These results would be recapitulating the GI distress generally reported in GRD patients.

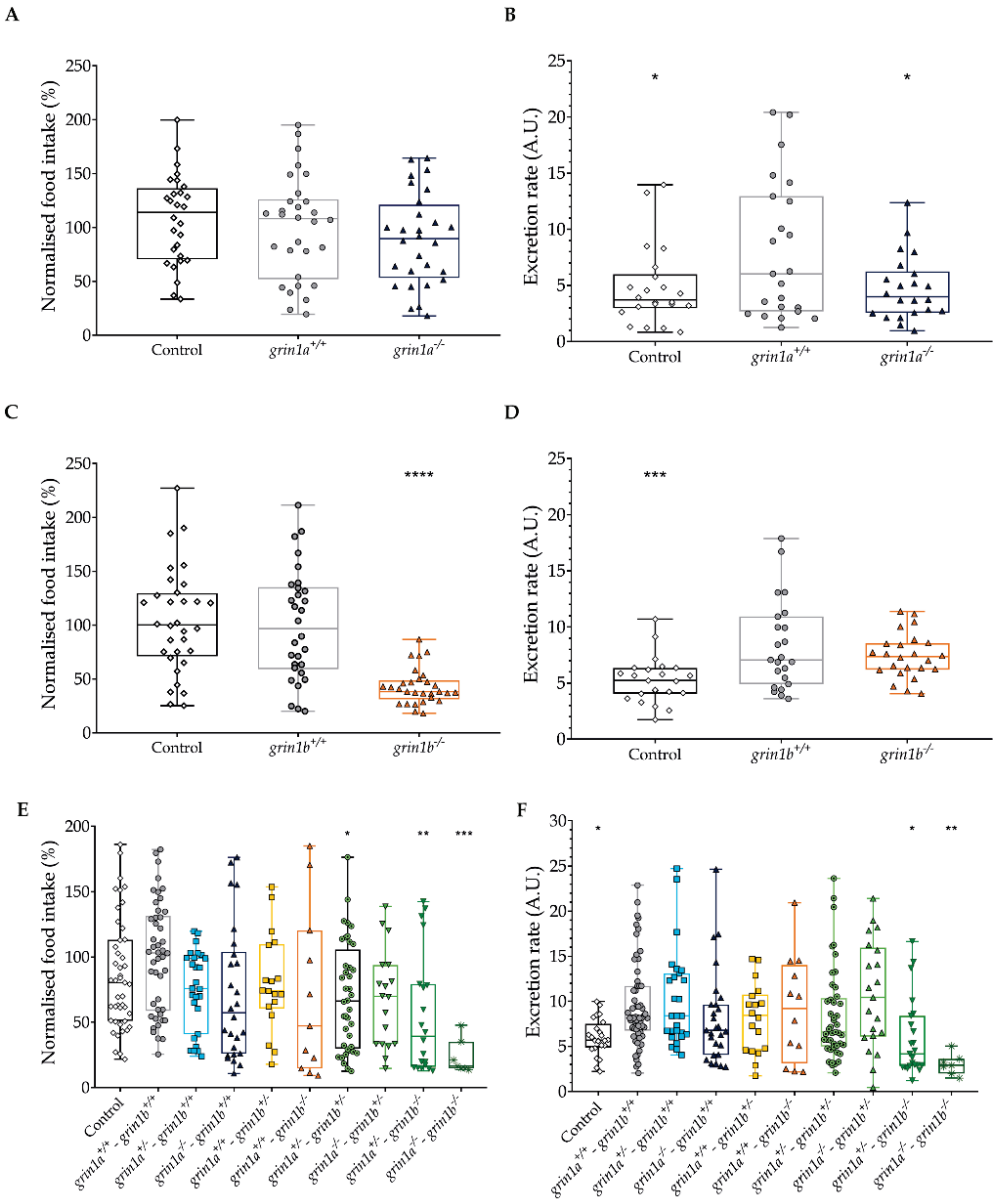

Figure 60. Evaluation of the intake and digestive performance of the *grin1* models. A. Normalised values of the initial intake of *grin1a* zebrafish model. B. Ratio of the two analysed timepoints to evaluate the digestive performance of *grin1a* larvae. C. Normalised values of the initial intake of *grin1b* zebrafish model. D. Ratio of the two analysed timepoints to evaluate the digestive performance of *grin1b* larvae. E. Normalised values of the initial intake of double *grin1a – grin1b* zebrafish model. F. Ratio of the two analysed timepoints to evaluate the digestive performance of *grin1a – grin1b* double mutant larvae. Control (Atropine-treated) larvae are represented in black and white, wild-type larvae are represented in grey, homozygous *grin1a*$^{-/-}$ in dark blue, homozygous *grin1b*$^{-/-}$ in orange, double heterozygous *grin1a*$^{+/-}$-*grin1b*$^{+/-}$ in lime, homozygous for *grin1a* and heterozygous for *grin1a, grin1a*$^{-/-}$-*grin1b*$^{+/-}$ in light green, heterozygous for *grin1a* and homozygous for *grin1b, grin1a*$^{+/-}$-*grin1b*$^{-/-}$ in green, and the double homozygous *grin1a*$^{-/-}$-*grin1b*$^{-/-}$, in dark green. *p<0.05, **p<0.01; ***p<0.001; ****p<0.0001 (One-Way ANOVA with Tukey's post-hoc analysis).

These results validated the experimental methodology to *in vivo* assess the functionality of GI tract, not only in a pharmacological model (atropine) but also in genetic models. Although the complete library of grin models generated have not been comprehensively assessed, the initial findings in *grin1* models (alterations on the rate of food intake and GI motility) recapitulate GRD-associated GI symptoms.

4.2. Characterisation of visual impairment through colour preference

Visual impairment is a common phenotype that has been reported in a subset of GRD patients (García-Recio et al., 2021). Therefore, visual alterations could be also present in genetic zebrafish *grin* models, and upon their putative identification might represent an *in vivo* readout. Considering the blue-colour preference of zebrafish larvae (a vision-dependent ethological innate response), we designed and developed a novel protocol to assess vision.

Based on the developmental establishment of the zebrafish visual system (formed and functional at 120 hpf, alike the CNS and movement behaviour), the colour preference test was performed with 120 hpf larvae placed in bottom-coloured wells, subdivided in blue and yellow. The behavioural evaluation consisted of quantifying the preference index, resulting from dividing the percentage of time spent in the preference area (blue) over the time spent in the non-preference area (yellow). Additionally, heatmaps were used to illustrate in a colour-based manner the time spent in each area of the well. Similarly to what was proposed in the gastrointestinal protocol, we decided to use *grin1* generated mutants to set up and optimise this new *in vivo* assay.

The analysis of *grin1a* and *grin1b* single mutants did not show an impairment or differences in the colour preference (Figure 61A-F), indicating the lack of visual deficits at this developmental stage. Interestingly, a significant impairment in the colour discrimination was observed only in the double homozygous *grin1a*$^{-/-}$ - *grin1b*$^{-/-}$ models, with no colour preference (Figure 61G-I). The visual impairment and the equal movement in both areas was confirmed when visualising the heatmap of the larval movement during the whole protocol (Figure 61G).

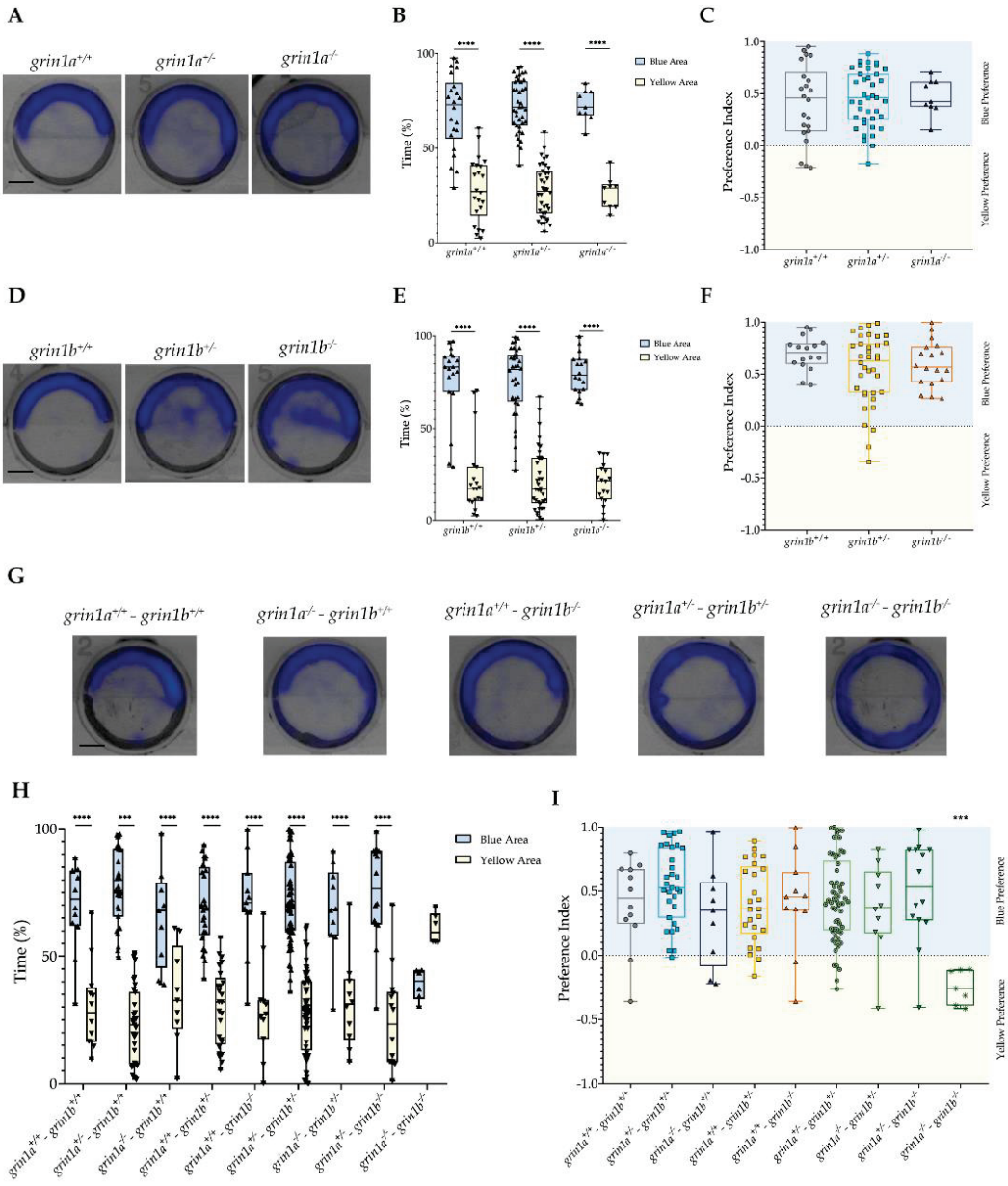

Figure 61. Evaluation of visual impairment in zebrafish larvae using a colour-preference based test. A. Representative images of the heatmap generated from the movement of *grin1a* larva during the trial. B. Percentage of time spent in blue and yellow areas of each *grin1a* larva. C. Preference index representation of the *grin1a* models. Values over zero refer to blue area preference, while values below zero refer to yellow area preference. D. Representative images of the heatmap generated from the movement of *grin1b* larva during the trial. E. Percentage of time spent in blue and yellow areas of each *grin1b* larva. F. Preference index representation of the *grin1* models. Values over zero refer to blue area preference, while values below zero refer to yellow area preference. G. Representative images of the heatmap generated from the movement of *grin1a - grin1b* larva during the trial. H. Percentage of time spent in blue and yellow areas of each *grin1a – grin1b* larva. I. Preference index representation of the *grin1a – grin1b* models. Values over zero refer to blue area preference, while values below zero refer to yellow area preference. Wild-type larvae are represented in grey, heterozygous *grin1a*$^{+/-}$ in light blue, homozygous *grin1a*$^{-/-}$ in dark blue, heterozygous *grin1b*$^{+/-}$ in yellow, homozygous *grin1b*$^{-/-}$ in orange, double heterozygous *grin1a*$^{+/-}$*-grin1b*$^{+/-}$ in lime, homozygous for *grin1a* and heterozygous for *grin1a*, *grin1a*$^{-/-}$*-grin1b*$^{+/-}$ in

light green, heterozygous for *grin1a* and homozygous for *grin1b*, *grin1a*$^{+/-}$-*grin1b*$^{-/-}$ in green, and the double homozygous *grin1a*$^{-/-}$-*grin1b*$^{-/-}$, in dark green. ***p<0.001, ****p<0.0001 (Two-way ANOVA ANOVA with Sidak's multiple comparisons test in the blue-yellow preference and One-way ANOVA with Tukey's post-hoc analysis in the preference index).

The development of this novel in vivo assay represents a novel tool for the functional assessment of the presence of GRD-associated visual impairment. Although the grin models library has not been comprehensively studies with this assay, the presence of a strong phenotype in the double homozygous grin1 model supports the involvement of the NMDAR in vision development and/or physiology.

5. PharmaGRIN: evaluation of tolerability and behavioural impact of novel potential NMDAR modulators

The final purpose of this Thesis research was to assess novel potential therapies primarily targeting the NMDAR, to expand the pharmacological tools for a precision medicine of GRD. Furthermore, glutamatergic neurotransmission disturbance and, more precisely the alteration of NMDAR function, has been widely associated to a plethora of neurological disorders Consequently, beyond the direct beneficial effects for GRD, the pharmacological study of novel NMDAR modulators can have a wide relevance for translational neurology.

With this objective, and born from the collaboration between Dr. Mireia Olivella, Dr. Xavier Altafaj and ZeClinics, a series of different compounds that potentially allosterically modulate NMDAR function were identified *in silico* (binding to a site on a receptor distinct from the active site). The proposed compounds were purchased and functionally characterized *in vitro*, using electrophysiological techniques (data not shown). From these experiments, a subset of five different compounds that showed a modulation of NMDAR function were selected and tested *in vivo*, using zebrafish larvae and performing toxicology and behavioural assays.

5.1. Toxicology analysis of NMDAR modulators in zebrafish larvae

Zebrafish possess several characteristics that highlight their potential as alternative animal models, notably their conserved metabolic processes. The ability to directly treat

larvae by adding compounds to their media reduces both the quantity of compounds required and the time needed for studies compared to more commonly used animal models.

For the toxicology analysis of the five selected compounds, numerically named from 1 to 5 to preserve their anonymity, 96 hpf wild-type larvae were treated for 24 hours. At 120 hpf, the mortality and toxicology traits were analysed under a stereoscope. Compounds 1, 2 and 3 showed a high lethality only at the highest tested concentration (1000µM, Figure 62A-C). Additionally, 100µM Compound 1 and 100µM Compound 3 caused toxic morphological phenotypes, such as heart and craniofacial oedema, body curvature defects or pigmentation loss. The surviving larvae in the highest concentration used of Compound 2 also developed similar toxicity traits (data not shown). Interestingly, Compounds 4 and 5 did not show any toxicological trait or mortality defects at any of the concentrations used, with only stochastic mortality at low concentrations (Figure 62D-E).

These results suggest that Compound 4 and Compound 5 could be safer regarding generalised toxicity characteristics. Additionally, Compound 1, Compound 2 and Compound 3 have potential toxicity at higher concentrations. Therefore, lower concentrations should be used to analyse their potential effect as NMDAR modulators and avoid toxicity.

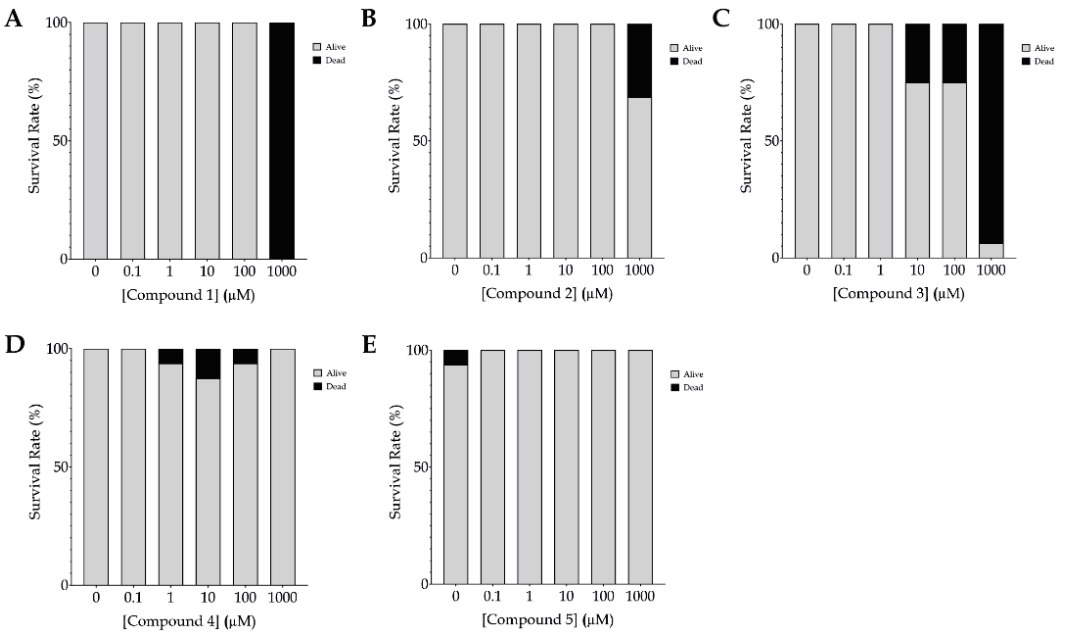

Figure 62. Toxicity analysis of the different compounds after 24-hour exposure in 96 hpf wild-type larvae. Graphs showing the survival rate of the treated wild-type larvae after 24-hour exposure to the different compounds. Alive larvae are represented in grey; dead larvae are represented in black. Between 16 and 20 larvae were analysed in each condition.

5.2. Analysis of the impact in behaviour of NMDAR modulators

For the proposed behavioural studies, dose-response experiments were performed for each candidate compound, with concentration range adapted from the toxicology data. The experimental conditions were homogenous with set-up parameters defined along pharmacological studies (MK-801, L-Serine and Spermine). To avoid toxicity, 120 hpf wild-type larvae were acutely treated 3 hours before each experiment. The different concentrations include values close to the BMD described from toxicology analysis (data not shown) and higher concentrations.

5.2.1. Locomotor behaviour analysis upon NMDAR modulators treatment

As for the characterisation of GRD models, the dark/light transitions paradigm was used to assess the impact of the candidate NMDAR modulators on locomotor activity of wildtype larvae (n=16-24 larvae / group; Figure 63). The effect was variable, in a compound- and dose-dependent manner. As shown in Figure 63, the Compounds 1, 2 and 3 significantly increased motor activity, leading to a hyperlocomotion in response to particular drug concentrations (50, 50 and 3.3µM, respectively). Remarkably, the hyperlocomotion was exclusively observed during the dark phase (Figure 63). Finally, for all the tested Compounds, no alterations were detected in terms of anxiety-related thigmotaxis index (percentage of time spent in the centre *vs*. periphery).

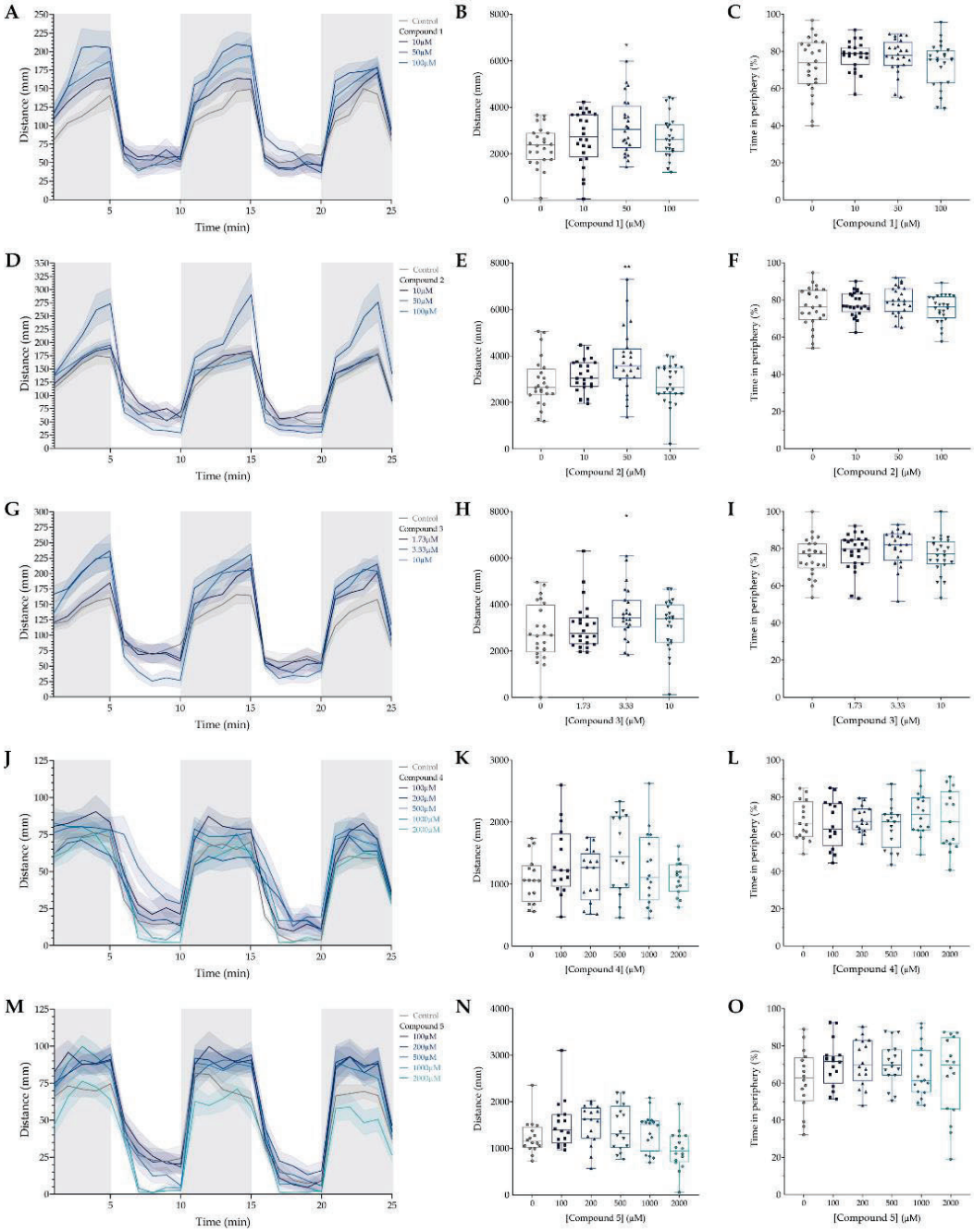

Figure 63. Locomotor analysis of the different compounds after 24-hour exposure in 96 hpf wild-type larvae. A, D, G, J, M. Representation of the distance moved by one-minute time bin during the 25-minute dark/light cycles. Dark cycles are annotated as grey vertical lines for better visualisation. B, E, H, K, N. Graph of the total distance moved (mm) of the larvae in the complete 25-minute protocol. C, F, I, L, O. Analysis of the average percentage of time spent in the peripherical area of the well to study anxiety. *p<0.05, **p<0.01 (One-way ANOVA with Tukey's post-hoc analysis).

5.2.2. *Immediate response and habituation to tapping analysis of NMDAR modulators treated larvae*

The effect of the candidate NMDAR modulator compounds on sensory function was evaluated by the analysis of response to external tactile stimuli. This analysis showed two types of responses: while compounds 1, 2 and 3 (n=24/group) decreased the response to tapping, larva treated with compounds 4 and 5 (n=16/group) did neither show a significant change of tapping response, nor the habituation (Figure 64).

Compound 1, Compound 2 and Compound 3 responded similarly to the tactile stimulation. The response to the tapping stipulation was decreased in larvae treated with these compounds. Alternatively, Compound 4 and Compound 5 produced a decrease of the response and lower habituation at low doses, while the opposite, an increase of the response and faster habituation was observed at higher doses, generating a dose-response curve.

Specifically, Compound 1 produced a mild decrease of the response at 10μM and 50μM. Interestingly, in the latest concentration, 100μ, we could observe that no response was produced in the larvae (Figure 64A-C). Compound 2 effect in the wild-type larvae was very similar, showing a decrease in the response at 10μM and 50μM, and a lack of response at 100μM concentration (Figure 64D-F). The decreased response to the tapping stimulus was more prominent in Compound 3 treated larvae. In all the tested concentrations, a significant decrease in the number of larvae responding to the stimulus was described. In fact, only few larvae were responding, while the majority did not react to the tap (Figure 64G-I).

Alternatively, Compound 4 (Figure 64J-L) and Compound 5 (Figure 64M-O) caused a mild increase in the response to the tapping at higher concentrations, 1000μM and 2000μM. These results were accompanied with a decrease in the time needed to habituate to the stimulus.

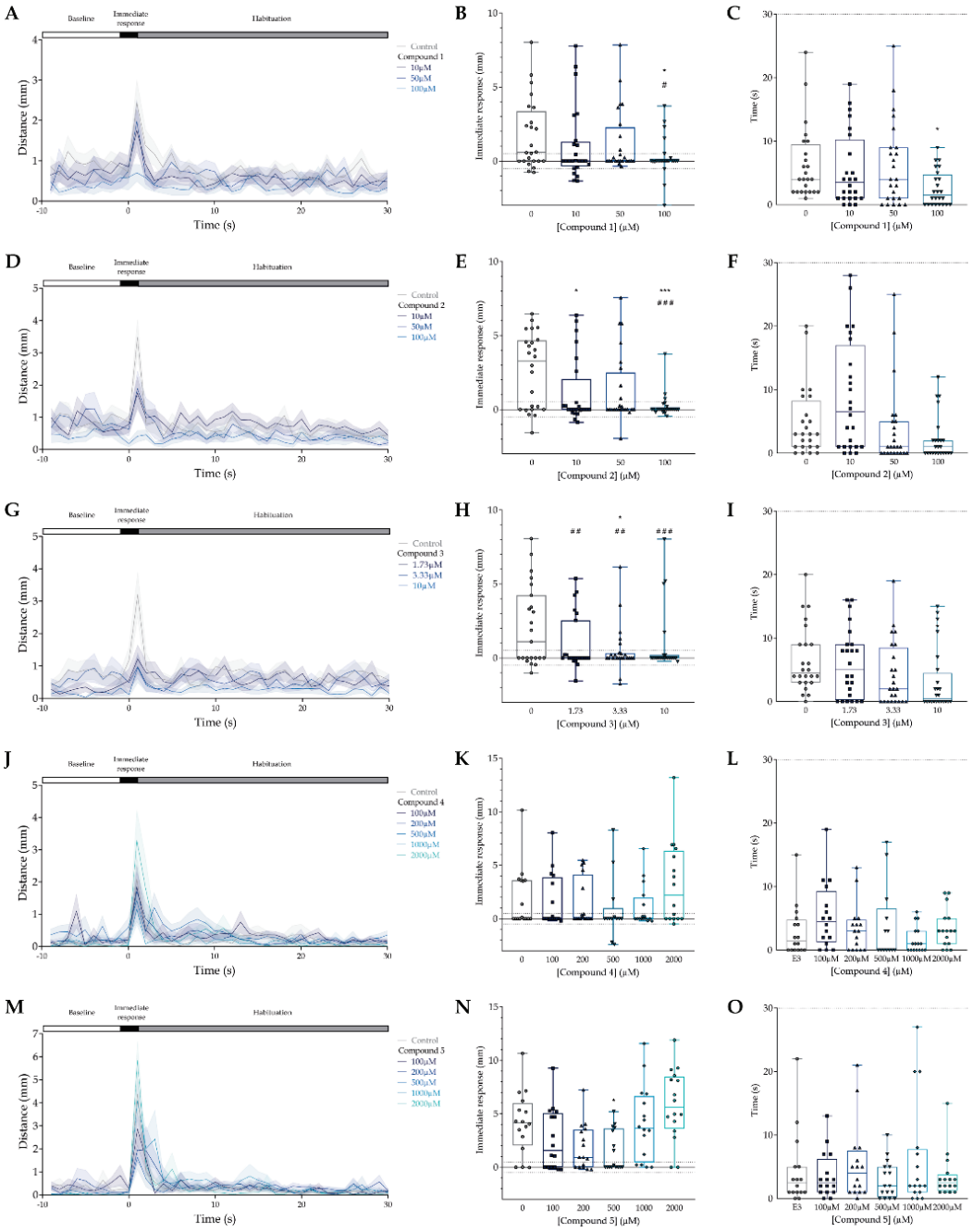

Figure 64. Immediate response and habituation analysis of the different compounds after 24-hour exposure in 96 hpf wild-type larvae. A, D, G, J, M. Graph of the distanced moved in one-second time bin. B, E, H, K, N. Graph representing the difference in the distance moved as a response to the first tap. Statistical analysis of the immediate response (mm) is represented with "*". Statistical analysis of the number of larvae responding (%) is represented with "#". C, F, I, L, O. Quantification of the habituation by measuring the time each larva takes to not respond to the stimulus, with a cut off at 30 seconds. Wild-type *grin1a*$^{+/+}$ larvae are represented in grey, heterozygous *grin1a*$^{+/-}$ in light blue and homozygous *grin1a*$^{-/-}$ in dark blue. *p<0.05, ***p<0.001 (One-way ANOVA with Tukey's post-hoc analysis). # p<0.05, ## p<0.01, ### p<0.001 (Two-way ANOVA with Sidak's multiple comparisons test).

5.2.3. Epilepsy-like response analysis after NMDAR modulators acute treatment

As in previous sections, the first analysis performed to evaluate epilepsy-like response to light flashes was the study of habituation in the consecutive stimulation. We did not observe habituation either in the maximum velocity achieved or the maximum number of turns performed in any of the studied compounds. Therefore, each flash was considered as an independent readout, and the average of the five consecutive light flashes was calculated to compare the performed responses.

The analysis of Compound 1 effect on larvae revealed an epilepsy-like behaviour at 50µM and 100µM concentrations, with a significant increase in both measured parameters. In addition, the visualisation of the travelled trajectory after the flashes supports the epilepsy-like behaviour analysed (Figure 65A-C).

No significative differences in the response to the light stimulus were observed in compound 2 treated larvae.

Upon Compound 3 exposure, larvae did not show a significant alteration in their behaviour when the light-flashes were applied. However, a mild but not significant increase in the number of bouts performed was observed in all the concentrations. This increase was not observed in the maximum velocity achieved.

Similarly, no significant alterations in the behaviour of Compound 4 treated larvae were observed. Interestingly, a dose-response curve of an increase in both parameters was observed, with an increase peak between 200µM and 500µM. Nevertheless, these results were not significantly different compared with their controls.

Finally, Compound 5 treatment revealed a decrease in the response, in both parameters, at 1000µM and 2000µM. Nevertheless, this decrease was only significant in maximum velocity analysis, and was more evident at the highest concentration.

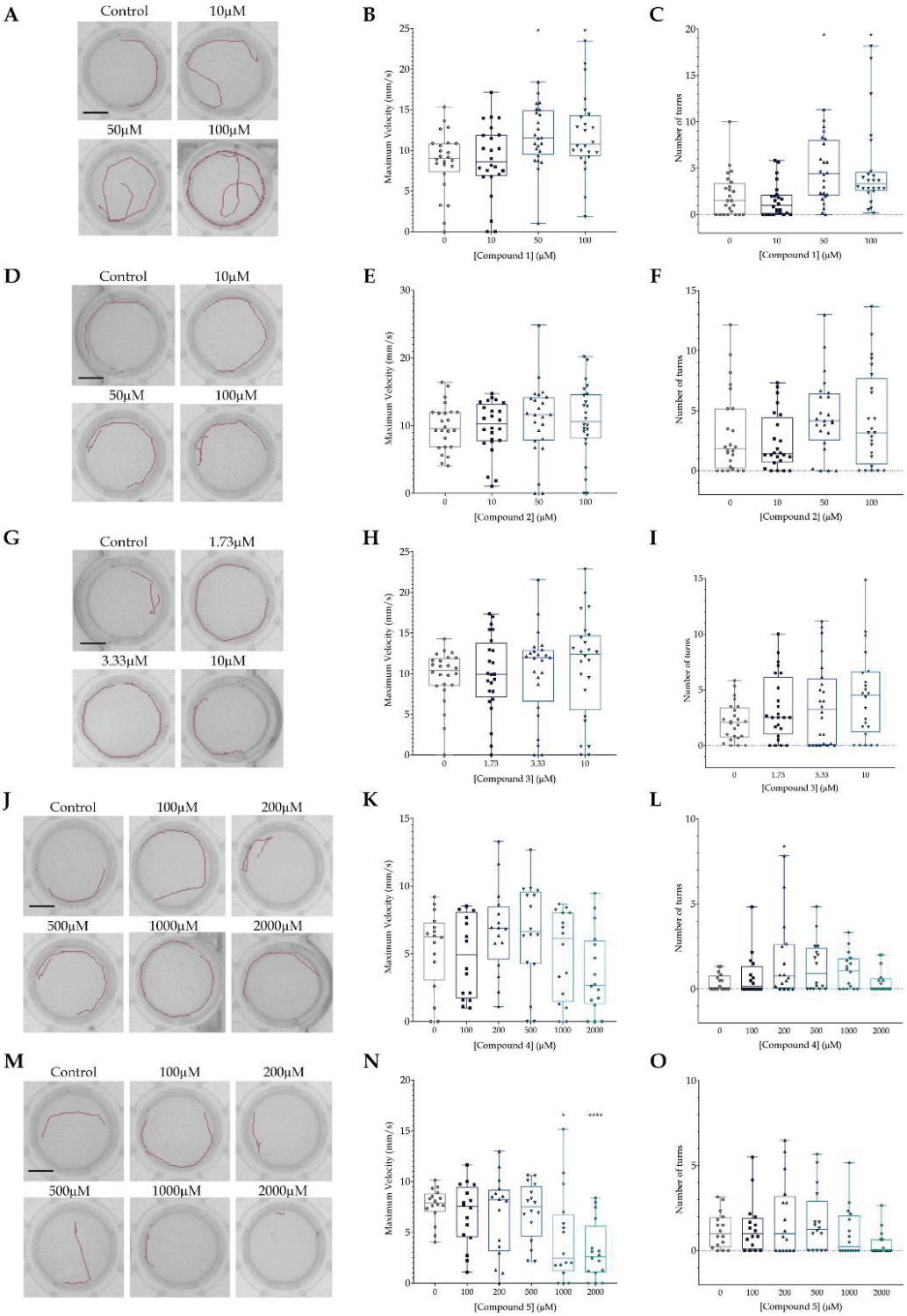

Figure 65. Epilepsy-like behaviour evaluation of the different compounds after 24-hour exposure in 96 hpf wild-type larvae. A, D, G, J, M. Representative images of the tracking of single larvae, recorded 2 seconds after the first applied flash. Scale bar = 6mm. B, E, H, K, N. Measurement of the maximum velocity (mm/s) achieved, comparing the different average of the five flashes performed. C, F, I, L, O. Measurement of the total number of angle turns performed, comparing the different average of five flashes performed. *p<0.05, ****p<0.0001 (One-way ANOVA with Tukey's post-hoc analysis).

Conclusively, the five different NMDAR modulators studied in this chapter do have an effect in zebrafish larval behaviour. Therefore, they are pharmacologically active and could be used in the generated GRD models to test their effect in NMDAR loss-of-function environment. Some of the results, such as the increase of locomotion in most cases or the decrease in light-induced responses, were promising and could be effective to treat and rescue some of the described phenotypes of GRD models.

Summary of the PharmaGRIN phenotypic characterisation

Paradigm	Variable	Compound 1	Compound 2	Compound 3	Compound 4	Compound 5
Dark/Light cycles	Total distance (mm)	↑↑	↑↑↑	↑↑	=	↑
	Percentage of time in periphery area	=	=	=	=	=
	Dark/Light transitions	↑↑	↑↑↑	↑↑	=	↑
Response and habituation to tapping	Quantitative response to the first stimulus (mm)	↓↓	↓↓	↓	=	=
	Qualitative response to the first stimulus (%)	↓↓	↓↓↓	↓↓↓	=	=
	Time for habituation (s)	↓↓	↓	↓	=	=
Light-induced epilepsy	Maximum velocity (s)	↑↑	=	↑	↓	↓
	Number of angle turns	↑↑	=	↑	↓↓↓	↓

Table 16. Summary of the described behaviours in the different studied paradigms. A code of arrows is used to simplify the observed results in all the concentrations. Up arrows refer to an increase in the response compared with the control group. Down arrows refer to a decrease in the response compared with the control group. Equal sign refers to no changes in the response compared with the control group. The number of arrows refers to the magnitude of the observed changes and its significance.

Chapter 2:

A zebrafish-based platform for high-throughput epilepsy modelling and drug screening in F0

The development of a fast-screening platform for evaluating pharmacological candidates in potential genetic targets represents a significant advancement in the field of genetic research and drug discovery. The generation of *GRIN* knockout models has revealed a series of limitations, including the extended time required to create KO lines, the necessity for individual genotyping of larvae, and the complexities associated with assessing epileptic phenotypes. These challenges underscore the need for refinement in the evaluation processes, as they can hinder the efficiency of identifying and validating new therapeutic targets. By addressing these limitations, the proposed screening platform has the potential to streamline future research on genetic disorders, facilitating more efficient target identification and validation studies as well as accelerating drug discovery efforts.

1. *Tyr* loss-of-function strategy for high-rate mutation's mutant selection

To reduce variability and maximize the utility of an F0 knock-out approach, it is necessary to cluster together genetic homogeneous populations. To this end, distinguishing between larvae carrying high and low rates of mutations is needed. To be able to perform such selection, we hypothesized that, if two genes are targeted simultaneously, their sequences will undergo a comparable mutagenesis process. As a consequence, the presence of a phenotype associated with the loss-of-function of one gene could be employed as a reporter for the efficient inactivation of the second gene. The rationale is that the efficiency of double strand breaks (DSB) is largely related to the injection procedure and timing. As such, embryo stage, at the time of the injection, as well as injection accuracy are critical to achieve high DSB rates. Therefore, a complete loss of function of the reporter gene might suggest a correct injection timing and high injection accuracy.

To this end, we thought to target, together with the candidate gene of interest, the tyrosinase (*tyr*) locus. The *tyr* gene encodes for a protein involved in melanin production and its disruption results in the absence of pigmentation, an easily identifiable phenotype that could be employed to select larvae in which the CRISPR/Cas9 system has efficiently disrupted the target genomic sequences (Jao et al., 2013).

First, we wanted to prove that *tyr* inactivation does not cause side developmental phenotypes other than the expected pigmentation deficiency in zebrafish larvae. To exclude the occurrence of morphological developmental defects in *tyr* crispants, wild-type one-cell stage embryos were injected with a mix containing Cas9/scrambled-sgRNA or Cas9/tyr-sgRNA. As expected, starting from 48 hpf, embryos carrying biallelic mutations in the *tyr* gene could be identified by the absence of pigmentation. This difference became particularly clear at 120 hpf (Figure 66A).

At this stage, we performed a comprehensive characterization of a panel of 9 qualitative (Table 17) and 3 quantitative (body length, eyes diameter and heart area) phenotypes. Importantly, we did not detect any significant morphological difference between scrambled and *tyr* crispants for qualitative phenotypes. A very mild but significant alteration was observed in the body length and eyes diameter of tyrosinase crispants (Figure 66A-D, Table 17).

	scrambled			***Tyrosinase***		
	Number of positive	**Total number**	**% of positive**	**number of positive**	**Total number**	**% of positive**
Body curvature	0	75	0	1	68	0.01
Snout jaw defects	2	75	0.03	0	68	0
Yolk edema	2	75	0.03	0	68	0
Necrosis	1	75	0.01	2	68	0.03
Tail bending	0	75	0	1	68	0.01
Notochord defects	0	75	0	0	68	0
Craniofacial edema	2	75	0.03	0	68	0
Fin absence	0	75	0	0	68	0
Scoliosis	0	75	0	0	68	0

Table 17. Qualitative phenotypes analysed

Once assessed the general morphology, we verified that larval locomotion and behaviour was not affected by *tyr* loss-of-function. To this end, we analysed the motor activity of crispants in response to different stimuli.

In the analysis of locomotion during dark/light phases and light-induced epileptic behaviour, *tyr* crispants did not show any significant difference when compared to control crispants (Figure 66E-G). Therefore, our data confirm that *tyr* loss-of-function does not cause motor defects and does not induce epilepsy-like behaviour.

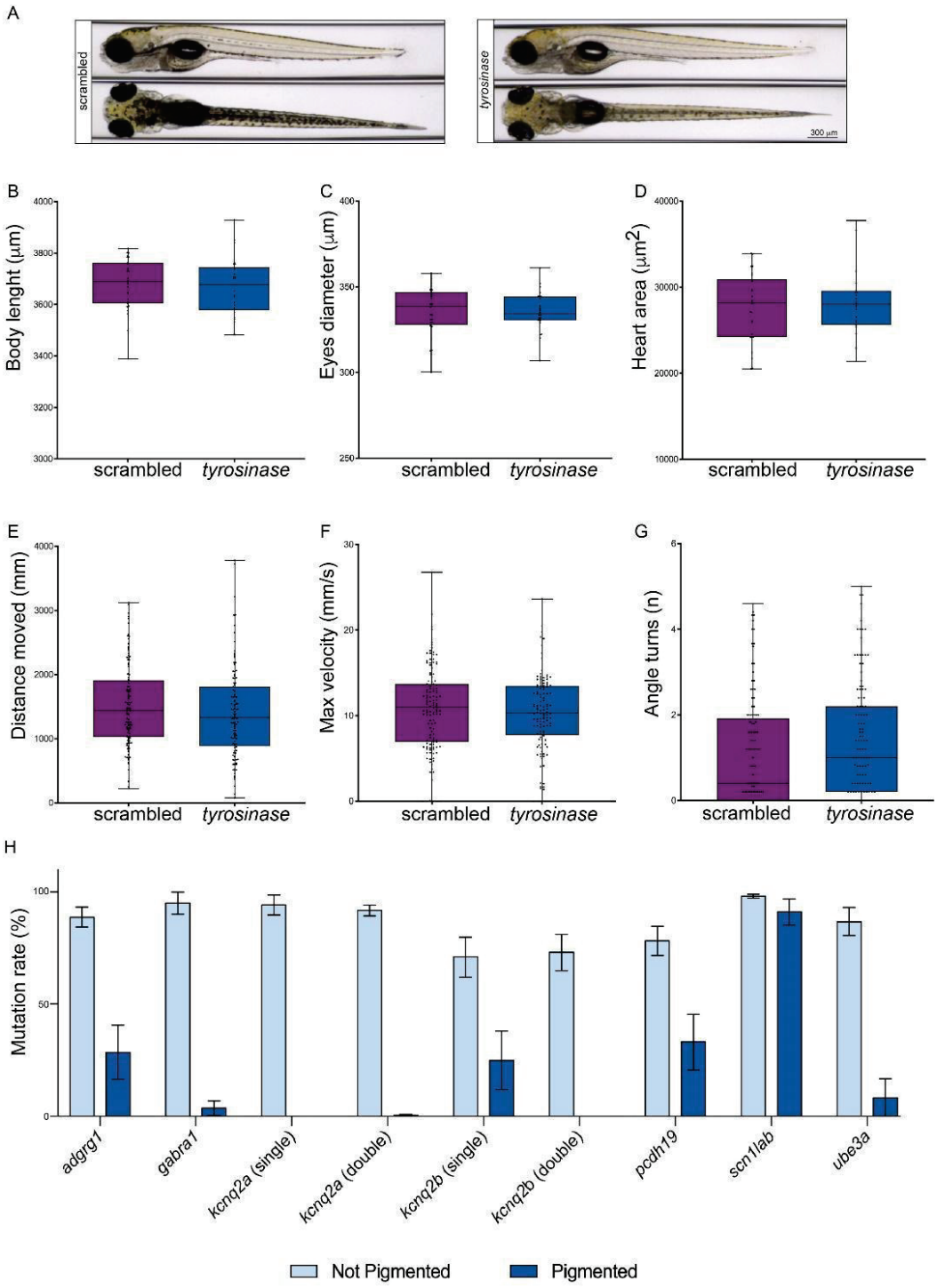

Figure 66. *tyr* loss-of-function analysis of pingmentation and behavioural and developmental parameters. A. Dorsal (lower panels) and lateral (upper panels) images of scrambled (left panels) and *tyrosinase* crispants (right panels), with a reduction in pigmentation in the latest. B,C,D. Analysis and comparison of different relevant morphological phenotypes in both crispants (scrambled are represented in purple; tyrosinase crispants are represented in blue. Error bar represents minimum to maximum values): body length (µm) (B), diameter of the eyes (µm) (C) and heart area (µm2) (D). E,F,G. Analysis and comparison of the most relevant parameters related with epilepsy in both crispants (scrambled are represented in purple; *tyrosinase* crispants are represented in blue. Error bar represents minimum to maximum values): distance moved (mm) during the dark/light cycles phase

(E), maximum velocity achieved after the light flashes (mm/s) (F) and number of angle turns after the light flashes (G). H. Bar-plot showing the mutagenesis efficiency observed in the targeted loci in pigmented larvae (dark blue) and unpigmented larvae (light blue). From left to right: mutation rate observed in the *adrgr1* CDS in *adrgr1* crispants; mutation rate observed in the *gabra1* CDS in *gabra1* crispants; mutation rate observed in the *kcnq2a* CDS in *kcnq2a* single crispants; mutation rate observed in the kcnq2a CDS in kcnq2a-kcnq2b double crispants; mutation rate observed in the *kcnq2b* CDS in *kcnq2b* single crispants; mutation rate observed in the *kcnq2b* CDS in *kcnq2a-kcnq2b* double crispants; mutation rate observed in the *pcdh19* CDS in *pcdh19* crispants; mutation rate observed in the *scn1lab* CDS in *scn1lab* crispants; mutation rate observed in the *ube3a* CDS in *ube3a* crispants. Error bars represent the standard error of the mean (SEM).

Having verified that *tyr* disruption does not affect larval morphology or behaviour, we wanted to prove that the loss of pigmentation could be employed as a reporter for the efficient disruption of the coding sequence (CDS) of a second gene. We tested our approach on the zebrafish orthologues of six genes whose loss-of-function has been associated with different kinds of genetic epilepsy (Table 18). One of the epilepsies associated genes (*KCNQ2*) has two orthologues in zebrafish (*kcnq2a* and *kcnq2b*). In this case, we generated three types of crispants: two single crispants in which only one of the two paralogues was targeted (single crispants) and a double crispant in which both paralogues were simultaneously targeted.

Human gene	Disease	Zebrafish orthologue
ADGRG1	Bilateral frontoparietal polymicrogyria (Bahi-Buisson et al., 2010)	*adgrg1*
GABRA1	Different epileptic disorders (Johannesen et al., 2016)	*gabra1*
KCNQ2	Benign familial neonatal seizures (Castaldo et al., 2002)	*kcnq2a; kcnq2b*
PCDH19	PCDH19 Epilepsy (Samanta, 2020)	*pcdh19*
SCN1A	Dravet syndrome (Depienne et al., 2008)	*scn1lab*
UBE3A	Angelman syndrome (Fang, 1999)	*ube3a*

Table 18. Candidate epilepsy-associated genes analysed in the study.

To confirm our hypothesis, we injected one-cell stage wild-type embryos with a mix containing the Cas9 protein together with three sgRNAs (one targeting the *tyr* and two targeting one of the selected target genes). To verify that the mutation rates of the two targeted genes correlate, we extracted the genomic DNA from individual pigmented and unpigmented larvae and sequenced the second locus targeted. As expected, unpigmented larvae displayed a higher mutagenesis rate than the one observed in their pigmented siblings (Figure 66H). In all analysed genes, more than 60% of unpigmented larvae displayed a mutation rate higher than 75%, leading us to the conclusion that it is possible to use *tyr* loss-of-function as a reliable reporter for Cas9 cutting efficiency.

2. Analysis of epilepsy-like behaviour in childhood epilepsy genes crispants

Once confirmed that the loss of pigmentation represents a powerful screening method to identify gene-specific crispants that carry a high rate of mutations, we used this approach in the following experiments. For the study of the phenotype induced by the loss-of-function of the different candidate epilepsy genes, we injected one-cell stage wild-type embryos with Cas9/sgRNA complexes, one sgRNA targeting the *tyr* locus and two sgRNA targeting the epilepsy gene of interest. For the negative control, we co-injected the *tyr* sgRNA and a scrambled sgRNA. We selected the unpigmented larvae for the experiments.

To evaluate the effects of the loss-of-function of the selected genes, we first looked for the presence of morphological alterations in the different gene-specific crispants. We observed that *adgrg1* crispants displayed significant morphological phenotypes (reduced size and presence of body curvature) possibly due to a developmental delay or to hypotonia and muscular defects related to the generated loss-of-function. The inactivation of other epilepsy-associated genes did not result in significant morphological deficiencies, with the exception of *gabra1*- and *pcdh19*- crispants (minor but significant decrease in body length) and *kcnq2a* and *kcnq2b*- crispants (minor but significant increase in body length and eye diameter.

Subsequently, we analysed the presence of locomotion alterations or the occurrence of epilepsy-like phenotypes.

First, we analysed the locomotion activity of control and gene-specific crispants in response to alternating dark/light cycles. Interestingly, most crispants did not show differences in their motor behaviour in response to the dark/light changes. Differently, *scn1lab* and *gabra1* crispants showed a reduced locomotion in comparison to scrambled crispants (Figure 67).

Next, we decided to test the possibility of inducing epilepsy-like behaviour by exposing the crispants to different epileptogenic stimuli. In order to trigger seizures, we employed two kinds of stimuli, namely the incubation with Pentylenetetrazole (PTZ) and the exposure to intermittent flashes of light.

In our experiment, crispants were exposed to two sub-optimal concentrations of PTZ (1 and 3 mM) and their locomotion activity was monitored for a sustained light period (15 minutes). The presence of locomotion alterations and spontaneous convulsions was evaluated by analysing the maximum velocity (mm/s) reached by each larva during the trial. Interestingly, we found that *pcdh19* and *ube3a* have an increased sensitivity to PTZ. Indeed, if the two genes were inactivated, the behavioural response of larvae treated with PTZ 3mM was significantly stronger than the one observed in scrambled controls exposed to the same concentration of the compound. In both cases, the incubation with a lower concentration of PTZ (1mM) was not sufficient to induce seizure-like activity. Differently, the KO of the other epilepsy-associated genes did not increase the susceptibility of crispants to PTZ.

When exposed to intermittent light as an epileptogenic stimulus, different crispants showed a different response. The exposure to quick and repeated light flashes had a strong impact on the behaviour of *adgrg1*, *gabra1*, *pcdh19* and *scn1lab* crispants. The presence of seizure-like behaviours could be visually detected by analysing the trajectory followed by each larva in the two seconds after the exposure to the light stimulus. While crispants injected with scrambled sgRNAs followed a linear trajectory along the wall of the well, *adgrg1*, *gabra1*, *pcdh19* and *scn1lab* crispants moved along an erratic trajectory in which they crossed the well and changed direction multiple times (Figure 67A). The analysis of the two kinematic parameters confirmed this observation (Figure 67C-D, 67F-G, 67I-J and 67L-M). Both parameters were significantly increased if compared to scrambled control, suggesting that the mutation of *adgrg1*, *gabra1*, *pcdh19* and *scn1lab* CDS increases the susceptibility to light-induced seizures.

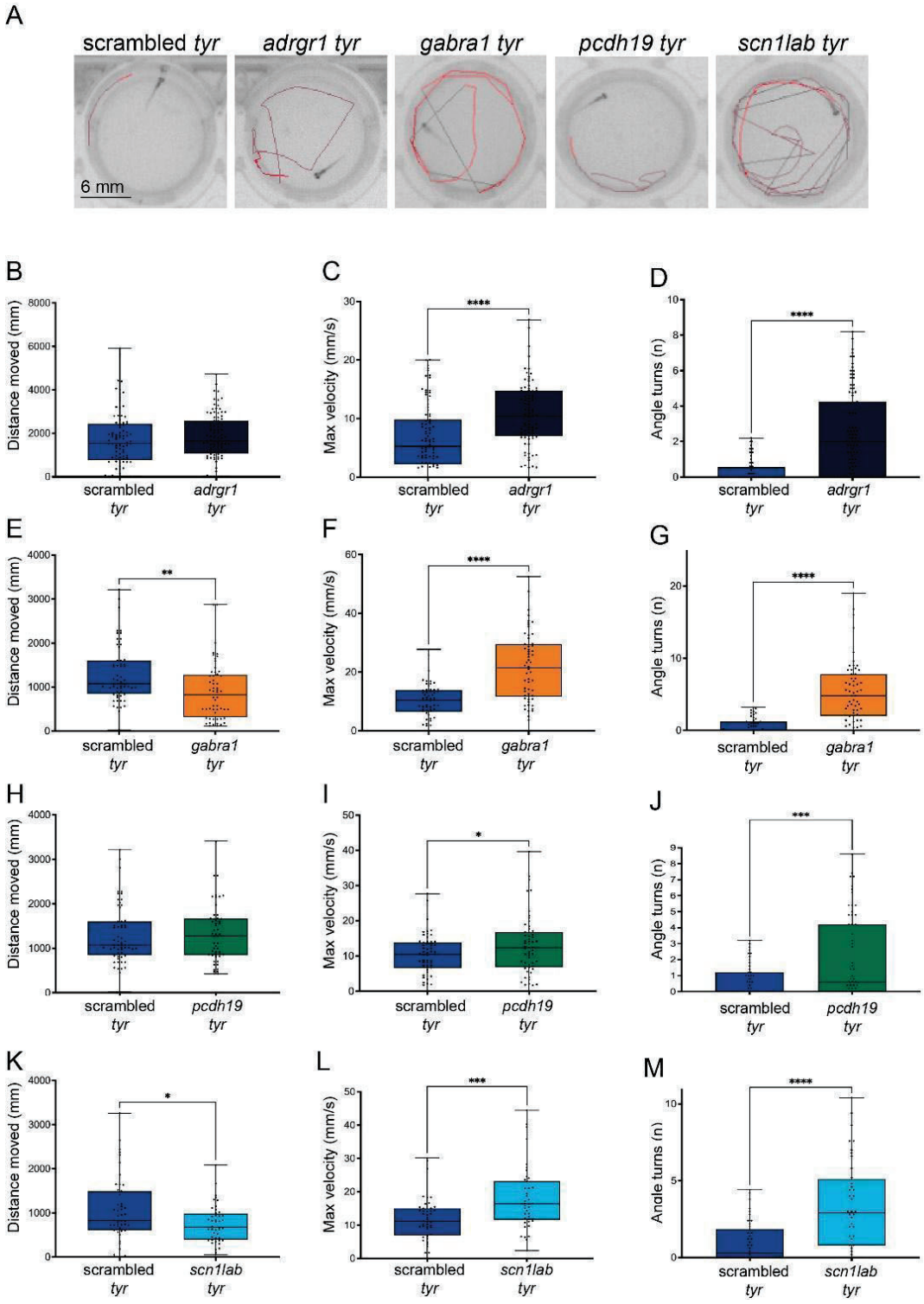

Figure 67. Characterization of *adgrg1, gabra1, pcdh19* and *scn1lab* crispants. A. Representative trajectories of the different mutant seconds after the light-flashes. B. Representation of *adgrg1* locomotion during dark/light cycles. C. Representation of the maximum velocity (mm/s) achieved by *adgrg1* crispants after the light stimuli. D. Representation of the number of angle turns performed by *adgrg1* crispants after the light stimuli. E. Representation of *gabra1* locomotion during dark/light cycles. F. Representation of the maximum velocity (mm/s) achieved by *gabra1* crispants after the light stimuli. G. Representation of the number of angle turns

performed by *gabra1* crispants after the light stimuli. H. Representation of *pcdh19* locomotion during dark/light cycles. I. Representation of the maximum velocity (mm/s) achieved by *pcdh19* crispants after the light stimuli. J. Representation of the number of angle turns performed by *pcdh19* crispants after the light stimuli. K. Representation of *scn1lab* locomotion during dark/light cycles. L. Representation of the maximum velocity (mm/s) achieved by *scn1lab* crispants after the light stimuli. M. Representation of the number of angle turns performed by *scn1lab* crispants after the light stimuli. *p<0.05, **p< 0.01, ***p< 0.005, ****p<0.001 (t-test).

3. Multiparametric analysis of behavioural response to light flashes for fine characterization of photosensitive epilepsy

To detect spontaneous seizures (e.g. in response to the incubation with PTZ), the behaviour of larvae has to be recorded for a relatively long time-window. Indeed, it is not possible to predict when the epileptic event is going to occur and, to increase the probabilities to track a seizure, it is necessary to monitor the locomotion activity of larvae for a long period of time. Differently, the use of flashes of light as a causative convulsive stimulus, allows to temporally control the manifestation of seizure-like events, making it possible to assess and characterize behavioural alterations in a timely-convenient manner.

Bearing in mind these considerations, we decided to focus on light-induced seizures in the following part of this study. We decided to perform a more detailed analysis of the behavioural response of zebrafish larvae to an epileptogenic stimulus in order to better classify the observed epilepsy-like responses.

To extract the most possible information from our dataset, we built a principal component analysis (PCA), considering those kinematic variables having the greatest relation and relevance in the study of epileptic seizures. To perform such analysis, we focused on parameters associated with a modification of the larval position or orientation in the space (Maximum velocity (mm/s), number of angle turns, maximum acceleration (mm/s^2), angular velocity (deg/s)) and variables reflecting a movement alteration (e.g. tremors or freezing behaviours) that do not cause a change in the position or orientation of larvae (mobility in the arena (%) and cumulative duration (s) of three different mobility states, immobile, mobile and highly mobile) (Figure 68A).

Data from all replicates and all different crispants were pooled in this multivariate analysis. Interestingly, we noticed that the samples were distributed in the PCA plot along different levels of overall "activity". Indeed, variables associated with increased motor activity (e.g. maximum velocity, maximum acceleration, highly mobile state)

pointed toward a similar direction, opposed to the one of variables reflecting low motor activity (e.g. immobile state) (Figure 68A). To our surprise, we did not observe a clear clusterisation of crispants versus scrambled controls but a dispersed sample distribution in which most observations localized in the centre of the plot.

Nonetheless, we noticed that a number of samples showed a highly aberrant behaviour, with higher values in different kinematic parameters (Figure 68B). We reasoned that analysed larvae could be classified in different groups depending on their activity level and we speculated that crispants of genes having a positive association with photosensitive epilepsy would have an increased representation in the more active group.

To explore this possibility, we decided to measure the Mahalanobis distance (MD) of all the observations in order to evaluate how each flash response differs from the average of the entire population. We speculated that this analysis would allow us to define the behavioural fingerprint of each larva and to classify their response to epileptogenic flashes of light based on the intensity of the observed motor activity.

Indeed, we distinguished and classified two regions of activity in our population: a region of low activity (MD<2.5 and p. value >0.1) and a region of high activity (MD>2.5 and p. value <0.1) (Figure 68C-D). This observation suggests that larvae with increased photosensitivity are prone to display a highly aberrant behaviour in response to the exposure of flashes of light, constituting a population of outliers distinguished by their higher motor activity. We assume that these extreme behaviours correspond to epilepsy-like seizures characterized by aberrant and excessive movements.

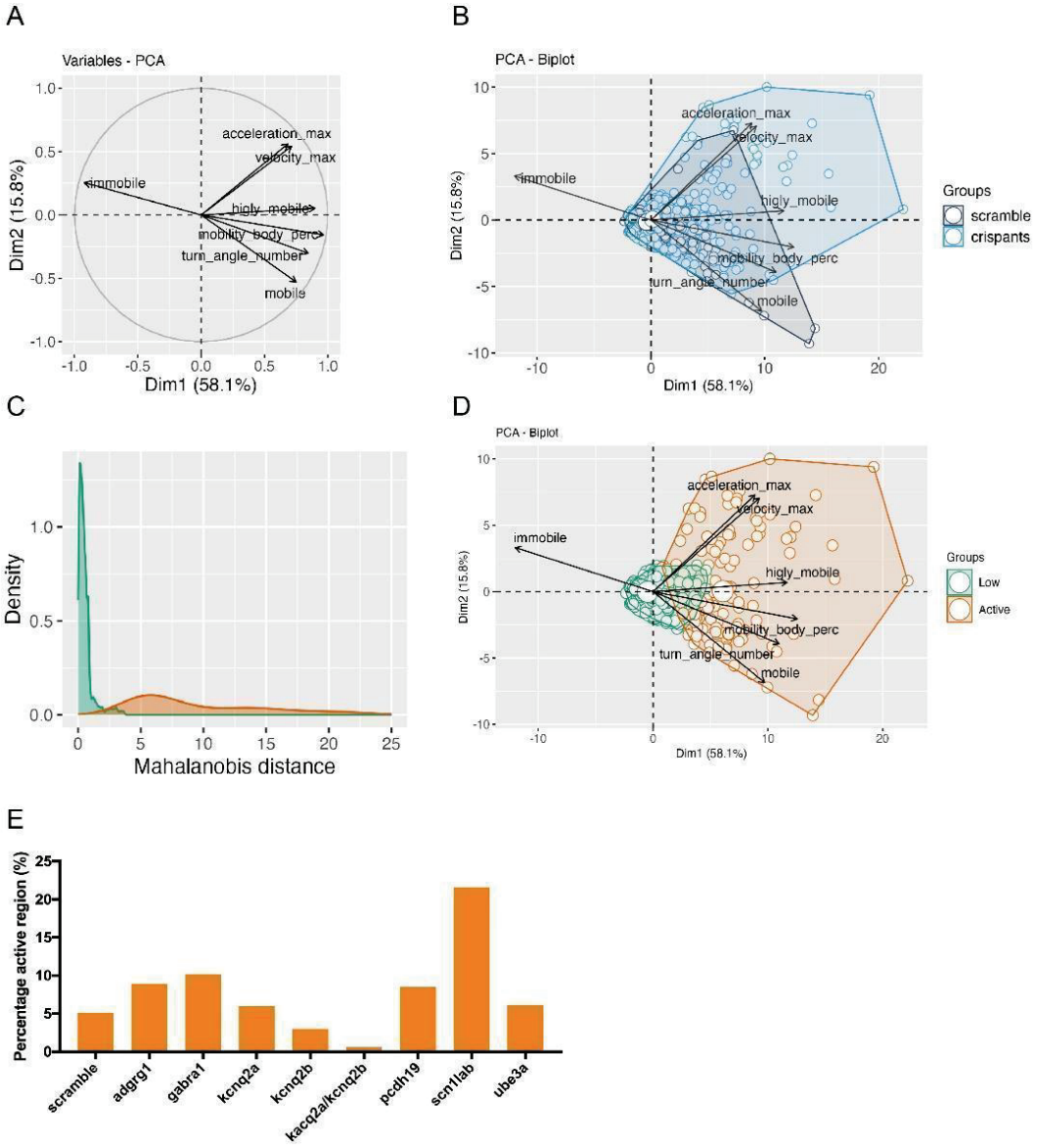

Figure 68. The identification of crispants with the greatest photosensitivity can be obtained through a multiparametric analysis of their reaction to light flashes. A. Bidimensional plot of the different variables selected as more relevant to perform the principal component analysis (PCA), with a vectorial representation. The selected variables are: maximum velocity (mm/s), number of angle turns, maximum acceleration (mm/s2), angular velocity (deg/s), mobility in the arena (%) and cumulative duration (s) of three different mobility states, immobile, mobile and highly mobile. B. PCA biplot comparing two main groups, the scrambled (in black) and the different studied crispants related with childhood epileptic genes (in blue). C. Definition of two different populations depending on their activity through the calculation of Mahalanobis distance. The low activity group (in green) represents the population of analysed larvae with a non-epileptic behaviour; the high activity group (in orange) represents the population of analysed larvae with an epilepsy-like behaviour in response to light-flashes. D. PCA biplot comparing the two main groups described through the Mahalanobis distance analysis, considering the different PCA variables. E. Representation of the percentage of larvae classified in the epilepsy-like population of the scrambled and all the selected crispants.

For each experimental group, we calculated the proportion of larvae whose level of activity was statistically classified as "low" or "high" (Table 19).

Target gene	Number of larvae	Number of flash responses	Percentage of high activity responses
scrambled	116	617	5.1%
adgrg1	86	282	8.9 %
gabra1	56	212	10.2 %
kcnq2a	57	219	6 %
kcnq2b	55	181	3 %
kcnq2a/kcnq2b	53	208	0.6 %
pcdh19	50	157	8.5 %
scn1lab	46	183	21.6 %
ube3a	44	150	6.1 %

Table 19. Proportion of active larvae in the different crispants

Interestingly, we observed that four crispants (*adgrg1*, *gabra1*, *pcdh19* and *scn1lab*) displayed an increased proportion of seizure-like responses if compared to control larvae. Among these, the crispants with the highest proportion of "highly active" responses were *gabra1*, accounting for a percentage of hyperactive responses double than the one observed in scrambled controls, and *scn1lab*, showing four times more "active responses" than scrambled controls (Figure 68E), suggesting that the inactivation of these genes has a strongest association with photosensitivity and, as a consequence, promoted the manifestation of seizure-like events in response to flashes of light.

4. Treatment of *scn1lab* crispants with antiepileptic compounds

Proven that *scn1lab* crispants display the highest susceptibility to light-induced seizures, we wanted to evaluate the effect of antiepileptic compounds on the behavioural phenotype described above.

Epilepsies, and especially childhood epilepsies, are known to present pharmaco-resistant seizures, highlighting the need of designing targeted therapeutic strategies. With the objective of evaluate different known antiepileptic drugs, three different compounds were selected: Valproic acid, Topiramate, and Fenfluramine. We speculated that the treatment of photosensitive crispants with effective antiepileptic drugs would reduce the number of seizure-like events, resulting in a reduced presence of treated crispants in the region of "high activity". To test this hypothesis, we incubated scn1lab crispants with two concentrations of the aforementioned compounds.

Upon incubation with the test compounds, control and gene-specific crispants were exposed to flashes of light to induce a convulsive behaviour. First, we evaluated the efficacy of the tested ASMs from a qualitative point of view, examining the trajectory followed by larvae in response to the flashes of light. As expected, the trajectory of DMSO-treated *scn1lab* crispants appeared more complex and fragmented than the one of DMSO-treated scrambled control (Figure 69A). Differently, treated larvae followed a less complex trajectory, even if we observed differences among different drugs (Figure 69A). Indeed, *scn1lab* crispants treated with the two selected concentrations (17.5 μM and 35 μM) of Fenfluramine and with the highest concentration of Valproic acid (100 μM) followed a linear trajectory comparable to the one of control individuals. Differently, larvae treated with the lowest concentration of Valproic acid (50 μM) and with the two chosen concentrations of Topiramate (50 μM and 100 μM) displayed a twistier trajectory (less complex than the one followed by DMSO-treated scn1lab crispants but more complex than the one described in scrambled control crispants).

Then, the kinematic parameters of each larva were extracted and analysed, and the response of each sample was classified into the "low" (normal behaviour) or "high" active region (epilepsy-like behaviour).

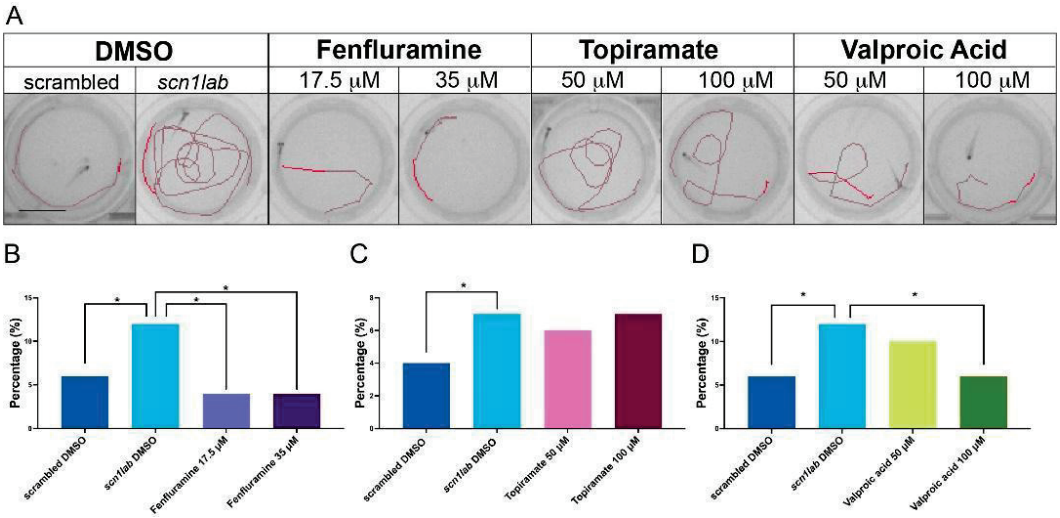

Figure 69. Evaluation of *scn1lab* crispants treated with antiepileptic compounds. A. Tracking plots of the different crispants 2 seconds after the light flashes. Scale bar= 6 mm. The different plots correspond (from left to right) to scrambled, *scn1lab* crispants treated with DMSO (vehicle), *scn1lab* crispants treated with two different concentrations of Fenfluramine (17.5μM and 35μM), Topiramate (50μM and 100μM) and Valproic acid (50μM and 100μM). B, C and D. Representation of the percentage of larvae classified in the high-activity region. Scrambled treated with DMSO are represented in dark blue in all plots, *scn1lab* crispants treated with DMSO are represented in light blue in all plots. B. *scn1lab* crispants treated with Fenfluramine 17.5μM are represented in light purple; *scn1lab* crispants treated with Fenfluramine 25μM are represented in dark purple. C. *scn1lab* crispants treated with Topiramate 50μM are represented in light pink; *scn1lab* crispants treated with Topiramate 100μM are represented in dark pink. *scn1lab* crispants treated with Valproic acid 50μM are represented in light green; *scn1lab* crispants treated with Valproic acid 100μM are represented in dark green. *p< 0.05 (binomial test).

As expected, for each of the treatments, the most represented group in the "high" active region was the one of DMSO- treated crispants (Figure 69B-D). This data confirms that *scn1lab* inactivation triggers an increased susceptibility to epileptic seizures. Differently, DMSO-treated scrambles constitute only a minority of the observations in the higher active regions (Figure 69B-D). Statistically, the proportions of *scn1lab* crispants in the "active" region are significantly different compared to scrambled larvae (binomial test with p-value < 0.05) in each of the three drug experiments. Most importantly, the treatment with both concentrations of Fenfluramine appeared to protect against the manifestation of aberrant light-induced behaviour. The treatment with topiramate did not show a protective effect. In the case of the valproic acid, the lowest concentration did not protect against epilepsy-like behaviours while the highest concentration efficiently protected against light-induced aberrant movement. Taken together, our data

demonstrate that F0 *scn1lab* mutants can be employed as a useful tool in the screening of anti-epileptic compounds.

Discussion

The principal goal of this Thesis was to develop an experimental platform to study NMDAR dysfunction in zebrafish and, importantly, to allow a high-throughput screening for NMDAR modulators. In consequence, new therapeutical compounds and targets could be discovered to treat GRD patients, but with potential to expand and treat several diseases that course with NMDAR dysfunction.

Glutamate is the main excitatory neurotransmitter in the brain, and the glutamatergic system is involved in multiple key functions of the body. The glutamatergic transmission is tightly regulated due to its important role in physiology, and alterations in its function can be related with severe neuronal disorders. Importantly, NMDAR play pivotal roles in the glutamatergic transmission and synaptic development, plasticity, neural survival and cognition. Therefore, NMDARs' function is tightly regulated, and both hyperactivity and hypoactivity are related with several pathologies, e.g. neurodegenerative diseases (AD, PD, HD), schizophrenia, autoimmune encephalitis, ASD, depression or neuropathic pain (Adell, 2020; Bermudo-Soriano et al., 2012; Bliss et al., 2016; Clayton et al., 2002; Dalmau et al., 2008, 2019; García-Recio et al., 2021; Ghasemi & Schachter, 2011; Gjerulfsen et al., 2024; Hanada, 2020; Husari & Dubey, 2019; Jelen & Stone, 2021; Kayser & Dalmau, 2016; E.-J. Lee et al., 2015; K. Lee et al., 2022; Liang et al., 2021; Marsden, 2011; Mony et al., 2009; Nozaki et al., 2015; O'Roak et al., 2012; Paoletti et al., 2013; Reutlinger et al., 2010; Rung et al., 2005; Tarabeux et al., 2011; Yi-Wen et al., 2021).

Recent advances on Next-Generation Sequencing revealed the association of *de novo* mutations affecting *GRIN* genes with neurodevelopmental disorders, so-called GRINpathies or GRIN-related disorders (GRD). GRD is a rare condition with a clinical spectrum dictated by both the affected *GRIN* gene and the functional outcomes of the mutated residue/s, primarily affecting glutamatergic neurotransmission and causing synaptopathies.

Accordingly, the generation of an *in vivo* library is required to delineate the neurological alterations and ultimately to identify personalized therapeutic approaches for GRDs. In the context of GRD, zebrafish appear as an optimal animal model, since it provides several advantages from biomedical and industrial points of view.

To address this objective, CRISPR-Cas9-based genome editing technology has been applied for the obtention of knockout models of Zebrafish paralogous *GRIN1*, *GRIN2A* and *GRIN2B* genes. The majority of the variants in *GRIN2C*, *GRIN2D*, *GRIN3A*, and

GRIN3B have been described as neutral variants. Therefore, they were not taken into consideration in the development of this Thesis (according to GRINdb, https://alf06.uab.es/grindb/home, (García-Recio et al., 2021)).

In the short term, the comprehensive phenotyping of Zebra-GRIN models will allow to define GRD-like alterations and, importantly, to evaluate the therapeutic efficacy of repurposed and EMA-approved putative NMDAR allosteric modulators, to ultimately allow personalized therapies for GRD patients.

1. Spatio-temporal characterisation of *grin* genes in zebrafish

At the beginning of this Thesis project, little was known about NMDAR spatio-temporal expression in zebrafish, either larval or adult stages. The embryonic expression of NMDAR gene family was studied by J.A. Cox in 2005, describing the homology and conservation of the NMDAR subunits across Zebrafish and Humans. Nevertheless, the spatio-temporal characterisation was limited only to the first 48 hpf. Precisely because of the developmental relevance of NMDAR and the described expression turnover in mice and humans, we believed that a description of NMDAR expression was needed at least up to 120 hpf.

To accomplish this objective, we decided to perform whole mount in situ hybridisation in larvae from 24 hpf to 120 hpf, analysing all the intermediate stages every 24 hours. With our experiments we were able to replicate the observations previously described. Moreover, we analysed in more depth the spatial expression of the different *grin* genes at 120 hpf, the larval stage in which the different behavioural assays were going to be performed.

With our findings, we were able to characterise the expression of *grin* genes in late developmental stages, confirming the conserved expression pattern of all the studied genes. These genes shared a similar expression pattern with their human orthologs, suggesting the conservation of their function. Nevertheless, a more exhaustive characterisation of the expression pattern could be obtained by sectioning the zebrafish samples and analysing the expression in more specific structures. In addition, analysis of NMDAR expression in the adult brain would also add interesting information to the current limited knowledge.

After the start of this project, similar experiments were performed, which confirmed the previous descriptions in literature and are in accordance with our findings (Zoodsma et al., 2020). In contrast with our findings, this last publication did not observe *grin1b* expression at early developmental stages, and the retinal expression of this gene also seemed reduced.

2. Design of a custom set of analysis for GRD zebrafish models

The symptomatology of GRD patients is highly variable. It depends on the gene where the mutation occurs, therefore on the altered subunit, but it also depends on the domain of the subunit. Moreover, both gain and loss of function mutations may cause similar functional alterations in the patients.

The high variety of symptoms that can be observed difficult the diagnosis of the patients, but also the study of the disease pathophysiology and the research for therapies that help with the different possible phenotypes.

For this reason, we decided to design a specific set of experiments that allowed us to characterise the majority and most important symptoms observed in the patients.

One of the most evident phenotypes in several GRD patients is the locomotor dysfunction and hypotonia. For this reason, the first characterisation was focused on locomotor alterations. With this aim, we decided to use the dark/light transitions paradigm, commonly used in zebrafish research and presenting a characteristic behaviour in wild-type animals (Peng et al., 2016). Moreover, this paradigm also allowed us to analyse the presence of an anxiety behaviour, observed in some cohorts of patients. In line with these observations, it has been reported that NMDAR dysfunction can be related with increased anxiety levels (Bermudo-Soriano et al., 2012).

Cognitive dysfunction and memory impairment are also relevant features described in GRD patients. In the research of paradigms related with patients' symptoms, one important readout was the cognitive impairment and/or memory deficits. Working with zebrafish larvae also have some limitations, and to our surprise, we couldn't find paradigms in larval zebrafish with this aim. However, we did find in the literature that zebrafish larvae have a limited ability to perform memory-related paradigms (Bruzzone et al., 2020). The ability to learn and memorise some characteristics of objects and environments is fundamental for several quotidian activities. For example, the

recognition of dangerous situations, interaction with other individuals or the obtention of the food. This memory is called recognition memory, and allows to discriminate a familiar stimuli from a novel ones and adjust the behaviour in accordance with the received stimulus (Antunes & Biala, 2012; Blaser & Heyser, 2015)(Antunes & Biala, 2012; Blaser & Heyser, 2015).

In addition, GRD families have reported hyper-reactivity and increased sensitivity for the surroundings of the patients. Therefore, we aimed to analyse these characteristics in the zebrafish models. To analyse the response to environmental tactile stimuli and the non-associative memory or habituation to the mentioned stimuli, we applied a paradigm in which the larvae received a tactile response from the outside of their environment, imitating a situation in which patients are exposed to external stimuli, like loud sounds or excessive movement (Best et al., 2008; Reemst et al., 2023).

Finally, we wanted to include an evaluation of epilepsy, since epilepsy is highly commonly reported in GRD patients. Moreover, *GRIN* genes have been found as key factors in some epilepsy patient cohorts (Gjerulfsen et al., 2024; Griffin et al., 2021; Howard & Baraban, 2017). Several approaches could be used, but to study the presence of epilepsy-like behaviour we decided to induce epileptic events with light flashes. Considering the advantages and limitations of this paradigm, we include it in our protocol in order to control the moment in time where the epileptic response could be happening.

Multiple other phenotypes could be assessed in juvenile and adult fish. However, we wanted to focus on the developmental stages of the zebrafish, considering both the advantages that the zebrafish provide and that GRD are considered a neurodevelopmental disease.

3. Characterisation of pharmacological models of NMDAR loss- and gain-of-function

Previous to the generation and characterisation of the GRD zebrafish models, we verified the potential of our in house designed pipeline to detect behavioural consequences of NMDAR dysfunction.

With this aim, we selected three different known compounds that modify NMDAR function. On one hand, we tested MK-801, a known and widely used NMDAR non-

competitive antagonist. On the other hand, we decided to use D-Serine, a NMDAR co-agonist and the active molecule of the only current treatment available, and Spermine, another known NMDAR positive allosteric modulator with potential use as a therapy.

3.1. Characterisation of MK-801 acute treatment effects on wild-type zebrafish larvae

MK-801 is commonly used in the literature as an NMDAR antagonist to model pharmacologically the loss-of-function of the receptor. Specifically in zebrafish, this compound has been used to model schizophrenia (Benvenutti et al., 2022), learning and memory impairment through contextual fear conditioning (Kenney et al., 2017), ASD through social behaviour alterations (Dreosti et al., 2015), locomotor alterations (F. Li et al., 2018) and retinal degeneration (Luo, 2019) among others. However, in the referred studies, except for the locomotion study, zebrafish are used in juvenile and/or adult stages. Therefore, the knowledge of the effect of MK-801 in larval stages is still limited. For this reason, we firstly performed an acute toxicity assay to determine the LD10 and select non-toxic concentrations to perform our experiments.

Our findings regarding locomotor alterations were in line with the ones previously described (F. Li et al., 2018), with a generalised hypolocomotion after MK-801 treatment and an absence of response to the dark/light cycle transitions. We hypothesise that the absence of response to light transitions may be caused by a disruption in the retinal function. In accordance with previous publications, in which MK-801 chronical exposure caused retinal neurodegeneration, we believe that acute exposure to the NMDAR antagonist could be impairing the signal transmission, resulting on a visual impairment or eyesight loss.

The response to external tactile or vibrating stimulus was also impaired after MK-801 acute treatment. We observed an increase in the response to the stimulus and, importantly, an absence in the habituation to the continuous stimulation. These results confirmed that with this proposed paradigm we could evaluate non-associative memory and habituation alterations. Moreover, these findings suggested that NMDAR loss-of-function disrupted the response to the applied stimulus, and similar results could be present in the Zebra-*grin* models.

The last part of the protocol consisted in evaluation of epilepsy-like behaviours. We did not observe convulsions or epilepsy-like behaviours in response to the light flashes. We

hypothesise that this may be caused because at these concentrations or with this exposure time there was no promotion of epilepsy. Additionally, the possible visual impairment could be interfering with the paradigm of light-induced epilepsy triggering, revealing a possible limitation of the selected test.

3.2. Characterisation of D-Serine and Spermine acute treatment effects on wild-type zebrafish larvae

Similarly to the study of NMDAR antagonists, we aimed to investigate the effect of positive NMDAR modulators in zebrafish wild-type larvae. This was performed not only to prove the conservation of pharmacology among species, but also to find a gain-of-function pharmacological model, analogous to the MK-801 and its loss-of-function effect.

Acute exposure to D-Serine did not cause any significant alterations in the different paradigms studied. The most remarkable phenotype observed is a mild but not significant alteration in locomotion, where we observe a mild increase in a dose-response manner. Interestingly, no toxic effects were observed in any of the concentrations used, either in the acute toxicology assessment or the behavioural characterisation. This data is in accordance with previous results, in which, in primary hippocampal cultures, D-Serine effect in wild-type conditions had no effect in chemicaly induced LTP assays (cLTP). However, the same treatment with D-Serine did have an effect in a loss-of-function mutation, specifically P553T in the GluN2B subunit (Soto et al., 2019). From these studies, and considering the absence of toxicity and, therefore, side effects related to D-Serine, this could become the only available treatment for LoF GRD (Juliá-Palacios et al., 2024).

Alternatively, Spermine acute treatment did have an effect in the treated wild-type animals. Spermine is a known polyamine, widely distributed in the body, which have the potential to modulate neuronal excitability by acting on various ion channels and receptors, like NMDAR. And specifically, Spermine potentiation shows a strict selectivity for GluN2B subunits (Mony et al., 2011). After Spermine treatment, wild-type larvae did present alterations in locomotion, showing hyperlocomotor activity in a dose-response manner, increased levels of anxiety at higher concentrations, a deficit in non-associative learning and a mild but significant increase in the response to light flashes. Treatment with Spermine did show important mortality and the appearance of toxic-

related phenotypes, like generalised oedema or body curvature. However, the adjustment to the dose to non-toxic levels had enough effect to alter the behaviour of zebrafish larvae. Therefore, after Spermine treatment we could also detect and analyse GRD related phenotypes by using our custom designed pipeline.

With these results, we could not confirm the use of these specific compounds as GoF models, since the effect was limited. However, it allowed us to confirm the potential of our designed protocol to evaluate behavioural alterations caused by alterations in NDMAR function. After this validation, we could proceed with the generation and evaluation of the GRD *in vivo* library.

4. Generation of Zebra-*grin* library of loss-of-function

To generate the loss-of-function library, we decided to use the CRISPR/Cas9 strategy to knockout the different *grin* genes. The knockout strategy consisted of the generation of large deletions (~200bp) that also caused a disruption in the code reading frame, inevitably causing not only the disruption of the protein sequence, but also a premature STOP codon, mimicking a truncation of the protein.

Noteworthy, the presence of premature STOP codon leads to mutant mRNAs that may undergo two distinct destinations: either the resultant proteins are inactivated or the translation does not occur, degrading the mRNA molecules. The first process should result in mutated proteins with a reduced size. Considering the early deletion and protein truncation, the truncated might be lacking the transmembrane domain, resulting in a loss-of-function (Santos-Gómez, Miguez-Cabello, García-Recio, et al., 2021). The latter process is known as nonsense-mediated mRNA decay, where mutant mRNA is prematurely degraded and not translated into proteins (Dzikiewicz & Szweykowska-Kulińska, 2006).

The generation of the knockout lines was accomplished in all the selected genes. Importantly, the annotation of *grin2Ba* gene in the available online databases is disorganised and not complete, which difficulted the generation of the mutant. However, we could confirm the deletion, a frameshift of the codon sequence and the premature STOP codon, equivalently to what we achieved with the other genes.

In this thesis project, we have successfully generated nine different *grin* loss-of-function lines: six different single knockout lines (*grin1a. grin1b, grin2Aa, grin2Ab, grin2Ba* and

grin2Bb) and three different double knockout lines, obtained by crossing the single knockout lines of each *grin* paralog (*grin1a-grin1b, grin2Aa-grin2Ab* and *grin2Ba-grin2Bb*).

5. Characterisation of the generated Zebra-*grin* KO models

5.1. Locomotion and anxiety in GRD models

As previously described, locomotor alterations are one important trait observed in GRD patients. For this reason, we decided to perform an analysis of the locomotion of the generated Zebra-*grin* models in order to characterise this potential alteration. Surprisingly, the observed alterations in locomotion, mainly in the single models, were milder than expected. In the double models, both *grin1a-grin1b* and *grin2Aa-grin2Ab*, stronger phenotypes of locomotor impairment were described. In line with these findings, we expect similar results after the evaluation of the double line *grin2Ba-grin2Bb*.

Previous experiments showed that 25 minutes with 5-minute cycles were sufficient to detect locomotor alterations. Therefore, we decided to adopt this timing to reduce the experimental time. However, and considering the obtained results and the hypotonia observed in patients, we believe that a longer evaluation of the generated models could unveil important information. The appearance of alterations dark/light transitions in the last two transitions of the protocol in some double mutants support this hypothesis.

5.2. Tapping, response to external stimulus and memory in larval zebrafish

Habituation is a non-associative learning process where animals initially respond to a stimulus and gradually modify the intensity of their response with repeated exposure. This basic form of learning has been preserved throughout evolution (McDiarmid et al., 2019). Therefore, this response can be useful to explore neuronal dysfunction.

In accordance with patients' behaviour, we could observe alterations both in the first response to the vibrating or tapping stimuli and in the habituation to the continuous stimulation, unveiling alterations in the non-associative learning process.

5.3. Epilepsy-like behaviour characterisation in zebrafish larvae

As previously stated, one of the common traits in GRD patients is epilepsy. We decided to perform the light-flashes to characterise specifically light-induced epilepsy-like behaviours because with this approach we are inducing the flashes, being able to control the time where they should occur and perform a more specific analysis. However, this analysis is restricted to light-sensitive epilepsy, and other epilepsy-like behaviours may be overseen.

With this specific protocol, we were able to detect and characterise epilepsy-like behaviours in several Zebra-*grin* models, and more prominently in *grin1b* and *grin2Ab* single knockout lines. These findings demonstrate the existence of an epilepsy-like behaviour in these lines, but restricted only to light-sensitive epilepsy. In GRD patients, different modalities of epileptic crisis have been described. For this reason, and in line with our findings, we believe that epilepsy in the generated models is a whole pipeline worth exploring. Not only from a behavioural perspective, but importantly and to truly classify the observed phenotypes as epilepsy, by performing electrophysiological studies.

The zebrafish transparent nature along with the transgenic background of the generated lines would allow to perform electrophysiological recordings with linving larvae (Baraban, 2013). This would not only expand our knowledge of how *grin* mutations generate epilepsy-like events, but importantly will allow the screening of several anti-epileptic compounds or NMDAR modulators with potential rescuing effect on this phenotype.

5.4. Characterisation of Zebra-grin models from homozygous parents

As mentioned in previous sections, the observed phenotypes were milder than expected, including the double mutants' phenotypic alterations. One possible explanation for this phenomenon is a compensation by the other *grin* paralog, *a* or *b* respectively.

In a complementary manner, the phenomenon of maternal contribution could also be affecting the observed results. During early zebrafish development, some of the transcriptional functions are silenced, and some developmental processes depend on maternal provided mRNA and proteins located in the larval yolk (Harvey et al., 2013).

Interestingly, the effects of this maternal contribution can be affecting part of the development even after the clearance of the maternal products. Therefore, maternal expressed genes could potentially alter the detrimental effect of the generated gene inactivation (Wolf & Wade, 2016).

To discard the maternal contribution effects, we decided to perform the same custom designed pipeline with mutant larvae coming from homozygous parents, avoiding positive contribution from heterozygous mothers. As in the previous experiments, to reduce the variability with the controls, we decided to use wild-type relatives as negative controls to compare with. With this aim, wild-type *grin*$^{+/+}$ and homozygous *grin*$^{-/-}$ F2 adult zebrafish were in-crossed, and the experiments were performed with the progeny, that was 100% *grin*$^{+/+}$ and *grin*$^{-/-}$ respectively. The same set of experiments was performed in all the single models, *grin1a* (Supplementary Figures 22-24), *grin1b* (Supplementary Figures 24-27), *grin2Aa* (Supplementary Figures 28-30), *grin2Ab* (Supplementary Figures 31-33), *grin2Ba* (Supplementary Figures 34-36) and *grin2Bb* lines (Supplementary Figures 37-39).

In addition, we performed an analysis on growing animals to decipher growing delay or alterations. A growing delay in *grin1* zebrafish models was already described by Zoodsma et al. 2020. With this aim, wild-type *grin*$^{+/+}$ and homozygous *grin*$^{-/-}$ F2 adult zebrafish were in-crossed, allowing the identification and segregation of larvae and fish during all the procedure. This procedure was performed in *grin1* and *grin2A* lines, analysing the measure and weight of individual siblings every two during sixteen weeks. To our surprise, and in accordance with previous results in this section, we did not observe significative differences between the wild-type and homozygous animals in any of the lines (Supplementary Figure 40). Following the previous results, we hypothesise that the growing alterations in the knockout lines could be notorious by using heterozygous parents. Nevertheless, individuals from homozygous parents present an attenuated phenotype. To confirm this hypothesis, the same protocol would be used to study growing stages of larvae coming from heterozygous parents.

The results of these experiments suggested that there was no maternal contribution involved in the performed experiments from heterozygous parents. The observed phenotypes observed in the larvae from homozygous parents were milder, and in some paradigms the performance was completely different. Some doubts arise from these experiments, since we were comparing some fish with wild-type no siblings, even if

they were closely related. Therefore, we observed some differences that may be significant due to environmental variations, and that could be altering our results. For this reason, we decided to finally focus on the heterozygous parents' experiments, where larvae could be compared with their direct wild-type siblings. Furthermore, the characterisation of heterozygous larval models could also be performed, which was obviated with this alternative experimental design.

5.5. Genetic compensation in the Zebra-grin models

Another possible explanation for the mild phenotypes observed during the characterisation of the generated Zebra-*grin* models is the genetic compensation triggered by mutant mRNA degradation. It has been reported in the literature that genetic mutations may trigger transcriptional adaptation. This is a process in which related genes are upregulated independently of protein feedback loops. In some situations, alleles that have defects on their transcription may also trigger mutant mRNA degradation through a sequence-dependent mechanism, leading to milder phenotypes (El-Brolosy et al., 2019).

In accordance with these findings, it has been proven that, specifically in the CNS, and as a response to a loss of function of one gene, the overexpression of paralogous genes may compensate their function (Etzion et al., 2020). For this reason, we hypothesise that in these situations both paralogs should be knocked out in order to observe the loss-of-function of the resulting proteins and to be comparable with humans' equivalent loss-of-function.

Recently, an extensive study of the zebrafish synapse proteomes was performed, concluding that the retention of duplicated synapse genes has generated an increase in molecular complexity in zebrafish. This is consistent with the view that the sub- and/or neofunctionalization of retained paralogs expanded synaptic molecular complexity and diversity, contributing to improved fitness. These findings need to be taken into consideration when studying disorders that influence the synapse protein structure and function. the additional zebrafish-specific paralogues arising from the TSGD will increase redundancy and potentially mask phenotypes in mutations within that gene family. The additional paralogues may also have undergone species-specific neofunctionalization resulting in species-specific phenotypes (Bayés et al., 2017).

The literature supports the idea that there might be a compensating effect blocking the loss-of-function of NMDAR when their codifying genes are mutated. This supports our data, in which the observed phenotypes are less robust when compared with pharmacological models. In consequence, and specifically for the generated ZeGRIN models, a transcriptomic analysis should be performed in order to obtain a realistic picture of the consequences of knocking out the expression of the different *grin* genes. The obtained information would not only better describe the synaptic situation of the generated models, but importantly will reveal potential genetic and pharmacological targets to modulate NMDAR function and restore normal synaptic function in a glutamatergic transmission dysfunction scenario.

6. Development of new tools related with GRD symptomatology

During the development of this Thesis, and thanks to the direct contact with GRD paediatric neurologists, GRD researchers and GRD families, novel phenotypes highly affecting patients' quality of life arised. Important but commonly omitted phenotypes include gastrointestinal dysfunction. Moreover, another known phenotype that has not been largely studied in GRD animal models is the visual impairment.

We decided to take advantage of our generated models to design and develop novel tools to evaluate these alterations. This would not only allow a better characterisation of these models, but importantly evaluate the effect of potential therapies in alleviating these phenotypes.

6.1. Novel imaging platform to study gastrointestinal alterations

Gastrointestinal dysfunction, specifically intake impairment and constipation, have been previously reported as GRD-related alterations. In accordance with this, constitutive *Grin2b*$^{-/-}$ knockout mice models are reported to be lethal in early stages due to lack of sucking reflex (Kutsuwada et al., 1996).

Undoubtedly, the impairment in the nutrient's intake and absorption is not only harmful itself, but can lead to malnutrition and several other related alterations. For this reason, we agreed on stablishing a new pipeline to describe possible gastrointestinal alterations. The development of this new tool will not only be useful for GRD modelling, and can be expanded to any other studies performed with zebrafish larvae.

This protocol has raised the interest of the ZeClinics company clients and has been included in the Services Portfolio. The performance of this evaluation has been solicited by some clients in order to evaluate gastrointestinal impairment caused by metabolic alterations or different tested diets.

6.2. Visual impairment evaluation through colour preference

Cortex visual problems have been reported in GRD patients (García-Recio et al., 2021). In the research of paradigms related with patients' symptoms, one important readout was the cognitive impairment and/or memory deficits. However, we did find in the literature that zebrafish larvae have a limited ability to perform memory-related paradigms (Bruzzone et al., 2020).

Interestingly, this same scientific article talking about memory paradigms showed a colour-preference in the zebrafish larvae. Specifically, it was shown that larvae had a preference for blue against the other colours, and specifically when compared to yellow. Importantly, this preference was maintained through different developmental and adult stages (Bruzzone et al., 2020). In accordance with these findings, another group proved the colour preference (Hagen et al., 2023). These investigations triggered our intention to use colour preference to evaluate visual function.

Thus, we adapted this information to our behavioural chamber, Noldus, and our larval models. With this aim, we generated the two-coloured 24 well-plate, in which the mutant larvae can freely swim and the colour preference could be evaluated. Despite the results being only preliminary, and the protocol still needs some refinement, the protocol seems promising. It allows us to rapidly evaluate the existence of a visual impairment.

Nevertheless, visual impairment can be caused by several dysfunctions, and the observed impairment can be originated in the retina, but also in higher structures. For this reason, this new tool or paradigm would be used as a filter or screening of the mutants with visual impairment and/or the compounds with an effect on visual function.

Although, to better define the origin of the visual dysfunction, further experiments should be performed. For example, a histological haematoxylin-eosin staining of the retina could be performed to confirm the retina integrity and the architecture of the

different retinal layers. Moreover, some markers of the retina could also be used in immunohistological staining to analyse the integrity of the rods and cones in the outer layers. In addition, the study of higher structures with markers of CNS or some specific receptors could be used in immunohistological analysis to determine alterations in the visual cortex or the transduction of the signal. Verifying the origin of the visual impairment in zebrafish models would give more robust results regarding the modelling and reproduction of GRD patients' symptoms.

Additional paradigms could be performed for further studies. One example that combines the visual and GI functions is the prey consumption paradigm (Abdel-Moneim et al., 2015; Zhao et al., 2023). Predatory hunting is an important type of innate behaviour typically composed of a set of sequential actions, including prey search, pursuit, attack and consumption Importantly, this behaviour is subject to control by the CNS. Therefore, the locomotion, visual and GI functions are involved and can be assessed in one single protocol. We believe these studies would add important information to our obtained phenotypic characterisation.

In addition, also more detailed analysis of eye-movement or locomotor movements triggered by alive prey could be analysed and improved applying innovative ML or AI approaches currently being developed by the ZeClinics group. Moreover, these analyses would bring light regarding the intake deficit observed in some models, unveiling the nature of the observed alterations: movement alterations affecting the consumption, lack of interest for the prey, jaw defects affecting the intake, etc.

Importantly, this paradigm is also compatible with drug discovery and pharmacological screening, allowing to observe directly the effect of possible therapies in the ingestion, an important issue reported by GRD families.

7. Pharma-*grin*, a platform to screen potential treatments for GRD

The results obtained are focused around developing new therapeutic strategies that target NMDAR dysfunction, with a focus on GRD, but with the potential for wider applicability to other diseases involving NMDAR-related dysfunctions. The study directly models the loss-of-function in GRIN genes, which plays a crucial role in NMDAR activity. This allows for an in-depth investigation of how NMDAR dysfunction affects the system, and it may also provide insights into other conditions where the glutamatergic synapse or neurotransmission is compromised.

A significant challenge in current treatments is the lack of selectivity in NMDAR modulators. These broad-spectrum drugs target multiple NMDAR subunits indiscriminately, leading to undesirable and often unbearable side effects. These side effects make it difficult to use NMDAR modulators as viable therapies, which highlights the need for more precise pharmacological tools. This research suggests that focusing on selective modulation of different GluN subunits of NMDAR could be a more effective and safer approach (Mony et al., 2009; Paoletti et al., 2013).

Additionally, there is a strong interplay between NMDAR function and GABAergic transmission, so targeting GABA signaling modulators could indirectly influence NMDAR function and help restore normal neural activity in conditions where NMDAR is dysfunctional. This opens up the possibility of exploring alternative therapeutic targets beyond NMDAR alone (Sadikot et al., 1998).

There are some studies also pointing the need of precision medicine when referring to NMDAR dysfunction, related with the lack of selectivity of the current drugs (Gale et al., 2021). Recently, some groups studying not only GRD but generally NMDAR function and dysfunction have emphasise the differential effect of different NMDAR modulators and its therapeutic potential (Geoffroy et al., 2022; Thapaliya et al., 2021).

The use of zebrafish as a model organism plays a key role in this research, as it provides a powerful platform for assessing the developmental toxicity, neurotoxicity, and overall safety of potential NMDAR-modulating compounds. The zebrafish model allows for rapid, high-throughput screening of these compounds before advancing to mammalian models, making the process both cost-effective and time-efficient. The early findings suggest that some of these modulators have the potential to reverse phenotypes associated with GRD, offering a promising step forward in the development of effective therapies.

Ultimately, the project aims to develop pharmacologically safe NMDAR modulators that could not only be applied to GRD patients but also to a wider range of neurological disorders associated with NMDAR dysfunction. The next steps will involve further testing of these compounds in more advanced models to assess their potential for therapeutic use across a broader spectrum of diseases.

8. Validity of the models

Our results suggest that the generated zebra-*grin* models have an elevated potential to be GRD models to study the systemic disruptions resulting from NMDAR dysfunction. Importantly, and given the previous results and recent literature supporting a conserved pharmacology, the models have an enormous potential to screen potential therapies and assess their toxicity. Nevertheless, a compensation mechanism may be attenuating the observed results. To elude or minimise the compensation, the double mutant lines are more promising models. Further comprehension of the compensatory mechanisms interfering in the generated lines is needed to better define our final GRD models.

9. Development of an F0 platform for high-throughput screening

From the GRD deep study, and the fact that the zebrafish model has emerged as a reference tool for phenotypic drug screening, we decided to develop a novel platform for high-throughput screening without the need of developing isogenic lines.

The study of neurodevelopmental disorders (NDDs) is one of the research fields that might benefit more from the establishment of a robust pipeline allowing the assessment of gene function in F0 larvae. It has been estimated that NDDs affect up to 15% of children and adolescents worldwide and cause deficits in mental performance, adaptive behaviour and motor skills (Francés et al., 2022). The genetic causes underlying these disorders are extremely complex, since, although common molecular players have been identified (Cristino et al., 2014), the nature of the disease-causing mutations is heterogeneous, resulting in variable clinical outcomes (Parenti et al., 2020). This is particularly true for epilepsy, which is regarded as an NDD due to the contribution of multiple developmental variables, including congenital brain abnormalities and aberrant neuronal signalling throughout embryonic life (Bozzi et al., 2012). Epilepsy is one of the most common neurological disorders, with over 70 million people diagnosed worldwide (Thijs et al., 2019; Turrini et al., 2022).

For this reason, we decided to focus on epilepsy to develop this new tool as a proof of principle. Our objective is to develop a zebrafish-based comprehensive platform enabling the functional validation of common and *de novo* rare loss-of-function mutations in a high-throughput fashion.

We successfully proved that co-targeting the gene of interest with a reporter gene whose loss of function is associated with an easily detectable phenotype, the *tyrosinase* gene, we could use this phenotype to screen zebrafish with high-rate of mutations in F0. Moreover, we coupled highly efficient gene inactivation with the automated analysis of the morphological developmental defects potentially induced by the gene inactivation and with a complex multiparametric behavioural analysis to describe seizure-like events.

With this multiparametric analysis we could describe two populations regarding parameters related with epileptic behaviour, describing a fingerprint that allowed us to describe the anti-epileptic effect of different anti-epileptic compounds. For this last part, we focused on *scn1lab* loss-of-function, commonly used to model Dravet's syndrome.

With the completion of this secondary project, and given its innovative nature, a scientific report has been recently published in the "International Journal of Molecular Sciences" peer-reviewed journal (Locubiche et al., 2024).

10. Future perspectives

Regarding the possible genetic compensation that takes place in *grin* genes (similar to what happens with other genes related with the synaptic activity), we should further investigate the genomics and, importantly, proteomics of the generated ZeGRIN models. This will not only allow to better describe the picture of the glutamatergic synapse in the generated models, but importantly to detect potential genetic and pharmacological targets. These targets could be easily further studied and potential novel therapies would surge from this analysis.

Some of the limitations encountered when phenotypically characterising the generated models were related with the age of the models. The study of zebrafish larvae was crucial for the characterisation of this neurodevelopmental disease. However, we believe that further analysis of the models in juvenile stages will be able to expand our characterisation, including memory and learning paradigms or social behaviour characterisation, tightly related with ASD traits that could be comparable with the patients' symptoms.

It is important to point and emphasise that NMDAR modulators or other targets related with the balance of the glutamatergic transmission would be potential therapies for

GRD patients, but also for several other diseases related with glutamatergic unbalance or NMDAR dysfunction. Among the different diseases, ASD or epilepsy, which are usually considered multiparametric or idiopathic would have possible treatments.

Regarding the pharmacological treatment, we have confirmed that zebrafish is a good model for pharmacological screening, and specifically for NMDAR modulators. With this concept in mind, our short future perspectives is to focus on pharmacological targets or therapeutic strategies that can be brought to the patients as fast as possible.

In collaboration with Dra. Mireia Olivella (UVic), Dr. Xavier Altafaj (UB) and Dra. Àngels García Cazorla (HSJD), an exhaustive study of multiple potential nutraceutics is being performed. Nutraceutics are the nutraceutical supplements already commercialised that may have a positive impact in neuronal function, but neutral or with reduced side-effects. This situation is what happened with L-Serine treatment, which is commercialised as a nutraceutical supplement that has shown to improve cognitive functions. L-Serine is transformed to D-Serine in the CNS, which have a co-agonist function of NMDAR. Its effect in wild-type animal models, cultures and patients is limited, but in front of a LoF it has proven to improve some of the phenotypes observed in patients. Recently a clinical trial has been completed In SJD by Natlaia Julià and Àngels García Cazorla, and nowadays D-Serine is the main compound prescribed to patients with LoF mutations.

This raises the important issue of having all the possible functional annotations of the known mutations. Functional annotation and stratification in GoF or LoF fastens the procedure, and allows to treat the patients in a faster manner.

For this reason, the following projects related with GRD and the Barcelona GRD Hub are also focused on continuing the functional annotation and the completion of the GRINdb. The three groups working together will accomplish that, few weeks after the diagnosis of GRD patients, the patient could already receive some kind of treatment.

Other possible collaborations are focused on the generation of a platform combining our findings with Artificial Intelligence (AI) and Machine Learning (ML) technology. Our objective on this side would be to build a knowledge graph (KG), potentiating the finding potential targets and compounds to treat not only GRD but any other disease that course with glutamatergic dysfunction. The building of this complex platform

could potentially be applied to several other disease, specially rare diseases, potentiating their study and the discovery of potential targets and compounds.

Conclusions

I. In zebrafish, two paralogous genes of human GRIN1, GRIN2A and GRIN2B are expressed. These genes display a high percentage of homology, specifically in the transmembrane domain and Mg^{2+} binding domain, suggesting a conservation in their function. Whole-mount in situ hybridization unveiled the spatio-temporal expression pattern of *grin1*, *grin2A* and *grin2B* paralogous genes in zebrafish larvae, *grin* genes are expressed in the zebrafish CNS, the retina and the gastrointestinal tract.

II. An *in vivo* library of loss-of-function GRD models has been generated by individually knocking out six different GRIN genes in zebrafish, applying CRISPR/Cas9 technology. We have generated six different single knockout lines (*grin1a. grin1b, grin2Aa, grin2Ab, grin2Ba* and *grin2Bb)* and three different double knockout lines, obtained by crossing the single knockout lines of each *grin* paralog (*grin1a-grin1b, grin2Aa-grin2Ab* and *grin2Ba-grin2Bb*).

III. An in vivo library of loss-of-function GRD models (ZeGRIN) has been generated by means of CRISPR/Cas9 technology, individually knocking out six different grin genes in zebrafish. We have generated six different single knockout lines (grin1a, grin1b, grin2Aa, grin2Ab, grin2Ba and grin2Bb) and three different double knockout lines (grin1a-grin1b, grin2Aa-grin2Ab and grin2Ba-grin2Bb).

IV. Zebrafish models of GRD allow to explore systemic disabling phenotypes associated with GRD. A behavioural phenotypation battery of zebrafish larvae has been designed and validated using pharmacological models of GRD.

V. Behavioural analysis of the single ZeGRIN models unveiled, in a genotype-dependent manner and with a light effect, discrete locomotor alterations, defects in response to tapping stimuli and epilepsy-like behaviour in response to light flashes.

VI. The double knockout ZeGRIN models exhibited strong phenotypes, suggesting that a genetic compensatory mechanism might be attenuating the phenotype alterations in single grin knockout lines.

VII. Pre-juvenile mortality was described in double homozygous grin1a-/- - grin1b-/- larvae, but not for all the other single and double knockout lines generated.

VIII. A new protocol for the in vivo assessment of the gastrointestinal function has been established and validated in zebrafish larvae. This new tool allowed the characterisation of an impairment in the gastrointestinal function of the generated ZeGRIN models, recapitulating GRD-associated GI distress.

IX. A new protocol for the in vivo assessment of potential visual function impairment has been designed and established in zebrafish larvae. Using this protocol, the colour preference test, we identified the presence of a visual impairment in double homozygous grin1a-/- - grin1b-/- larvae.

X. The pharmacological and genetic ZeGRIN models show the zebrafish larvae as a suitable model for high-throughput screening of NMDAR modulators. Using this model, our proof-of-concept studies showed a differential tolerability and behavioural effect of *in silico*-identified novel NMDAR modulators.

XI. A novel platform of high-throughput epilepsy modelling and drug screening in F0 larvae has been generated. The *in vivo* combination of F0 gene targeting and phenotypic fingerprinting of zebrafish larvae represents a powerful tool for functional genomics, drug screening and personalized medicine development that can be scalable from epilepsy to other neurodevelopmental disorders and, in principle, to a vast array of indications.

XII. The zebrafish is a suitable model to generate an *in vivo* library of GRD avatars, allowing to perform a comprehensive phenotypic assessment and a high-throughput screening of potential therapies in a fast, trusty and economic way.

References

- Abdel-Moneim, A., Moreira-Santos, M., & Ribeiro, R. (2015). A short-term sublethal toxicity assay with zebra fish based on preying rate and its integration with mortality. *Chemosphere*, *120*, 568–574. https://doi.org/10.1016/j.chemosphere.2014.09.083
- Adell, A. (2020). Brain NMDA Receptors in Schizophrenia and Depression. *Biomolecules*, *10*(6), 947. https://doi.org/10.3390/biom10060947
- Akram, M. (2014). Citric Acid Cycle and Role of its Intermediates in Metabolism. *Cell Biochemistry and Biophysics*, *68*(3), 475–478. https://doi.org/10.1007/s12013-013-9750-1
- Amador, A., Bostick, C. D., Olson, H., Peters, J., Camp, C. R., Krizay, D., Chen, W., Han, W., Tang, W., Kanber, A., Kim, S., Teoh, J., Sah, M., Petri, S., Paek, H., Kim, A., Lutz, C. M., Yang, M., Myers, S. J., … Frankel, W. N. (2020). Modelling and treating GRIN2A developmental and epileptic encephalopathy in mice. *Brain*, *143*(7), 2039–2057. https://doi.org/10.1093/brain/awaa147
- Anaparti, V., Ilarraza, R., Orihara, K., Stelmack, G. L., Ojo, O. O., Mahood, T. H., Unruh, H., Halayko, A. J., & Moqbel, R. (2015). NMDA receptors mediate contractile responses in human airway smooth muscle cells. *American Journal of Physiology-Lung Cellular and Molecular Physiology*, *308*(12), L1253–L1264. https://doi.org/10.1152/ajplung.00402.2014
- Antunes, M., & Biala, G. (2012). The novel object recognition memory: Neurobiology, test procedure, and its modifications. *Cognitive Processing*, *13*(2), 93–110. https://doi.org/10.1007/s10339-011-0430-z
- Araque, A., Parpura, V., Sanzgiri, R. P., & Haydon, P. G. (1999). Tripartite synapses: Glia, the unacknowledged partner. *Trends in Neurosciences*, *22*(5), 208–215. https://doi.org/10.1016/S0166-2236(98)01349-6
- Bahi-Buisson, N., Poirier, K., Boddaert, N., Fallet-Bianco, C., Specchio, N., Bertini, E., Caglayan, O., Lascelles, K., Elie, C., Rambaud, J., Baulac, M., An, I., Dias, P., Des Portes, V., Moutard, M. L., Soufflet, C., El Maleh, M., Beldjord, C., Villard, L., & Chelly, J. (2010). GPR56-related bilateral frontoparietal polymicrogyria: Further evidence for an overlap with the cobblestone complex. *Brain*, *133*(11), Article 11. https://doi.org/10.1093/brain/awq259
- Bak, L. K., Schousboe, A., & Waagepetersen, H. S. (2006). The glutamate/GABA-glutamine cycle: Aspects of transport, neurotransmitter homeostasis and ammonia transfer. *Journal of Neurochemistry*, *98*, 641–653.
- Bannerman, D. M., Niewoehner, B., Lyon, L., Romberg, C., Schmitt, W. B., Taylor, A., Sanderson, D. J., Cottam, J., Sprengel, R., Seeburg, P. H., Köhr, G., & Rawlins, J. N. P. (2008). NMDA Receptor Subunit NR2A Is Required for Rapidly Acquired Spatial Working Memory But Not Incremental Spatial Reference Memory. *The Journal of Neuroscience*, *28*(14), 3623–3630. https://doi.org/10.1523/JNEUROSCI.3639-07.2008
- Baraban, S. C. (2013). Forebrain Electrophysiological Recording in Larval Zebrafish. *Journal of Visualized Experiments*, *71*, 50104. https://doi.org/10.3791/50104

- Baraban, S. C., Dinday, M. T., & Hortopan, G. A. (2013). Drug screening in Scn1a zebrafish mutant identifies clemizole as a potential Dravet syndrome treatment. *Nature Communications*, *4*(1), Article 1. https://doi.org/10.1038/ncomms3410
- Baraban, S. C., Taylor, M. R., Castro, P. A., & Baier, H. (2005). Pentylenetetrazole induced changes in zebrafish behavior, neural activity and c-fos expression. *Neuroscience*, *131*(3), Article 3. https://doi.org/10.1016/j.neuroscience.2004.11.031
- Bayés, À., Collins, M. O., Reig-Viader, R., Gou, G., Goulding, D., Izquierdo, A., Choudhary, J. S., Emes, R. D., & Grant, S. G. N. (2017). Evolution of complexity in the zebrafish synapse proteome. *Nature Communications*, *8*(1), 14613. https://doi.org/10.1038/ncomms14613
- Benke, T. A., Park, K., Krey, I., Camp, C. R., Song, R., Ramsey, A. J., Yuan, H., Traynelis, S. F., & Lemke, J. (2021). Clinical and therapeutic significance of genetic variation in the GRIN gene family encoding NMDARs. *Neuropharmacology*, *199*, 108805. https://doi.org/10.1016/j.neuropharm.2021.108805
- Benvenutti, R., Gallas-Lopes, M., Marcon, M., Reschke, C. R., Herrmann, A. P., & Piato, A. (2022). Glutamate NMDA Receptor Antagonists with Relevance to Schizophrenia:A Review of Zebrafish Behavioral Studies. *Current Neuropharmacology*, *20*(3), 494–509. https://doi.org/10.2174/1570159X19666210215121428
- Bermudo-Soriano, C. R., Perez-Rodriguez, M. M., Vaquero-Lorenzo, C., & Baca-Garcia, E. (2012). New perspectives in glutamate and anxiety. *Pharmacology Biochemistry and Behavior*, *100*(4), 752–774. https://doi.org/10.1016/j.pbb.2011.04.010
- Bertocchi, I., Cifarelli, L., Oberto, A., Eva, C. E., Sprengel, R., Mirza, N. R., & Muglia, P. (2024). Radiprodil, a selective GluN2B negative allosteric modulator, rescues audiogenic seizures in mice carrying the GluN2A(N615S) mutation. *British Journal of Pharmacology*, *181*(12), 1886–1894. https://doi.org/10.1111/bph.16361
- Best, J. D., Berghmans, S., Hunt, J. J. F. G., Clarke, S. C., Fleming, A., Goldsmith, P., & Roach, A. G. (2008). Non-Associative Learning in Larval Zebrafish. *Neuropsychopharmacology*, *33*(5), 1206–1215. https://doi.org/10.1038/sj.npp.1301489
- Blaser, R., & Heyser, C. (2015). Spontaneous object recognition: A promising approach to the comparative study of memory. *Frontiers in Behavioral Neuroscience*, *9*. https://doi.org/10.3389/fnbeh.2015.00183
- Bliss, T. V. P., & Collingridge, G. L. (1993). A synaptic model of memory: Long-term potentiation in the hippocampus. *Nature*, *361*, 31–39.
- Bliss, T. V. P., Collingridge, G. L., Kaang, B.-K., & Zhuo, M. (2016). Synaptic plasticity in the anterior cingulate cortex in acute and chronic pain. *Nature Reviews Neuroscience*, *17*(8), 485–496. https://doi.org/10.1038/nrn.2016.68
- Borghuis, B. G., Looger, L. L., Tomita, S., & Demb, J. B. (2014). Kainate Receptors Mediate Signaling in Both Transient and Sustained OFF Bipolar Cell Pathways in Mouse Retina. *The Journal of Neuroscience*, *34*(18), 6128–6139. https://doi.org/10.1523/JNEUROSCI.4941-13.2014

- Boueid, M.-J., El-Hage, O., Schumacher, M., Degerny, C., & Tawk, M. (2023). Zebrafish as an emerging model to study estrogen receptors in neural development. *Frontiers in Endocrinology*, *14*, 1240018. https://doi.org/10.3389/fendo.2023.1240018
- Bouvier, G., Bidoret, C., Casado, M., & Paoletti, P. (2015). Presynaptic NMDA receptors: Roles and rules. *Neuroscience*, *311*, 322–340. https://doi.org/10.1016/j.neuroscience.2015.10.033
- Boyce-Rustay, J. M., & Holmes, A. (2006). Genetic Inactivation of the NMDA Receptor NR2A Subunit has Anxiolytic- and Antidepressant-Like Effects in Mice. *Neuropsychopharmacology*, *31*(11), 2405–2414. https://doi.org/10.1038/sj.npp.1301039
- Bozzi, Y., Casarosa, S., & Caleo, M. (2012). Epilepsy as a Neurodevelopmental Disorder. *Frontiers in Psychiatry*, *3*. https://doi.org/10.3389/fpsyt.2012.00019
- Brigman, J. L., Feyder, M., Saksida, L. M., Bussey, T. J., Mishina, M., & Holmes, A. (2008). Impaired discrimination learning in mice lacking the NMDA receptor NR2A subunit. *Learning & Memory*, *15*(2), 50–54. https://doi.org/10.1101/lm.777308
- Bruzzone, M., Gatto, E., Lucon Xiccato, T., Dalla Valle, L., Fontana, C. M., Meneghetti, G., & Bisazza, A. (2020). Measuring recognition memory in zebrafish larvae: Issues and limitations. *PeerJ*, *8*, e8890. https://doi.org/10.7717/peerj.8890
- Burnashev, N., & Szepetowski, P. (2015). NMDA receptor subunit mutations in neurodevelopmental disorders. *Current Opinion in Pharmacology*, *20*, 73–82. https://doi.org/10.1016/j.coph.2014.11.008
- Camp, C. R., Vlachos, A., Klöckner, C., Krey, I., Banke, T. G., Shariatzadeh, N., Ruggiero, S. M., Galer, P., Park, K. L., Caccavano, A., Kimmel, S., Yuan, X., Yuan, H., Helbig, I., Benke, T. A., Lemke, J. R., Pelkey, K. A., McBain, C. J., & Traynelis, S. F. (2023). Loss of Grin2a causes a transient delay in the electrophysiological maturation of hippocampal parvalbumin interneurons. *Communications Biology*, *6*(1), 952. https://doi.org/10.1038/s42003-023-05298-9
- Carrillo, E., Gonzalez, C. U., Berka, V., & Jayaraman, V. (2021). Delta glutamate receptors are functional glycine- and D-serine–gated cation channels in situ. *Science Advances*, *7*(52), eabk2200. https://doi.org/10.1126/sciadv.abk2200
- Carvill, G. L., Regan, B. M., Yendle, S. C., O'Roak, B. J., Lozovaya, N., Bruneau, N., Burnashev, N., Khan, A., Cook, J., Geraghty, E., Sadleir, L. G., Turner, S. J., Tsai, M.-H., Webster, R., Ouvrier, R., Damiano, J. A., Berkovic, S. F., Shendure, J., Hildebrand, M. S., … Mefford, H. C. (2013). GRIN2A mutations cause epilepsy-aphasia spectrum disorders. *Nature Genetics*, *45*(9), 1073–1076. https://doi.org/10.1038/ng.2727
- Cassar, S., Huang, X., & Cole, T. (2018). High-throughput Measurement of Gut Transit Time Using Larval Zebrafish. *Journal of Visualized Experiments*, *140*, 58497. https://doi.org/10.3791/58497
- Castaldo, P., Del Giudice, E. M., Coppola, G., Pascotto, A., Annunziato, L., & Taglialatela, M. (2002). Benign Familial Neonatal Convulsions Caused by Altered Gating of KCNQ2/KCNQ3 Potassium Channels. *The Journal of Neuroscience*, *22*(2), Article 2. https://doi.org/10.1523/JNEUROSCI.22-02-j0003.2002

- Chandrasekhar, A., Moens, C. B., Warren, J. T., Kimmel, C. B., & Kuwada, J. Y. (1997). Development of branchiomotor neurons in zebrafish. *Development*, *124*(13), 2633–2644. https://doi.org/10.1242/dev.124.13.2633
- Chapouton, P., & Godinho, L. (2010). Neurogenesis. In *Methods in Cell Biology* (Vol. 100, pp. 72–126). Elsevier. https://doi.org/10.1016/B978-0-12-384892-5.00004-9
- Charu C. Aggarwal. (2017). *Outlier Analysis* (2nd ed.). Springer Cham. https://doi.org/10.1007/978-3-319-47578-3
- Chen, W., Shieh, C., Swanger, S. A., Tankovic, A., Au, M., McGuire, M., Tagliati, M., Graham, J. M., Madan-Khetarpal, S., Traynelis, S. F., Yuan, H., & Pierson, T. M. (2017). GRIN1 mutation associated with intellectual disability alters NMDA receptor trafficking and function. *Journal of Human Genetics*, *62*(6), 589–597. https://doi.org/10.1038/jhg.2017.19
- Chenu, C., Serre, C. M., Raynal, C., Burt-Pichat, B., & Delmas, P. D. (1998). Glutamate Receptors Are Expressed by Bone Cells and Are Involved in Bone Resorption. *Bone*, *22*(4), 295–299. https://doi.org/10.1016/S8756-3282(97)00295-0
- Chitnis, A., & Kuwada, J. (1990). Axonogenesis in the brain of zebrafish embryos. *The Journal of Neuroscience*, *10*(6), 1892–1905. https://doi.org/10.1523/JNEUROSCI.10-06-01892.1990
- Clayton, D. A., Mesches, M. H., Alvarez, E., Bickford, P. C., & Browning, M. D. (2002). A Hippocampal NR2B Deficit Can Mimic Age-Related Changes in Long-Term Potentiation and Spatial Learning in the Fischer 344 Rat. *The Journal of Neuroscience*, *22*(9), 3628–3637. https://doi.org/10.1523/JNEUROSCI.22-09-03628.2002
- Collier, A. D., Abdulai, A. R., & Leibowitz, S. F. (2023). Utility of the Zebrafish Model for Studying Neuronal and Behavioral Disturbances Induced by Embryonic Exposure to Alcohol, Nicotine, and Cannabis. *Cells*, *12*(20), 2505. https://doi.org/10.3390/cells12202505
- Collingridge, G. L., Olsen, R. W., Peters, J., & Spedding, M. (2009). A nomenclature for ligand-gated ion channels. *Neuropharmacology*, *56*(1), 2–5. https://doi.org/10.1016/j.neuropharm.2008.06.063
- Concordet, J.-P., & Haeussler, M. (2018). CRISPOR: Intuitive guide selection for CRISPR/Cas9 genome editing experiments and screens. *Nucleic Acids Research*, *46*(W1), W242–W245. https://doi.org/10.1093/nar/gky354
- Conroy, J., McGettigan, P. A., McCrear, D., Shah, N., Collins, K., Parry-Fielder, B., Moran, M., Hanrahan, D., Deonna, T. W., Korff, C. M., Webb, D., Ennis, S., Lynch, S. A., & King, M. D. (2014). Towards the identification of a genetic basis for Landau-Kleffner syndrome. *Epilepsia*, *55*(6), 858–865.
- Cornet, C., Calzolari, S., Miñana-Prieto, R., Dyballa, S., Van Doornmalen, E., Rutjes, H., Savy, T., D'Amico, D., & Terriente, J. (2017). ZeGlobalTox: An Innovative Approach to Address Organ Drug Toxicity Using Zebrafish. *International Journal of Molecular Sciences*, *18*(4), 864. https://doi.org/10.3390/ijms18040864

- Cox, J. A., Kucenas, S., & Voigt, M. M. (2005). Molecular characterization and embryonic expression of the family of *N* -methyl- D -aspartate receptor subunit genes in the zebrafish. *Developmental Dynamics*, *234*(3), 756–766. https://doi.org/10.1002/dvdy.20532
- Cristino, A. S., Williams, S. M., Hawi, Z., An, J.-Y., Bellgrove, M. A., Schwartz, C. E., Costa, L. D. F., & Claudianos, C. (2014). Neurodevelopmental and neuropsychiatric disorders represent an interconnected molecular system. *Molecular Psychiatry*, *19*(3), Article 3. https://doi.org/10.1038/mp.2013.16
- Cull-Candy, S., Brickley, S., & Farrant, M. (2001). NMDA receptor subunits: Diversity, development and disease. *Current Opinion in Neurobiology*, *11*(3), 327–335. https://doi.org/10.1016/S0959-4388(00)00215-4
- Curtis, D., Phillis, J., & Watkins, J. (1959). Chemical Excitation of Spinal Neurones. *Nature*, *183*.
- Curtis, D. R., & Johnston, G. A. R. (1974). Amino acid transmitters in the mammalian central nervous system. In *Reviews of Physiology* (Vol. 69, pp. 97–188). DOI: 10.1007/3-540-06498-2_3
- Dalmau, J., Armangué, T., Planagumà, J., Radosevic, M., Mannara, F., Leypoldt, F., Geis, C., Lancaster, E., Titulaer, M. J., Rosenfeld, M. R., & Graus, F. (2019). An update on anti-NMDA receptor encephalitis for neurologists and psychiatrists: Mechanisms and models. *The Lancet Neurology*, *18*(11), 1045–1057. https://doi.org/10.1016/S1474-4422(19)30244-3
- Dalmau, J., Gleichman, A. J., Hughes, E. G., Rossi, J. E., Peng, X., Lai, M., Dessain, S. K., Rosenfeld, M. R., Balice-Gordon, R., & Lynch, D. R. (2008). Anti-NMDA-receptor encephalitis: Case series and analysis of the effects of antibodies. *The Lancet Neurology*, *7*(12), 1091–1098. https://doi.org/10.1016/S1474-4422(08)70224-2
- De Ligt, J., Willemsen, M. H., Van Bon, B. W. M., Kleefstra, T., Yntema, H. G., Kroes, T., Vulto-van Silfhout, A. T., Koolen, D. A., De Vries, P., Gilissen, C., Del Rosario, M., Hoischen, A., Scheffer, H., De Vries, B. B. A., Brunner, H. G., Veltman, J. A., & Vissers, L. E. L. M. (2012). Diagnostic Exome Sequencing in Persons with Severe Intellectual Disability. *New England Journal of Medicine*, *367*(20), 1921–1929. https://doi.org/10.1056/NEJMoa1206524
- Den Hollander, B., Veenvliet, A. R. J., Rothuizen-Lindenschot, M., Van Essen, P., Peters, G., Santos-Gómez, A., Olivella, M., Altafaj, X., Brands, M. M., Jacobs, B. A. W., & Van Karnebeek, C. D. (2023). Evidence for effect of l-serine, a novel therapy for GRIN2B-related neurodevelopmental disorder. *Molecular Genetics and Metabolism*, *138*(3), 107523. https://doi.org/10.1016/j.ymgme.2023.107523
- DeOliveira-Mello, L., Baronio, D., & Panula, P. (2023). Zebrafish embryonically exposed to valproic acid present impaired retinal development and sleep behavior. *Autism Research*, *16*(10), Article 10. https://doi.org/10.1002/aur.3010
- Depienne, C., Trouillard, O., Saint-Martin, C., Gourfinkel-An, I., Bouteiller, D., Carpentier, W., Keren, B., Abert, B., Gautier, A., Baulac, S., Arzimanoglou, A., Cazeneuve, C., Nabbout, R., & LeGuern, E. (2008). Spectrum of SCN1A gene mutations associated with Dravet syndrome: Analysis of 333 patients. *Journal of Medical Genetics*, *46*(3), Article 3. https://doi.org/10.1136/jmg.2008.062323

- DeVries, S. P., & Patel, A. D. (2013). Two Patients With a GRIN2A Mutation and Childhood-onset Epilepsy. *Pediatric Neurology*, *49*(6), 482–485. https://doi.org/10.1016/j.pediatrneurol.2013.08.023
- Dimassi, S., Labalme, A., Lesca, G., Rudolf, G., Bruneau, N., Hirsch, E., Arzimanoglou, A., Motte, J., De Saint Martin, A., Boutry-Kryza, N., Cloarec, R., Benitto, A., Ameil, A., Edery, P., Ryvlin, P., De Bellescize, J., Szepetowski, P., & Sanlaville, D. (2014). A subset of genomic alterations detected in rolandic epilepsies contains candidate or known epilepsy genes including *GRIN 2A* and *PRRT 2* . *Epilepsia*, *55*(2), 370–378. https://doi.org/10.1111/epi.12502
- Dinday, M. T., & Baraban, S. C. (2015). Large-Scale Phenotype-Based Antiepileptic Drug Screening in a Zebrafish Model of Dravet Syndrome. *Eneuro*, *2*(4), Article 4. https://doi.org/10.1523/ENEURO.0068-15.2015
- Dolino, D. M., Rezaei Adariani, S., Shaikh, S. A., Jayaraman, V., & Sanabria, H. (2016). Conformational Selection and Submillisecond Dynamics of the Ligand-binding Domain of the N-Methyl-d-aspartate Receptor. *Journal of Biological Chemistry*, *291*(31), 16175–16185. https://doi.org/10.1074/jbc.M116.721274
- Doszyn, O., Dulski, T., & Zmorzynska, J. (2024). Diving into the zebrafish brain: Exploring neuroscience frontiers with genetic tools, imaging techniques, and behavioral insights. *Frontiers in Molecular Neuroscience*, *17*, 1358844. https://doi.org/10.3389/fnmol.2024.1358844
- Dreosti, E., Lopes, G., Kampff, A. R., & Wilson, S. W. (2015). Development of social behavior in young zebrafish. *Frontiers in Neural Circuits*, *9*. https://doi.org/10.3389/fncir.2015.00039
- Du, J., Li, X.-H., & Li, Y.-J. (2016). Glutamate in peripheral organs: Biology and pharmacology. *European Journal of Pharmacology*, *784*, 42–48. https://doi.org/10.1016/j.ejphar.2016.05.009
- Duncan, G. E., Miyamoto, S., Gu, H., Lieberman, J. A., Koller, B. H., & Snouwaert, J. N. (2002). Alterations in regional brain metabolism in genetic and pharmacological models of reduced NMDA receptor function. *Brain Research*, *951*(2), 166–176. https://doi.org/10.1016/S0006-8993(02)03156-6
- Duncan, G. E., Moy, S. S., Perez, A., Eddy, D. M., Zinzow, W. M., Lieberman, J. A., Snouwaert, J. N., & Koller, B. H. (2004). Deficits in sensorimotor gating and tests of social behavior in a genetic model of reduced NMDA receptor function. *Behavioural Brain Research*, *153*(2), 507–519. https://doi.org/10.1016/j.bbr.2004.01.008
- Dzikiewicz, A., & Szweykowska-Kulińska, Z. (2006). Nonsense-mediated mRNA decay (NMD) on guard of mRNA quality. *Popstepy Biochemii*, *52*(4), 390–398.
- Dzirasa, K., Ramsey, A. J., Takahashi, D. Y., Stapleton, J., Potes, J. M., Williams, J. K., Gainetdinov, R. R., Sameshima, K., Caron, M. G., & Nicolelis, M. A. L. (2009). Hyperdopaminergia and NMDA Receptor Hypofunction Disrupt Neural Phase Signaling. *Journal of Neuroscience*, *29*(25), 8215–8224. https://doi.org/10.1523/JNEUROSCI.1773-09.2009
- El-Brolosy, M. A., Kontarakis, Z., Rossi, A., Kuenne, C., Günther, S., Fukuda, N., Kikhi, K., Boezio, G. L. M., Takacs, C. M., Lai, S.-L., Fukuda, R., Gerri, C., Giraldez, A. J., & Stainier, D.

Y. R. (2019). Genetic compensation triggered by mutant mRNA degradation. *Nature*, *568*(7751), 193–197. https://doi.org/10.1038/s41586-019-1064-z

- Ellis, L. D., Seibert, J., & Soanes, K. H. (2012). Distinct models of induced hyperactivity in zebrafish larvae. *Brain Research*, *1449*, 46–59. https://doi.org/10.1016/j.brainres.2012.02.022
- Endele, S., Rosenberger, G., Geider, K., Popp, B., Tamer, C., Stefanova, I., Milh, M., Kortüm, F., Fritsch, A., Pientka, F. K., Hellenbroich, Y., Kalscheuer, V. M., Kohlhase, J., Moog, U., Rappold, G., Rauch, A., Ropers, H.-H., Von Spiczak, S., Tönnies, H., … Kutsche, K. (2010). Mutations in GRIN2A and GRIN2B encoding regulatory subunits of NMDA receptors cause variable neurodevelopmental phenotypes. *Nature Genetics*, *42*(11), 1021–1026. https://doi.org/10.1038/ng.677
- Epi4K Consortium & Epilepsy Phenome/Genome Project. (2013). De novo mutations in epileptic encephalopathies. *Nature*, *501*(7466), 217–221. https://doi.org/10.1038/nature12439
- Erdem, F. A., Ilic, M., Koppensteiner, P., Gołacki, J., Lubec, G., Freissmuth, M., & Sandtner, W. (2019). A comparison of the transport kinetics of glycine transporter 1 and glycine transporter 2. *Journal of General Physiology*, *151*(8), 1035–1050. https://doi.org/10.1085/jgp.201912318
- Etzion, T., Zmora, N., Zohar, Y., Levavi-Sivan, B., Golan, M., & Gothilf, Y. (2020). Ectopic over expression of kiss1 may compensate for the loss of kiss2. *General and Comparative Endocrinology*, *295*, 113523. https://doi.org/10.1016/j.ygcen.2020.113523
- Fang, P. (1999). The spectrum of mutations in UBE3A causing Angelman syndrome. *Human Molecular Genetics*, *8*(1), Article 1. https://doi.org/10.1093/hmg/8.1.129
- Farsi, Z., Nicolella, A., Simmons, S. K., Aryal, S., Shepard, N., Brenner, K., Lin, S., Herzog, L., Moran, S. P., Stalnaker, K. J., Shin, W., Gazestani, V., Song, B. J., Bonanno, K., Keshishian, H., Carr, S. A., Pan, J. Q., Macosko, E. Z., Datta, S. R., … Sheng, M. (2023). Brain-region-specific changes in neurons and glia and dysregulation of dopamine signaling in Grin2a mutant mice. *Neuron*, *111*(21), 3378-3396.e9. https://doi.org/10.1016/j.neuron.2023.08.004
- Fonnum, F. (1984). Glutamate: A Neurotransmitter in Mammalian Brain. *Journal of Neurochemistry*, *42*(1), 1–11. https://doi.org/10.1111/j.1471-4159.1984.tb09689.x
- Fonnum, F., Gottesfeld, Z., & Grofova, I. (1978). Distribution of glutamate decarboxylase, choline acetyl-transferase and aromatic amino acid decarboxylase in the basal ganglia of normal and operated rats. Evidence for striatopallidal, striatoentopeduncular and striatonigral gabaergic fibres. *Brain Research*, *143*(1), 125–138. https://doi.org/10.1016/0006-8993(78)90756-4
- Fonnum, F., Grofová, I., & Rinvik, E. (1978). Origin and distribution of glutamate decarboxylase in the nucleus subthalamicus of the cat. *Brain Research*, *153*(2), 370–374. https://doi.org/10.1016/0006-8993(78)90417-1
- Fonnum, F., Soreide, A., Kvale, I., Walker, J., & Walaas, I. (1981). Glutamate in cortical fibers. *Advances in Biochemical Psychopharmacology*, *27*, 29–41.

- Forrest, D., Yuzaki, M., Soares, H. D., Ng, L., Luk, D. C., Sheng, M., Stewart, C. L., Morgan, J. I., Connor, J. A., & Curran, T. (1994). Targeted disruption of NMDA receptor 1 gene abolishes NMDA response and results in neonatal death. *Neuron*, *13*(2), 325–338. https://doi.org/10.1016/0896-6273(94)90350-6
- Francés, L., Quintero, J., Fernández, A., Ruiz, A., Caules, J., Fillon, G., Hervás, A., & Soler, C. V. (2022). Current state of knowledge on the prevalence of neurodevelopmental disorders in childhood according to the DSM-5: A systematic review in accordance with the PRISMA criteria. *Child and Adolescent Psychiatry and Mental Health*, *16*(1), Article 1. https://doi.org/10.1186/s13034-022-00462-1
- Freunscht, I., Popp, B., Blank, R., Endele, S., Moog, U., Petri, H., Prott, E.-C., Reis, A., Rübo, J., Zabel, B., Zenker, M., Hebebrand, J., & Wieczorek, D. (2013). Behavioral phenotype in five individuals with de novo mutations within the GRIN2B gene. *Behavioral and Brain Functions*, *9*(1), 20. https://doi.org/10.1186/1744-9081-9-20
- Furukawa, H., Singh, S. K., Mancusso, R., & Gouaux, E. (2005). Subunit arrangement and function in NMDA receptors. *Nature*, *438*(7065), 185–192. https://doi.org/10.1038/nature04089
- Gale, J. R., Kosobucki, G. J., Hartnett-Scott, K. A., & Aizenman, E. (2021). Imprecision in Precision Medicine: Differential Response of a Disease-Linked GluN2A Mutant to NMDA Channel Blockers. *Frontiers in Pharmacology*, *12*, 773455. https://doi.org/10.3389/fphar.2021.773455
- García-Recio, A., Santos-Gómez, A., Juliá-Palacios, N., García-Cazorla, À., Altafaj, X., & Olivella, M. (2021). GRIN database: A unified and manually curated repertoire of GRIN variants. *Human Mutation*, *42*, 8–18.
- Genever, P. G., Maxfield, S. J., Skerry, T. M., Kennovin, G. D., Maltman, J., Bowgen, C. J., & Raxworthy, M. J. (1999). Evidence for a Novel Glutamate-Mediated Signaling Pathway in Keratinocytes. *Journal of Investigative Dermatology*, *112*(3), 337–342. https://doi.org/10.1046/j.1523-1747.1999.00509.x
- Geoffroy, C., Paoletti, P., & Mony, L. (2022). Positive allosteric modulation of NMDA receptors: Mechanisms, physiological impact and therapeutic potential. *The Journal of Physiology*, *600*(2), 233–259. https://doi.org/10.1113/JP280875
- Ghasemi, M., & Schachter, S. C. (2011). The NMDA receptor complex as a therapeutic target in epilepsy: A review. *Epilepsy & Behavior*, *22*(4), 617–640. https://doi.org/10.1016/j.yebeh.2011.07.024
- Gibson, L. L., Pollak, T. A., Blackman, G., Thornton, M., Moran, N., & David, A. S. (2019). The Psychiatric Phenotype of Anti-NMDA Receptor Encephalitis. *The Journal of Neuropsychiatry and Clinical Neurosciences*, *31*(1), 70–79. https://doi.org/10.1176/appi.neuropsych.17120343
- Gill, S. S., & Pulido, O. M. (2001). Review Article: Glutamate Receptors in Peripheral Tissues: Current Knowledge, Future Research, and Implications for Toxicology. *Toxicologic Pathology*, *29*(2), 208–223. https://doi.org/10.1080/019262301317052486

- Gill, S., Veinot, J., Kavanagh, M., & Pulido, O. (2007). Human Heart Glutamate Receptors—Implications for Toxicology, Food Safety, and Drug Discovery. *Toxicologic Pathology*, *35*(3), 411–417. https://doi.org/10.1080/01926230701230361
- Gjerulfsen, C. E., Krey, I., Klöckner, C., Rubboli, G., Lemke, J. R., & Møller, R. S. (2024). Spctrum of NMDA Receptor Variants in Neurodevelopmental Disorders and Epilepsy. In *NMDA Receptors* (Vol. 2799, pp. 1–11).
- Glasauer, S. M. K., & Neuhauss, S. C. F. (2014). Whole-genome duplication in teleost fishes and its evolutionary consequences. *Molecular Genetics and Genomics*, *289*(6), 1045–1060. https://doi.org/10.1007/s00438-014-0889-2
- Goldsmith, J. R., & Jobin, C. (2012). Think Small: Zebrafish as a Model System of Human Pathology. *Journal of Biomedicine and Biotechnology*, *2012*, 1–12. https://doi.org/10.1155/2012/817341
- Goldsmith, P. (2004). Zebrafish as a pharmacological tool: The how, why and when. *Current Opinion in Pharmacology*, *4*(5), 504–512. https://doi.org/10.1016/j.coph.2004.04.005
- Griffin, A., Carpenter, C., Liu, J., Paterno, R., Grone, B., Hamling, K., Moog, M., Dinday, M. T., Figueroa, F., Anvar, M., Ononuju, C., Qu, T., & Baraban, S. C. (2021). Phenotypic analysis of catastrophic childhood epilepsy genes. *Communications Biology*, *4*(1), Article 1. https://doi.org/10.1038/s42003-021-02221-y
- GRIN Therapeutics. (2024). GRIN Therapeutics Announces Positive Topline Data from Honeycomb Trial of Radiprodil in GRIN-Related Neurodevelopmental Disorder. *Https://Curegrin.Org/*.
- Grone, B. P., Qu, T., & Baraban, S. C. (2017). Behavioral Comorbidities and Drug Treatments in a Zebrafish *scn1lab* Model of Dravet Syndrome. *Eneuro*, *4*(4), Article 4. https://doi.org/10.1523/ENEURO.0066-17.2017
- Guo, S. (2009). Using zebrafish to assess the impact of drugs on neural development and function. *Expert Opinion on Drug Discovery*, *4*(7), 715–726. https://doi.org/10.1517/17460440902988464
- Hagen, E. V., Zhang, Y., & Hamilton, T. J. (2023). Innate colour preference in zebrafish (Danio rerio). *MethodsX*, *11*, 102342. https://doi.org/10.1016/j.mex.2023.102342
- Halene, T. B., Ehrlichman, R. S., Liang, Y., Christian, E. P., Jonak, G. J., Gur, T. L., Blendy, J. A., Dow, H. C., Brodkin, E. S., Schneider, F., Gur, R. C., & Siegel, S. J. (2009). Assessment of NMDA receptor NR1 subunit hypofunction in mice as a model for schizophrenia. *Genes, Brain and Behavior*, *8*(7), 661–675. https://doi.org/10.1111/j.1601-183X.2009.00504.x
- Hamdan, F. F., Gauthier, J., Araki, Y., Lin, D.-T., Yoshizawa, Y., Higashi, K., Park, A.-R., Spiegelman, D., Dobrzeniecka, S., Piton, A., Tomitori, H., Daoud, H., Massicotte, C., Henrion, E., Diallo, O., Shekarabi, M., Marineau, C., Shevell, M., Maranda, B., … Michaud, J. L. (2011). Excess of De Novo Deleterious Mutations in Genes Associated with Glutamatergic Systems in Nonsyndromic Intellectual Disability. *The American Journal of Human Genetics*, *88*(3), 306–316. https://doi.org/10.1016/j.ajhg.2011.02.001

- Hanada, T. (2020). Ionotropic Glutamate Receptors in Epilepsy: A Review Focusing on AMPA and NMDA Receptors. *Biomolecules*, *10*(3), 464. https://doi.org/10.3390/biom10030464
- Hansen, K. B., Naur, P., Kurtkaya, N. L., Kristensen, A. S., Gajhede, M., Kastrup, J. S., & Traynelis, S. F. (2009). Modulation of the Dimer Interface at Ionotropic Glutamate-Like Receptor δ2 by d-Serine and Extracellular Calcium. *The Journal of Neuroscience*, *29*(4), 907–917. https://doi.org/10.1523/JNEUROSCI.4081-08.2009
- Hardingham, G. E., & Bading, H. (2010). Synaptic versus extrasynaptic NMDA receptor signalling: Implications for neurodegenerative disorders. *Nature Reviews Neuroscience*, *11*(10), 682–696. https://doi.org/10.1038/nrn2911
- Harvey, S. A., Sealy, I., Kettleborough, R., Fenyes, F., White, R., Stemple, D., & Smith, J. C. (2013). Identification of the zebrafish maternal and paternal transcriptomes. *Development*, *140*(13), 2703–2710. https://doi.org/10.1242/dev.095091
- Hashimoto, M., & Hibi, M. (2012). Development and evolution of cerebellar neural circuits. *Development, Growth & Differentiation*, *54*(3), 373–389. https://doi.org/10.1111/j.1440-169X.2012.01348.x
- Hayashi, T. (2021). Post-translational palmitoylation of ionotropic glutamate receptors in excitatory synaptic functions. *British Journal of Pharmacology*, *178*, 784–797.
- Hibi, M., & Shimizu, T. (2012). Development of the cerebellum and cerebellar neural circuits. *Developmental Neurobiology*, *72*(3), 282–301. https://doi.org/10.1002/dneu.20875
- Higashijima, S., Mandel, G., & Fetcho, J. R. (2004). Distribution of prospective glutamatergic, glycinergic, and GABAergic neurons in embryonic and larval zebrafish. *Journal of Comparative Neurology*, *480*(1), 1–18. https://doi.org/10.1002/cne.20278
- Hogan-Cann, A. D., & Anderson, C. M. (2016). Physiological Roles of Non-Neuronal NMDA Receptors. *Trends in Pharmacological Sciences*, *37*(9), 750–767. https://doi.org/10.1016/j.tips.2016.05.012
- Hollmann, M., & Heinemann, S. (1994). Cloned Glutamate Receptors. *Annual Review of Neuroscience*, *17*, 31–108.
- Horak, M., & Wenthold, R. J. (2009). Different Roles of C-terminal Cassettes in the Trafficking of Full-length NR1 Subunits to the Cell Surface. *Journal of Biological Chemistry*, *284*(15), 9683–9691. https://doi.org/10.1074/jbc.M807050200
- Howard, M. A., & Baraban, S. C. (2017). Catastrophic Epilepsies of Childhood. *Annual Review of Neuroscience*, *40*(1), 149–166. https://doi.org/10.1146/annurev-neuro-072116-031250
- Howe, K., Clark, M. D., Torroja, C. F., Torrance, J., Berthelot, C., Muffato, M., Collins, J. E., Humphray, S., McLaren, K., Matthews, L., McLaren, S., Sealy, I., Caccamo, M., Churcher, C., Scott, C., Barrett, J. C., Koch, R., Rauch, G.-J., White, S., … Stemple, D. L. (2013). The zebrafish reference genome sequence and its relationship to the human genome. *Nature*, *496*(7446), 498–503. https://doi.org/10.1038/nature12111
- Hsu, P. D., Scott, D. A., Weinstein, J. A., Ran, F. A., Konermann, S., Agarwala, V., Li, Y., Fine, E. J., Wu, X., Shalem, O., Cradick, T. J., Marraffini, L. A., Bao, G., & Zhang, F. (2013). DNA

targeting specificity of RNA-guided Cas9 nucleases. *Nature Biotechnology*, *31*(9), 827–832. https://doi.org/10.1038/nbt.2647

- Hu, C., Chen, W., Myers, S. J., Yuan, H., & Traynelis, S. F. (2016). Human GRIN2B variants in neurodevelopmental disorders. *Journal of Pharmacological Sciences*, *132*(2), 115–121. https://doi.org/10.1016/j.jphs.2016.10.002
- Hughes, E. G., Peng, X., Gleichman, A. J., Lai, M., Zhou, L., Tsou, R., Parsons, T. D., Lynch, D. R., Dalmau, J., & Balice-Gordon, R. J. (2010). Cellular and Synaptic Mechanisms of Anti-NMDA Receptor Encephalitis. *The Journal of Neuroscience*, *30*(17), 5866–5875. https://doi.org/10.1523/JNEUROSCI.0167-10.2010
- Husari, K. S., & Dubey, D. (2019). Autoimmune Epilepsy. *Neurotherapeutics*, *16*(3), 685–702. https://doi.org/10.1007/s13311-019-00750-3
- Ingham, P. (1997). Zebrafish genetics and its implications for understanding vertebrate development. *Human Molecular Genetics*, *6*(10), 1755–1760. https://doi.org/10.1093/hmg/6.10.1755
- Ito, I., Futai, K., Katagiri, H., & Watanabe, M. (1997). Synapse-selective impairment of NMDA receptor functions in mice lacking NMDA receptor eI or e2 subunit. *Journal of Physiology*, *500*(2), 401–408.
- Itoh, M., Piot, L., Mony, L., Paoletti, P., & Yuzaki, M. (2024). Lack of evidence for direct ligand-gated ion channel activity of GluD receptors. *Proceedings of the National Academy of Sciences*, *121*(31), e2406655121. https://doi.org/10.1073/pnas.2406655121
- James, D. M., Kozol, R. A., Kajiwara, Y., Wahl, A. L., Storrs, E. C., Buxbaum, J. D., Klein, M., Moshiree, B., & Dallman, J. E. (2019). Intestinal dysmotility in a zebrafish (Danio rerio) shank3a;shank3b mutant model of autism. *Molecular Autism*, *10*(1), 3. https://doi.org/10.1186/s13229-018-0250-4
- Jao, L.-E., Wente, S. R., & Chen, W. (2013). Efficient multiplex biallelic zebrafish genome editing using a CRISPR nuclease system. *Proceedings of the National Academy of Sciences*, *110*(34), Article 34. https://doi.org/10.1073/pnas.1308335110
- Jarque, S., Rubio-Brotons, M., Ibarra, J., Ordoñez, V., Dyballa, S., Miñana, R., & Terriente, J. (2020). Morphometric analysis of developing zebrafish embryos allows predicting teratogenicity modes of action in higher vertebrates. *Reproductive Toxicology*, *96*, 337–348. https://doi.org/10.1016/j.reprotox.2020.08.004
- Jelen, L. A., & Stone, J. M. (2021). Ketamine for depression. *International Review of Psychiatry*, *33*(3), 207–228. https://doi.org/10.1080/09540261.2020.1854194
- Johannesen, K., Marini, C., Pfeffer, S., Møller, R. S., Dorn, T., Niturad, C. E., Gardella, E., Weber, Y., Søndergård, M., Hjalgrim, H., Nikanorova, M., Becker, F., Larsen, L. H. G., Dahl, H. A., Maier, O., Mei, D., Biskup, S., Klein, K. M., Reif, P. S., … Maljevic, S. (2016). Phenotypic spectrum of GABRA1: From generalized epilepsies to severe epileptic encephalopathies. *Neurology*, *87*(11), Article 11. https://doi.org/10.1212/WNL.0000000000003087

- Juliá-Palacios, N., Olivella, M., Sigatullina Bondarenko, M., Ibáñez-Micó, S., Muñoz-Cabello, B., Alonso-Luengo, O., Soto-Insuga, V., García-Navas, D., Cuesta-Herraiz, L., Andreo-Lillo, P., Aguilera-Albesa, S., Hedrera-Fernández, A., González Alguacil, E., Sánchez-Carpintero, R., Martín Del Valle, F., Jiménez González, E., Cean Cabrera, L., Medina-Rivera, I., Perez-Ordoñez, M., … García-Cazorla, Á. (2024). L-serine treatment in patients with *GRIN* -related encephalopathy: A phase 2A, non-randomized study. *Brain*, *147*(5), 1653–1666. https://doi.org/10.1093/brain/awae041
- Kaniakova, M., Krausova, B., Vyklicky, V., Korinek, M., Lichnerova, K., Vyklicky, L., & Horak, M. (2012). Key Amino Acid Residues within the Third Membrane Domains of NR1 and NR2 Subunits Contribute to the Regulation of the Surface Delivery of N-methyl-d-aspartate Receptors. *Journal of Biological Chemistry*, *287*(31), 26423–26434. https://doi.org/10.1074/jbc.M112.339085
- Kannangara, T. S., Bostrom, C. A., Ratzlaff, A., Thompson, L., Cater, R. M., Gil-Mohapel, J., & Christie, B. R. (2014). Deletion of the NMDA Receptor GluN2A Subunit Significantly Decreases Dendritic Growth in Maturing Dentate Granule Neurons. *PLoS ONE*, *9*(8), e103155. https://doi.org/10.1371/journal.pone.0103155
- Kannangara, T. S., Eadie, B. D., Bostrom, C. A., Morch, K., Brocardo, P. S., & Christie, B. R. (2015). GluN2A $^{-/-}$ Mice Lack Bidirectional Synaptic Plasticity in the Dentate Gyrus and Perform Poorly on Spatial Pattern Separation Tasks. *Cerebral Cortex*, *25*(8), 2102–2113. https://doi.org/10.1093/cercor/bhu017
- Karakas, E., Simorowski, N., & Furukawa, H. (2009). Structure of the zinc-bound amino-terminal domain of the NMDA receptor NR2B subunit. *The EMBO Journal*, *28*(24), 3910–3920. https://doi.org/10.1038/emboj.2009.338
- Kartvelishvily, E., Shleper, M., Balan, L., Dumin, E., & Wolosker, H. (2006). Neuron-derived D-Serine Release Provides a Novel Means to Activate N-Methyl-D-aspartate Receptors. *Journal of Biological Chemistry*, *281*(20), 14151–14162. https://doi.org/10.1074/jbc.M512927200
- Kayser, M. S., & Dalmau, J. (2016). Anti-NMDA receptor encephalitis, autoimmunity, and psychosis. *Schizophrenia Research*, *176*(1), 36–40. https://doi.org/10.1016/j.schres.2014.10.007
- Kearse, M., Moir, R., Wilson, A., Stones-Havas, S., Cheung, M., Sturrock, S., Buxton, S., Cooper, A., Markowitz, S., Duran, C., Thierer, T., Ashton, B., Meintjes, P., & Drummond, A. (2012). Geneious Basic: An integrated and extendable desktop software platform for the organization and analysis of sequence data. *Bioinformatics*, *28*(12), 1647–1649. https://doi.org/10.1093/bioinformatics/bts199
- Kellner, S., Abbasi, A., Carmi, I., Heinrich, R., Garin-Shkolnik, T., Hershkovitz, T., Giladi, M., Haitin, Y., Johannesen, K. M., Steensbjerre Møller, R., & Berlin, S. (2021). Two de novo GluN2B mutations affect multiple NMDAR-functions and instigate severe pediatric encephalopathy. *eLife*, *10*, e67555. https://doi.org/10.7554/eLife.67555

- Kennedy, M. B. (2018). The Protein Biochemistry of the Postsynaptic Density in Glutamatergic Synapses Mediates Learning in Neural Networks. *Biochemistry*, *57*(27), 4005–4009. https://doi.org/10.1021/acs.biochem.8b00496
- Kenney, J. W., Scott, I. C., Josselyn, S. A., & Frankland, P. W. (2017). Contextual fear conditioning in zebrafish. *Learning & Memory*, *24*(10), 516–523. https://doi.org/10.1101/lm.045690.117
- Kenny, E. M., Cormican, P., Furlong, S., Heron, E., Kenny, G., Fahey, C., Kelleher, E., Ennis, S., Tropea, D., Anney, R., Corvin, A. P., Donohoe, G., Gallagher, L., Gill, M., & Morris, D. W. (2014). Excess of rare novel loss-of-function variants in synaptic genes in schizophrenia and autism spectrum disorders. *Molecular Psychiatry*, *19*(8), 872–879. https://doi.org/10.1038/mp.2013.127
- Kim, P. M., Aizawa, H., Kim, P. S., Huang, A. S., Wickramasinghe, S. R., Kashani, A. H., Barrow, R. K., Huganir, R. L., Ghosh, A., & Snyder, S. H. (2005). Serine racemase: Activation by glutamate neurotransmission via glutamate receptor interacting protein and mediation of neuronal migration. *Proceedings of the National Academy of Sciences*, *102*(6), 2105–2110. https://doi.org/10.1073/pnas.0409723102
- Kimmel, C. B., Ballard, W. W., Kimmel, S. R., Ullmann, B., & Schilling, T. F. (1995). Stages of embryonic development of the zebrafish. *Developmental Dynamics*, *203*(3), 253–310. https://doi.org/10.1002/aja.1002030302
- Kiyama, Y., Manabe, T., Sakimura, K., Kawakami, F., Mori, H., & Mishina, M. (1998). Increased Thresholds for Long-Term Potentiation and Contextual Learning in Mice Lacking the NMDA-type Glutamate Receptor □1 Subunit. *The Journal of Neuroscience*, *18*(17), 6704–6712.
- Koseki, N., Deguchi, J., Yamashita, A., Miyawaki, I., & Funabashi, H. (2014). Establishment of a novel experimental protocol for drug-induced seizure liability screening based on a locomotor activity assay in zebrafish. *The Journal of Toxicological Sciences*, *39*(4).
- Koshiba-Takeuchi, K. (2018). Whole-Mount and Section In Situ Hybridization in Mouse Embryos for Detecting mRNA Expression and Localization. In *Mouse Embryogenesis* (Vol. 1752, pp. 123–131). Humana Press.
- Kozol, R. A., Abrams, A. J., James, D. M., Buglo, E., Yan, Q., & Dallman, J. E. (2016). Function Over Form: Modeling Groups of Inherited Neurological Conditions in Zebrafish. *Frontiers in Molecular Neuroscience*, *9*. https://doi.org/10.3389/fnmol.2016.00055
- Krebs, H. A. (1935). Metabolism of amino-acids: Deamination of amino-acids. *The Biochemical Journal*, *29*(7), 1620–1644.
- Krey, I., Von Spiczak, S., Johannesen, K. M., Hikel, C., Kurlemann, G., Muhle, H., Beysen, D., Dietel, T., Møller, R. S., Lemke, J. R., & Syrbe, S. (2022). L-Serine Treatment is Associated with Improvements in Behavior, EEG, and Seizure Frequency in Individuals with GRIN-Related Disorders Due to Null Variants. *Neurotherapeutics*, *19*(1), 334–341. https://doi.org/10.1007/s13311-021-01173-9

- Kutsuwada, T., Sakimura, K., Manabe, T., Takayama, C., Katakura, N., Kushiya, E., Natsume, R., Watanabe, M., Inoue, Y., Yagi, T., Aizawa, S., Arakawa, M., Takahashi, T., Nakamura, Y., Mori, H., & Mishina, M. (1996). Impairment of Suckling Response, Trigeminal Neuronal Pattern Formation, and Hippocampal LTD in NMDA Receptor □2 Subunit Mutant Mice. *Neuron*, *16*, 333–344.
- LaCoursiere, C. (2024). Zebrafish models of candidate human epilepsy-associated genes provide evidence of hyperexcitability. *bioRxiv*.
- Lai, Y.-H., Ding, Y.-J., Moses, D., & Chen, Y.-H. (2017). Teratogenic Effects of Topiramate in a Zebrafish Model. *International Journal of Molecular Sciences*, *18*(8), Article 8. https://doi.org/10.3390/ijms18081721
- Lalo, U., Koh, W., Lee, C. J., & Pankratov, Y. (2021). The tripartite glutamatergic synapse. *Neuropharmacology*, *199*, 108758. https://doi.org/10.1016/j.neuropharm.2021.108758
- Laurie, D. J., & Seeburg, P. H. (1994). Regional and Developmental Heterogeneity in Splicing of the Rat Bran NMDAR1 mRNA. *The Journal of Neuroscience*, *14*(5), 3180–3194.
- Lee, D., Xiong, S., & Xiong, W.-C. (2013). General Introdution to In Situ Hybridization Protocol Using Nonradioactively Labeled Probes to Detect mRNAs on Tissue Sections. In *Neural Development* (Vol. 1018, pp. 165–174). Humana Press.
- Lee, E.-J., Choi, S. Y., & Kim, E. (2015). NMDA receptor dysfunction in autism spectrum disorders. *Current Opinion in Pharmacology*, *20*, 8–13. https://doi.org/10.1016/j.coph.2014.10.007
- Lee, K., Mills, Z., Cheung, P., Cheyne, J. E., & Montgomery, J. M. (2022). The Role of Zinc and NMDA Receptors in Autism Spectrum Disorders. *Pharmaceuticals*, *16*(1), 1. https://doi.org/10.3390/ph16010001
- Lemke, J. R. (2020). Predicting incidences of neurodevelopmental disorders. *Brain*, *143*, 1046–1056.
- Lemke, J. R., Hendrickx, R., Geider, K., Laube, B., Schwake, M., Harvey, R. J., James, V. M., Pepler, A., Steiner, I., Hörtnagel, K., Neidhardt, J., Ruf, S., Wolff, M., Bartholdi, D., Caraballo, R., Platzer, K., Suls, A., De Jonghe, P., Biskup, S., & Weckhuysen, S. (2014). *GRIN2B* mutations in west syndrome and intellectual disability with focal epilepsy. *Annals of Neurology*, *75*(1), 147–154. https://doi.org/10.1002/ana.24073
- Lemke, J. R., Lal, D., Reinthaler, E. M., Steiner, I., Nothnagel, M., Alber, M., Geider, K., Laube, B., Schwake, M., Finsterwalder, K., Franke, A., Schilhabel, M., Jähn, J. A., Muhle, H., Boor, R., Van Paesschen, W., Caraballo, R., Fejerman, N., Weckhuysen, S., … Von Spiczak, S. (2013). Mutations in GRIN2A cause idiopathic focal epilepsy with rolandic spikes. *Nature Genetics*, *45*(9), 1067–1072. https://doi.org/10.1038/ng.2728
- Lesca, G., Rudolf, G., Bruneau, N., Lozovaya, N., Labalme, A., Boutry-Kryza, N., Salmi, M., Tsintsadze, T., Addis, L., Motte, J., Wright, S., Tsintsadze, V., Michel, A., Doummar, D., Lascelles, K., Strug, L., Waters, P., De Bellescize, J., Vrielynck, P., … Szepetowski, P. (2013). GRIN2A mutations in acquired epileptic aphasia and related childhood focal epilepsies and

encephalopathies with speech and language dysfunction. *Nature Genetics*, *45*(9), 1061–1066. https://doi.org/10.1038/ng.2726

- Lesca, G., Rudolf, G., Labalme, A., Hirsch, E., Arzimanoglou, A., Genton, P., Motte, J., De Saint Martin, A., Valenti, M.-P., Boulay, C., De Bellescize, J., Kéo-Kosal, P., Boutry-Kryza, N., Edery, P., Sanlaville, D., & Szepetowski, P. (2012). Epileptic encephalopathies of the Landau-Kleffner and continuous spike and waves during slow-wave sleep types: Genomic dissection makes the link with autism. *Epilepsia*, *53*(9), 1526–1538.
- Lewis, K. E., & Eisen, J. S. (2003). From cells to circuits: Development of the zebrafish spinal cord. *Progress in Neurobiology*, *69*(6), 419–449. https://doi.org/10.1016/S0301-0082(03)00052-2
- Li, F., Lin, J., Liu, X., Li, W., Ding, Y., Zhang, Y., Zhou, S., Guo, N., & Li, Q. (2018). Characterization of the locomotor activities of zebrafish larvae under the influence of various neuroactive drugs. *Annals of Translational Medicine*, *6*(10), 173–173. https://doi.org/10.21037/atm.2018.04.25
- Li, J., Zhang, J., Tang, W., Mizu, R. K., Kusumoto, H., XiangWei, W., Xu, Y., Chen, W., Amin, J. B., Hu, C., Kannan, V., Keller, S. R., Wilcox, W. R., Lemke, J. R., Myers, S. J., Swanger, S. A., Wollmuth, L. P., Petrovski, S., Traynelis, S. F., & Yuan, H. (2019). De novo GRIN variants and NMDA receptor M2 channel pore-forming loop are associated with neurological diseases. *Human Mutation*, *40*, 2393–2413.
- Li, Q., Lin, J., Zhang, Y., Liu, X., Chen, X. Q., Xu, M.-Q., He, L., Li, S., & Guo, N. (2015). Differential behavioral responses of zebrafish larvae to yohimbine treatment. *Psychopharmacology*, *232*(1), 197–208. https://doi.org/10.1007/s00213-014-3656-5
- Liang, Y., Ma, Y., Wang, J., Nie, L., Hou, X., Wu, W., Zhang, X., & Tian, Y. (2021). Leptin Contributes to Neuropathic Pain via Extrasynaptic NMDAR-nNOS Activation. *Molecular Neurobiology*, *58*(3), 1185–1195. https://doi.org/10.1007/s12035-020-02180-1
- Lipina, T., Men, X., Blundell, M., Salahpour, A., & Ramsey, A. J. (2022). Abnormal sensory perception masks behavioral performance of Grin1 knockdown mice. *Genes, Brain and Behavior*, *21*(6), e12825. https://doi.org/10.1111/gbb.12825
- Liu, C.-Y., Yang, Y., Ju, W.-N., Wang, X., & Zhang, H.-L. (2018). Emerging Roles of Astrocytes in Neuro-Vascular Unit and the Tripartite Synapse With Emphasis on Reactive Gliosis in the Context of Alzheimer's Disease. *Frontiers in Cellular Neuroscience*, *12*, 193. https://doi.org/10.3389/fncel.2018.00193
- Locubiche, S., Ordóñez, V., Abad, E., Scotto Di Mase, M., Di Donato, V., & De Santis, F. (2024). A Zebrafish-Based Platform for High-Throughput Epilepsy Modeling and Drug Screening in F0. *International Journal of Molecular Sciences*, *25*(5), 2991. https://doi.org/10.3390/ijms25052991
- Lodish, H., Berk, A., Zipursky, S. L., Matsudaira, P., Baltimore, D., & Darnell, J. (2000). Neurotransmitters, Synapses, and Impulse Transmission. In *Molecular Cell Biology* (4th ed.).

- Loganathan, D., Wu, S.-H., & Chen, C.-Y. (2023). Behavioural responses of zebrafish with sound stimuli in microfluidics. *Lab on a Chip*, *23*(1), 106–114. https://doi.org/10.1039/D2LC00758D
- Lomeli, H., Sprengel, R., Laurie, D. J., Köhr, G., Herb, A., Seeburg, P. H., & Wisden, W. (1993). The rat delta-1 and delta-2 subunits extend the excitatory amino acid receptor family. *Federation of European Biochemical Scieties*, *315*(3), 318–322.
- Lu, D., Ma, R., Xie, Q., Xu, Z., Yuan, J., Ren, M., Li, J., Li, Y., & Wang, J. (2021). Application and advantages of zebrafish model in the study of neurovascular unit. *European Journal of Pharmacology*, *910*, 174483. https://doi.org/10.1016/j.ejphar.2021.174483
- Luo, Z.-W. (2019). Establishment of an adult zebrafish model of retinal neurodegeneration induced by NMDA. *International Journal of Ophthalmology*, *12*(8), 1250–1261. https://doi.org/10.18240/ijo.2019.08.04
- MacPhail, R. C., Brooks, J., Hunter, D. L., Padnos, B., Irons, T. D., & Padilla, S. (2009). Locomotion in larval zebrafish: Influence of time of day, lighting and ethanol. *NeuroToxicology*, *30*(1), Article 1. https://doi.org/10.1016/j.neuro.2008.09.011
- MacRae, C. A., & Peterson, R. T. (2015). Zebrafish as tools for drug discovery. *Nature Reviews Drug Discovery*, *14*(10), 721–731. https://doi.org/10.1038/nrd4627
- Maki, B. A., Aman, T. K., Amico-Ruvio, S. A., Kussius, C. L., & Popescu, G. K. (2012). C-terminal Domains of N-Methyl-d-aspartic Acid Receptor Modulate Unitary Channel Conductance and Gating. *Journal of Biological Chemistry*, *287*(43), 36071–36080. https://doi.org/10.1074/jbc.M112.390013
- Mannara, F., Radosevic, M., Planagumà, J., Soto, D., Aguilar, E., García-Serra, A., Maudes, E., Pedreño, M., Paul, S., Doherty, J., Quirk, M., Dai, J., Gasull, X., Lewis, M., & Dalmau, J. (2020). Allosteric modulation of NMDA receptors prevents the antibody effects of patients with anti-NMDAR encephalitis. *Brain*, *143*(9), 2709–2720. https://doi.org/10.1093/brain/awaa195
- Marsden, W. N. (2011). Stressor-induced NMDAR dysfunction as a unifying hypothesis for the aetiology, pathogenesis and comorbidity of clinical depression. *Medical Hypotheses*, *77*(4), 508–528. https://doi.org/10.1016/j.mehy.2011.06.021
- Martin, S. C., Heinrich, G., & Sandell, J. H. (1998). Sequence and expression of glutamic acid decarboxylase isoforms in the developing zebrafish. *Journal of Comparative Neurology*, *396*(2), 253–266. https://doi.org/10.1002/(SICI)1096-9861(19980629)396:2<253::AID-CNE9>3.0.CO;2-#
- Marvin, J. S., Borghuis, B. G., Tian, L., Cichon, J., Harnett, M. T., Akerboom, J., Gordus, A., Renninger, S. L., Chen, T.-W., Bargmann, C. I., Orger, M. B., Schreiter, E. R., Demb, J. B., Gan, W.-B., Hires, S. A., & Looger, L. L. (2013). An optimized fluorescent probe for visualizing glutamate neurotransmission. *Nature Methods*, *10*(2), 162–170. https://doi.org/10.1038/nmeth.2333
- Massey, P. V., Johnson, B. E., Moult, P. R., Auberson, Y. P., Brown, M. W., Molnar, E., Collingridge, G. L., & Bashir, Z. I. (2004). Differential Roles of NR2A and NR2B-Containing

NMDA Receptors in Cortical Long-Term Potentiation and Long-Term Depression. *The Journal of Neuroscience*, *24*(36), 7821–7828. https://doi.org/10.1523/JNEUROSCI.1697-04.2004

- Mattson, M. P. (2008). Glutamate and Neurotrophic Factors in Neuronal Plasticity and Disease. *Annals of the New York Academy of Sciences*, *1144*(1), 97–112. https://doi.org/10.1196/annals.1418.005
- Maudes, E., Jamet, Z., Marmolejo, L., Dalmau, J. O., & Groc, L. (2024). Positive Allosteric Modulation of NMDARs Prevents the Altered Surface Dynamics Caused by Patients' Antibodies. *Neurology Neuroimmunology & Neuroinflammation*, *11*(4), e200261. https://doi.org/10.1212/NXI.0000000000200261
- McDiarmid, T. A., Yu, A. J., & Rankin, C. H. (2019). Habituation Is More Than Learning to Ignore: Multiple Mechanisms Serve to Facilitate Shifts in Behavioral Strategy. *BioEssays*, *41*(9), 1900077. https://doi.org/10.1002/bies.201900077
- McKenna, M. C. (2007). The Glutamate-Glutamine Cycle Is Not Stoichiometric: Fates of Glutamate in Brain. *Journal of Neuroscience Research*, *85*, 3347–3358.
- McLean, D. L., & Fetcho, J. R. (2008). Using imaging and genetics in zebrafish to study developing spinal circuits *in vivo*. *Developmental Neurobiology*, *68*(6), 817–834. https://doi.org/10.1002/dneu.20617
- Mielnik, C. A., Binko, M. A., Chen, Y., Funk, A. J., Johansson, E. M., Intson, K., Sivananthan, N., Islam, R., Milenkovic, M., Horsfall, W., Ross, R. A., Groc, L., Salahpour, A., McCullumsmith, R. E., Tripathy, S., Lambe, E. K., & Ramsey, A. J. (2021). Consequences of NMDA receptor deficiency can be rescued in the adult brain. *Molecular Psychiatry*, *26*(7), 2929–2942. https://doi.org/10.1038/s41380-020-00859-4
- Miyamoto, Y., Yamada, K., Noda, Y., Mori, H., Mishina, M., & Nabeshima, T. (2001). Hyperfunction of Dopaminergic and Serotonergic Neuronal Systems in Mice Lacking the NMDA Receptor □1 Subunit. *The Journal of Neuroscience*, *21*(2), 750–757.
- Mohn, A. R., Gainetdinov, R. R., Caron, M. G., & Koller, B. H. (1999). Mice with Reduced NMDA Receptor Expression Display Behaviors Related to Schizophrenia. *Cell*, *98*(4), 427–436. https://doi.org/10.1016/S0092-8674(00)81972-8
- Mony, L., Kew, J. N. C., Gunthorpe, M. J., & Paoletti, P. (2009). Allosteric modulators of NR2B-containing NMDA receptors: Molecular mechanisms and therapeutic potential. *British Journal of Pharmacology*, *157*, 1301–1317.
- Mony, L., Zhu, S., Carvalho, S., & Paoletti, P. (2011). Molecular basis of positive allosteric modulation of GluN2B NMDA receptors by polyamines. *The EMBO Journal*, *30*(15), 3134–3146. https://doi.org/10.1038/emboj.2011.203
- Moog, M., & Baraban, S. C. (2022). Clemizole and trazodone are effective antiseizure treatments in a zebrafish model of STXBP1 disorder. *Epilepsia Open*, *7*(3), Article 3. https://doi.org/10.1002/epi4.12604

- Moy, S. S., Perez, A., Koller, B. H., & Duncan, G. E. (2006). Amphetamine-induced disruption of prepulse inhibition in mice with reduced NMDA receptor function. *Brain Research*, *1089*(1), 186–194. https://doi.org/10.1016/j.brainres.2006.03.073
- Myers, R. A., Casals, F., Gauthier, J., Hamdan, F. F., Keebler, J., Boyko, A. R., Bustamante, C. D., Piton, A. M., Spiegelman, D., Henrion, E., Zilversmit, M., Hussin, J., Quinlan, J., Yang, Y., Lafrenière, R. G., Griffing, A. R., Stone, E. A., Rouleau, G. A., & Awadalla, P. (2011). A Population Genetic Approach to Mapping Neurological Disorder Genes Using Deep Resequencing. *PLoS Genetics*, *7*(2), e1001318. https://doi.org/10.1371/journal.pgen.1001318
- Myers, S. J., Yuan, H., Kang, J.-Q., Tan, F. C. K., Traynelis, S. F., & Low, C.-M. (2019). Distinct roles of GRIN2A and GRIN2B variants in neurological conditions. *F1000Research*, *8*, 1940. https://doi.org/10.12688/f1000research.18949.1
- Myers, S. J., Yuan, H., Perszyk, R. E., Zhang, J., Kim, S., Nocilla, K. A., Allen, J. P., Bain, J. M., Lemke, J. R., Lal, D., Benke, T. A., & Traynelis, S. F. (2023). Classification of missense variants in the *N* -methyl- D -aspartate receptor *GRIN* gene family as gain- or loss-of-function. *Human Molecular Genetics*, *32*(19), 2857–2871. https://doi.org/10.1093/hmg/ddad104
- Nicoletti, F., Bockaert, J., Collingridge, G. L., Conn, P. J., Ferraguti, F., Schoepp, D. D., Wroblewski, J. T., & Pin, J. P. (2011). Metabotropic glutamate receptors: From the workbench to the bedside. *Neuropharmacology*, *60*(7–8), 1017–1041. https://doi.org/10.1016/j.neuropharm.2010.10.022
- Nishida, H., & Okabe, S. (2007). Direct Astrocytic Contacts Regulate Local Maturation of Dendritic Spines. *The Journal of Neuroscience*, *27*(2), 331–340. https://doi.org/10.1523/JNEUROSCI.4466-06.2007
- Noriega-Prieto, J. A., & Araque, A. (2021). Sensing and Regulating Synaptic Activity by Astrocytes at Tripartite Synapse. *Neurochemical Research*, *46*(10), 2580–2585. https://doi.org/10.1007/s11064-021-03317-x
- Nozaki, C., Markert, A., & Zimmer, A. (2015). Inhibition of FAAH reduces nitroglycerin-induced migraine-like pain and trigeminal neuronal hyperactivity in mice. *European Neuropsychopharmacology*, *25*(8), 1388–1396. https://doi.org/10.1016/j.euroneuro.2015.04.001
- Nutt, J. G., Gunzler, S. A., Kirchhoff, T., Hogarth, P., Weaver, J. L., Krams, M., Jamerson, B., Menniti, F. S., & Landen, J. W. (2008). Effects of a NR2B Selective NMDA Glutamate Antagonist CP-101,606, on Dyskinesia and Parkinsonism. *Movement Disorders*, *23*(13), 1860–1866.
- O'Roak, B. J., Vives, L., Girirajan, S., Karakoc, E., Krumm, N., Coe, B. P., Levy, R., Ko, A., Lee, C., Smith, J. D., Turner, E. H., Stanaway, I. B., Vernot, B., Malig, M., Baker, C., Reilly, B., Akey, J. M., Borenstein, E., Rieder, M. J., … Eichler, E. E. (2012). Sporadic autism exomes reveal a highly interconnected protein network of de novo mutations. *Nature*, *485*(7397), 246–250. https://doi.org/10.1038/nature10989

- Padilla, S., Hunter, D. L., Padnos, B., Frady, S., & MacPhail, R. C. (2011). Assessing locomotor activity in larval zebrafish: Influence of extrinsic and intrinsic variables. *Neurotoxicology and Teratology*, *33*(6), Article 6. https://doi.org/10.1016/j.ntt.2011.08.005
- Paoletti, P. (2011). Molecular basis of NMDA receptor functional diversity: NMDA receptor functional diversity. *European Journal of Neuroscience*, *33*(8), 1351–1365. https://doi.org/10.1111/j.1460-9568.2011.07628.x
- Paoletti, P., Bellone, C., & Zhou, Q. (2013). NMDA receptor subunit diversity: Impact on receptor properties, synaptic plasticity and disease. *Nature Reviews Neuroscience*, *14*(6), 383–400. https://doi.org/10.1038/nrn3504
- Parenti, I., Rabaneda, L. G., Schoen, H., & Novarino, G. (2020). Neurodevelopmental Disorders: From Genetics to Functional Pathways. *Trends in Neurosciences*, *43*(8), Article 8. https://doi.org/10.1016/j.tins.2020.05.004
- Parng, C., Seng, W. L., Semino, C., & McGrath, P. (2002). Zebrafish: A Preclinical Model for Drug Screening. *ASSAY and Drug Development Technologies*, *1*(1), 41–48. https://doi.org/10.1089/154065802761001293
- Peng, X., Lin, J., Zhu, Y., Liu, X., Zhang, Y., Ji, Y., Yang, X., Zhang, Y., Guo, N., & Li, Q. (2016). Anxiety-related behavioral responses of pentylenetetrazole-treated zebrafish larvae to light-dark transitions. *Pharmacology Biochemistry and Behavior*, *145*, 55–65. https://doi.org/10.1016/j.pbb.2016.03.010
- Perea, G., Navarrete, M., & Araque, A. (2009). Tripartite synapses: Astrocytes process and control synaptic information. *Trends in Neurosciences*, *32*(8), 421–431. https://doi.org/10.1016/j.tins.2009.05.001
- Petroff, O. A. C. (2002). Book Review: GABA and Glutamate in the Human Brain. *The Neuroscientist*, *8*(6), 562–573. https://doi.org/10.1177/1073858402238515
- Pierson, T. M., Yuan, H., Marsh, E. D., Fuentes-Fajardo, K., Adams, D. R., Markello, T., Golas, G., Simenov, D. R., Holloman, C., Tankovic, A., Karamchandani, M. M., Schreiber, J. M., Mullikin, J. C., Tifft, C. J., Toro, C., Boerkoel, C. F., Traynelis, S. F., & Gahl, W. A. (2014). GRIN2A mutation and early-onset epileptic encephalopathy: Personalized therapy with memantine. *Annals of Clinical and Translational Neurology*, *1*(3), 190–198.
- Pin, J.-P., & Duvoisin, R. (1995). The metabotropic glutamate receptors: Structure and functions. *Neuropharmacology*, *34*(1), 1–26. https://doi.org/10.1016/0028-3908(94)00129-G
- Pinheiro, P. S., & Mulle, C. (2008). Presynaptic glutamate receptors: Physiological functions and mechanisms of action. *Nature Reviews Neuroscience*, *9*(6), 423–436. https://doi.org/10.1038/nrn2379
- Planagumà, J., Haselmann, H., Mannara, F., Petit-Pedrol, M., Grünewald, B., Aguilar, E., Röpke, L., Martín-García, E., Titulaer, M. J., Jercog, P., Graus, F., Maldonado, R., Geis, C., & Dalmau, J. (2016). Ephrin-B2 prevents N-methyl-D-aspartate receptor antibody effects on memory and neuroplasticity. *Annals of Neurology*, *80*, 388–400.

- Platzer, K., & Lemke, J. R. (2018). GRIN2B-Related Neurodevelopmental Disorder. *GeneReviews*.
- Platzer, K., Yuan, H., Schütz, H., Winschel, A., Chen, W., Hu, C., Kusumoto, H., Heyne, H. O., Helbig, K. L., Tang, S., Willing, M. C., Tinkle, B. T., Adams, D. J., Depienne, C., Keren, B., Mignot, C., Frengen, E., Strømme, P., Biskup, S., … Lemke, J. R. (2017). *GRIN2B* encephalopathy: Novel findings on phenotype, variant clustering, functional consequences and treatment aspects. *Journal of Medical Genetics*, *54*(7), 460–470. https://doi.org/10.1136/jmedgenet-2016-104509
- Radosevic, M., Planagumà, J., Mannara, F., Mellado, A., Aguilar, E., Sabater, L., Landa, J., García-Serra, A., Maudes, E., Gasull, X., Lewis, M., & Dalmau, J. (2022). Allosteric Modulation of NMDARs Reverses Patients' Autoantibody Effects in Mice. *Neurology Neuroimmunology & Neuroinflammation*, *9*(1), e1122. https://doi.org/10.1212/NXI.0000000000001122
- Rajesh, V., Deepan, N., Anitha, V., Kalaiselvan, D., Jayaseelan, S., Sivakumar, P., & Ganesan, V. (2020). Heart malformation is an early response to valproic acid in developing zebrafish. *Naunyn-Schmiedeberg's Archives of Pharmacology*, *393*(12), Article 12. https://doi.org/10.1007/s00210-020-01949-4
- Ramsey, A. J., Milenkovic, M., Oliveira, A. F., Escobedo-Lozoya, Y., Seshadri, S., Salahpour, A., Sawa, A., Yasuda, R., & Caron, M. G. (2011). Impaired NMDA receptor transmission alters striatal synapses and DISC1 protein in an age-dependent manner. *Proceedings of the National Academy of Sciences*, *108*(14), 5795–5800. https://doi.org/10.1073/pnas.1012621108
- Rebola, N., Srikumar, B. N., & Mulle, C. (2010). Activity-dependent synaptic plasticity of NMDA receptors. *The Journal of Physiology*, *588*(1), 93–99. https://doi.org/10.1113/jphysiol.2009.179382
- Reemst, K., Shahin, H., & Shahar, O. D. (2023). Learning and memory formation in zebrafish: Protein dynamics and molecular tools. *Frontiers in Cell and Developmental Biology*, *11*, 1120984. https://doi.org/10.3389/fcell.2023.1120984
- Rennekamp, A. J. (2018). Modulation of Threat Response in Larval Zebrafish. In *Phenotypic Screening* (Vol. 1787, pp. 147–159).
- Reutlinger, C., Helbig, I., Gawelczyk, B., Subero, J. I. M., Tönnies, H., Muhle, H., Finsterwalder, K., Vermeer, S., Pfundt, R., Sperner, J., Stefanova, I., Gillessen-Kaesbach, G., Von Spiczak, S., Van Baalen, A., Boor, R., Siebert, R., Stephani, U., & Caliebe, A. (2010). Deletions in 16p13 including *GRIN2A* in patients with intellectual disability, various dysmorphic features, and seizure disorders of the rolandic region. *Epilepsia*, *51*(9), 1870–1873. https://doi.org/10.1111/j.1528-1167.2010.02555.x
- Rieger, S., Wang, F., & Sagasti, A. (2011). Time-Lapse Imaging of Neural Development: Zebrafish Lead the Way Into the Fourth Dimension. *Genesis*, *49*, 534–545.
- Roberts, E. (1981). Strategies for identifying sources and sites of formation of GABA-precursor or transmitter glutamate in brain. *Advances in Biochemical Psychopharmacology*, *27*, 91–102.

- Rossi, D. (2015). Astrocyte physiopathology: At the crossroads of intercellular networking, inflammation and cell death. *Progress in Neurobiology*, *130*, 86–120. https://doi.org/10.1016/j.pneurobio.2015.04.003
- Rung, J. P., Carlsson, A., Rydén Markinhuhta, K., & Carlsson, M. L. (2005). (+)-MK-801 induced social withdrawal in rats; a model for negative symptoms of schizophrenia. *Progress in Neuro-Psychopharmacology and Biological Psychiatry*, *29*(5), 827–832. https://doi.org/10.1016/j.pnpbp.2005.03.004
- Sadikot, A. F., Burhan, A. M., Bélanger, M.-C., & Sasseville, R. (1998). NMDA receptor antagonists influence early development of GABAergic interneurons in the mammalian striatum. *Developmental Brain Research*, *105*(1), 35–42. https://doi.org/10.1016/S0165-3806(97)00148-X
- Saint-Amant, L. (2010). Development of motor rhythms in zebrafish embryos. In *Progress in Brain Research* (Vol. 187, pp. 47–61). Elsevier. https://doi.org/10.1016/B978-0-444-53613-6.00004-6
- Salmi, M., Del Gallo, F., Minlebaev, M., Zakharov, A., Pauly, V., Perron, P., Pons-Bennaceur, A., Corby-Pellegrino, S., Aniksztejn, L., Lenck-Santini, P.-P., Epsztein, J., Khazipov, R., Burnashev, N., Bertini, G., & Szepetowski, P. (2019). Impaired vocal communication, sleep-related discharges, and transient alteration of slow-wave sleep in developing mice lacking the GluN2A subunit of N-methyl-D-aspartate receptors. *Epilepsia*, *60*, 1424–1437. https://doi.org/DOI: 10.1111/epi.16060
- Samanta, D. (2020). PCDH19-Related Epilepsy Syndrome: A Comprehensive Clinical Review. *Pediatric Neurology*, *105*, 3–9. https://doi.org/10.1016/j.pediatrneurol.2019.10.009
- Santello, M., Calì, C., & Bezzi, P. (2012). Gliotransmission and the Tripartite Synapse. In *Synaptic Plasticity* (Vol. 970, pp. 307–331).
- Santos-Gómez, A., Miguez-Cabello, F., García-Recio, A., Locubiche-Serra, S., García-Díaz, R., Soto-Insuga, V., Guerrero-López, R., Juliá-Palacios, N., Ciruela, F., García-Cazorla, À., Soto, D., Olivella, M., & Altafaj, X. (2021). Disease-associated GRIN protein truncating variants trigger NMDA receptor loss-of-function. *Human Molecular Genetics*, *29*(24), 3859–3871. https://doi.org/10.1093/hmg/ddaa220
- Santos-Gómez, A., Miguez-Cabello, F., Juliá-Palacios, N., García-Navas, D., Soto-Insuga, V., García-Peñas, J. J., Fuentes, P., Ibáñez-Micó, S., Cuesta, L., Cancho, R., Andreo-Lillo, P., Gutiérrez-Aguilar, G., Alonso-Luengo, O., Málaga, I., Hedrera-Fernández, A., García-Cazorla, À., Soto, D., Olivella, M., & Altafaj, X. (2021). Paradigmatic De Novo GRIN1 Variants Recapitulate Pathophysiological Mechanisms Underlying GRIN1-Related Disorder Clinical Spectrum. *International Journal of Molecular Sciences*, *22*(23), 12656. https://doi.org/10.3390/ijms222312656
- Sanz-Clemente, A., Nicoll, R. A., & Roche, K. W. (2013). Diversity in NMDA Receptor Composition: Many Regulators, Many Consequences. *The Neuroscientist*, *19*(1), 62–75. https://doi.org/10.1177/1073858411435129

- Schell, M. J., Molliver, M. E., & Snyder, S. H. (1995). D-serine, an endogenous synaptic modulator: Localization to astrocytes and glutamate-stimulated release. *Proceedings of the National Academy of Sciences*, *92*(9), 3948–3952. https://doi.org/10.1073/pnas.92.9.3948
- Schindelin, J., Arganda-Carreras, I., Frise, E., Kaynig, V., Longair, M., Pietzsch, T., Preibisch, S., Rueden, C., Saalfeld, S., Schmid, B., Tinevez, J.-Y., White, D. J., Hartenstein, V., Eliceiri, K., Tomancak, P., & Cardona, A. (2012). Fiji: An open-source platform for biological-image analysis. *Nature Methods*, *9*(7), 676–682. https://doi.org/10.1038/nmeth.2019
- Schmid, S. M., & Hollmann, M. (2008). To Gate or not to Gate: Are the Delta Subunits in the Glutamate Receptor Family Functional Ion Channels? *Molecular Neurobiology*, *37*(2–3), 126–141. https://doi.org/10.1007/s12035-008-8025-0
- Schmidt, R., Strähle, U., & Scholpp, S. (2013). Neurogenesis in zebrafish – from embryo to adult. *Neural Development*, *8*(1), 3. https://doi.org/10.1186/1749-8104-8-3
- Schneider, C. A., Rasband, W. S., & Eliceiri, K. W. (2012). NIH Image to ImageJ: 25 years of image analysis. *Nature Methods*, *9*(7), 671–675. https://doi.org/10.1038/nmeth.2089
- Schweitzer, J., & Driever, W. (2009). Development of the Dopamine Systems in Zebrafish. In R. J. Pasterkamp, M. P. Smidt, & J. P. H. Burbach (Eds.), *Development and Engineering of Dopamine Neurons* (Vol. 651, pp. 1–14). Springer New York. https://doi.org/10.1007/978-1-4419-0322-8_1
- Sheng, M., & Kim, E. (2011). The Postsynaptic Organization of Synapses. *Cold Spring Harbor Perspectives in Biology*, *3*(12), a005678–a005678. https://doi.org/10.1101/cshperspect.a005678
- Shin, W., Kim, K., Serraz, B., Cho, Y. S., Kim, D., Kang, M., Lee, E.-J., Lee, H., Bae, Y. C., Paoletti, P., & Kim, E. (2020). Early correction of synaptic long-term depression improves abnormal anxiety-like behavior in adult GluN2B-C456Y-mutant mice. *PLOS Biology*, *18*(4), e3000717. https://doi.org/10.1371/journal.pbio.3000717
- Simon, P., Dupuis, R., & Costentin, J. (1994). Thigmotaxis as an index of anxiety in mice. Influence of dopaminergic transmissions. *Behavioural Brain Research*, *61*(1), 59–64. https://doi.org/10.1016/0166-4328(94)90008-6
- Soto, D., Olivella, M., Grau, C., Armstrong, J., Alcon, C., Gasull, X., Santos-Gómez, A., Locubiche, S., Gómez De Salazar, M., García-Díaz, R., Gratacòs-Batlle, E., Ramos-Vicente, D., Chu-Van, E., Colsch, B., Fernández-Dueñas, V., Ciruela, F., Bayés, À., Sindreu, C., López-Sala, A., … Altafaj, X. (2019). L -Serine dietary supplementation is associated with clinical improvement of loss-of-function *GRIN2B* -related pediatric encephalopathy. *Science Signaling*, *12*(586), eaaw0936. https://doi.org/10.1126/scisignal.aaw0936
- Strehlow, V., Myers, K. A., Morgan, A. T., Hons, A., Scheffer, I. E., & Lemke, J. R. (2016). GRIN2A-Related Disorders. *GeneReviews*.
- Sullivan, M. T., Tidball, P., Yan, Y., Intson, K., Chen, W., Xu, Y., Venkatesan, S., Horsfall, W., Georgiou, J., Finnie, P. S. B., Lambe, E. K., Traynelis, S. F., Salahpour, A., Yuan, H., Collingridge, G. L., & Ramsey, A. J. (2024). Grin1 $^{Y\ 647\ S/+}$ *Mice: A Preclinical Model of* GRIN1 *-Related Neurodevelopmental Disorder*. https://doi.org/10.1101/2024.08.21.608984

- Sun, X.-Y., Tuo, Q.-Z., Liuyang, Z.-Y., Xie, A.-J., Feng, X.-L., Yan, X., Qiu, M., Li, S., Wang, X.-L., Cao, F.-Y., Wang, X.-C., Wang, J.-Z., & Liu, R. (2016). Extrasynaptic NMDA receptor-induced tau overexpression mediates neuronal death through suppressing survival signaling ERK phosphorylation. *Cell Death & Disease*, *7*(11), e2449–e2449. https://doi.org/10.1038/cddis.2016.329
- Swain, H. A., Sigstad, C., & Scalzo, F. M. (2004). Effects of dizocilpine (MK-801) on circling behavior, swimming activity, and place preference in zebrafish (Danio rerio). *Neurotoxicology and Teratology*, *26*(6), 725–729. https://doi.org/10.1016/j.ntt.2004.06.009
- Takahashi, H., Yokoi, N., & Seino, S. (2019). Glutamate as intracellular and extracellular signals in pancreatic islet functions. *Proceedings of the Japan Academy, Series B*, *95*(6), 246–260. https://doi.org/10.2183/pjab.95.017
- Tarabeux, J., Kebir, O., Gauthier, J., Hamdan, F. F., Xiong, L., Piton, A., Spiegelman, D., Henrion, É., Millet, B., S2D team, Fathalli, F., Joober, R., Rapoport, J. L., DeLisi, L. E., Fombonne, É., Mottron, L., Forget-Dubois, N., Boivin, M., Michaud, J. L., … Krebs, M.-O. (2011). Rare mutations in N-methyl-D-aspartate glutamate receptors in autism spectrum disorders and schizophrenia. *Translational Psychiatry*, *1*(11), e55–e55. https://doi.org/10.1038/tp.2011.52
- Thapaliya, E. R., Mony, L., Sanchez, R., Serraz, B., Paoletti, P., & Ellis-Davies, G. C. R. (2021). Photochemical Control of Drug Efficacy: A Comparison of Uncaging and Photoswitching Ifenprodil on NMDA Receptors. *ChemPhotoChem*, *5*(5), 445–454. https://doi.org/10.1002/cptc.202000240
- Thijs, R. D., Surges, R., O'Brien, T. J., & Sander, J. W. (2019). Epilepsy in adults. *The Lancet*, *393*(10172), Article 10172. https://doi.org/10.1016/S0140-6736(18)32596-0
- Thisse, B., & Thisse, C. (2004). Fast Release Clones: A High Throughput Expression Analysis. *ZFIN Direct Data Submission*.
- Tiedeken, J. A., & Ramsdell, J. S. (2007). Embryonic Exposure to Domoic Acid Increases the Susceptibility of Zebrafish Larvae to the Chemical Convulsant Pentylenetetrazole. *Environmental Health Perspectives*, *115*(11), Article 11. https://doi.org/10.1289/ehp.10344
- Tomé, D. (2018). The Roles of Dietary Glutamate in the Intestine. *Annals of Nutrition and Metabolism*, *73*(Suppl. 5), 15–20. https://doi.org/10.1159/000494777
- Traynelis, S. F., Wollmuth, L. P., McBain, C. J., Menniti, F. S., Vance, K. M., Ogden, K. K., Hansen, K. B., Yuan, H., Myers, S. J., & Dingledine, R. (2010). Glutamate Receptor Ion Channels: Structure, Regulation, and Function. *Pharmacological Reviews*, *62*(3), 405–496. https://doi.org/10.1124/pr.109.002451
- Turrini, L., Sorelli, M., De Vito, G., Credi, C., Tiso, N., Vanzi, F., & Pavone, F. S. (2022). Multimodal Characterization of Seizures in Zebrafish Larvae. *Biomedicines*, *10*(5), 951. https://doi.org/10.3390/biomedicines10050951
- Umemori, J., Takao, K., Koshimizu, H., Hattori, S., Furuse, T., Wakana, S., & Miyakawa, T. (2013). ENU-mutagenesis mice with a non-synonymous mutation in Grin1 exhibit abnormal

anxiety-like behaviors, impaired fear memory, and decreased acoustic startle response. *BMC Research Notes*, *6*(1), 203. https://doi.org/10.1186/1756-0500-6-203

- Von Engelhardt, J., Doganci, B., Jensen, V., Hvalby, Ø., Göngrich, C., Taylor, A., Barkus, C., Sanderson, D. J., Rawlins, J. N. P., Seeburg, P. H., Bannerman, D. M., & Monyer, H. (2008). Contribution of Hippocampal and Extra-Hippocampal NR2B-Containing NMDA Receptors to Performance on Spatial Learning Tasks. *Neuron*, *60*(5), 846–860. https://doi.org/10.1016/j.neuron.2008.09.039
- Vorhees, C. V., Williams, M. T., Hawkey, A. B., & Levin, E. D. (2021). Translating Neurobehavioral Toxicity Across Species From Zebrafish to Rats to Humans: Implications for Risk Assessment. *Frontiers in Toxicology*, *3*, 629229. https://doi.org/10.3389/ftox.2021.629229
- Wang, G., Qi, W., Liu, Q.-H., & Guan, W. (2024). GluN2A: A promising target for developing novel antidepressants. *International Journal of Neuropsychopharmacology*, pyae037. https://doi.org/10.1093/ijnp/pyae037
- Warming, H., Pegasiou, C.-M., Pitera, A. P., Kariis, H., Houghton, S. D., Kurbatskaya, K., Ahmed, A., Grundy, P., Vajramani, G., Bulters, D., Altafaj, X., Deinhardt, K., & Vargas-Caballero, M. (2019). A primate-specific short GluN2A-NMDA receptor isoform is expressed in the human brain. *Molecular Brain*, *12*(1), 64. https://doi.org/10.1186/s13041-019-0485-9
- Westerfield, M. (2000). *The Zebrafish Book. A Guide for the Laboratory Use of Zebrafish (Danio rerio).* (4th ed.).
- Wolf, J. B., & Wade, M. J. (2016). Evolutionary genetics of maternal effects: EVOLUTIONARY GENETICS OF MATERNAL EFFECTS. *Evolution*, *70*(4), 827–839. https://doi.org/10.1111/evo.12905
- Wu, L.-J., & Zhuo, M. (2009). Targeting the NMDA Receptor Subunit NR2B for the Treatment of Neuropathic Pain. *Neurotherapeutics*, *6*(4), 693–702. https://doi.org/10.1016/j.nurt.2009.07.008
- XiangWei, W., Jiang, Y., & Yuan, H. (2018). De novo mutations and rare variants occurring in NMDA receptors. *Current Opinion in Physiology*, *2*, 27–35. https://doi.org/10.1016/j.cophys.2017.12.013
- Xu, Y., Song, R., Perszyk, R. E., Chen, W., Kim, S., Park, K. L., Allen, J. P., Nocilla, K. A., Zhang, J., XiangWei, W., Tankovic, A., McDaniels, E. D., Sheikh, R., Mizu, R. K., Karamchandani, M. M., Hu, C., Kusumoto, H., Pecha, J., Cappuccio, G., … Traynelis, S. F. (2024). De novo GRIN variants in M3 helix associated with neurological disorders control channel gating of NMDA receptor. *Cellular and Molecular Life Sciences*, *81*(1), 153. https://doi.org/10.1007/s00018-023-05069-z
- Yang, X., Lin, J., Peng, X., Zhang, Q., Zhang, Y., Guo, N., Zhou, S., & Li, Q. (2017). Effects of picrotoxin on zebrafish larvae behaviors: A comparison study with PTZ. *Epilepsy & Behavior*, *70*, 224–231. https://doi.org/10.1016/j.yebeh.2017.03.023

- Yano, S., Tokumitsu, H., & Soderling, T. R. (1998). Calcium promotes cell survival through CaM-K kinase activation of the protein-kinase-B pathway. *Nature*, *396*(6711), 584–587. https://doi.org/10.1038/25147
- Yi-Wen, W., Yao-Yao, Z., Zheng-Yuan, W., Er-Deng, C., Yan-Qi, C., Wen, S., & Su-Ming, Z. (2021). *GluN2B-BDNF pathway in the cerebrospinal fluid-contacting nucleus mediates nerve injury-induced neuropathic pain in rats*.
- Yong, X. L. H., Zhang, L., Yang, L., Chen, X., Tan, J. Z. A., Yu, X., Chandra, M., Livingstone, E., Widagdo, J., Vieira, M. M., Roche, K. W., Lynch, J. W., Keramidas, A., Collins, B. M., & Anggono, V. (2021). Regulation of NMDA receptor trafficking and gating by activity-dependent CaMKIIα phosphorylation of the GluN2A subunit. *Cell Reports*, *36*(1), 109338. https://doi.org/10.1016/j.celrep.2021.109338
- Zada, D., Schulze, L., Yu, J.-H., Tarabishi, P., Napoli, J. L., Milan, J., & Lovett-Barron, M. (2024). Development of neural circuits for social motion perception in schooling fish. *Current Biology*, *34*(15), 3380-3391.e5. https://doi.org/10.1016/j.cub.2024.06.049
- Zeron, M. M., Hansson, O., Chen, N., Wellington, C. L., Leavitt, B. R., Brundin, P., Hayden, M. R., & Raymond, L. A. (2002). Increased Sensitivity to N-Methyl-D-Aspartate Receptor-Mediated Excitotoxicity in a Mouse Model of Huntington's Disease. *Neuron*, *33*(6), 849–860. https://doi.org/10.1016/S0896-6273(02)00615-3
- Zhang, Y., Kecskés, A., Copmans, D., Langlois, M., Crawford, A. D., Ceulemans, B., Lagae, L., De Witte, P. A. M., & Esguerra, C. V. (2015). Pharmacological Characterization of an Antisense Knockdown Zebrafish Model of Dravet Syndrome: Inhibition of Epileptic Seizures by the Serotonin Agonist Fenfluramine. *PLOS ONE*, *10*(5), Article 5. https://doi.org/10.1371/journal.pone.0125898
- Zhao, T., Zhong, R., Zhang, X., Li, G., Zhou, C., Fang, S., Ding, Y., & Lin, W. (2023). Efavirenz restored NMDA receptor dysfunction and inhibited epileptic seizures in GluN2A/Grin2a mutant mice. *Frontiers in Neuroscience*, *17*, 1086462. https://doi.org/10.3389/fnins.2023.1086462
- Zhou, Y., & Danbolt, N. C. (2014). Glutamate as a neurotransmitter in the healthy brain. *Journal of Neural Transmission*, *121*(8), 799–817. https://doi.org/10.1007/s00702-014-1180-8
- Zon, L. I. (1999). Zebrafish: A New Model for Human Disease: Figure 1. *Genome Research*, *9*(2), 99–100. https://doi.org/10.1101/gr.9.2.99
- Zoodsma, J. D., Chan, K., Bhandiwad, A. A., Golann, D. R., Liu, G., Syed, S. A., Napoli, A. J., Burgess, H. A., Sirotkin, H. I., & Wollmuth, L. P. (2020). A Model to Study NMDA Receptors in Early Nervous System Development. *The Journal of Neuroscience*, *40*(18), 3631–3645. https://doi.org/10.1523/JNEUROSCI.3025-19.2020
- Zoodsma, J. D., Keegan, E. J., Moody, G. R., Bhandiwad, A. A., Napoli, A. J., Burgess, H. A., Wollmuth, L. P., & Sirotkin, H. I. (2022). Disruption of grin2B, an ASD-associated gene, produces social deficits in zebrafish. *Molecular Autism*, *13*(1), 38. https://doi.org/10.1186/s13229-022-00516-3

-

Supplementary Figures

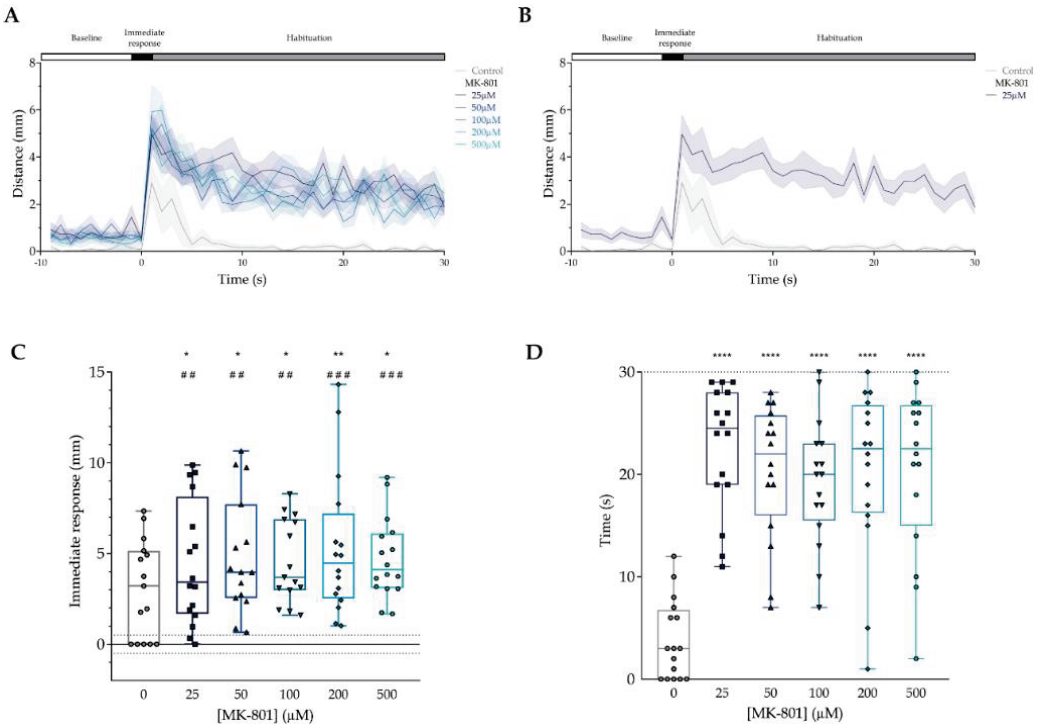

Supplementary Figure 1. MK-801 exposure effects in the response and habituation to tactile stimuli in a in a 15-minute spaced set of tappings. A Dose-response effect of MK-801 on locomotor response (distance travelled) in one-second time. B. Graph of the distance moved in one-second time bin of 25µM MK-801 as a representative example of the tapping response. C. Graph representing the difference in the distance moved as a response to the first tap. Statistical analysis of the immediate response (mm) is represented with "*". Statistical analysis of the number of larvae responding (%) is represented with "#". D. Quantification of the habituation by measuring the time each larva takes to not respond to the stimulus, with a cut off at 30 seconds. In panels A and B, data is represented as mean ± SEM; in panels C and D, data is represented with box and whisker plots, showing the median, minimum and maximum, showing all points. N=16 in all groups. "#". *p<0.05, ** p<0.01, ****p<0.0001 (One-way ANOVA with Tukey's post-hoc analysis). ##p<0.01, ###p<0.001 (Two-way ANOVA with Sidak's multiple comparisons test).

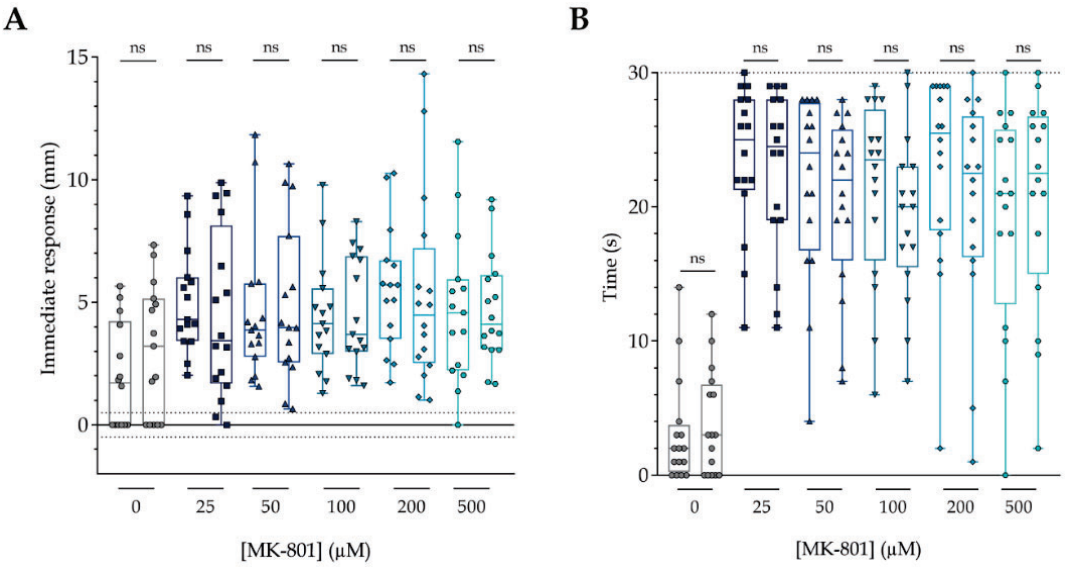

Supplementary Figure 2. Comparison of 15-minute spaced tapping responses after MK-801 exposure. A. Graph representing the difference in the distance moved as a response to the first tap, comparing the first set (left) to the second set (right) of tappings. B. Quantification of the habituation by measuring the time each larva takes to not respond to the stimulus, with a cut off at 30 seconds, comparing the first set (left) to the second set (right) of tappings. Data is represented with box and whisker plots, showing the median, minimum and maximum, showing all points. N=16 in all groups. (One-way ANOVA with Tukey's post-hoc analysis).

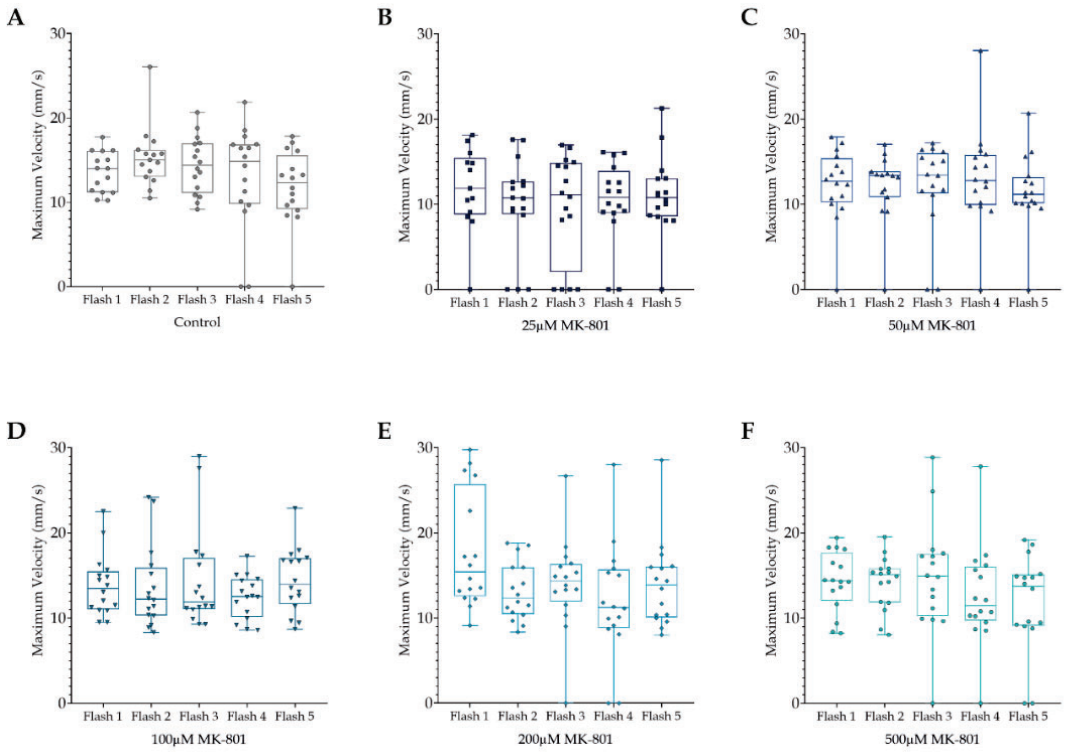

Supplementary Figure 3. Analysis of maximum velocity of independent flashes response of MK-801 treated larvae. Measurement of the maximum velocity (mm/s) achieved, comparing the different responses to each flash of Control larvae (A) and all the tested MK-801 concentrations, 25µM MK-801 (B), 50µM MK-801 (C), 100µM MK-801 (D), 200µM MK-801 (E) and 500µM MK-801 (F). The data is represented with box and whisker plots, showing the median, minimum and maximum, showing all points. N=16 in all groups. (One-way ANOVA with Tukey's post-hoc analysis).

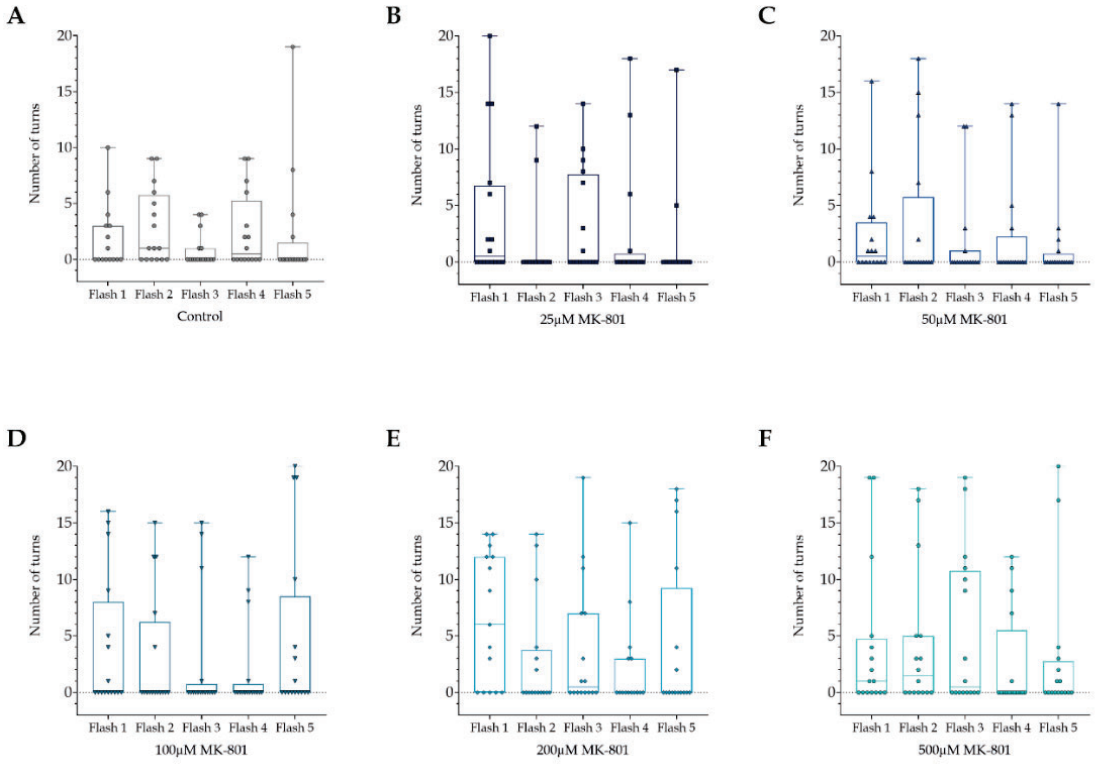

Supplementary Figure 4. Analysis of number of turns of independent flashes response of MK-801 treated larvae. Measurement of the number of turns performed, comparing the different responses to each flash of Control larvae (A) and all the tested MK-801 concentrations, 25µM MK-801 (B), 50µM MK-801 (C), 100µM MK-801 (D), 200µM MK-801 (E) and 500µM MK-801 (F). The data is represented with box and whisker plots, showing the median, minimum and maximum, showing all points. N=16 in all groups. (One-way ANOVA with Tukey's post-hoc analysis).

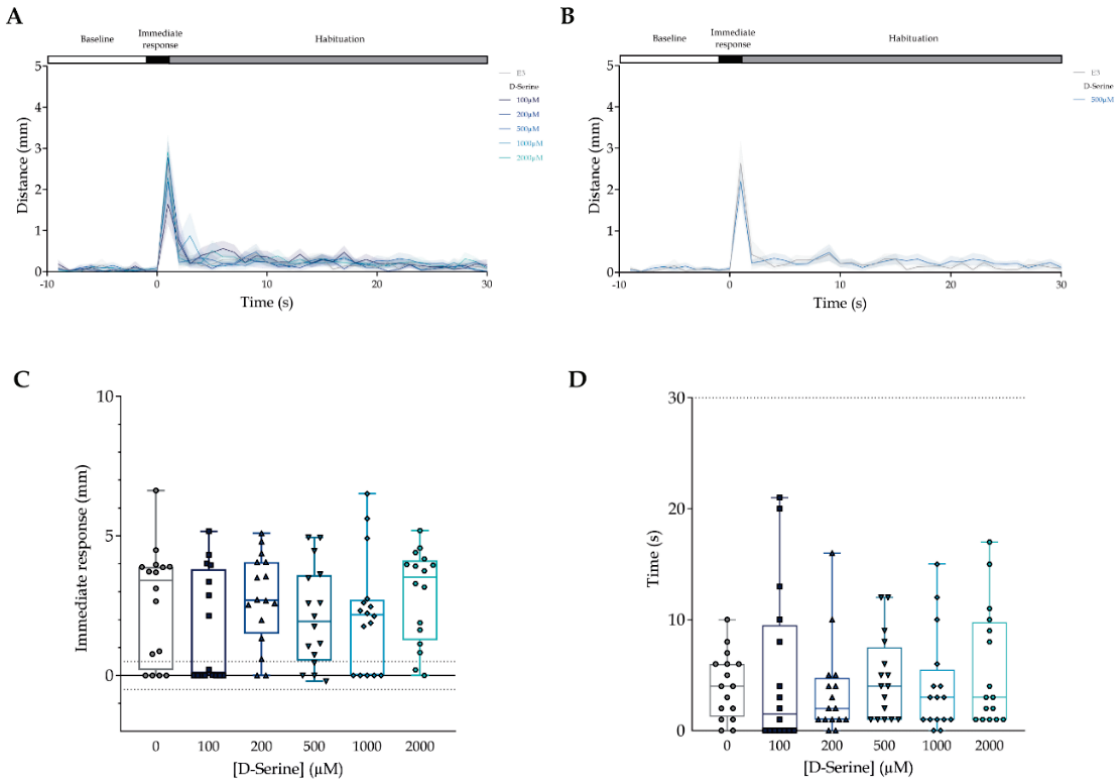

Supplementary Figure 5. D-Serine exposure effects in the response and habituation to tactile stimuli in a in a 15-minute spaced set of tappings. A Dose-response effect of D-Serine on locomotor response (distance travelled) in one-second time. B. Graph of the distance moved in one-second time bin of 500µM D-Serine as a representative example of the tapping response. C. Graph representing the difference in the distance moved as a response to the first tap. D. Quantification of the habituation by measuring the time each larva takes to not respond to the stimulus, with a cut off at 30 seconds. In panels A and B, data is represented as mean ± SEM; in panels C and D, data is represented with box and whisker plots, showing the median, minimum and maximum, showing all points. N=16 in all groups. (One-way ANOVA with Tukey's post-hoc analysis).

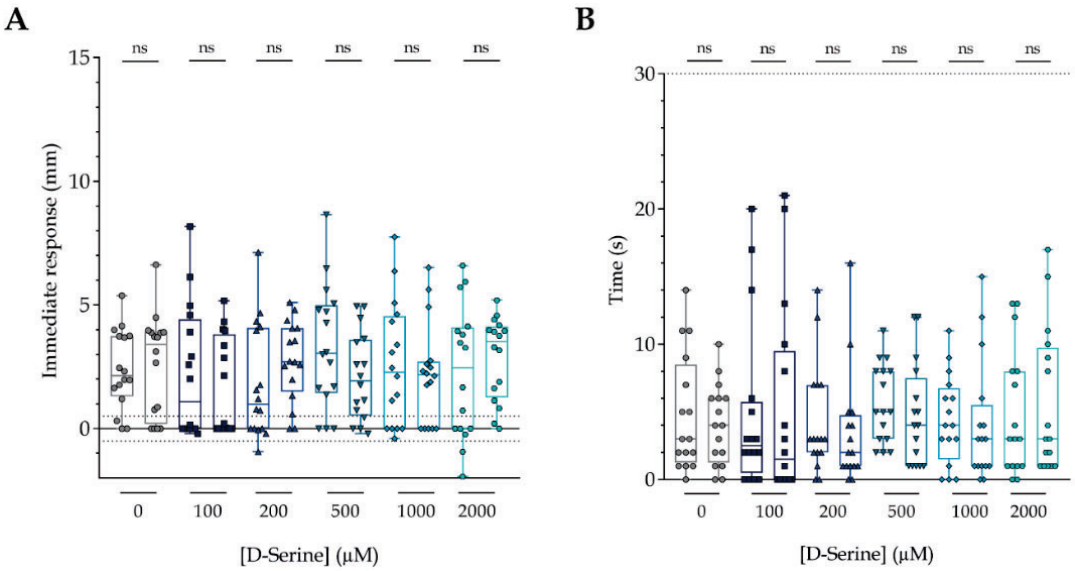

Supplementary Figure 6. Comparison of 15-minute spaced tapping responses after D-Serine exposure. A. Graph representing the difference in the distance moved as a response to the first tap, comparing the first set (left) to the second set (right) of tappings. B. Quantification of the habituation by measuring the time each larva takes to not respond to the stimulus, with a cut off at 30 seconds, comparing the first set (left) to the second set (right) of tappings. Data is represented with box and whisker plots, showing the median, minimum and maximum, showing all points. N=16 in all groups. (One-way ANOVA with Tukey's post-hoc analysis).

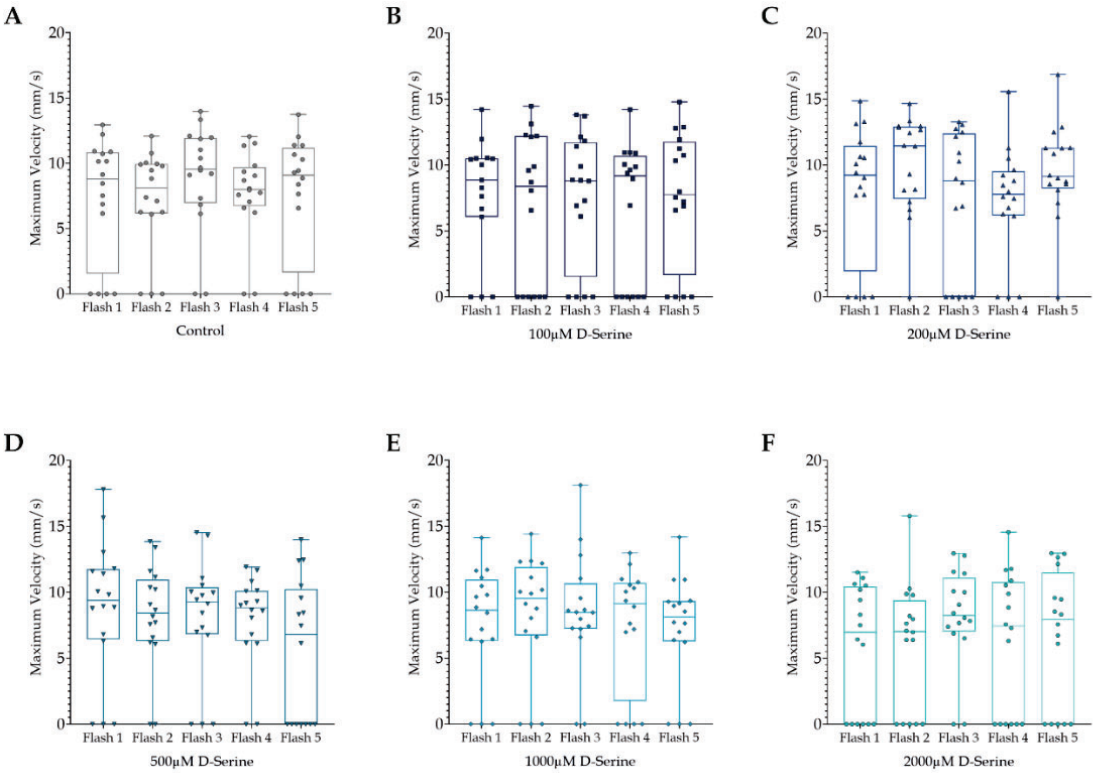

Supplementary Figure 7. Analysis of maximum velocity of independent flashes response of D-Serine treated larvae. Measurement of the maximum velocity (mm/s) achieved, comparing the different responses to each flash of Control larvae (A) and all the tested D-Serine concentrations, 100µM D-Serine (B), 200µM D-Serine (C), 500µM D-Serine (D), 1000µM D-Serine (E) and 2000µM D-Serine (F). The data is represented with box and whisker plots, showing the median, minimum and maximum, showing all points. N=16 in all groups. (One-way ANOVA with Tukey's post-hoc analysis).

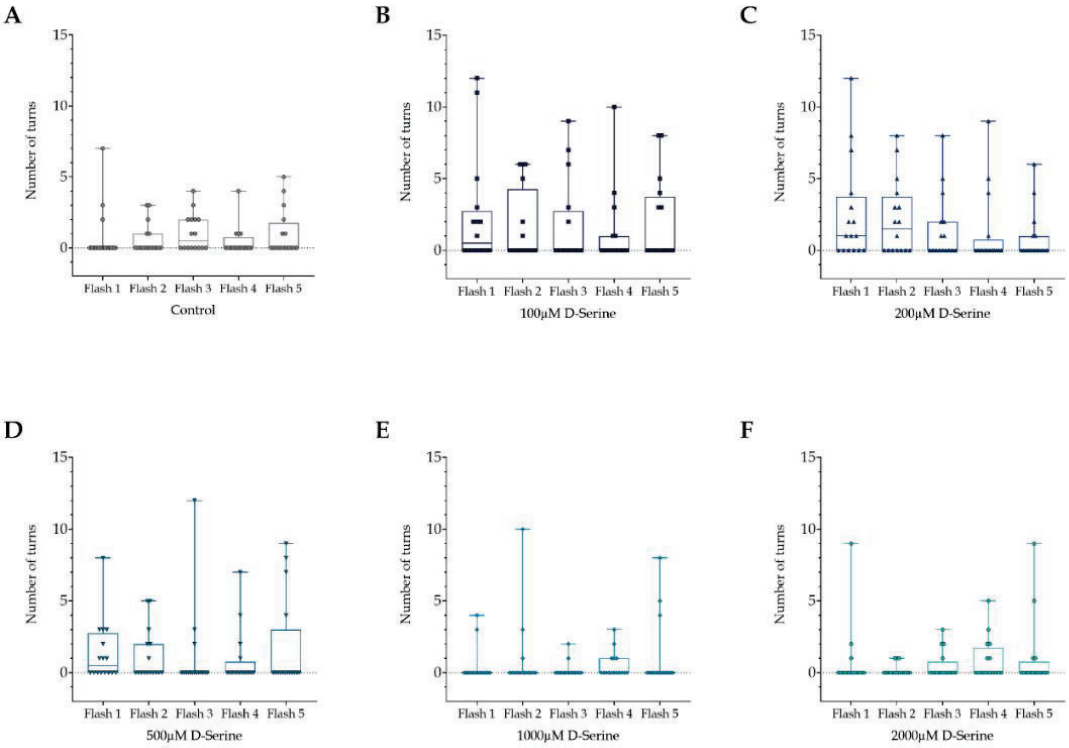

Supplementary Figure 8. Analysis of number of turns of independent flashes response of MK-801 treated larvae. Measurement of the number of turns performed, comparing the different responses to each flash of Control larvae (A) and all the tested D-Serine concentrations, 100µM D-Serine (B), 200µM D-Serine (C), 500µM D-Serine (D), 1000µM D-Serine (E) and 2000µM D-Serine (F). The data is represented with box and whisker plots, showing the median, minimum and maximum, showing all points. N=16 in all groups. (One-way ANOVA with Tukey's post-hoc analysis).

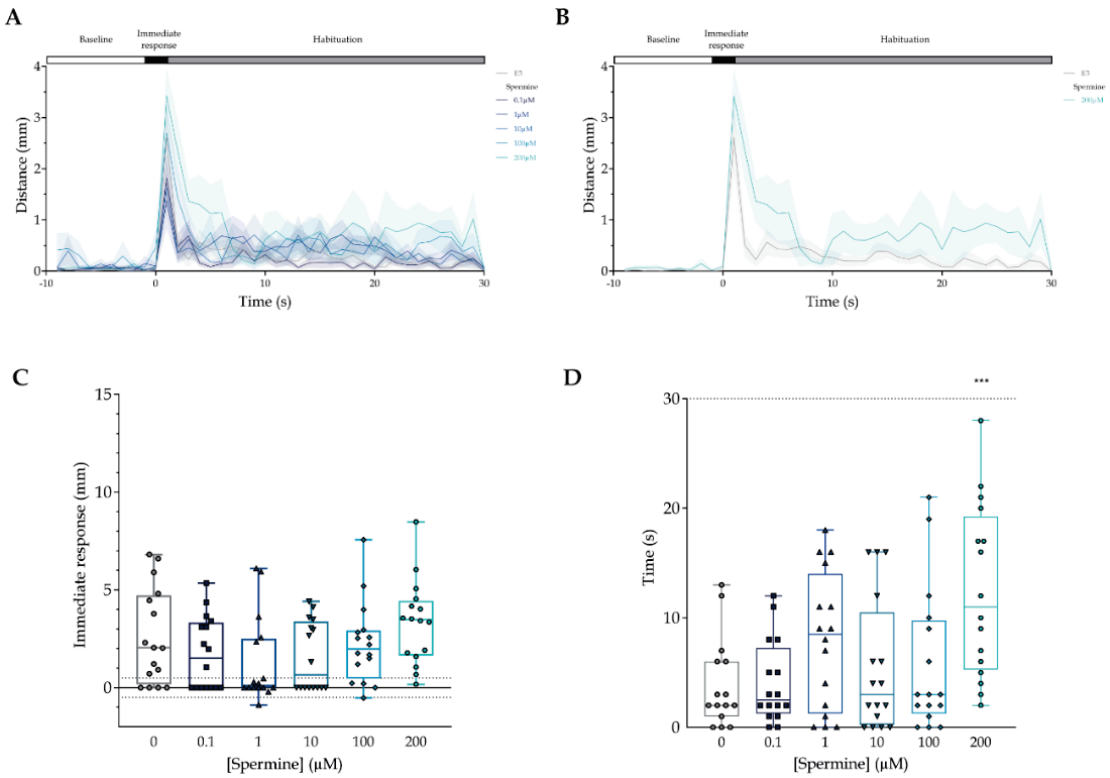

Supplementary Figure 9. Spermine exposure effects in the response and habituation to tactile stimuli in a in a 15-minute spaced set of tappings. A Dose-response effect of Spermine on locomotor response (distance travelled) in one-second time. B. Graph of the distance moved in one-second time bin of 200µM Spermine as a representative example of the tapping response. C. Graph representing the difference in the distance moved as a response to the first tap. D. Quantification of the habituation by measuring the time each larva takes to not respond to the stimulus, with a cut off at 30 seconds. In panels A and B, data is represented as mean ± SEM; in panels C and D, data is represented with box and whisker plots, showing the median, minimum and maximum, showing all points. N=16 in all groups. ***p<0.001 (One-way ANOVA with Tukey's post-hoc analysis).

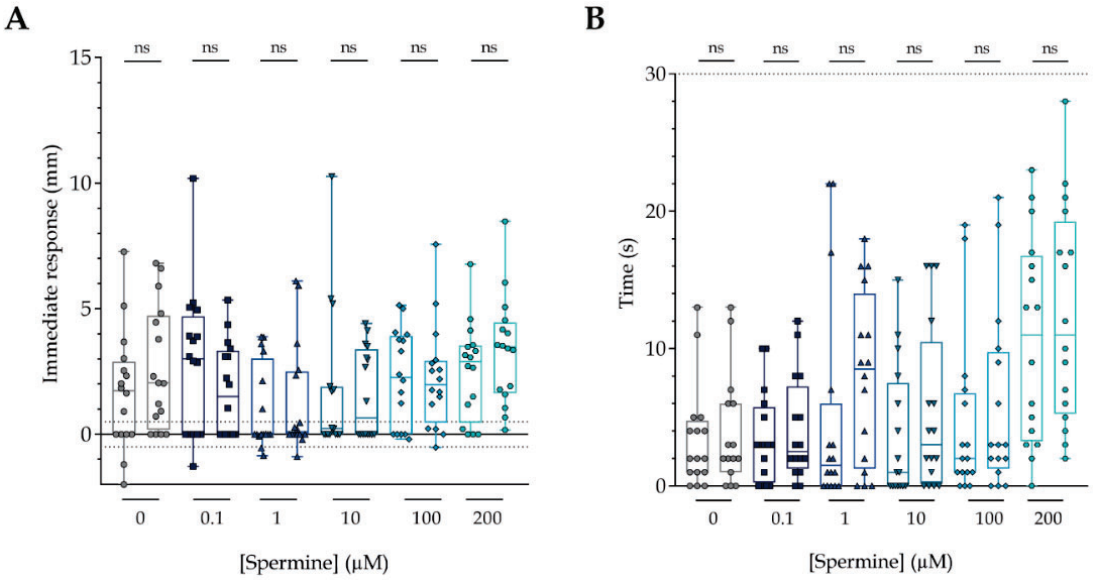

Supplementary Figure 10. Comparison of 15-minute spaced tapping responses after Spermine exposure. A. Graph representing the difference in the distance moved as a response to the first tap, comparing the first set (left) to the second set (right) of tappings. B. Quantification of the habituation by measuring the time each larva takes to not respond to the stimulus, with a cut off at 30 seconds, comparing the first set (left) to the second set (right) of tappings. Data is represented with box and whisker plots, showing the median, minimum and maximum, showing all points. N=16 in all groups. (One-way ANOVA with Tukey's post-hoc analysis).

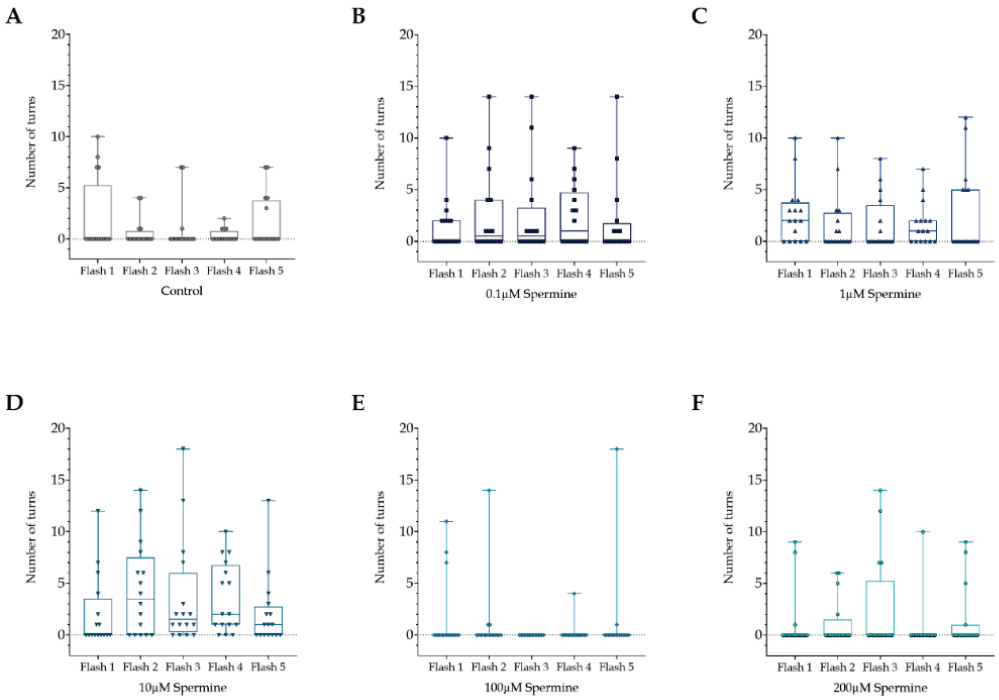

Supplementary Figure 11. Analysis of maximum velocity of independent flashes response of Spermine treated larvae. Measurement of the maximum velocity (mm/s) achieved, comparing the different responses to each flash of Control larvae (A) and all the tested Spermine concentrations, 0.1µM Spermine (B), 1µM Spermine (C), 10µM Spermine (D), 100µM Spermine (E) and 200µM Spermine (F). The data is represented with box and whisker plots, showing the median, minimum and maximum, showing all points. N=16 in all groups. (One-way ANOVA with Tukey's post-hoc analysis).

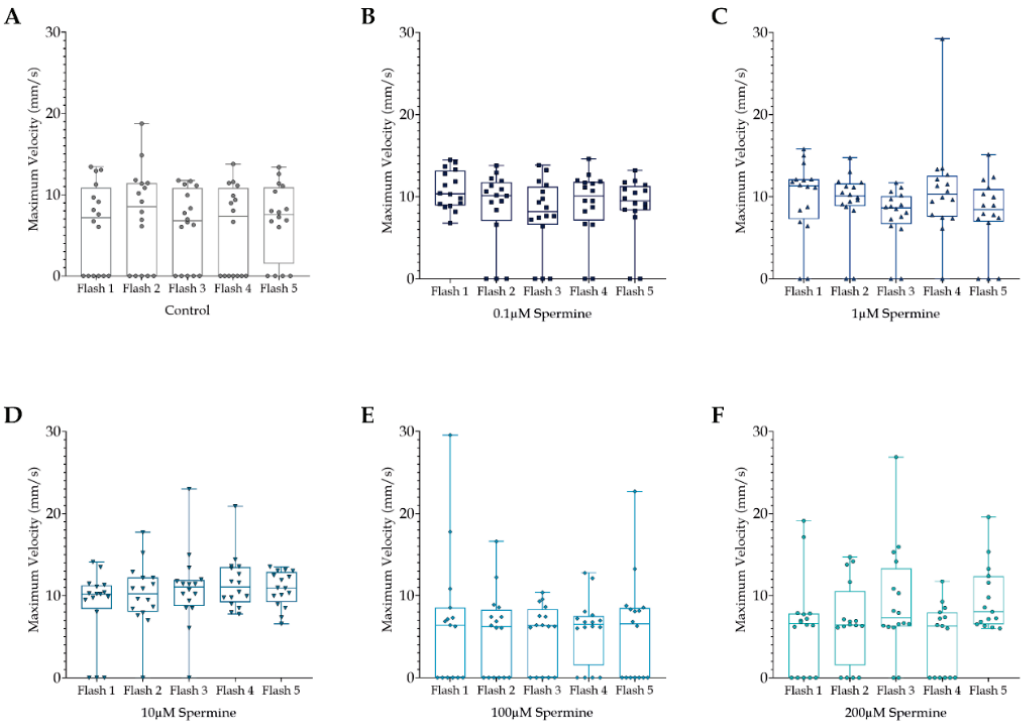

Supplementary Figure 12. Analysis of number of turns of independent flashes response of Spermine treated larvae. Measurement of the number of turns performed, comparing the different responses to each flash of Control larvae (A) and all the tested Spermine concentrations, 0.1µM Spermine (B), 1µM Spermine (C), 10µM Spermine (D), 100µM Spermine (E) and 200µM Spermine (F). The data is represented with box and whisker plots, showing the median, minimum and maximum, showing all points. N=16 in all groups. (One-way ANOVA with Tukey's post-hoc analysis).

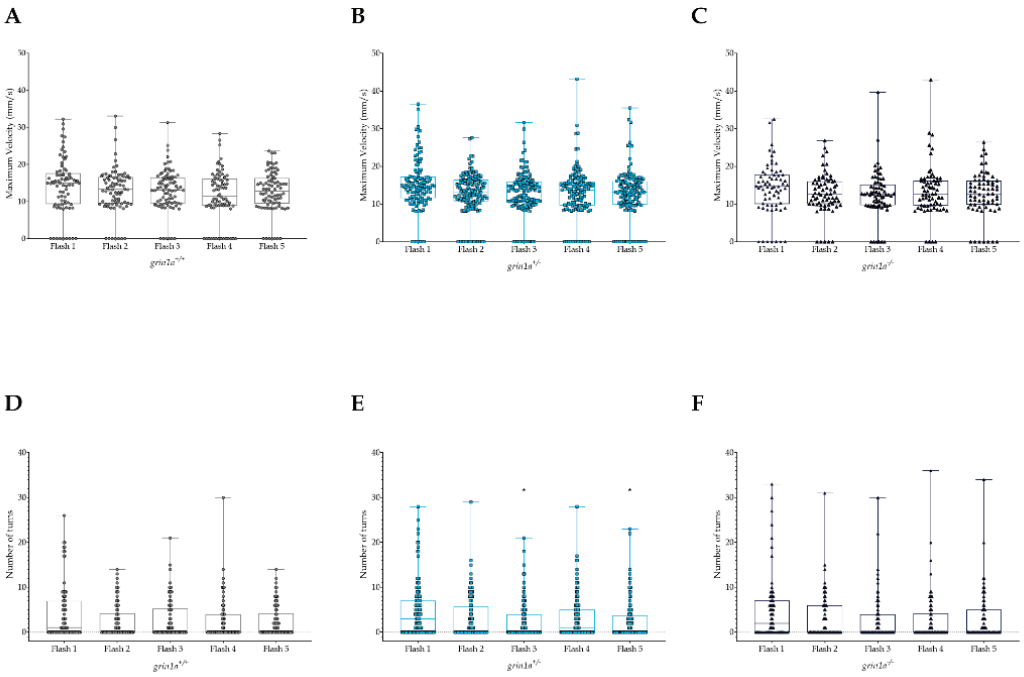

Supplementary Figure 13. Analysis of maximum velocity and angle turns of independent flashes response of *grin1a* larvae. A. B. C. Measurement of the maximum velocity (mm/s) achieved, comparing the different responses to each flash of wild-type larvae (A), heterozygous *grin1a*$^{+/-}$ (B) and homozygous *grin1a*$^{-/-}$ (C). D. E. F. Measurement of the number of angle turns performed, comparing the different responses to each flash of wild-type larvae (D), heterozygous *grin1a*$^{+/-}$ (E) and homozygous *grin1a*$^{-/-}$ (F). The data is represented with box and whisker plots, showing the median, minimum and maximum, showing all points. (One-way ANOVA with Tukey's post-hoc analysis).

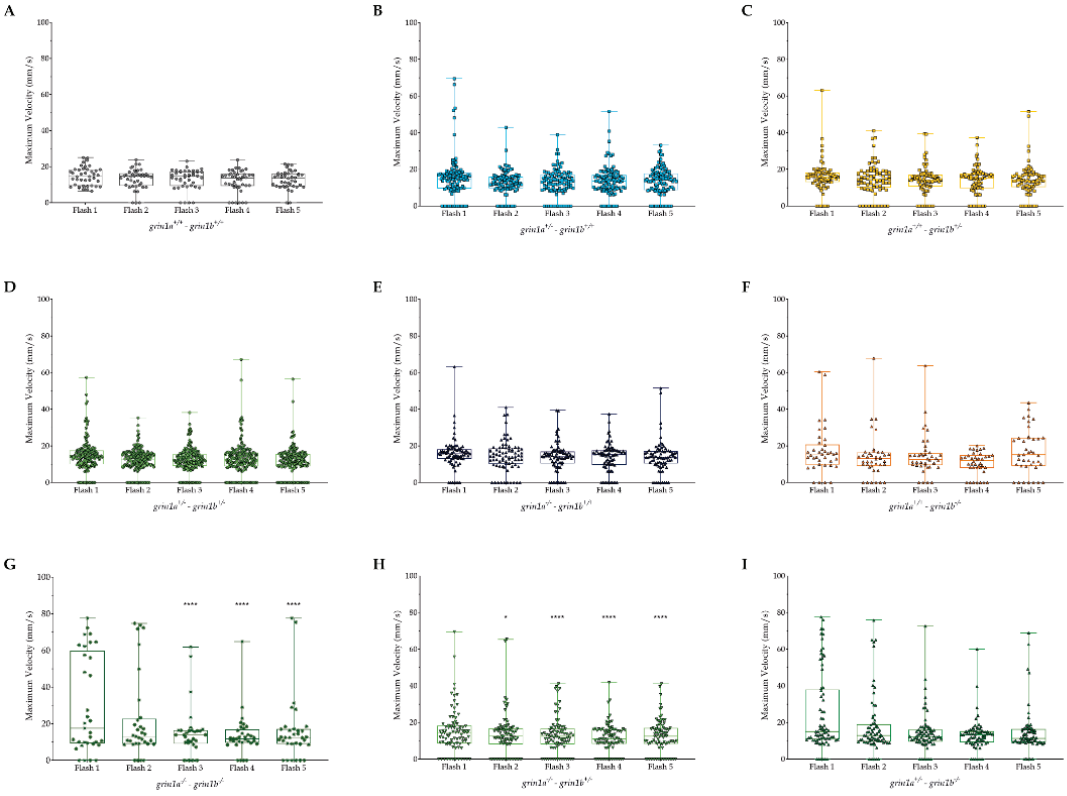

Supplementary Figure 14. Analysis of maximum velocity of independent flashes response of double mutant *grin1* larvae. Measurement of the maximum velocity (mm/s) achieved, comparing the different responses to each flash of wild-type *grin1a*$^{+/+}$-*grin1b*$^{+/+}$ larvae (A), heterozygous *grin1a*$^{+/-}$ (B), heterozygous *grin1b*$^{+/-}$ (C), double heterozygous *grin1a*$^{+/-}$-*grin1b*$^{+/-}$ (D), homozygous *grin1a*$^{-/-}$ (E), homozygous *grin1b*$^{-/-}$ (F), homozygous for *grin1a* and heterozygous for *grin1a, grin1a*$^{-/-}$-*grin1b*$^{+/-}$ (G), heterozygous for *grin1a* and homozygous for *grin1b*, *grin1a*$^{+/-}$-*grin1b*$^{-/-}$ (H), and the double homozygous *grin1a*$^{-/-}$-*grin1b*$^{-/-}$ (I). The data is represented with box and whisker plots, showing the median, minimum and maximum, showing all points. Wild-type *grin1a*$^{+/+}$-*grin1b*$^{+/+}$ larvae are represented in grey (N=43), heterozygous *grin1a*$^{+/-}$ in light blue (N=104), homozygous *grin1a*$^{-/-}$ in dark blue (N=41), heterozygous *grin1b*$^{+/-}$ in yellow (N=78), homozygous *grin1b*$^{-/-}$ in orange (N=40), double heterozygous *grin1a*$^{+/-}$-*grin1b*$^{+/-}$ in lime (N=171), homozygous for *grin1a* and heterozygous for *grin1a, grin1a*$^{-/-}$-*grin1b*$^{+/-}$ in light green (N=88), heterozygous for *grin1a* and homozygous for *grin1b*, *grin1a*$^{+/-}$-*grin1b*$^{-/-}$ in green (N=73), and the double homozygous *grin1a*$^{-/-}$-*grin1b*$^{-/-}$, in dark green (N=33). *p<0.05, ****p<0.0001 (One-way ANOVA with Tukey's post-hoc analysis).

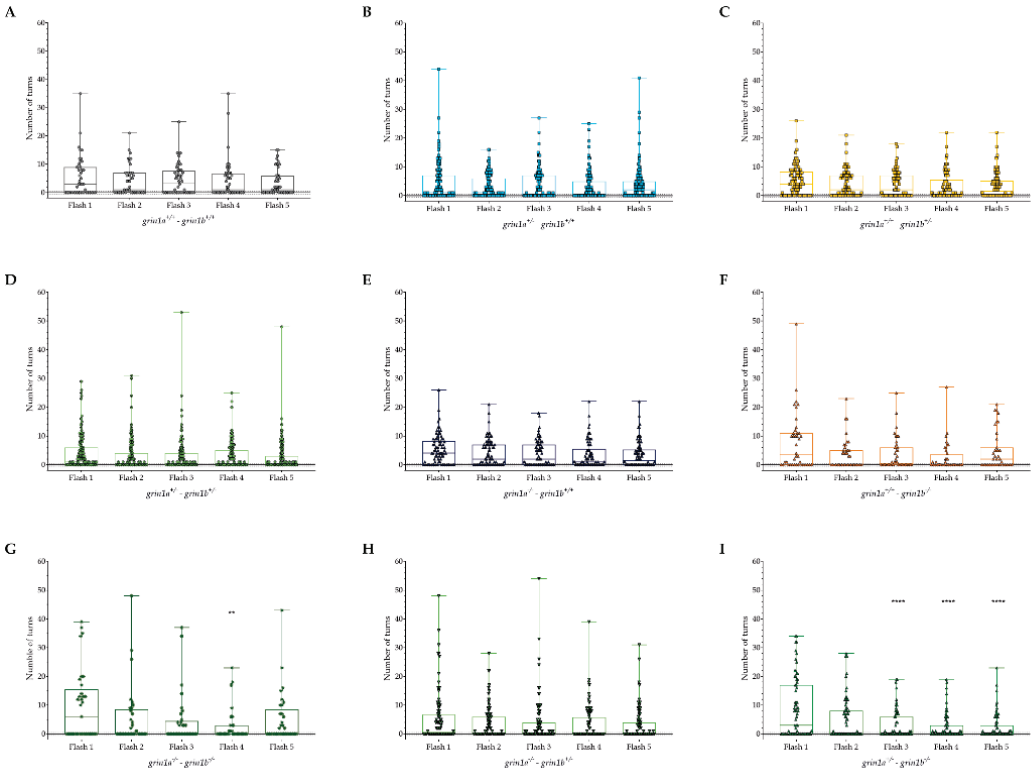

Supplementary Figure 15. Analysis of angle turns of independent flashes response of double mutant *grin1* larvae. Measurement of the number of angle turns performed, comparing the different responses to each flash of wild-type *grin1a*$^{+/+}$-*grin1b*$^{+/+}$ larvae (A), heterozygous *grin1a*$^{+/-}$ (B), heterozygous *grin1b*$^{+/-}$ (C), double heterozygous *grin1a*$^{+/-}$-*grin1b*$^{+/-}$ (D), homozygous *grin1a*$^{-/-}$ (E), homozygous *grin1b*$^{-/-}$ (F), homozygous for *grin1a* and heterozygous for *grin1a, grin1a*$^{-/-}$-*grin1b*$^{+/-}$ (G), heterozygous for *grin1a* and homozygous for *grin1b*, *grin1a*$^{+/-}$-*grin1b*$^{-/-}$ (H), and the double homozygous *grin1a*$^{-/-}$-*grin1b*$^{-/-}$ (I). The data is represented with box and whisker plots, showing the median, minimum and maximum, showing all points. Wild-type *grin1a*$^{+/+}$-*grin1b*$^{+/+}$ larvae are represented in grey (N=43), heterozygous *grin1a*$^{+/-}$ in light blue (N=104), homozygous *grin1a*$^{-/-}$ in dark blue (N=41), heterozygous *grin1b*$^{+/-}$ in yellow (N=78), homozygous *grin1b*$^{-/-}$ in orange (N=40), double heterozygous *grin1a*$^{+/-}$-*grin1b*$^{+/-}$ in lime (N=171), homozygous for *grin1a* and heterozygous for *grin1a, grin1a*$^{-/-}$-*grin1b*$^{+/-}$ in light green (N=88), heterozygous for *grin1a* and homozygous for *grin1b*, *grin1a*$^{+/-}$-*grin1b*$^{-/-}$ in green (N=73), and the double homozygous *grin1a*$^{-/-}$-*grin1b*$^{-/-}$, in dark green (N=33). *p<0.05, **p<0.01, ****p<0.0001 (One-way ANOVA with Tukey's post-hoc analysis).

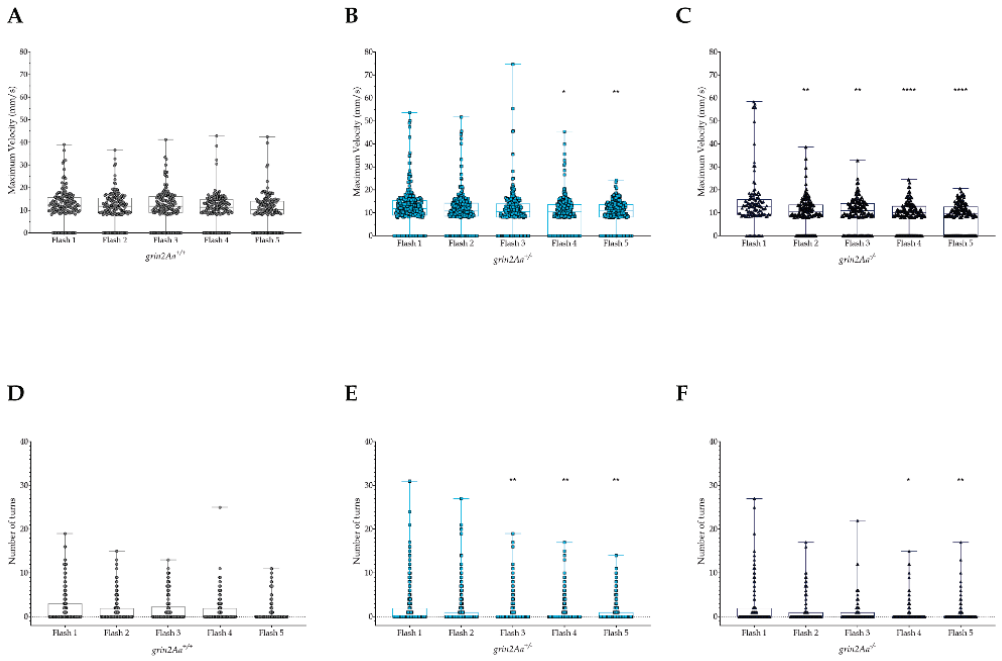

Supplementary Figure 16. Analysis of maximum velocity and angle turns of independent flashes response of *grin2Aa* larvae. A. B. C. Measurement of the maximum velocity (mm/s) achieved, comparing the different responses to each flash of wild-type larvae (A), heterozygous *grin2Aa*$^{+/-}$ (B) and homozygous *grin2Aa*$^{-/-}$ (C). D. E. F. Measurement of the number of angle turns performed, comparing the different responses to each flash of wild-type larvae (D), heterozygous *grin2Aa*$^{+/-}$ (E) and homozygous *grin2Aa*$^{-/-}$ (F). The data is represented with box and whisker plots, showing the median, minimum and maximum, showing all points. Wild-type *grin2Aa*$^{+/+}$ larvae are represented in grey (N=142), heterozygous *grin2Aa*$^{+/-}$ in light blue (N=266) and homozygous *grin2Aa*$^{-/-}$ in dark blue (N=117). *p<0.05; **p<0.01; ****p<0.0001 (One-way ANOVA with Tukey's post-hoc analysis).

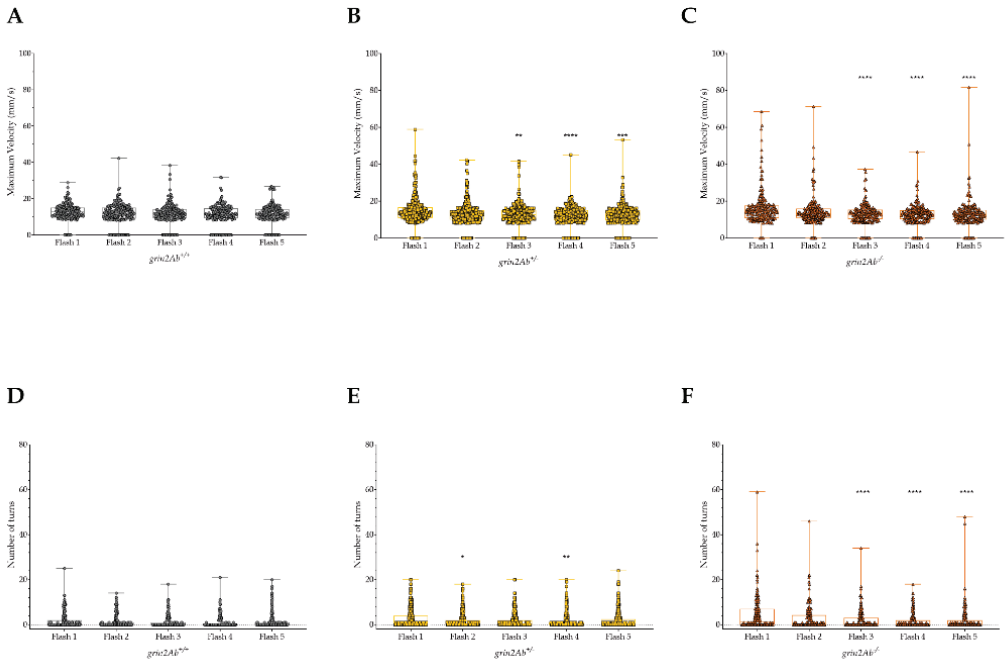

Supplementary Figure 17. Analysis of maximum velocity and angle turns of independent flashes response of *grin2Ab* larvae. A. B. C. Measurement of the maximum velocity (mm/s) achieved, comparing the different responses to each flash of wild-type larvae (A), heterozygous *grin2Ab*$^{+/-}$ (B) and homozygous *grin2Ab*$^{-/-}$ (C). D. E. F. Measurement of the number of angle turns performed, comparing the different responses to each flash of wild-type larvae (D), heterozygous *grin2Ab*$^{+/-}$ (E) and homozygous *grin2Ab*$^{-/-}$ (F). The data is represented with box and whisker plots, showing the median, minimum and maximum, showing all points. Wild-type *grin2Ab*$^{+/+}$ larvae are represented in grey (N=166), heterozygous *grin2Ab*$^{+/-}$ in yellow (N=353) and homozygous *grin2Ab*$^{-/-}$ in orange (N=198). *p<0.05; **p<0.01; ***p<0.001; ****p<0.0001 (One-way ANOVA with Tukey's post-hoc analysis).

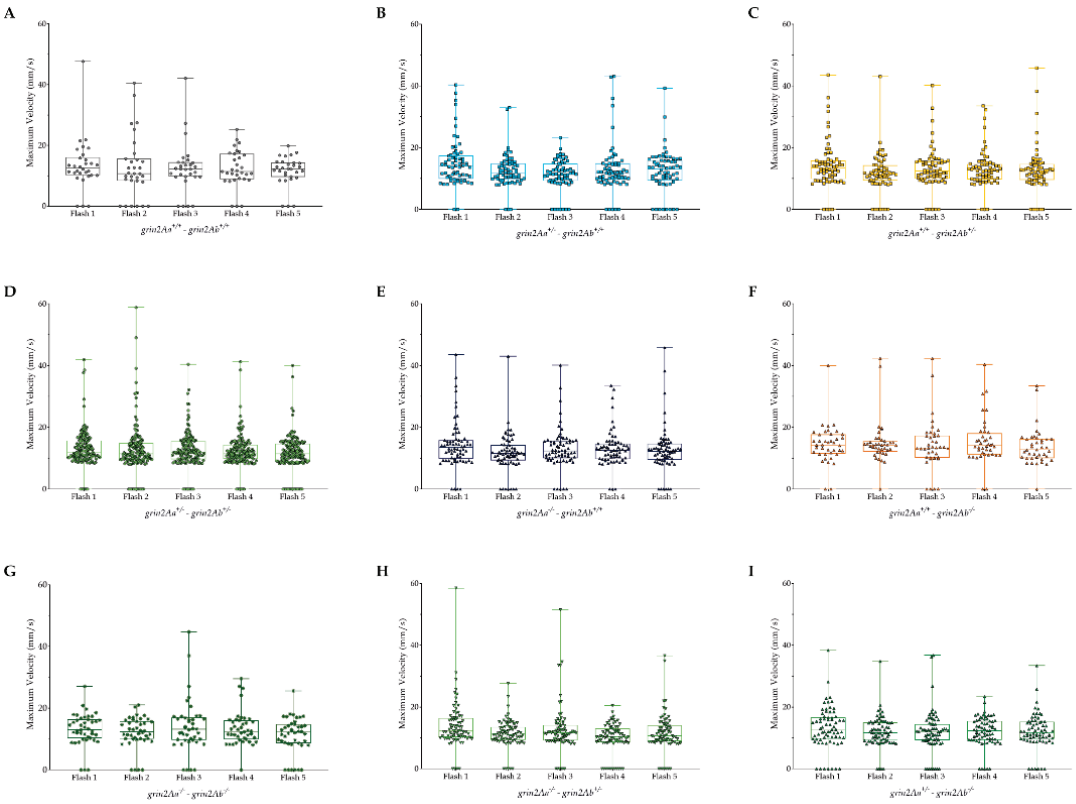

Supplementary Figure 18. Analysis of maximum velocity of independent flashes response of double mutant *grin2A* larvae. Measurement of the maximum velocity (mm/s) achieved, comparing the different responses to each flash of wild-type *grin2Aa*$^{+/+}$-*grin2Ab*$^{+/+}$ larvae (A), heterozygous *grin2Aa*$^{+/-}$ (B), heterozygous *grin2Ab*$^{+/-}$ (C), double heterozygous *grin2Aa*$^{+/-}$-*grin2Ab*$^{+/-}$ (D), homozygous *grin2Aa*$^{-/-}$ (E), homozygous *grin2Ab*$^{-/-}$ (F), homozygous for *grin2Aa* and heterozygous for *grin2Aa*, *grin2Aa*$^{-/-}$-*grin2Ab*$^{+/-}$ (G), heterozygous for *grin2Aa* and homozygous for *grin2Ab*, *grin2Aa*$^{+/-}$-*grin2Ab*$^{-/-}$ (H), and the double homozygous *grin2Aa*$^{-/-}$-*grin2Ab*$^{-/-}$ (I). The data is represented with box and whisker plots, showing the median, minimum and maximum, showing all points. Wild-type *grin2Aa*$^{+/+}$-*grin2Ab*$^{+/+}$ larvae are represented in grey (N=31), heterozygous *grin2Aa*$^{+/-}$ in light blue (N=66), homozygous *grin2Aa*$^{-/-}$ in dark blue (N=37), heterozygous *grin2Ab*$^{+/-}$ in yellow (N=68), homozygous *grin2Ab*$^{-/-}$ in orange (N=40), double heterozygous *grin2Aa*$^{+/-}$-*grin2Ab*$^{+/-}$ in lime (N=144), homozygous for *grin2Aa* and heterozygous for *grin2Aa*, *grin2Aa*$^{-/-}$-*grin2Ab*$^{+/-}$ in light green (N=78), heterozygous for *grin2Aa* and homozygous for *grin2Ab*, *grin2Aa*$^{+/-}$-*grin2Ab*$^{-/-}$ in green (N=70), and the double homozygous *grin2Aa*$^{-/-}$-*grin2Ab*$^{-/-}$, in dark green (N=42). *p<0.05, ****p<0.0001 (One-way ANOVA with Tukey's post-hoc analysis).

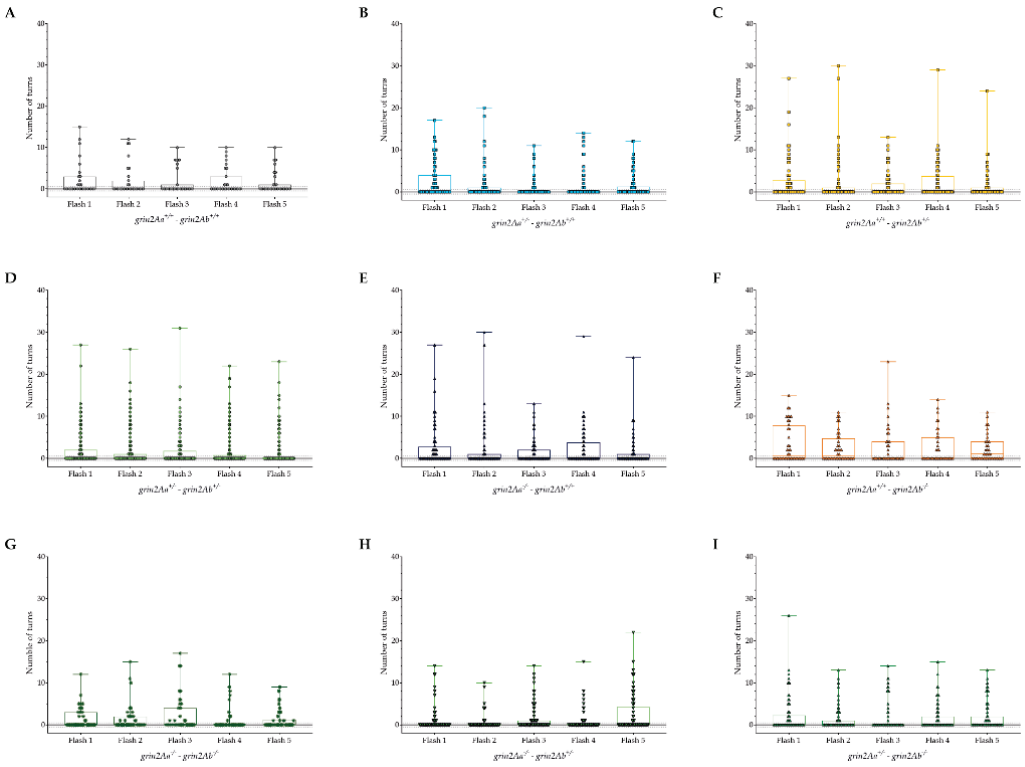

Supplementary Figure 19. Analysis of angle turns of independent flashes response of double mutant *grin2A* larvae. Measurement of the number of angle turns performed, comparing the different responses to each flash of wild-type *grin2Aa*$^{+/+}$-*grin2Ab*$^{+/+}$ larvae (A), heterozygous *grin2Aa*$^{+/-}$ (B), heterozygous *grin2Ab*$^{+/-}$ (C), double heterozygous *grin2Aa*$^{+/-}$-*grin2Ab*$^{+/-}$ (D), homozygous *grin2Aa*$^{-/-}$ (E), homozygous *grin2Ab*$^{-/-}$ (F), homozygous for *grin2Aa* and heterozygous for *grin2Aa, grin2Aa*$^{-/-}$-*grin2Ab*$^{+/-}$ (G), heterozygous for *grin2Aa* and homozygous for *grin2Ab*, *grin2Aa*$^{+/-}$-*grin2Ab*$^{-/-}$ (H), and the double homozygous *grin2Aa*$^{-/-}$-*grin2Ab*$^{-/-}$ (I). The data is represented with box and whisker plots, showing the median, minimum and maximum, showing all points. Wild-type *grin2Aa*$^{+/+}$-*grin2Ab*$^{+/+}$ larvae are represented in grey (N=31), heterozygous *grin2Aa*$^{+/-}$ in light blue (N=66), homozygous *grin2Aa*$^{-/-}$ in dark blue (N=37), heterozygous *grin2Ab*$^{+/-}$ in yellow (N=68), homozygous *grin2Ab*$^{-/-}$ in orange (N=40), double heterozygous *grin2Aa*$^{+/-}$-*grin2Ab*$^{+/-}$ in lime (N=144), homozygous for *grin2Aa* and heterozygous for *grin2Aa, grin2Aa*$^{-/-}$-*grin2Ab*$^{+/-}$ in light green (N=78), heterozygous for *grin2Aa* and homozygous for *grin2Ab*, *grin2Aa*$^{+/-}$-*grin2Ab*$^{-/-}$ in green (N=70), and the double homozygous *grin2Aa*$^{-/-}$-*grin2Ab*$^{-/-}$, in dark green (N=42). *p<0.05, **p<0.01, ****p<0.0002A (One-way ANOVA with Tukey's post-hoc analysis).

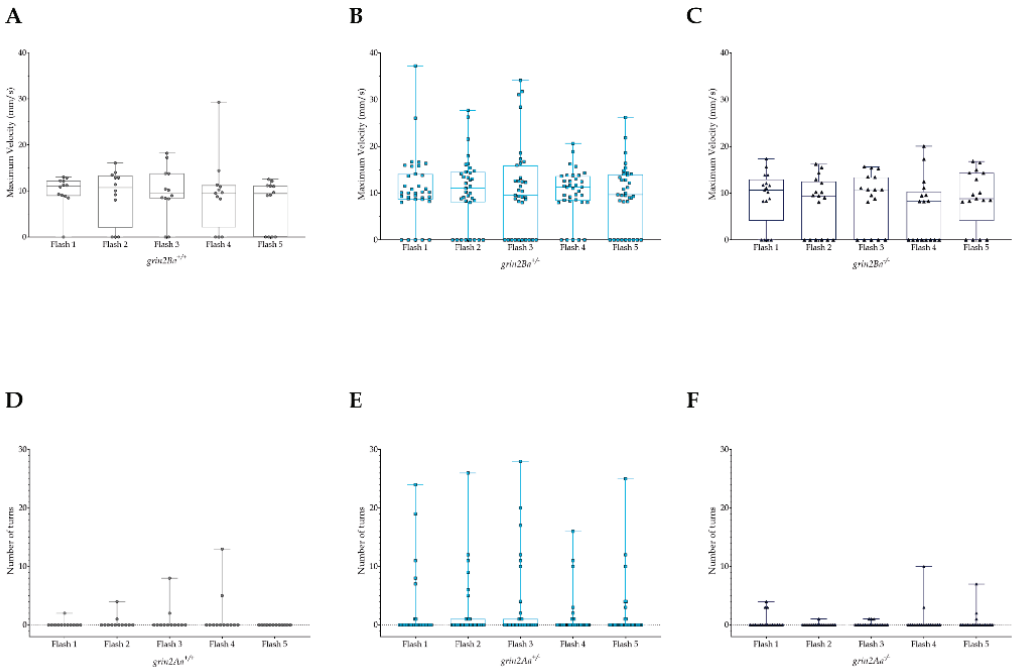

Supplementary Figure 20. Analysis of maximum velocity and angle turns of independent flashes response of *grin2Ba* larvae. A. B. C. Measurement of the maximum velocity (mm/s) achieved, comparing the different responses to each flash of wild-type larvae (A), heterozygous *grin2Ba*$^{+/-}$ (B) and homozygous *grin2Ba*$^{-/-}$ (C). D. E. F. Measurement of the number of angle turns performed, comparing the different responses to each flash of wild-type larvae (D), heterozygous *grin2Ba*$^{+/-}$ (E) and homozygous *grin2Ba*$^{-/-}$ (F). The data is represented with box and whisker plots, showing the median, minimum and maximum, showing all points. Wild-type *grin2Ba*$^{+/+}$ larvae are represented in grey (N=12), heterozygous *grin2Ba*$^{+/-}$ in light blue (N=35) and homozygous *grin2Ba*$^{-/-}$ in dark blue (N=17). *p<0.05; **p<0.01; ****p<0.0001 (One-way ANOVA with Tukey's post-hoc analysis).

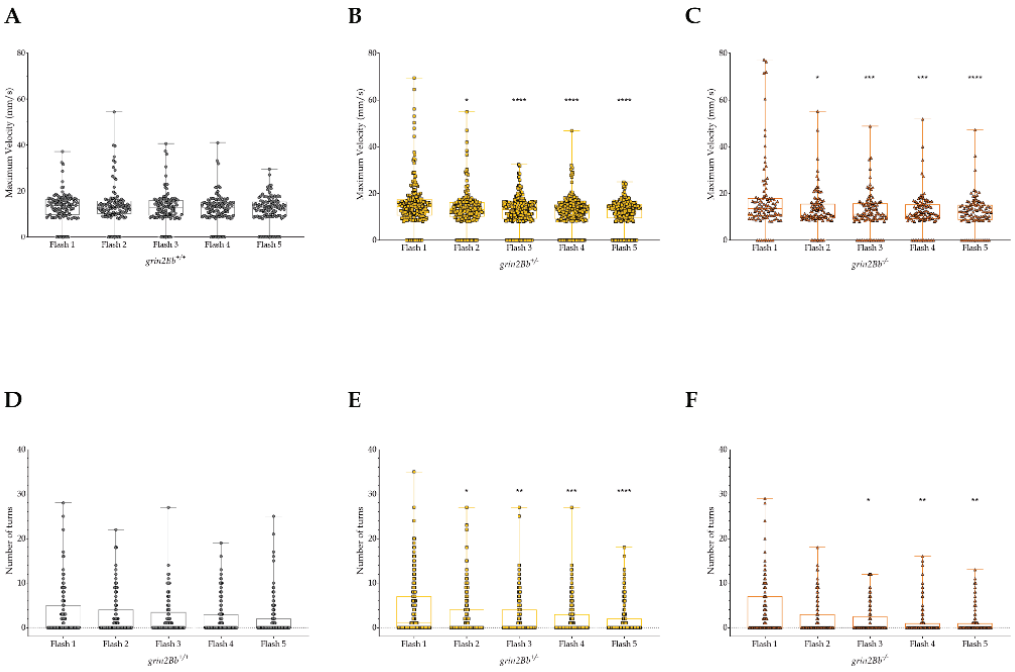

Supplementary Figure 21. Analysis of maximum velocity and angle turns of independent flashes response of *grin2Bb* larvae. A. B. C. Measurement of the maximum velocity (mm/s) achieved, comparing the different responses to each flash of wild-type larvae (A), heterozygous *grin2Bb*$^{+/-}$ (B) and homozygous *grin2Bb*$^{-/-}$ (C). D. E. F. Measurement of the number of angle turns performed, comparing the different responses to each flash of wild-type larvae (D), heterozygous *grin2Bb*$^{+/-}$ (E) and homozygous *grin2Bb*$^{-/-}$ (F). The data is represented with box and whisker plots, showing the median, minimum and maximum, showing all points. Wild-type *grin2Bb*$^{+/+}$ larvae are represented in grey (N=109), heterozygous *grin2Bb*$^{+/-}$ in yellow (N=353) and homozygous *grin2Bb*$^{-/-}$ in orange (N=100). *p<0.05; **p<0.01; ***p<0.001; ****p<0.0001 (One-way ANOVA with Tukey's post-hoc analysis).

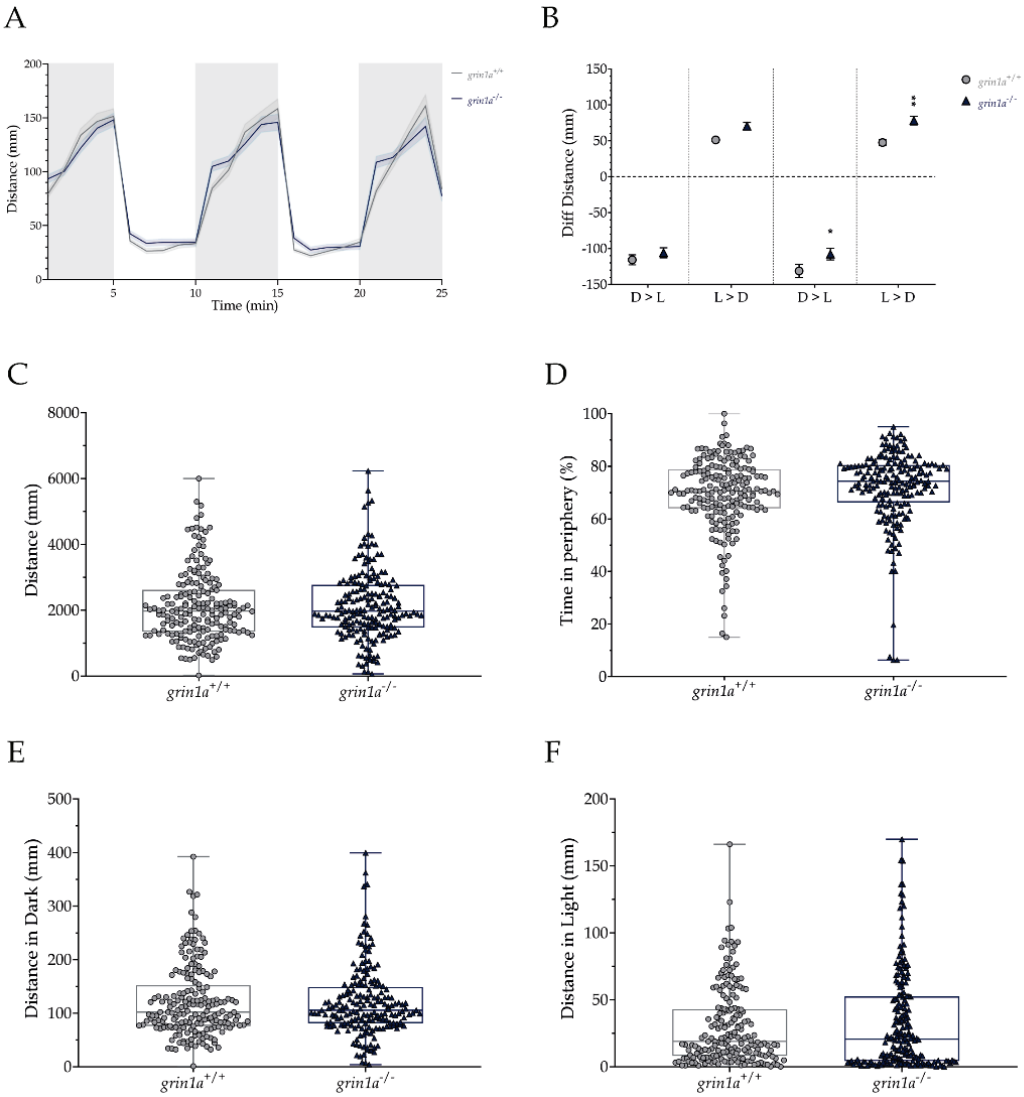

Supplementary Figure 22. Analysis of the locomotor performance of *grin1a* mutant zebrafish larvae. A. Representation of the distance moved by one-minute time bin during the 25-minute dark/light cycles. Dark cycles are annotated as grey vertical lines for better visualisation. B. Representation of the difference of the distance moved in the transitions from dark to light (D>L) and from light to dark (L>D). C. Graph of the total distance moved (mm) of the larvae in the complete 25-minute protocol. D. Analysis of the average percentage of time spent in the peripherical area of the well. E. Graph of the total distance moved (mm) only in the dark phases of the dark/light cycle protocol. F. Graph of the total distance moved (mm) only in the light phases of the dark/light cycle protocol. In panels A and B, data is represented as mean ± SEM; in panels C to F, data is represented with box and whisker plots, showing the median, minimum and maximum, showing all points. Wild-type *grin1a*$^{+/+}$ larvae are represented in grey, and homozygous *grin1a*$^{-/-}$ in dark blue. N=192. *p<0.05 (One-Way ANOVA with Tukey's post-hoc analysis).

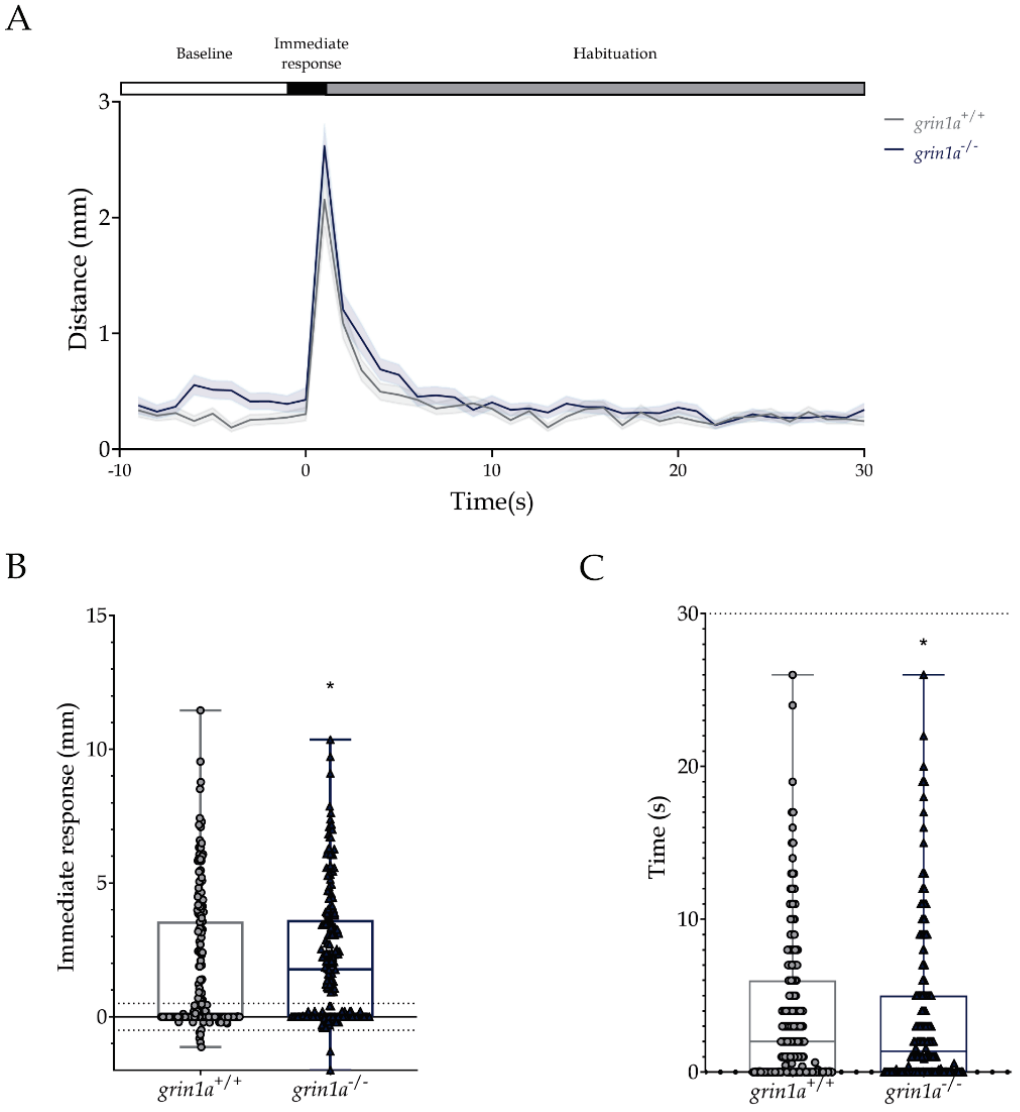

Supplementary Figure 23. Evaluation to the immediate response and habituation to tapping in *grin1a* mutant larvae. A. Graph of the distanced moved in one-second time bin. B. Graph representing the difference in the distance moved as a response to the first tap. Statistical analysis of the immediate response (mm) is represented with "*". Statistical analysis of the number of larvae responding (%) is represented with "#". C. Quantification of the habituation by measuring the time each larva takes to not respond to the stimulus, with a cut off at 30 seconds. Wild-type *grin1a*$^{+/+}$ larvae are represented in grey, and homozygous *grin1a*$^{-/-}$ in dark blue. N=192. * $p<0.05$ (One-way ANOVA with Tukey's post-hoc analysis).

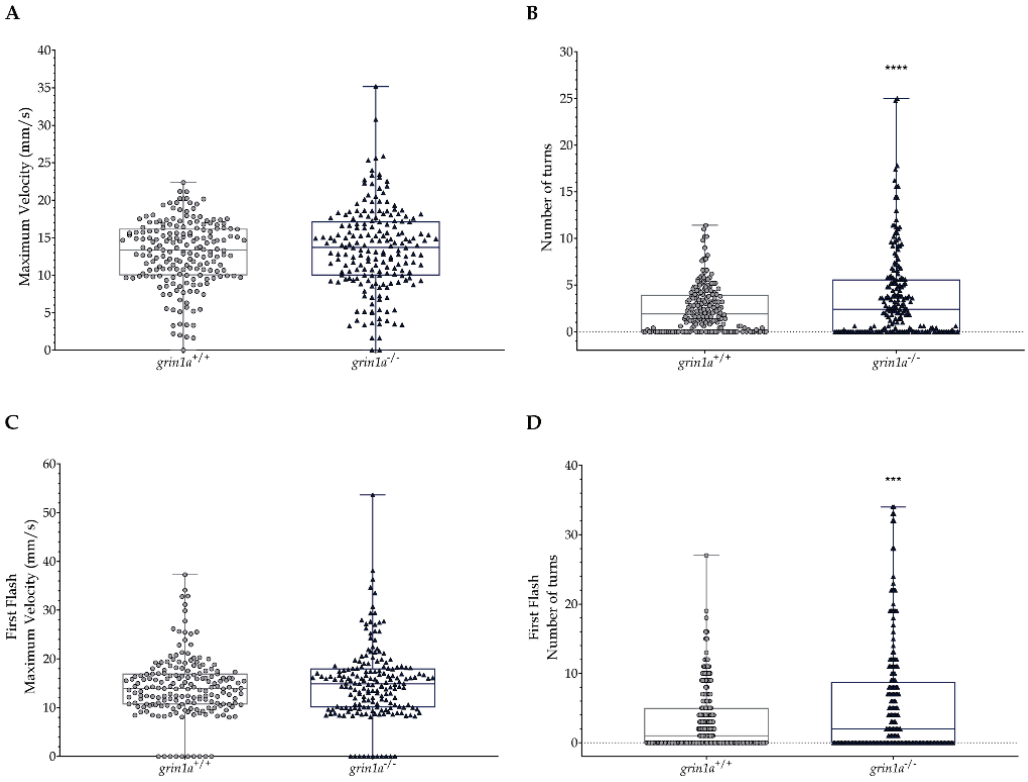

Supplementary Figure 24. Light-induced epilepsy-like response evaluation in *grin1a* mutant larvae. A. Measurement of the maximum velocity (mm/s) achieved, comparing the average of the five trials. B. Measurement of the total number of angle turns performed, comparing the average of the five trials. C. Measurement of the maximum velocity (mm/s) achieved, comparing only the response to the first flash. D. Measurement of the total number of angle turns performed, comparing only the response to the first flash. The data is represented with box and whisker plots, showing the median, minimum and maximum, showing all points. Wild-type *grin1a*$^{+/+}$ larvae are represented in grey, and homozygous *grin1a*$^{-/-}$ in dark blue. N=192. *** $p<0.001$, **** $p<0.0001$ (One-way ANOVA with Tukey's post-hoc analysis).

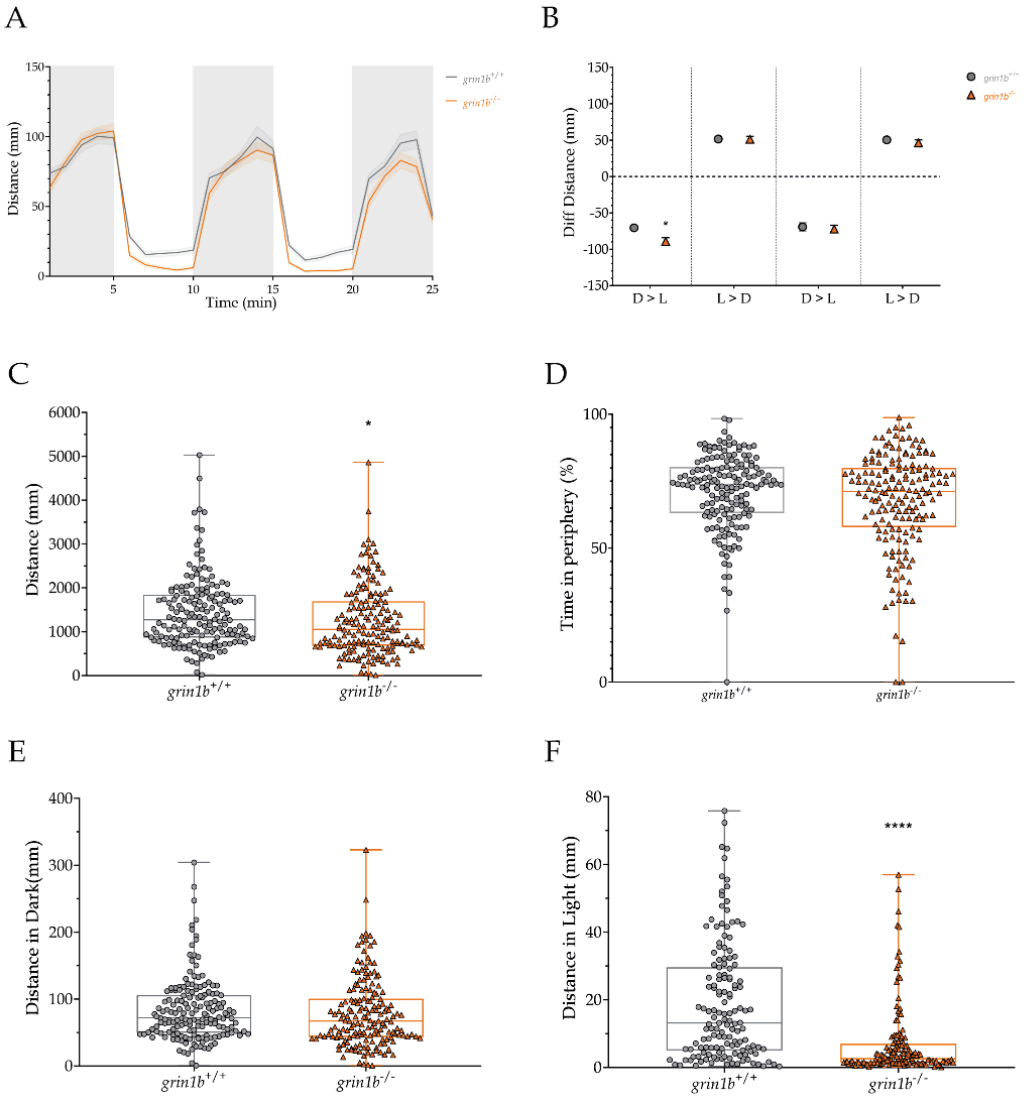

Supplementary Figure 25. Analysis of the locomotor performance of *grin1b* mutant zebrafish larvae. A. Representation of the distance moved by one-minute time bin during the 25-minute dark/light cycles. Dark cycles are annotated as grey vertical lines for better visualisation. B. Representation of the difference of the distance moved in the transitions from dark to light (D>L) and from light to dark (L>D). C. Graph of the total distance moved (mm) of the larvae in the complete 25-minute protocol. D. Analysis of the average percentage of time spent in the peripherical area of the well. E. Graph of the total distance moved (mm) only in the dark phases of the dark/light cycle protocol. F. Graph of the total distance moved (mm) only in the light phases of the dark/light cycle protocol. In panels A and B, data is represented as mean ± SEM; in panels C to F, data is represented with box and whisker plots, showing the median, minimum and maximum, showing all points. Wild-type *grin1b*$^{+/+}$ larvae are represented in grey, and homozygous *grin1b*$^{-/-}$ in orange. N=168. *p<0.05, ****p<0.0001 (One-Way ANOVA with Tukey's post-hoc analysis).

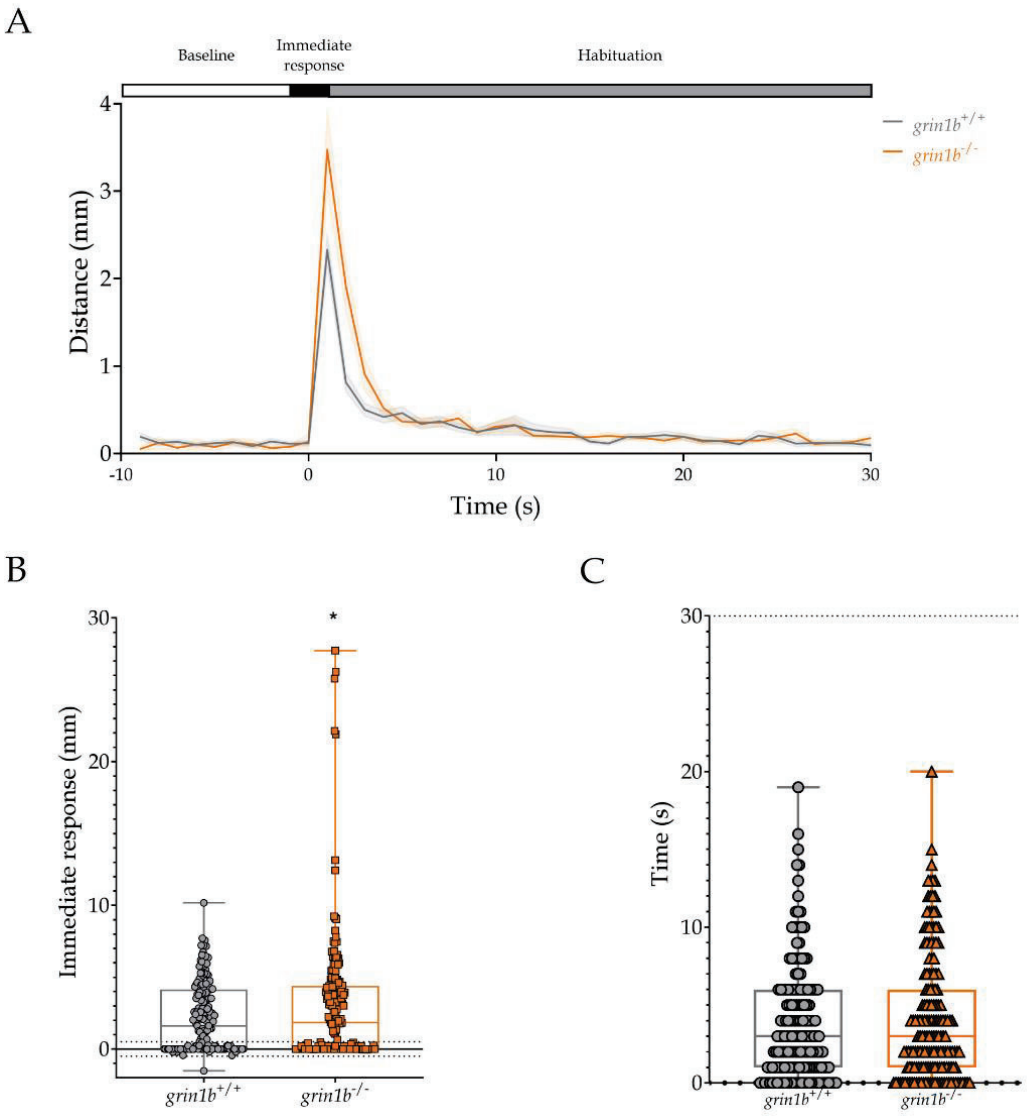

Supplementary Figure 26. Evaluation to the immediate response and habituation to tapping in *grin1b* mutant larvae. A. Graph of the distanced moved in one-second time bin. B. Graph representing the difference in the distance moved as a response to the first tap. Statistical analysis of the immediate response (mm) is represented with "*". Statistical analysis of the number of larvae responding (%) is represented with "#". C. Quantification of the habituation by measuring the time each larva takes to not respond to the stimulus, with a cut off at 30 seconds. Wild-type *grin1b*$^{+/+}$ larvae are represented in grey, and homozygous *grin1b*$^{-/-}$ in orange. N=168. * $p<0.05$ (One-way ANOVA with Tukey's post-hoc analysis).

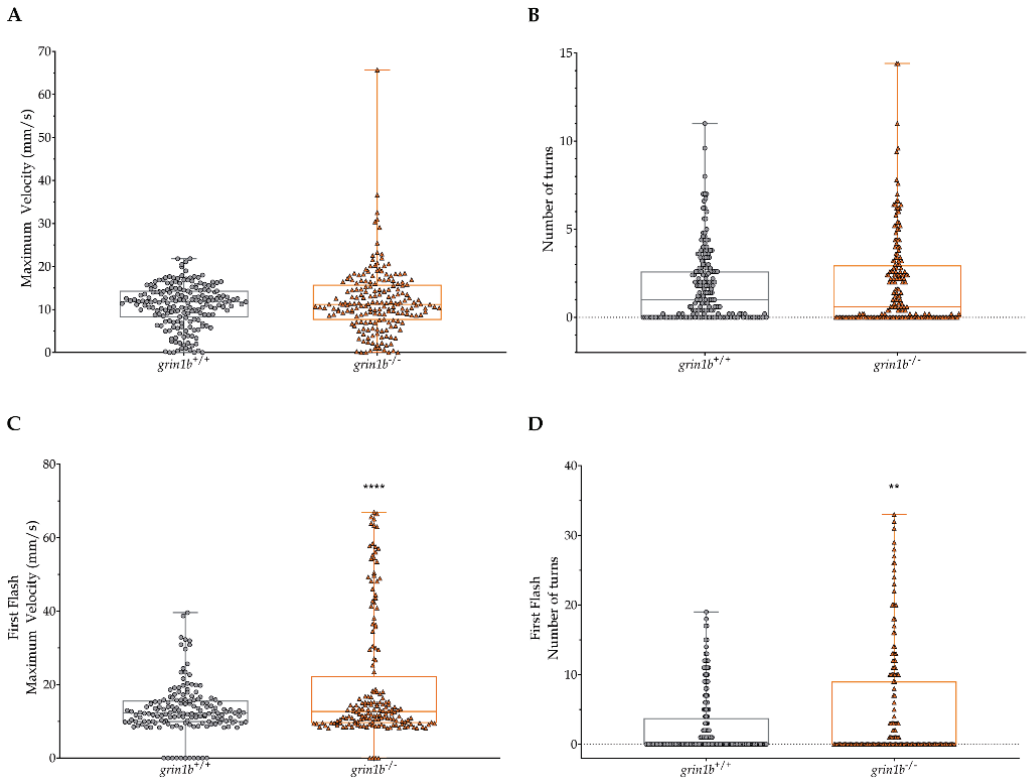

Supplementary Figure 27. Light-induced epilepsy-like response evaluation in *grin1b* mutant larvae. A. Measurement of the maximum velocity (mm/s) achieved, comparing the average of the five trials. B. Measurement of the total number of angle turns performed, comparing the average of the five trials. C. Measurement of the maximum velocity (mm/s) achieved, comparing only the response to the first flash. D. Measurement of the total number of angle turns performed, comparing only the response to the first flash. The data is represented with box and whisker plots, showing the median, minimum and maximum, showing all points. Wild-type *grin1b*$^{+/+}$ larvae are represented in grey, and homozygous *grin1b*$^{-/-}$ in orange. N=168. ** p<0.01, ****p<0.0001 (One-way ANOVA with Tukey's post-hoc analysis).

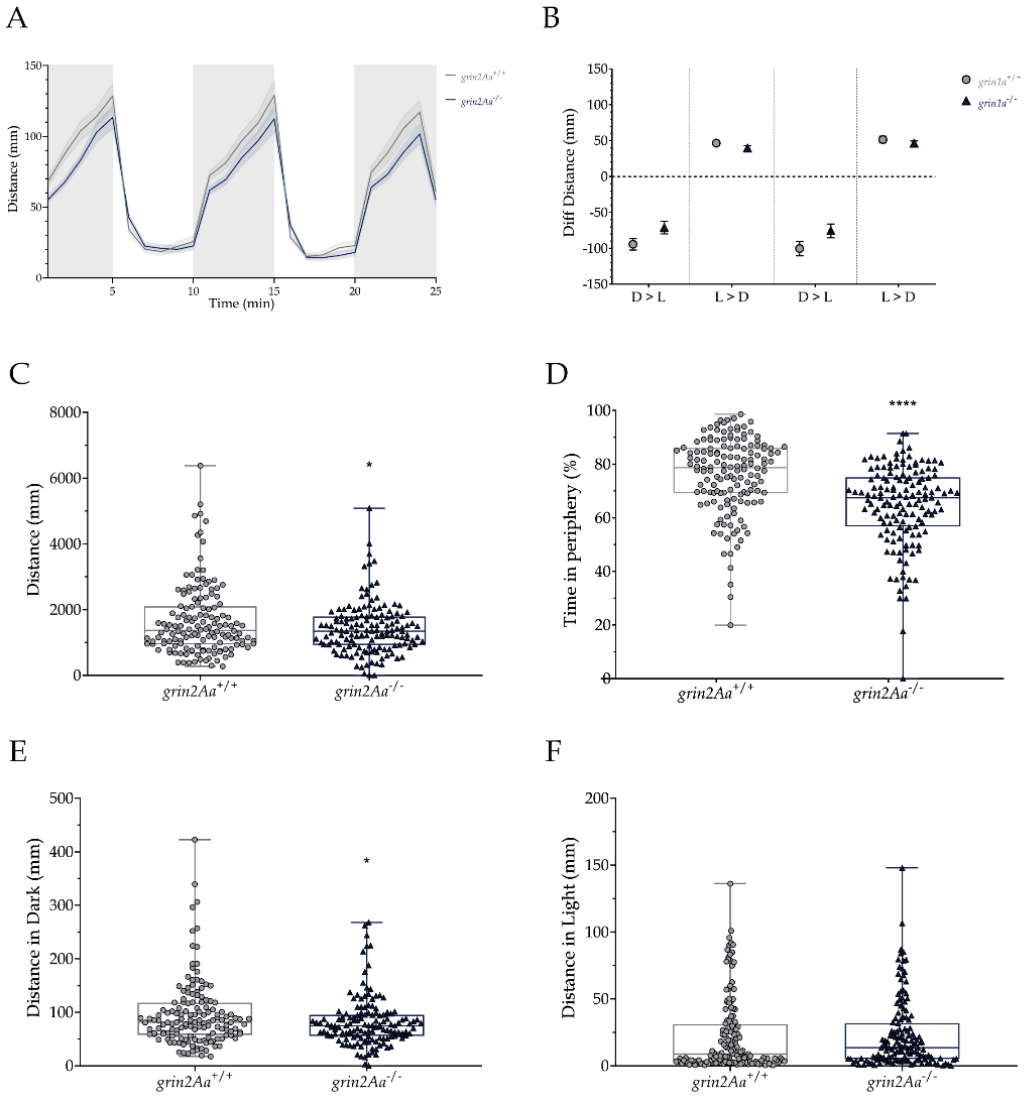

Supplementary Figure 28. Analysis of the locomotor performance of *grin2Aa* mutant zebrafish larvae. A. Representation of the distance moved by one-minute time bin during the 25-minute dark/light cycles. Dark cycles are annotated as grey vertical lines for better visualisation. B. Representation of the difference of the distance moved in the transitions from dark to light (D>L) and from light to dark (L>D). C. Graph of the total distance moved (mm) of the larvae in the complete 25-minute protocol. D. Analysis of the average percentage of time spent in the peripherical area of the well. E. Graph of the total distance moved (mm) only in the dark phases of the dark/light cycle protocol. F. Graph of the total distance moved (mm) only in the light phases of the dark/light cycle protocol. In panels A and B, data is represented as mean ± SEM; in panels C to F, data is represented with box and whisker plots, showing the median, minimum and maximum, showing all points. Wild-type *grin2Aa*$^{+/+}$ larvae are represented in grey, and homozygous *grin2Aa*$^{-/-}$ in dark blue. N=144. *p<0.05, ****p<0.0001 (One-Way ANOVA with Tukey's post-hoc analysis).

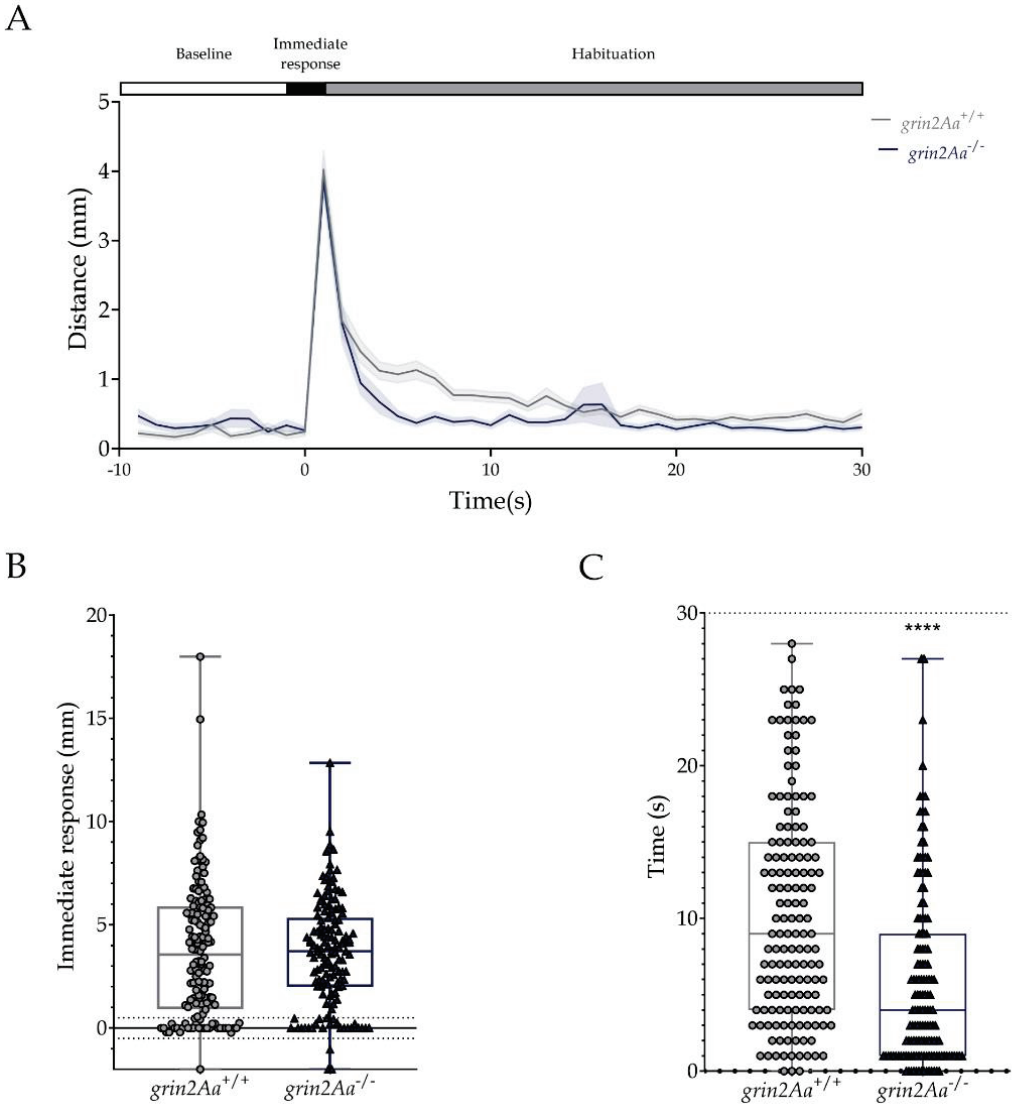

Supplementary Figure 29. Evaluation to the immediate response and habituation to tapping in *grin2Aa* mutant larvae. A. Graph of the distanced moved in one-second time bin. B. Graph representing the difference in the distance moved as a response to the first tap. Statistical analysis of the immediate response (mm) is represented with "*". Statistical analysis of the number of larvae responding (%) is represented with "#". C. Quantification of the habituation by measuring the time each larva takes to not respond to the stimulus, with a cut off at 30 seconds. Wild-type *grin2Aa*$^{+/+}$ larvae are represented in grey, and homozygous *grin2Aa*$^{-/-}$ in dark blue. N=144. **** p<0.0001 (One-way ANOVA with Tukey's post-hoc analysis).

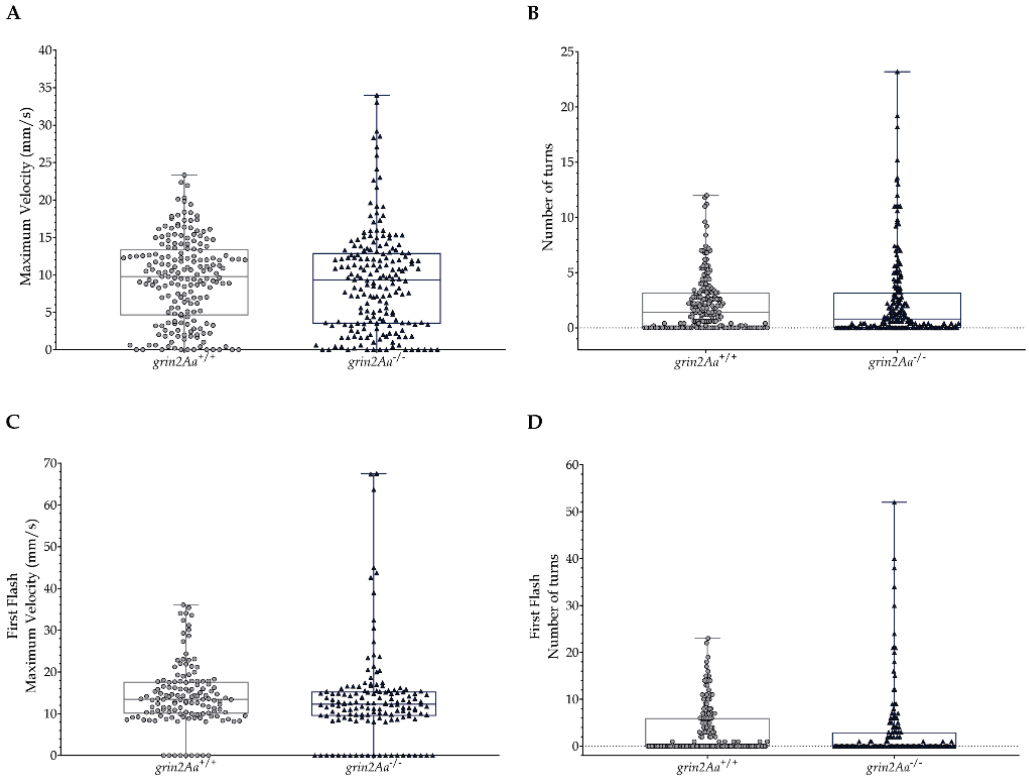

Supplementary Figure 30. Light-induced epilepsy-like response evaluation in *grin2Aa* mutant larvae. A. Measurement of the maximum velocity (mm/s) achieved, comparing the average of the five trials. B. Measurement of the total number of angle turns performed, comparing the average of the five trials. C. Measurement of the maximum velocity (mm/s) achieved, comparing only the response to the first flash. D. Measurement of the total number of angle turns performed, comparing only the response to the first flash. The data is represented with box and whisker plots, showing the median, minimum and maximum, showing all points. Wild-type *grin2Aa*$^{+/+}$ larvae are represented in grey, and homozygous *grin2Aa*$^{-/-}$ in dark blue. N=144.

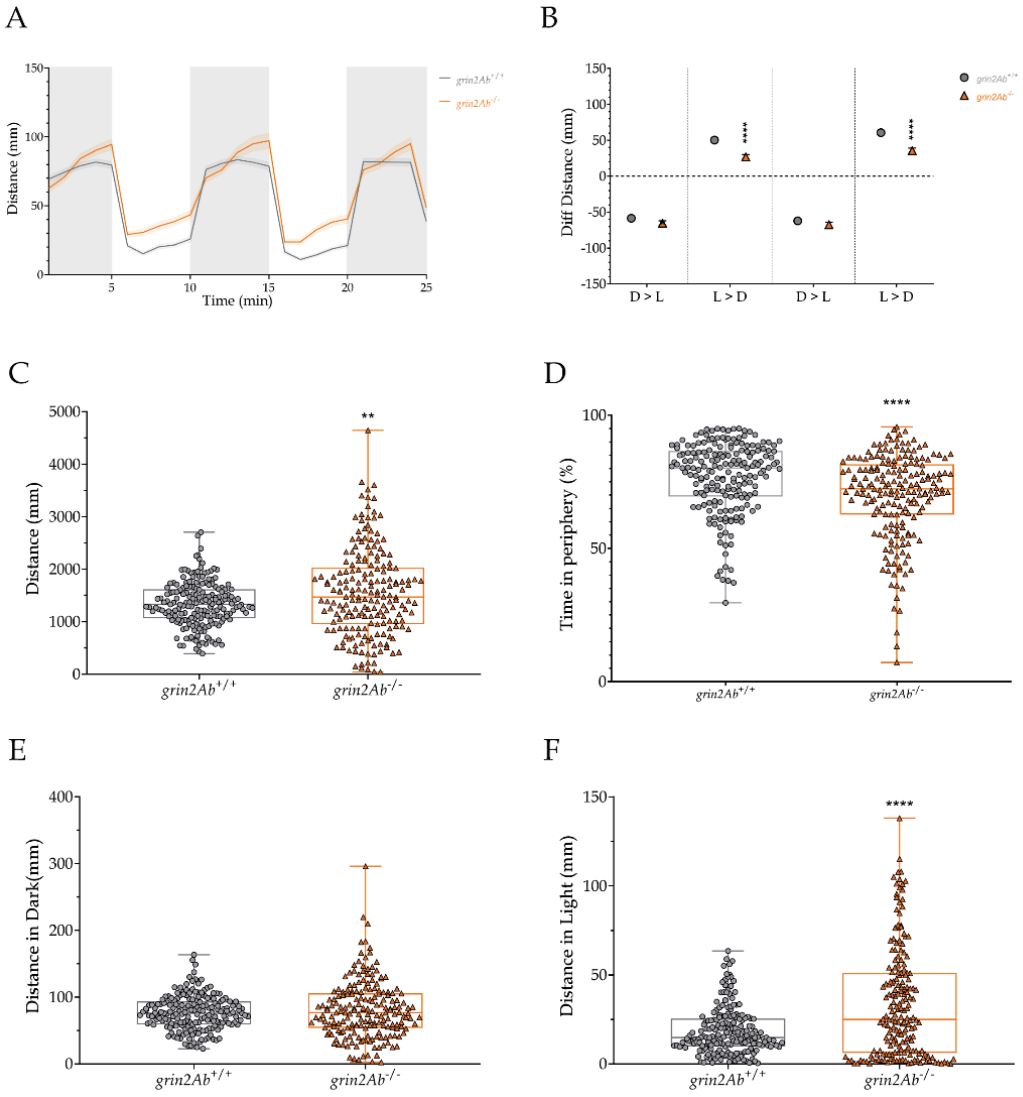

Supplementary Figure 31. Analysis of the locomotor performance of *grin2Ab* mutant zebrafish larvae. A. Representation of the distance moved by one-minute time bin during the 25-minute dark/light cycles. Dark cycles are annotated as grey vertical lines for better visualisation. B. Representation of the difference of the distance moved in the transitions from dark to light (D>L) and from light to dark (L>D). C. Graph of the total distance moved (mm) of the larvae in the complete 25-minute protocol. D. Analysis of the average percentage of time spent in the peripherical area of the well. E. Graph of the total distance moved (mm) only in the dark phases of the dark/light cycle protocol. F. Graph of the total distance moved (mm) only in the light phases of the dark/light cycle protocol. In panels A and B, data is represented as mean ± SEM; in panels C to F, data is represented with box and whisker plots, showing the median, minimum and maximum, showing all points. Wild-type *grin2Ab*$^{+/+}$ larvae are represented in grey, and homozygous *grin2Ab*$^{-/-}$ in orange. N=192. ****p<0.0001 (One-Way ANOVA with Tukey's post-hoc analysis).

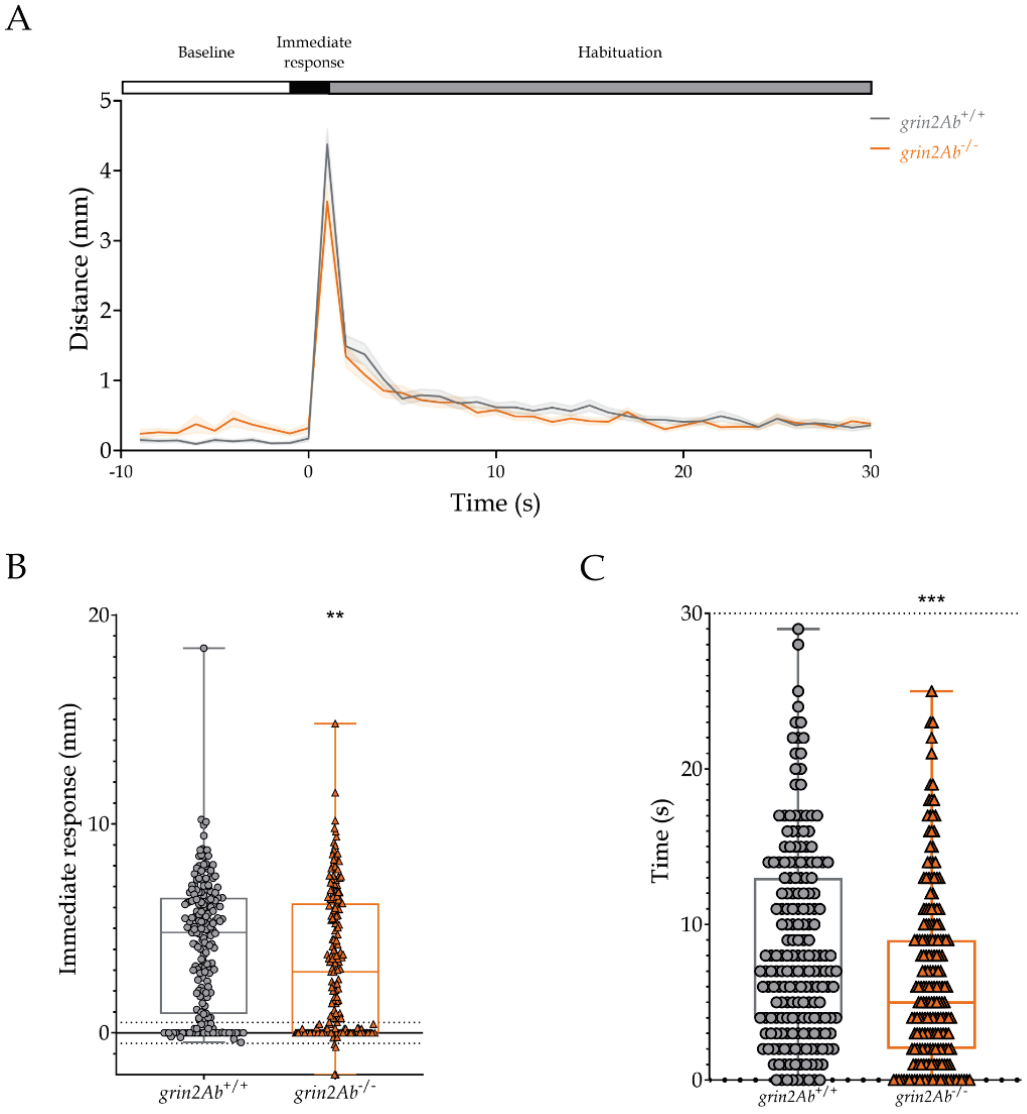

Supplementary Figure 32. Evaluation to the immediate response and habituation to tapping in *grin2Ab* mutant larvae. A. Graph of the distanced moved in one-second time bin. B. Graph representing the difference in the distance moved as a response to the first tap. Statistical analysis of the immediate response (mm) is represented with "*". Statistical analysis of the number of larvae responding (%) is represented with "#". C. Quantification of the habituation by measuring the time each larva takes to not respond to the stimulus, with a cut off at 30 seconds. Wild-type *grin2Ab*$^{+/+}$ larvae are represented in grey, and homozygous *grin2Ab*$^{-/-}$ in orange. N=192. ** p<0.01, ***p<0.001 (One-way ANOVA with Tukey's post-hoc analysis).

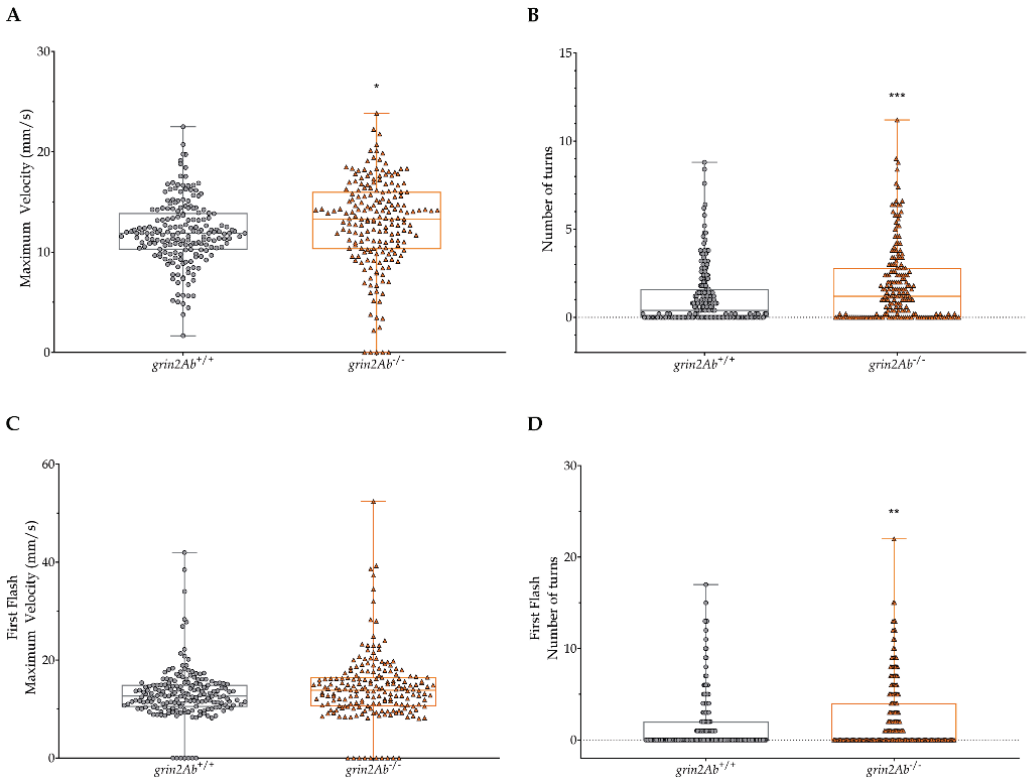

Supplementary Figure 33. Light-induced epilepsy-like response evaluation in *grin2Ab* mutant larvae. A. Measurement of the maximum velocity (mm/s) achieved, comparing the average of the five trials. B. Measurement of the total number of angle turns performed, comparing the average of the five trials. C. Measurement of the maximum velocity (mm/s) achieved, comparing only the response to the first flash. D. Measurement of the total number of angle turns performed, comparing only the response to the first flash. The data is represented with box and whisker plots, showing the median, minimum and maximum, showing all points. Wild-type *grin2Ab*$^{+/+}$ larvae are represented in grey, and homozygous *grin2Ab*$^{-/-}$ in orange. N=192. **p<0.01, *** p<0.001 (One-way ANOVA with Tukey's post-hoc analysis).

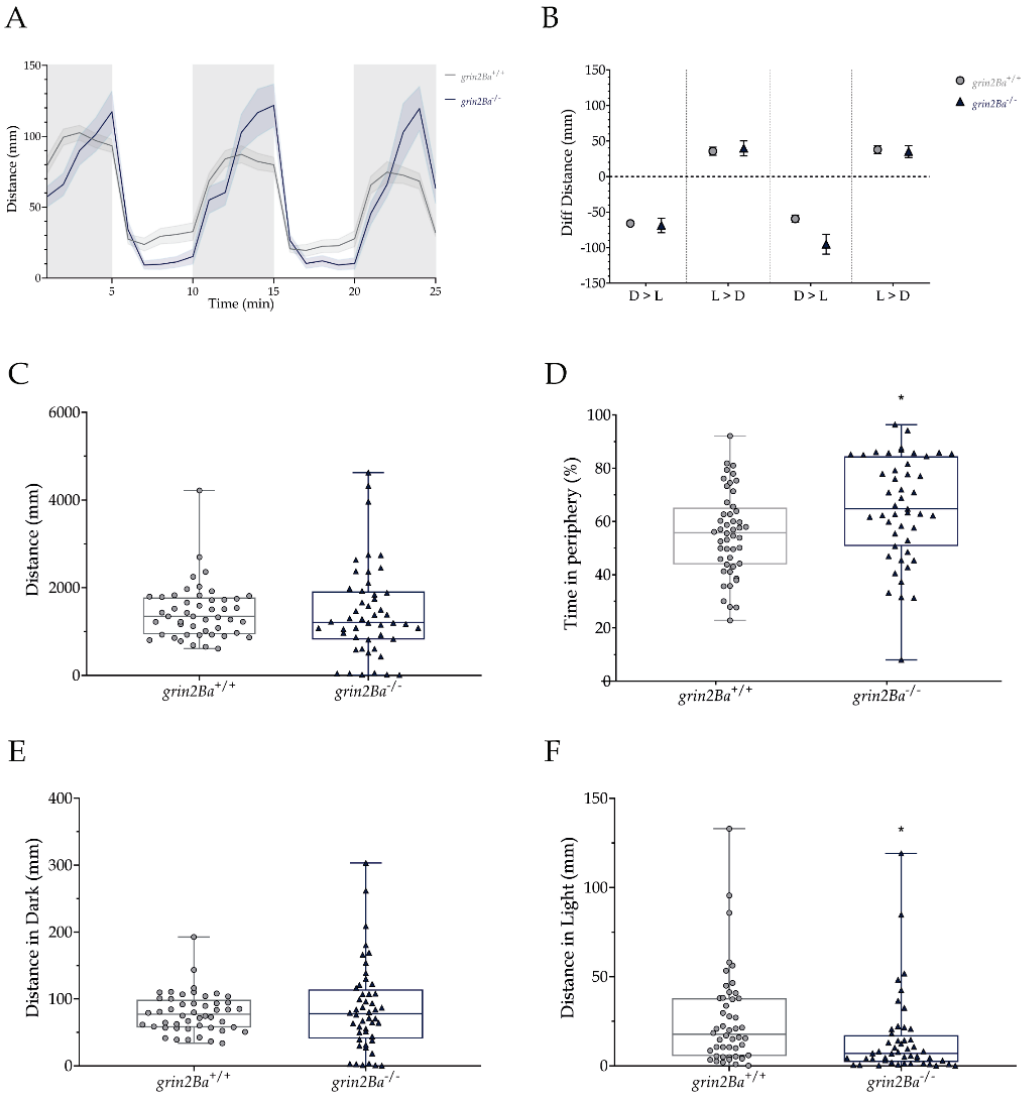

Supplementary Figure 34. Analysis of the locomotor performance of *grin2Ba* mutant zebrafish larvae. A. Representation of the distance moved by one-minute time bin during the 25-minute dark/light cycles. Dark cycles are annotated as grey vertical lines for better visualisation. B. Representation of the difference of the distance moved in the transitions from dark to light (D>L) and from light to dark (L>D). C. Graph of the total distance moved (mm) of the larvae in the complete 25-minute protocol. D. Analysis of the average percentage of time spent in the peripherical area of the well. E. Graph of the total distance moved (mm) only in the dark phases of the dark/light cycle protocol. F. Graph of the total distance moved (mm) only in the light phases of the dark/light cycle protocol. In panels A and B, data is represented as mean ± SEM; in panels C to F, data is represented with box and whisker plots, showing the median, minimum and maximum, showing all points. Wild-type *grin2Ba*$^{+/+}$ larvae are represented in grey, and homozygous *grin2Ba*$^{-/-}$ in dark blue. N=48. *p<0.05 (One-Way ANOVA with Tukey's post-hoc analysis).

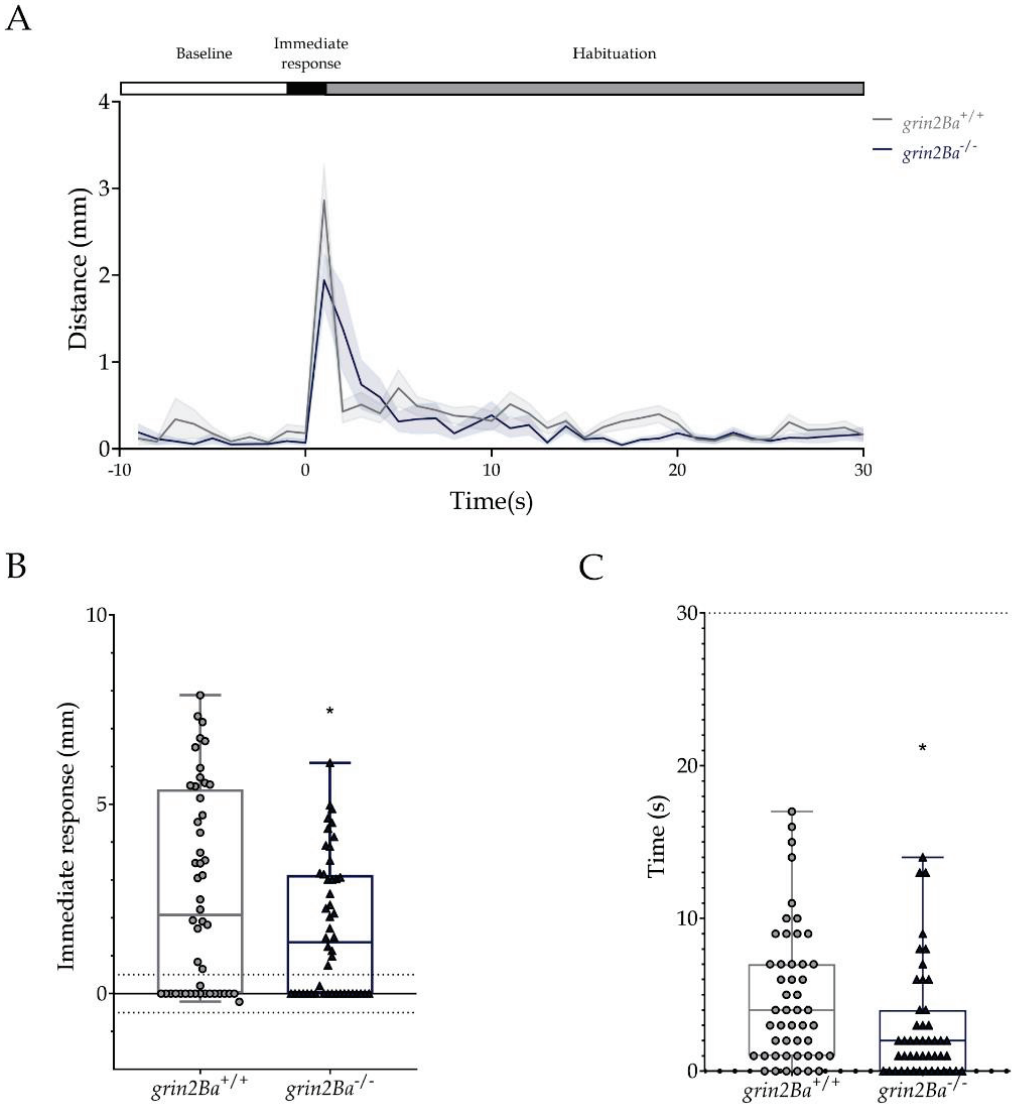

Supplementary Figure 35. Evaluation to the immediate response and habituation to tapping in *grin2Ba* mutant larvae. A. Graph of the distanced moved in one-second time bin. B. Graph representing the difference in the distance moved as a response to the first tap. Statistical analysis of the immediate response (mm) is represented with "*". Statistical analysis of the number of larvae responding (%) is represented with "#". C. Quantification of the habituation by measuring the time each larva takes to not respond to the stimulus, with a cut off at 30 seconds. Wild-type *grin2Ba*$^{+/+}$ larvae are represented in grey, and homozygous *grin2Ba*$^{-/-}$ in dark blue. N=48. * $p<0.05$ (One-way ANOVA with Tukey's post-hoc analysis).

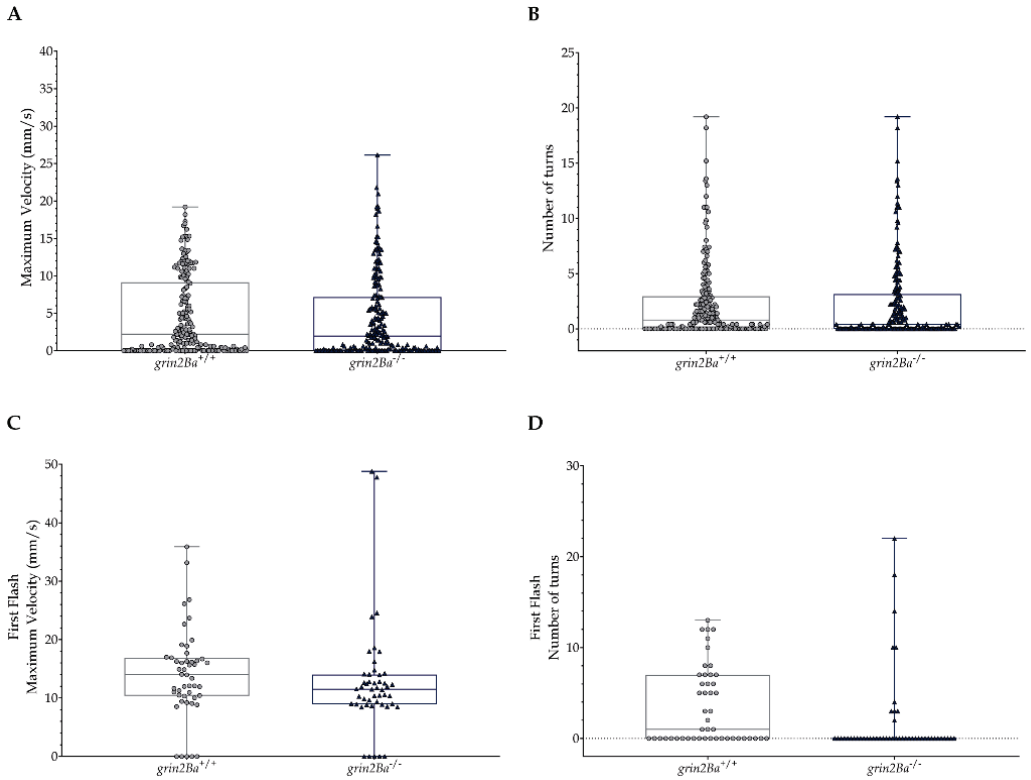

Supplementary Figure 36. Light-induced epilepsy-like response evaluation in *grin2Ba* mutant larvae. A. Measurement of the maximum velocity (mm/s) achieved, comparing the average of the five trials. B. Measurement of the total number of angle turns performed, comparing the average of the five trials. C. Measurement of the maximum velocity (mm/s) achieved, comparing only the response to the first flash. D. Measurement of the total number of angle turns performed, comparing only the response to the first flash. The data is represented with box and whisker plots, showing the median, minimum and maximum, showing all points. Wild-type *grin2Ba*$^{+/+}$ larvae are represented in grey, and homozygous *grin2Ba*$^{-/-}$ in dark blue. N=48. *** $p<0.001$, ****$p<0.0001$ (One-way ANOVA with Tukey's post-hoc analysis).

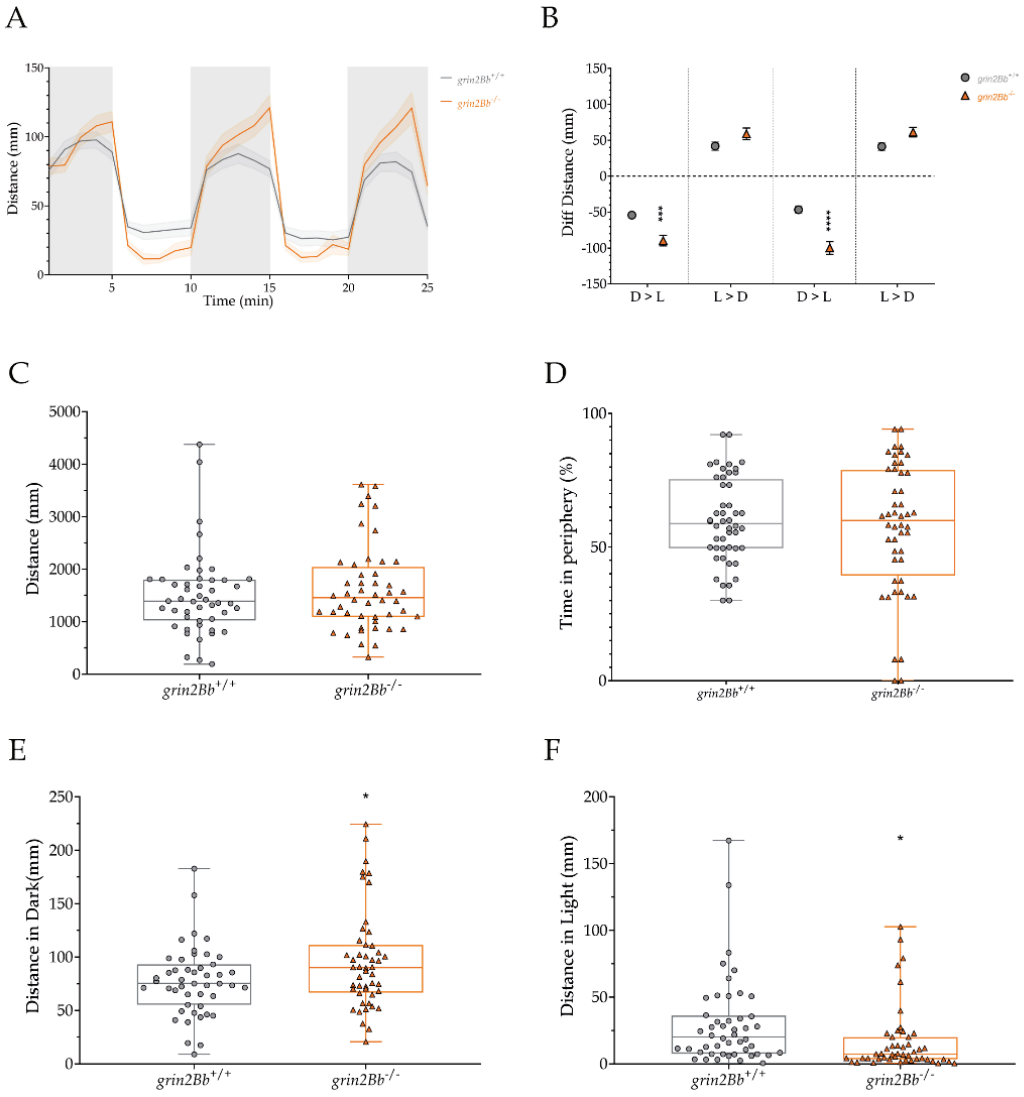

Supplementary Figure 37. Analysis of the locomotor performance of *grin2Bb* mutant zebrafish larvae. A. Representation of the distance moved by one-minute time bin during the 25-minute dark/light cycles. Dark cycles are annotated as grey vertical lines for better visualisation. B. Representation of the difference of the distance moved in the transitions from dark to light (D>L) and from light to dark (L>D). C. Graph of the total distance moved (mm) of the larvae in the complete 25-minute protocol. D. Analysis of the average percentage of time spent in the peripherical area of the well. E. Graph of the total distance moved (mm) only in the dark phases of the dark/light cycle protocol. F. Graph of the total distance moved (mm) only in the light phases of the dark/light cycle protocol. In panels A and B, data is represented as mean ± SEM; in panels C to F, data is represented with box and whisker plots, showing the median, minimum and maximum, showing all points. Wild-type *grin2Bb*$^{+/+}$ larvae are represented in grey, and homozygous *grin2Bb*$^{-/-}$ in orange. N=192. *p<0.05 (One-Way ANOVA with Tukey's post-hoc analysis).

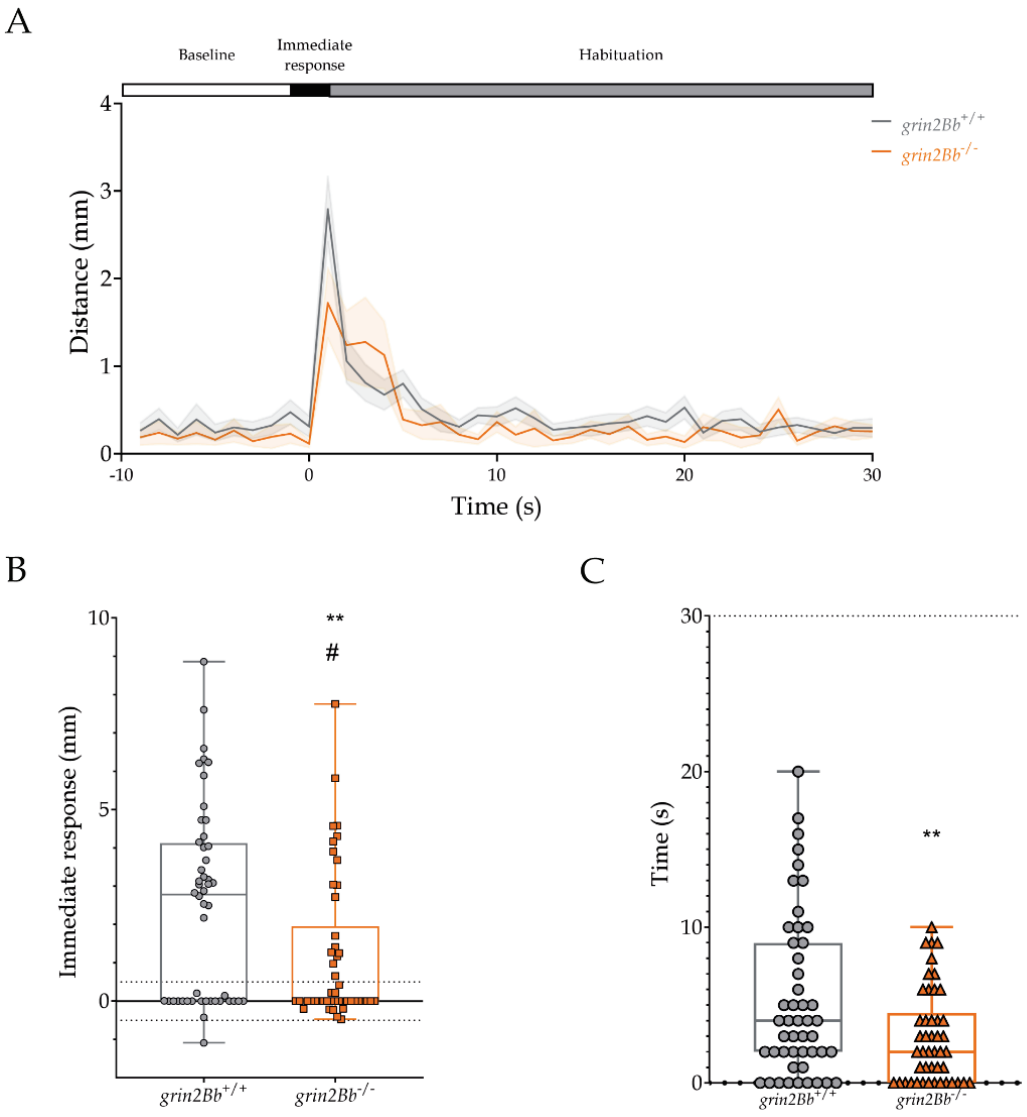

Supplementary Figure 38. Evaluation to the immediate response and habituation to tapping in *grin2Bb* mutant larvae. A. Graph of the distanced moved in one-second time bin. B. Graph representing the difference in the distance moved as a response to the first tap. Statistical analysis of the immediate response (mm) is represented with "*". Statistical analysis of the number of larvae responding (%) is represented with "#". C. Quantification of the habituation by measuring the time each larva takes to not respond to the stimulus, with a cut off at 30 seconds. Wild-type *grin2Bb*$^{+/+}$ larvae are represented in grey, and homozygous *grin2Bb*$^{-/-}$ in orange. N=192. * p<0.05 (One-way ANOVA with Tukey's post-hoc analysis).

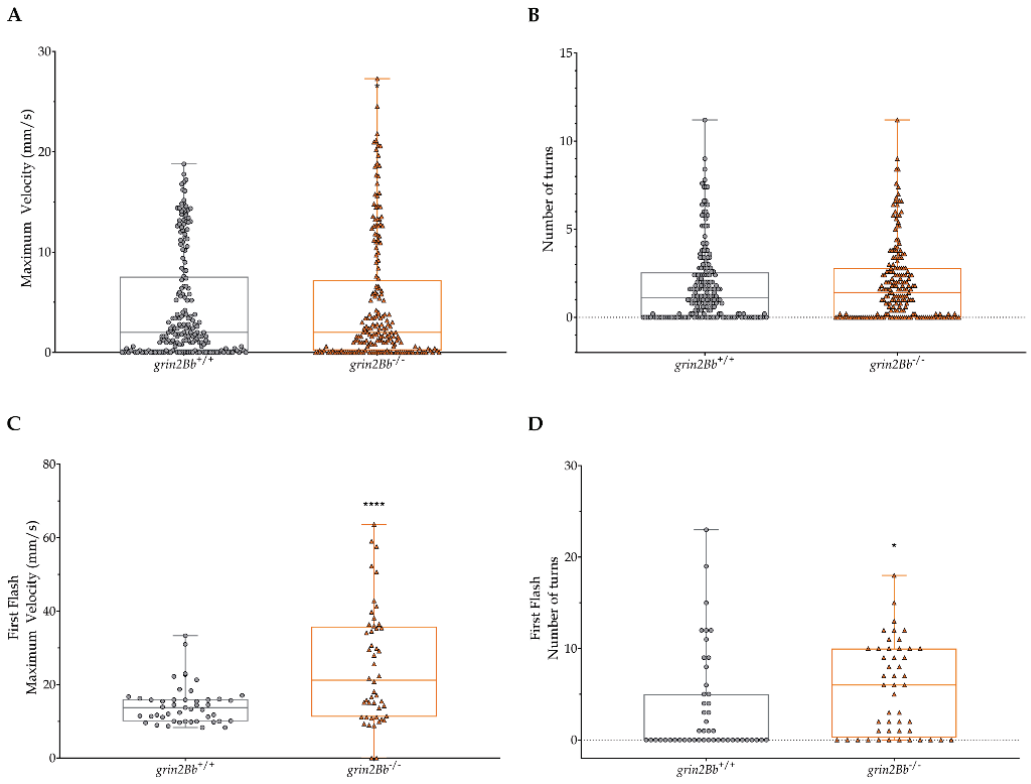

Supplementary Figure 39. Light-induced epilepsy-like response evaluation in *grin2Bb* mutant larvae. A. Measurement of the maximum velocity (mm/s) achieved, comparing the average of the five trials. B. Measurement of the total number of angle turns performed, comparing the average of the five trials. C. Measurement of the maximum velocity (mm/s) achieved, comparing only the response to the first flash. D. Measurement of the total number of angle turns performed, comparing only the response to the first flash. The data is represented with box and whisker plots, showing the median, minimum and maximum, showing all points. Wild-type *grin2Bb*$^{+/+}$ larvae are represented in grey, and homozygous *grin2Bb*$^{-/-}$ in orange. N=192. *** p<0.001, ****p<0.0001 (One-way ANOVA with Tukey's post-hoc analysis).

Index of Figures and Tables

Figures

Tables

Supplementary Figures